



**HAL**  
open science

# Contribution à l'étude de mélange en pellets composé d'argilite CO<sub>x</sub> et de bentonite MX80 pour le remplissage des stockages géologiques

Danai Panagiota Tyri

## ► To cite this version:

Danai Panagiota Tyri. Contribution à l'étude de mélange en pellets composé d'argilite CO<sub>x</sub> et de bentonite MX80 pour le remplissage des stockages géologiques. Génie civil. Université de Lyon, 2021. Français. NNT : 2021LYSEI001 . tel-03219187

**HAL Id: tel-03219187**

**<https://theses.hal.science/tel-03219187>**

Submitted on 6 May 2021

**HAL** is a multi-disciplinary open access archive for the deposit and dissemination of scientific research documents, whether they are published or not. The documents may come from teaching and research institutions in France or abroad, or from public or private research centers.

L'archive ouverte pluridisciplinaire **HAL**, est destinée au dépôt et à la diffusion de documents scientifiques de niveau recherche, publiés ou non, émanant des établissements d'enseignement et de recherche français ou étrangers, des laboratoires publics ou privés.



N°d'ordre NNT : 2021LYSEI001

**THESE de DOCTORAT DE L'UNIVERSITE DE LYON**  
opérée au sein de  
**INSA Lyon**

**Ecole Doctorale ED 162**  
**MEGA : Mécanique – Energétique – Génie Civil - Acoustique**

**Spécialité/ discipline de doctorat** : Génie Civil

Soutenue publiquement le 07/01/2021, par :  
**Danai Panagiota TYRI**

---

**Contribution to the study of  
pelletized mixture composed of  
COx argillite and MX80 bentonite  
as backfill for geological repositories**

---

Devant le jury composé de :

|                     |  |                       |
|---------------------|--|-----------------------|
| LEVACHER Daniel     | Professeur, Université de Caen Normandie       | Président             |
| COSENZA Philippe    | Professeur, Université de Poitiers             | Rapporteur            |
| LANOS Christophe    | Professeur, Université Rennes 1                | Rapporteur            |
| KALLIOGLOU Polyxeni | Maître de conférences, Université de Thessalie | Examinatrice          |
| PLAS Frédéric       | Directeur R&D, ANDRA                           | Examineur             |
| ZGHONDI Jad         | Docteur/Ingénieur de recherche, ANDRA          | Examineur             |
| DJERAN-MAIGRE Irini | Professeure, INSA Lyon                         | Directrice de thèse   |
| ROBINET Jean-Claude | HDR, Directeur EGC                             | Co-directeur de thèse |
| IMBERT Christophe   | Ingénieur de recherche, CEA                    | Invité                |



# INSA

**THESE de DOCTORAT DE L'UNIVERSITE DE LYON**  
opérée au sein de  
**INSA Lyon**

**Ecole Doctorale ED 162**  
**MEGA : Mécanique – Energétique – Génie Civil - Acoustique**

**Spécialité/ discipline de doctorat : Génie Civil**

Soutenue publiquement le 07/01/2021, par :  
**Danai Panagiota TYRI**

---

## **Contribution to the study of pelletized mixture composed of COx argillite and MX80 bentonite as backfill for geological repositories**

---

En collaboration avec :

EGC





Département FEDORA – INSA Lyon - Ecoles Doctorales – Quinquennal 2016-2020

| SIGLE            | ECOLE DOCTORALE  | NOM ET COORDONNEES DU RESPONSABLE  |
|------------------|--|--|
| <b>CHIMIE</b>    | <b><u>CHIMIE DE LYON</u></b><br><a href="http://www.edchimie-lyon.fr">http://www.edchimie-lyon.fr</a><br>Sec. : Renée EL MELHEM<br>Bât. Blaise PASCAL, 3e étage<br><a href="mailto:secretariat@edchimie-lyon.fr">secretariat@edchimie-lyon.fr</a><br>INSA : R. GOURDON   | <b>M. Stéphane DANIELE</b><br>Institut de recherches sur la catalyse et l'environnement de Lyon<br>IRCELYON-UMR 5256<br>Équipe CDFA<br>2 Avenue Albert EINSTEIN<br>69 626 Villeurbanne CEDEX<br><a href="mailto:directeur@edchimie-lyon.fr">directeur@edchimie-lyon.fr</a>   |
| <b>E.E.A.</b>    | <b><u>ÉLECTRONIQUE,</u></b><br><b><u>ÉLECTROTECHNIQUE,</u></b><br><b><u>AUTOMATIQUE</u></b><br><a href="http://edeea.ec-lyon.fr">http://edeea.ec-lyon.fr</a><br>Sec. : M.C. HAVGOUDOUKIAN<br><a href="mailto:ecole-doctorale.eea@ec-lyon.f">ecole-doctorale.eea@ec-lyon.f</a>  | <b>M. Gérard SCORLETTI</b><br>École Centrale de Lyon<br>36 Avenue Guy DE COLLONGUE<br>69 134 Écully<br>Tél : 04.72.18.60.97 Fax 04.78.43.37.17<br><a href="mailto:gerard.scorletti@ec-lyon.fr">gerard.scorletti@ec-lyon.fr</a>   |
| <b>E2M2</b>      | <b><u>ÉVOLUTION, ÉCOSYSTÈME,</u></b><br><b><u>MICROBIOLOGIE, MODÉLISATION</u></b><br><a href="http://e2m2.universite-lyon.fr">http://e2m2.universite-lyon.fr</a><br>Sec. : Sylvie ROBERJOT<br>Bât. Atrium, UCB Lyon 1<br>Tél : 04.72.44.83.62<br>INSA : H. CHARLES<br><a href="mailto:secretariat.e2m2@univ-lyon1.fr">secretariat.e2m2@univ-lyon1.fr</a> | <b>M. Philippe NORMAND</b><br>UMR 5557 Lab. d'Ecologie Microbienne<br>Université Claude Bernard Lyon 1<br>Bâtiment Mendel<br>43, boulevard du 11 Novembre 1918<br>69 622 Villeurbanne CEDEX<br><a href="mailto:philippe.normand@univ-lyon1.fr">philippe.normand@univ-lyon1.fr</a>  |
| <b>EDISS</b>     | <b><u>INTERDISCIPLINAIRE</u></b><br><b><u>SCIENCES-SANTÉ</u></b><br><a href="http://www.ediss-lyon.fr">http://www.ediss-lyon.fr</a><br>Sec. : Sylvie ROBERJOT<br>Bât. Atrium, UCB Lyon 1<br>Tél : 04.72.44.83.62<br>INSA : M. LAGARDE<br><a href="mailto:secretariat.ediss@univ-lyon1.fr">secretariat.ediss@univ-lyon1.fr</a>                            | <b>Mme Sylvie RICARD-BLUM</b><br>Institut de Chimie et Biochimie Moléculaires et<br>Supramoléculaires<br>(ICBMS) - UMR 5246 CNRS - Université Lyon 1<br>Bâtiment Curien - 3ème étage Nord<br>43 Boulevard du 11 novembre 1918<br>69622 Villeurbanne Cedex<br>Tel : +33(0)4 72 44 82 32<br><a href="mailto:sylvie.ricard-blum@univ-lyon1.fr">sylvie.ricard-blum@univ-lyon1.fr</a> |
| <b>INFOMATHS</b> | <b><u>INFORMATIQUE ET</u></b><br><b><u>MATHÉMATIQUES</u></b><br><a href="http://edinfomaths.universite-lyon.fr">http://edinfomaths.universite-lyon.fr</a><br>Sec. : Renée EL MELHEM<br>Bât. Blaise PASCAL, 3e étage<br>Tél : 04.72.43.80.46<br><a href="mailto:infomaths@univ-lyon1.fr">infomaths@univ-lyon1.fr</a>                                      | <b>M. Hamamache KHEDDOUCI</b><br>Bât. Nautibus<br>43, Boulevard du 11 novembre 1918<br>69 622 Villeurbanne Cedex France<br>Tel : 04.72.44.83.69<br><a href="mailto:hamamache.kheddouci@univ-lyon1.fr">hamamache.kheddouci@univ-lyon1.fr</a>  |
| <b>Matériaux</b> | <b><u>MATÉRIAUX DE LYON</u></b><br><a href="http://ed34.universite-lyon.fr">http://ed34.universite-lyon.fr</a><br>Sec. : Stéphanie CAUVIN<br>Tél : 04.72.43.71.70<br>Bât. Direction<br><a href="mailto:ed.materiaux@insa-lyon.fr">ed.materiaux@insa-lyon.fr</a>  | <b>M. Jean-Yves BUFFIÈRE</b><br>INSA de Lyon<br>MATEIS - Bât. Saint-Exupéry<br>7 Avenue Jean CAPELLE<br>69 621 Villeurbanne CEDEX<br>Tél : 04.72.43.71.70 Fax : 04.72.43.85.28<br><a href="mailto:jean-yves.buffiere@insa-lyon.fr">jean-yves.buffiere@insa-lyon.fr</a>   |
| <b>MEGA</b>      | <b><u>MÉCANIQUE, ÉNERGÉTIQUE,</u></b><br><b><u>GÉNIE CIVIL, ACOUSTIQUE</u></b><br><a href="http://edmega.universite-lyon.fr">http://edmega.universite-lyon.fr</a><br>Sec. : Stéphanie CAUVIN<br>Tél : 04.72.43.71.70<br>Bât. Direction<br><a href="mailto:mega@insa-lyon.fr">mega@insa-lyon.fr</a>   | <b>M. Jocelyn BONJOUR</b><br>INSA de Lyon<br>Laboratoire CETHIL<br>Bâtiment Sadi-Carnot<br>9, rue de la Physique<br>69 621 Villeurbanne CEDEX<br><a href="mailto:jocelyn.bonjour@insa-lyon.fr">jocelyn.bonjour@insa-lyon.fr</a>  |

|             |  |   |
|-------------|--|---|
| <b>ScSo</b> | <b><u>ScSo*</u></b><br><a href="http://ed483.univ-lyon2.fr">http://ed483.univ-lyon2.fr</a><br>Sec. : Véronique GUICHARD<br>INSA : J.Y. TOUSSAINT<br>Tél : 04.78.69.72.76<br><a href="mailto:veronique.cervantes@univ-lyon2.fr">veronique.cervantes@univ-lyon2.fr</a> | <b>M. Christian MONTES</b><br>Université Lyon 2<br>86 Rue Pasteur<br>69 365 Lyon CEDEX 07<br><a href="mailto:christian.montes@univ-lyon2.fr">christian.montes@univ-lyon2.fr</a> |
|-------------|--|---|

\*ScSo : Histoire, Géographie, Aménagement, Urbanisme, Archéologie, Science politique, Sociologie, Anthropologie



# Acknowledgments

The work presented in this PhD thesis was carried out in the laboratories of GEOMAS (INSA Lyon) and Euro-Geomat-Consulting and was financially supported by Andra. I would like to express my sincere gratitude to many people for their help and support these three years.

I would like to sincerely thank those who guided me through these years. My director Irini Djeran-Maigre and my co-director Jean-Claude Robinet for first and foremost giving me this opportunity, their insight, as well as their patience with my French. In particular, Irini, for her advice and encouragement and Jean-Claude for his constant motivation for work. I thank Andra for funding my research study and especially Jad Zghondi who has followed my work over the three years and has regularly advised me.

I warmly thank my two reviewers, Philippe Cosenza and Christophe Lanos for graciously accepting to review my thesis and giving me their detailed comments and suggestions on the subject. Further thanks to all the members of the jury for being able to attend my oral defense. Daniel Levacher and Frédéric Plas for having accepted to be my thesis examiners and giving their precious feedback. Allow me to single out Jenny Kallioglou, for also being the very first person who believed I was capable of doing a PhD. I would also like to thank Christophe Imbert for his insight and pleasant collaboration in CEA.

The valuable support of Stéphane Vacherie and Bui Quoc Huy Ly is undeniable for helping me to carry out the experimental work in both labs. I would like to also thank Jean Talandier and Nathalie Conil that were happy to share with me their scientific ideas over these years.

I could never forget the friends I made at INSA: Francois and Alexis, Nicole, Rosy, Jose and Atefeh (we were by far the best office), Nour, Adnan and those I did not have the chance to know more.

Last but certainly not least, I owe a huge “thank you” to my family and my friends who helped and supported me, from the beginning of this journey regardless the distance.



# Abstract

The safe operation of the geological disposal facilities for radioactive waste indicates the galleries progressive closure, by installing sealing and backfill materials. The French disposal concept examines the crushed excavated Callovo-Oxfordian (COx) claystone with bentonite additive (MX80) as backfill material. One of the ongoing studied backfill solutions considers the pelletized implementation of the mixture, due to potential set-up advantages. The pelletized mixture is emplaced inside the galleries at dry state, presenting initially a granular structure, gradually homogenised, due to swelling upon hydration from the groundwater of the surrounding rock.

Objective of the PhD thesis is the determination and manufacturing of the pelletized mixture, as well as the analysis of its hydro-mechanical behaviour. The pelletized granulometry is selected to result in the highest possible packing density, defining the optimum grain size distribution (GSD). The implemented COx/MX80 backfill needs to present hydro-mechanical properties capable of limiting the voids after the saturation on the drift as well as blocking the concrete movement when liners cracking will occur in the long-term.

Numerical and experimental gravitational deposits are conducted, to study the compactness of a granular material, without mechanical compaction. Simulations using the Discrete Element Method (DEM) investigate the granulometric effect on the granular material's packing state, determining an optimum GSD. Supplementary experiments are used to evaluate and finalise the granulometric selection maximising the resulting density. Both studies investigate the effect of additional parameters (implementation protocol, inter-particle friction, deposit height,...) on the packing state.

The pelletization of the selected GSD is performed for the first time on COx/MX80 powdered mixtures, by applying the compression method on a reconditioned tablet machine. The process is analysed to successfully fabricate pellets and optimise the challenging pellet production.

COx/MX80 mixtures hydro-mechanical behaviour is experimentally investigated by performing infiltration tests under free and confined volume conditions. A parametric study on various powdered mixtures is conducted to characterise the materials physicochemical properties and evaluate their swelling capacity at densities expected on the backfill implementation. On the other hand, the finalised pellets assembly on various compositions is directly tested in terms of swelling pressure and hydraulic conductivity.

**Keywords:** pellets, Callovo-Oxfordian claystone, MX80-bentonite, maximum packing density, optimum grain size distribution, DEM, hydro-mechanical behavior, swelling potential, swelling pressure, hydraulic conductivity

# Résumé

Lors de la fermeture du stockage géologique des déchets radioactifs, l'ensemble des galeries souterraines sont remblayées et localement des scellements sont installés pour limiter la circulation de l'eau dans les ouvrages. Pour le remblaiement des galeries de Cigéo, l'argilite du Callovo-Oxfordien (COx) remaniée, mélangée avec de la bentonite (MX80) est envisagée par l'Andra. Différentes solutions d'installation sont à l'étude et en particulier la forme de granules (pellets), une solution qui pourra offrir des avantages opérationnels. L'assemblage de pellets est mis en place dans des galeries à l'état sec. Cette structure granulaire est progressivement homogénéisée par le gonflement lors de l'hydratation par l'eau issue de la roche encaissante.

Cette thèse se concentre sur la détermination et la fabrication de mélanges de pellets, ainsi que l'évaluation de son comportement hydromécanique. La granulométrie des pellets est choisie pour aboutir à la densité de mise en place la plus élevée possible, qui est caractérisée comme étant la granulométrie optimale. Le mélange COx/MX80 doit produire un comportement hydromécanique adéquat de manière à reprendre les vides technologiques inhérent à la mise en place, et à long terme, réduire le déplacement des blocs de revêtements lors de la rupture de celui-ci. L'objectif est de limiter un endommagement de la roche environnante.

Des dépôts gravitationnels sont réalisés numériquement et expérimentalement, pour étudier la compacité d'un matériau granulaire, sans compactage mécanique. Des simulations utilisant la méthode des éléments discrets étudient l'effet granulométrique sur la densité de la mise en place, définissant un fuseau optimal. Des expériences supplémentaires sont menées pour évaluer et finaliser la sélection granulométrique qui maximise la densité du mélange. Les études examinent l'effet de paramètres supplémentaires (protocole de mise en place, frottement inter-particules, hauteur de dépôt,...) sur la compacité.

La pelletization sur la base de la granulométrie choisie est réalisée pour la première fois sur des mélanges COx/MX80. La méthode de compression est appliquée en utilisant une machine à comprimés reconditionnée. La fabrication des pellets et l'optimisation de la production est analysée.

Le comportement hydromécanique des mélanges COx/MX80 est étudié expérimentalement par des essais d'infiltration à volume libre et constant. Une étude paramétrique sur mélanges COx/MX80 en poudre est menée pour caractériser les propriétés physico-chimiques et évaluer leur capacité de gonflement aux densités attendues à la mise en place. En revanche, l'ensemble des pellets finalisé avec diverses compositions est directement testé en termes de pression de gonflement et de conductivité hydraulique.

**Mots clés:** pellets, argilite du Callovo-Oxfordien, MX80 bentonite, densité de la mise en place maximale, granulométrie optimale, DEM, comportement hydromécanique, potentiel de gonflement, pression de gonflement, conductivité hydraulique

# Table of Contents

|  |           |
|--|-----------|
| Acknowledgments .....  | i         |
| Abstract .....   | iii       |
| Résumé .....   | v         |
| Table of Contents .....  | vii       |
| List of Tables.....  | xi        |
| List of Figures .....  | xiii      |
| List of Notations.....   | xxiii     |
| List of Symbols .....  | xxv       |
| <br>   |           |
| <b>Chapter 1 - Introduction.....</b>   | <b>1</b>  |
| 1.1 General context of deep geological disposal - Project Cigeo.....   | 2         |
| 1.2 Pelletized CO <sub>x</sub> /MX80 mixture as backfill .....   | 7         |
| 1.3 Objective and outline of the thesis .....  | 7         |
| <br>   |           |
| <b>Chapter 2 - State of the art.....</b>   | <b>11</b> |
| 2.1 Introduction .....   | 12        |
| 2.2 Hydro-mechanical behaviour of remoulded CO <sub>x</sub> argillite .....  | 12        |
| 2.2.1 Mineralogical composition of CO <sub>x</sub> argillite.....  | 12        |
| 2.2.2 Reminder of swelling mechanism in clays and experimental techniques for swelling capacity measurement at macroscopic scale ..... | 13        |
| 2.2.3 Swelling capacity of remoulded CO <sub>x</sub> argillite.....  | 20        |
| 2.2.4 Conclusions and necessity for supplementary swelling behaviour .....   | 22        |
| 2.3 Swelling clay presence in remoulded soil materials: Bentonite case .....   | 23        |
| 2.3.1 Structure arrangement: pore families determination .....   | 23        |
| 2.3.2 Pore structure at the as-compacted state.....  | 24        |
| 2.3.3 Fabric evolution upon hydration path .....   | 26        |
| 2.3.4 Influential parameters of swelling behaviour.....  | 28        |
| 2.3.4.1 Smectite content.....  | 28        |
| 2.3.4.2 Mechanical loading prior to hydration.....   | 29        |
| 2.3.4.3 Hydration path.....  | 32        |
| 2.3.4.4 Chemical interactions with infiltrated fluid.....  | 34        |
| 2.3.4.5 Temperature effect.....  | 36        |

|  |   |           |
|--|---|-----------|
| 2.3.4.6  | Conclusions.....  | 36        |
| 2.4  | Implementation techniques of remoulded materials on radioactive waste disposal    | 37        |
| 2.5  | Swelling clay pellets at disposal systems .....                                   | 40        |
| 2.5.1  | Pellet fabrication.....   | 40        |
| 2.5.2  | Pelletized material at initial state.....   | 42        |
| 2.5.3  | Evolution upon hydration and hydro-mechanical response.....                       | 44        |
| 2.6  | Packing state of granular materials on emplacement conditions.....                | 47        |
| 2.7  | Identification of needs and proposed strategy of the present Phd study.....       | 51        |
| <br><b>Chapter 3 - Numerical study for optimisation of pellets assembly.....</b> |   | <b>55</b> |
| 3.1  | Introduction .....  | 56        |
| 3.2  | Numerical approach: theoretical aspects and calculations .....                    | 56        |
| 3.2.1  | Numerical model.....  | 57        |
| 3.2.2  | Simulation procedure.....   | 57        |
| 3.3  | Bimodal and trimodal samples: Results, parametric study and discussion .....      | 61        |
| 3.3.1  | Sample's porosity found in literature.....  | 61        |
| 3.3.2  | Resulting packing density of pelletized samples.....                              | 64        |
| 3.3.2.1  | Bimodal samples.....  | 64        |
| 3.3.2.2  | Trimodal samples.....   | 66        |
| 3.3.2.3  | Discussion on bimodal versus trimodal samples.....                                | 71        |
| 3.3.2.4  | Parametric study on optimum DEM Grain Size Distribution.....                      | 72        |
| 3.4  | Conclusions and optimum GSD obtained by DEM.....                                  | 74        |
| <br><b>Chapter 4 - Pelletizing process.....</b>                                  |   | <b>75</b> |
| 4.1  | Introduction .....  | 76        |
| 4.2  | Studied soil materials: physical parameters.....                                  | 76        |
| 4.2.1  | Parametric study of COx/MX80 mixtures: characterisation and compressibility ..... | 79        |
| 4.2.1.1  | Index properties.....   | 79        |
| 4.2.1.2  | Confined uniaxial compression tests.....  | 81        |
| 4.3  | Pellet machine and fabricated accessories.....                                    | 90        |
| 4.4  | Optimisation of COx/MX80 pellet production: Influential factors .....             | 93        |
| 4.4.1  | Realisation of pellet fabrication.....  | 93        |
| 4.4.2  | Optimisation of pellet production.....  | 96        |
| 4.5  | Conclusions .....   | 99        |

|  |     |
|--|-----|
| <b>Chapter 5 - Experimental optimisation of the resulting packing density of pellets assembly</b> .....                              | 101 |
| 5.1 Introduction .....   | 102 |
| 5.2 Studied materials and experimental set-up.....   | 102 |
| 5.3 Results and discussions .....  | 105 |
| 5.3.1 Evaluation of optimum pelletized DEM Grain Size Distribution.....  | 105 |
| 5.3.1.1 Resulting packing density.....   | 107 |
| 5.3.1.2 Discussion on experimental and numerical results.....  | 108 |
| 5.3.2 Supplementary experimental study on density maximisation .....   | 110 |
| 5.3.2.1 Resulting packing density for different mixture types.....   | 110 |
| 5.3.2.2 Effect of the proportions of finer grains.....   | 112 |
| 5.4 Conclusions and optimised resulting packing density.....   | 113 |
| <br>   |     |
| <b>Chapter 6 - Hydro-mechanical parametric study of COx/MX80 pelletized material from compacted COx/MX80 powdered mixtures</b> ..... | 115 |
| 6.1 Introduction .....   | 116 |
| 6.2 Tested materials and infiltrated fluids used in the experiments .....  | 117 |
| 6.3 Experimental methods and program.....  | 119 |
| 6.3.1 Physicochemical properties .....   | 119 |
| 6.3.2 Swelling capacity of compacted powdered samples .....  | 120 |
| 6.3.2.1 Samples preparation.....   | 120 |
| 6.3.2.2 Swelling under constant vertical stress.....   | 121 |
| 6.3.2.3 Swelling under constant volume conditions.....   | 123 |
| 6.4 Experimental results .....   | 125 |
| 6.4.1 Physicochemical properties.....  | 125 |
| 6.4.2 Swelling potential .....   | 128 |
| 6.4.3 Swelling pressure.....   | 135 |
| 6.5 Discussion .....   | 139 |
| 6.5.1 Chemical of infiltrated solutions on swelling capacity.....  | 139 |
| 6.5.2 Effect of initial dry density on swelling capacity .....   | 140 |
| 6.5.3 Preliminary estimation of backfill's swelling capacity .....   | 142 |
| 6.6 Conclusions .....  | 146 |

|  |     |
|--|-----|
| <b>Chapter 7 - Hydro-mechanical study of CO<sub>x</sub>/MX80 pelletized materials</b> .....                | 149 |
| 7.1 Introduction .....   | 150 |
| 7.2 Tested materials and infiltrated fluids used in the experiments .....                                  | 150 |
| 7.3 Experimental method and set-up .....   | 153 |
| 7.3.1 Samples preparation .....  | 154 |
| 7.3.2 Constant volume cell .....   | 156 |
| 7.3.3 Saturated hydraulic conductivity .....   | 158 |
| 7.4 Experimental results .....   | 159 |
| 7.4.1 Swelling pressure.....   | 159 |
| 7.4.2 Hydraulic conductivity .....   | 162 |
| 7.5 Discussion .....   | 164 |
| 7.5.1 Effect of finer grains type on hydro-mechanical behaviour.....                                       | 164 |
| 7.5.2 Pellets/Sand mixture: equivalent dry density of pellets.....   | 170 |
| 7.5.3 Clayey mixtures: pelletized material versus compacted powders .....                                  | 169 |
| 7.6 Conclusions .....  | 174 |
| <br>   |     |
| <b>Chapter 8 - General conclusions and perspectives</b> .....  | 177 |
| 8.1 Conclusions .....  | 178 |
| 8.1.1 Pelletized GSD and resulting packing density .....   | 178 |
| 8.1.2 CO <sub>x</sub> /MX80 pellet fabrication.....  | 180 |
| 8.1.3 Hydro-mechanical response of compacted CO <sub>x</sub> /MX80 powdered and pelletized materials ..... | 181 |
| 8.2 Perspectives .....   | 182 |
| <br>   |     |
| References .....   | 185 |
| Appendix A: Tablet machine.....  | 197 |
| Appendix B: Examination of pellet production in semi-industrial scale.....                                 | 201 |
| Résumé de thèse.....   | 202 |

# List of Tables

|  |     |
|--|-----|
| Table 2-1 Summary of clay mineral characteristics (after Mitchell and Soga, 2005). .....   | 16  |
| Table 2-2 Ideal grain size distribution curves resulting in optimum packing (Ghasemi, 2017).<br>.....  | 49  |
| Table 3-1 Results of considered cases of spherical particles with diameters of 12.7 mm, 9.6 mm and 6 mm: experimental data reported by Standish and Borger (1979) compared with global and re-calculated porosities of present study. .... | 63  |
| Table 3-2 Geometrical parameters of the tested bimodal and trimodal samples. ....  | 65  |
| Table 3-3 Results of (a) global density and (b) re-calculated density for trimodal tested samples (the two highest values of density are highlighted with red and black bold letters)..  | 69  |
| Table 4-1 Details regarding the grain size distribution of COx and MX80 soil materials. ....   | 77  |
| Table 4-2 Physical and chemical characteristics of the studied materials. ....   | 78  |
| Table 4-3 Experimental program followed at uniaxial compression tests. ....  | 82  |
| Table 5-1 Details of studied pelletized materials. ....  | 103 |
| Table 5-2 Granulometric details of studied sandy materials. ....   | 104 |
| Table 5-3 Experimental program followed on density optimisation tests. ....  | 106 |
| Table 6-1 Receipt for the preparation of synthetic waters. ....  | 118 |
| Table 6-2 Ionic concentration of synthetic waters. ....  | 118 |
| Table 6-3 Properties of infiltrated fluids used in the experiments. ....   | 118 |
| Table 6-4 Details of the experimental program of the conducted swelling under constant vertical stress tests. ....   | 123 |
| Table 6-5 Details of the experimental program of the conducted swelling pressure tests. ...  | 125 |
| Table 6-6 Summary of final results for all swelling potential tests. ....  | 135 |
| Table 6-7 Summary of final results for all swelling pressure tests. ....   | 139 |
| Table 6-8 Curve fitting parameters calculated from the swelling potential tests. ....  | 143 |
| Table 7-1 Composition and physical parameters of the tested pelletized materials. ....   | 151 |
| Table 7-2 Water content and granulometric parameters of the tested finer grains. ....  | 152 |
| Table 7-3 Details of investigated pelletized mixtures. ....  | 153 |
| Table 7-4 Receipt for the preparation of synthetic waters. ....  | 153 |
| Table 7-5 Ionic concentration and properties of infiltrated site water. ....   | 153 |
| Table 7-6 Details of the pelletized samples tested on swelling under constant volume conditions. ....  | 156 |
| Table 7-7 Results of swelling pressure tests on pelletized samples hydrated under constant volume conditions. ....   | 162 |
| Table 7-8 Results of hydraulic conductivity tests on pelletized samples under constant volume conditions. ....   | 164 |

Table 8-1 Considered parameters of CO<sub>x</sub>/MX80 pellets and sand for future optimisation.

..... **Erreur ! Signet non défini.**

# List of Figures

|  |    |
|--|----|
| Figure 1-1 3D Geological diagram of the underground research laboratory location.....  | 2  |
| Figure 1-2 Illustration of (a) Cigeo underground facility and (b) basic engineering design stage on final phase (after Andra, 2016b). .....  | 3  |
| Figure 1-3 Illustration of (a) HLW cell and (b) ILW cell in Cigeo disposal facility.....   | 4  |
| Figure 1-4 Schematic diagram for closing structures (seals, backfill) on horizontal and vertical configurations of Cigeo disposal system. ....   | 5  |
| Figure 1-5 Illustration of (a) HLW cell and (b) ILW cell in Cigeo disposal facility on the closing phase (Andra, 2016).....  | 6  |
| Figure 2-1 Sheet structure (left) and presentation (right) of (a) tetrahedral and (b) octahedral units (after Mitchell and Soga, 2005). ....   | 14 |
| Figure 2-2 Schematic diagram of the organization of “TOT” clay mineral (after Jacinto et al., 2016).....   | 14 |
| Figure 2-3 Schematic presentation of two montmorillonite unit layers with interlayer cations and water molecules (Karnland et al., 2006). ....   | 16 |
| Figure 2-4 Inter-crystalline swelling on montmorillonite structure upon water adsorption (Kraehenbuehl et al., 1987). ....   | 17 |
| Figure 2-5 Schematic diagram of the unit layer arrangement upon double layer diffusion development (after Schanz and Tripathy, 2009). ....   | 18 |
| Figure 2-6 Experimental techniques for swelling pressure measurement (after Sridharan et al., 1986).....   | 19 |
| Figure 2-7 Micrographs of COx aggregates at (a) RH = 27% and (b) the enlarged domain outlined in red. (c) Hydrated aggregate at RH = 85% (Wang et al., 2013b). ....  | 20 |
| Figure 2-8 Evolution of swelling pressure at constant volume conditions on compacted COx argillite at initial dry density of 2 Mg/m <sup>3</sup> : (a) hydration with suction control and (b) direct hydration with distilled water (Tang et al., 2011a).....              | 21 |
| Figure 2-9 Evolution of swelling pressure of compacted COx argillite at adjusted constant volume conditions: different vertical stresses were applied before flooding under constant volume conditions (Tang et al., 2011a). ....  | 22 |
| Figure 2-10 Swelling pressure of compacted COx argillite as function of sample’s dry density (after Zeng et al., 2019). ....   | 22 |
| Figure 2-11 Pore size distribution of compacted MX80 bentonite ( $\rho_d = 1.8 \text{ Mg/m}^3$ ), COx/MX80 ( $\rho_d = 2.0 \text{ Mg/m}^3$ ) and sand/MX80 mixture ( $\rho_d = 1.8 \text{ Mg/m}^3$ ) (Manca et al., 2015; Seiphoori et al., 2014; Zeng et al., 2020). .... | 25 |
| Figure 2-12 Pore size distribution of Febex bentonite compacted at different dry densities (Lloret and Villar, 2007).....  | 26 |

|   |    |
|---|----|
| Figure 2-13 Micrographs of Febex bentonite compacted with hygroscopic water content at dry density of (a) 1.40 Mg/m <sup>3</sup> and (b) 1.65 Mg/m <sup>3</sup> (Lloret and Villar, 2007).....  | 26 |
| Figure 2-14 Evolution of pore size distribution of samples containing (a) MX80 bentonite (Seiphoori et al., 2014) and (b) Sand/MX80 mixture (Manca et al., 2015) during wetting at constant volume conditions. ....   | 27 |
| Figure 2-15 Pore size distribution of Febex bentonite samples at the as-compacted state ( $\rho d=1.40$ Mg/m <sup>3</sup> ) and after wetting at non-constant volume conditions (under constant vertical load) (Lloret and Villar, 2007). ....              | 28 |
| Figure 2-16 Bentonite/sand mixtures compacted at similar dry densities, in various fractions; results of (a) swelling potential (MX80/sand) and (b) swelling pressure (Kunigen-V1/sand) (after Muntohar, 2004 and Komine and Ogata 1999 respectively). .... | 29 |
| Figure 2-17 Final developed swelling pressure for sand/MX80 bentonite samples (80/20), prepared in different dry densities (Manca et al., 2015).....  | 30 |
| Figure 2-18 Final swelling potential for Febex bentonite samples prepared at different dry densities and hydrated under various vertical stresses (Hoffmann et al., 2005).....  | 30 |
| Figure 2-19 Swelling under constant vertical stress of MX80 bentonite, for (a) normally consolidated and (b) over-consolidated samples (Dang, 2007).....  | 31 |
| Figure 2-20 Swelling pressure obtained from swelling pressure tests and swelling under constant vertical stress tests (Villar and Lloret, 2008). ....   | 32 |
| Figure 2-21 Swelling pressure development over time for (a) MX80 bentonite compacted at 1.60 Mg/m <sup>3</sup> (Pusch, 1982) and (b) MX80/COx mixture (70/30) compacted at initial dry density of 1.70 Mg/m <sup>3</sup> (Wang et al., 2012). ....          | 33 |
| Figure 2-22 Swelling pressure of MX80 bentonite on suction controlled constant volume conditions $\rho d = 1.40$ Mg/m <sup>3</sup> : Evolution (a) upon time and (b) upon suction decrease (Yigzaw et al., 2016).....                                       | 34 |
| Figure 2-23 Final swelling strains of Febex bentonite, hydrated with different solutions under the different vertical stresses (Castellanos et al., 2008). ....   | 35 |
| Figure 2-24 GMZ01 bentonite saturated with solutions of different pH: results of (a) swelling pressure measurements and (b) X-ray diffraction profiles of compacted samples (Ye et al., 2014).....  | 36 |
| Figure 2-25 Effect of temperature on final swelling pressure of Febex bentonite compacted in different dry densities (Villar et al., 2010). ....  | 37 |
| Figure 2-26 Presentation of Backfilling Demonstrator experiment (“Remblayage de Richwiller”- 2004) (Londe et al., 2008). ....   | 38 |
| Figure 2-27 Construction of seal walls of bentonite/sand (40/60) bricks inside the drift for the NSC experiment (de la Vaissière et al., 2014). ....  | 39 |

|  |    |
|--|----|
| Figure 2-28 Design concept, construction and installation of pelletized swelling claycore seal during FSS experiment (Andra, 2016a).....   | 39 |
| Figure 2-29 Extruded pellets composed of IBECO bentonite (Johnsson and Sandén, 2013). 41   |    |
| Figure 2-30 FoCa clay pellets fabricated by roller compaction (Imbert and Villar, 2006). ....  | 42 |
| Figure 2-31 Pictures of bentonite pellets obtained (a) by compaction of MX80 bentonite and (b) by crushing highly compacted Febex bentonite (Dardé, 2019; Alonso et al., 2011).....                                | 42 |
| Figure 2-32 Pore size distribution of MX80 bentonite pellet at the initial state (Molinero-Guerra et al., 2019).....   | 43 |
| Figure 2-33 Pore size distribution of Febex bentonite pellet mixtures at different densities. Lowest density obtained by pluviation, higher densities by compaction (Hoffmann et al., 2007).....                   | 43 |
| Figure 2-34 Granular structure and macrovoids of bentonite in: (a) pellets mixture (Hoffmann et al., 2007) and (b) pellet/powder (80/20) mixture at initial non-hydrated state (Molinero Guerra et al., 2017)..... | 44 |
| Figure 2-35 Visualization of density evolution on FoCa clay pellet/powder (50/50) mixture at initial state, after two weeks of hydration and 6 weeks of hydration (Van Geet et al., 2005). 45                      |    |
| Figure 2-36 Evolution of the granular structure of a MX80 bentonite pellet/powder mixture during hydration (Molinero Guerra et al., 2018).....   | 45 |
| Figure 2-37 Saturated permeability of bentonite pellet mixtures prepared at different dry densities (Hoffmann et al., 2007). ....  | 46 |
| Figure 2-38 Evolution of swelling pressure of pelletized and non-pelletized material (FoCa bentonite) over time, for different dry densities (Imbert and Villar, 2006).....  | 47 |
| Figure 2-39 Evolution of porosity in relation to sphericity on mono-sized spherical and spherical particles: (a) at loose deposit and (b) after tapping (Zou and Yu, 1996). ....                                   | 48 |
| Figure 2-40 Packing of soil particles following idealized Fuller's curve (Head, 2006).....   | 49 |
| Figure 2-41 Effect of GSD on packing state on bimodal mixtures and (Yu et al., 1992). ....   | 50 |
| Figure 2-42 Effect of vibration time of specimens with different GSD on packing state (Liu et al., 2019).....  | 51 |
| Figure 3-1 Non-Smooth Contact Dynamics: (a) Approach of contact on a binary body system, (b) Signorini unilateral contact law and (c) Coulomb law of dry friction (after Jean, 1999).....                          | 57 |
| Figure 3-2 Schematic view of the numerical simulation: (a) sample generation and (b) sample deposit, for a given deposit height.....   | 58 |
| Figure 3-3 Snapshots during deposit of random granular mixture inside the cell using the LMGC <sup>90</sup> software: (a) the beginning of deposit, (b) during the deposit (c) at the final step of deposit. ....  | 59 |

|   |    |
|---|----|
| Figure 3-4 Determination of the final compaction state: (a) creation of fictional spherical boundary and (b) considered cases for solid volume calculation inside fictional boundary. . .   | 60 |
| Figure 3-5 Comparison of experimentally measured porosity (Standish and Borger, 1979) and numerical porosity obtained by global and re-calculated results (present study).....  | 62 |
| Figure 3-6 Achieved dry density of tested bimodal samples in relation to volumetric proportion of maximum sphere on each sample: (a) global results and (b) results after re-calculation. ....  | 66 |
| Figure 3-7 Effect of size ratio on the highest achieved dry density of bimodal tested samples: (a) global results and (b) results after re-calculation. ....  | 66 |
| Figure 3-8 Trimodal tested samples: global dry density in relation to volumetric proportion of (a) maximum, (b) medium and (c) minimum diameter and re-calculated dry density in relation to volumetric proportion of (d) maximum, (d) medium and (f) minimum diameter..... | 70 |
| Figure 3-9 Effect of size ratio of (a) medium diameter and (b) minimum diameter on the highest achieved density of trimodal tested samples.....   | 71 |
| Figure 3-10 Comparison of maximum obtained density for bimodal and trimodal samples with identical maximum and minimum diameters: (a) 12-7-4 mm 12-4 mm and (b) 12-4-3 mm and 12-3 mm. ....   | 71 |
| Figure 3-11 Influence of deposit height on the dry density of the chosen optimum GSD (16, 10 and 4 mm in 60, 10 and 30% respectively). ....   | 73 |
| Figure 3-12 Influence of friction coefficient on the achieved dry density for the chosen optimum GSD (16, 10 and 4 mm in 60, 10 and 30% respectively) deposited from 0 and 0.160 m: (a) global and (b) re-calculated results.....   | 73 |
| Figure 4-1 The grain size distribution and photographs of the studied materials at reception conditions. ....   | 77 |
| Figure 4-2 Water absorption test results on COx argillite and MX80 bentonite using demineralized water. ....  | 78 |
| Figure 4-3 Evolution of: (a) liquid limit and (b) plastic limit in relation to bentonite content for COx/MX80 mixtures. ....  | 79 |
| Figure 4-4 Plasticity chart for the different materials.....  | 80 |
| Figure 4-5 Free swelling index in relation to bentonite content for COx/MX80 mixtures. ....   | 80 |
| Figure 4-6 Schematic representation of the oedometric apparatus used for the uniaxial compression tests.....  | 82 |
| Figure 4-7 Results of uniaxial compression tests at COx and COx/MX80 at initial water content conditions as function of vertical pressure (in logarithmic scale): (a) void ratio and (b) dry density.....   | 83 |
| Figure 4-8 Variation of (a) compression and (b) swelling index for COx/MX80 mixtures, in relation to MX80 content.....  | 84 |

|  |    |
|--|----|
| Figure 4-9 Variation on radial stresses with the applied vertical stress during the loading and un-loading paths of compression tests on CO <sub>x</sub> /MX80 at their initial conditions.....  | 84 |
| Figure 4-10 Variation of coefficient of earth pressure at rest for CO <sub>x</sub> /MX80 mixtures, in relation to MX80 content.....  | 85 |
| Figure 4-11 Compacted CO <sub>x</sub> /MX80 mixture at reception conditions, at the end of uniaxial compression tests, containing (a) 10%MX80, (b) 20%MX80, (c) 30%MX80 and (d) 40%MX80. ....  | 85 |
| Figure 4-12 Evolution of void ratio with the applied vertical stress (in logarithmic scale) for different water content conditions of CO <sub>x</sub> /MX80 mixtures containing: (a) 10%, (b) 20%, (c) 30% and (d) 40% of MX80. ....   | 87 |
| Figure 4-13 Evolution radial stress with the applied vertical stress for different water content conditions of CO <sub>x</sub> /MX80 mixtures containing: (a) 10%, (b) 20%, (c) 30% and (d) 40% of MX80.....   | 88 |
| Figure 4-14 Variation of coefficient of earth pressure at rest for various CO <sub>x</sub> /MX80 mixtures, in relation to imposed water content. ....  | 88 |
| Figure 4-15 Evolution of void ratio with the applied vertical stress (in logarithmic scale) for different displacement rates (0.04-0.40-0.85 mm/min) of CO <sub>x</sub> /MX80 mixtures with water content of ~ 15%, containing: (a) 10%, (b) 20%, (c) 30% and (d) 40% of MX80..... | 89 |
| Figure 4-16 Maximum obtained dry density as function of the applied displacement rate for different CO <sub>x</sub> /MX80 mixtures. ....   | 90 |
| Figure 4-17 Target pellet shape.....   | 91 |
| Figure 4-18 (a) Frogerais 1B tablet press machine used on the present study, and detailed description of (b) the machine's metallic frame and (c) part of mould and punch tools.....   | 91 |
| Figure 4-19 Fabrication of accessories for target sizes (4 mm, 10 mm and 16 mm): moulds and punch tools.....   | 92 |
| Figure 4-20 Scratches observed in the first type of fabricated punch tools.....  | 94 |
| Figure 4-21 Rupture of punch tool's ending occurred after the fabrication of approximately 50 kg of pellets. ....  | 94 |
| Figure 4-22 Observed soil attachment to the punch tool with the initial curvature.....   | 95 |
| Figure 4-23 Schematic presentation of the adopted approach for realisation of pellet fabrication.....  | 95 |
| Figure 4-24 Effect of CO <sub>x</sub> argillite's initial state on pellet production: (a) percentage of particles finer than 200 μm, (b) water content. ....   | 96 |
| Figure 4-25 Effect of initial CO <sub>x</sub> /MX80 mixture's water content on pellet production using the modified CO <sub>x</sub> granulometry.....  | 97 |
| Figure 4-26 Effect of CO <sub>x</sub> /MX80 mixture's composition on pellet production using the modified CO <sub>x</sub> granulometry.\ .....   | 98 |

|  |     |
|--|-----|
| Figure 4-27 Schematic presentation of the adopted approach for optimisation of pellet production.....  | 98  |
| Figure 4-28 Fabricated pellets with diameter of 16 mm and 10 mm (CO <sub>x</sub> /MX80 mixture) and 4 mm (pure MX80).....  | 99  |
| Figure 5-1 Granulometry and pictures of materials used for the experimental study of density maximisation. ....  | 103 |
| Figure 5-2 Transparent cells used for the density measurement of the pelletized mixture: (a) cubic and (b) cylindrical container. ....   | 104 |
| Figure 5-3 Experimental results of the resulting dry density for the optimum GSD defined by DEM (16mm-10mm-4mm in 60%-10%-30%) prepared by blending and layering methods. ....   | 107 |
| Figure 5-4 Presentation of the pelletized DEM granulometry deposited inside the cubic cell by (a) blending and (b) layering method. ....   | 107 |
| Figure 5-5 Comparison between numerical (a) global and (b) re-calculated density with experimental density obtained by two methods. ....   | 108 |
| Figure 5-6 Photograph of experimental pellet pile formed by the optimum DEM GSD. ....  | 109 |
| Figure 5-7 Experimental dry density of different mixture types for density optimisation. ...   | 111 |
| Figure 5-8 Effect of finer grains proportion on the resulting dry density. ....  | 113 |
| Figure 5-9 Pictures of the two mixtures reported the highest resulting dry density deposited on cylindrical cell: (a) 16 mm, 4 mm and well-graded sand (60%, 10% and 30%) and (b) 16 mm, 10mm and well-graded sand (60%, 10% and 30%). ....  | 114 |
| Figure 6-1 Grain size distribution and presentation of the materials used on the hydro-mechanical study of powdered mixtures. ....   | 117 |
| Figure 6-2 Specimens compaction steps. ....  | 120 |
| Figure 6-3 Experimental system used on swelling under constant vertical stress tests.....  | 122 |
| Figure 6-4 Experimental system used on swelling under constant volume tests. ....  | 124 |
| Figure 6-5 Effect of infiltrated solution on (a) liquid limit and (b) plastic limit in relation to bentonite content for CO <sub>x</sub> /MX80 mixtures.....   | 126 |
| Figure 6-6 Results of Free Swelling capacity index.....  | 126 |
| Figure 6-7 Results of standard Proctor tests on CO <sub>x</sub> /MX80 mixtures prepared with site and cementitious water.....  | 127 |
| Figure 6-8 Evolution of (a) optimum dry density and (b) optimum water content, with MX80 bentonite content on CO <sub>x</sub> /MX80 wetted with site and cementitious water. ....  | 128 |
| Figure 6-9 Results of swelling potential tests under different vertical stresses on CO <sub>x</sub> /MX80 mixture containing 10%MX80: (a) $\rho d = 1.60 \text{ Mg/m}^3$ hydrated with site water, (b) $\rho d = 1.45 \text{ Mg/m}^3$ hydrated with site water, (c) $\rho d = 1.60 \text{ Mg/m}^3$ hydrated with cementitious water, (d) $\rho d = 1.45 \text{ Mg/m}^3$ hydrated with cementitious water. .... | 129 |

|   |     |
|---|-----|
| Figure 6-10 Results of swelling potential tests under different vertical stresses on CO <sub>x</sub> /MX80 mixture containing 20%MX80: (a) $\rho d = 1.60 \text{ Mg/m}^3$ hydrated with site water, (b) $\rho d = 1.45 \text{ Mg/m}^3$ hydrated with site water, (c) $\rho d = 1.60 \text{ Mg/m}^3$ hydrated with cementitious water, (d) $\rho d = 1.45 \text{ Mg/m}^3$ hydrated with cementitious water. .... | 130 |
| Figure 6-11 Results of swelling potential tests under different vertical stresses on CO <sub>x</sub> /MX80 mixture containing 30%MX80: (a) $\rho d = 1.60 \text{ Mg/m}^3$ hydrated with site water, (b) $\rho d = 1.45 \text{ Mg/m}^3$ hydrated with site water, (c) $\rho d = 1.60 \text{ Mg/m}^3$ hydrated with cementitious water, (d) $\rho d = 1.45 \text{ Mg/m}^3$ hydrated with cementitious water. .... | 131 |
| Figure 6-12 Results of swelling potential tests under different vertical stresses on CO <sub>x</sub> /MX80 mixture containing 40%MX80: (a) $\rho d = 1.60 \text{ Mg/m}^3$ hydrated with site water, (b) $\rho d = 1.45 \text{ Mg/m}^3$ hydrated with site water, (c) $\rho d = 1.60 \text{ Mg/m}^3$ hydrated with cementitious water, (d) $\rho d = 1.45 \text{ Mg/m}^3$ hydrated with cementitious water. .... | 132 |
| Figure 6-13 Evolution of CO <sub>x</sub> /MX80 mixtures obtained swelling potential with bentonite content for different initial dry densities and infiltrated fluid: (a) under 6 kPa and (b) under 100 kPa. ....   | 133 |
| Figure 6-14 Results of swelling potential tests under $\sigma_v = 6 \text{ kPa}$ using site water, on samples with initial dry density of $\rho d = 1.60 \text{ Mg/m}^3$ prepared with the modified CO <sub>x</sub> granulometry: (a) CO <sub>x</sub> /MX80 mixtures and (b) CO <sub>x</sub> /MX80/sand mixtures. ....  | 134 |
| Figure 6-15 Evolution of swelling potential obtained for CO <sub>x</sub> /MX80 mixtures of original granulometry, CO <sub>x</sub> /MX80 mixtures with modified granulometry and CO <sub>x</sub> /MX80/sand mixtures, under $\sigma_v = 6 \text{ kPa}$ using site water ( $\rho d = 1.60 \text{ Mg/m}^3$ ). ....   | 134 |
| Figure 6-16 Evolution of swelling pressure with time for samples compacted at initial dry density of $\rho d = 1.45 \text{ Mg/m}^3$ and $\rho d = 1.60 \text{ Mg/m}^3$ : CO <sub>x</sub> /MX80 mixtures containing (a) 10%, (b) 20%, (c) 30% and (d) 40% of MX80. ....  | 136 |
| Figure 6-17 Influence of MX80 bentonite content on final swelling pressure of CO <sub>x</sub> /MX80 mixtures compacted at different initial dry densities. ....   | 137 |
| Figure 6-18 Evolution of swelling pressure with time for samples compacted at initial dry density of $\rho d = 1.60 \text{ Mg/m}^3$ with water content of reception and optimum water content: CO <sub>x</sub> /MX80 mixtures containing (a) 10%, (b) 20%, (c) 30% and (d) 40% of MX80. ....  | 138 |
| Figure 6-19 Influence of MX80 bentonite content on final swelling pressure of CO <sub>x</sub> /MX80 mixtures compacted at initial dry density $\rho d = 1.60 \text{ Mg/m}^3$ at water content of reception and optimum water content conditions. ....   | 138 |
| Figure 6-20 Evolution of swelling potential with initial dry density for various CO <sub>x</sub> /MX80 mixtures: applied vertical stress of (a) $\sigma_v = 6 \text{ kPa}$ , (b) $\sigma_v = 52 \text{ kPa}$ and (c) $\sigma_v = 100 \text{ kPa}$ (hydration with SW). ....   | 141 |

|  |     |
|--|-----|
| Figure 6-21 Evolution of swelling pressure with initial dry density for various CO <sub>x</sub> /MX80 mixtures (hydration with SW).....  | 141 |
| Figure 6-22 Influence of the applied vertical stress on the developed swelling potential of CO <sub>x</sub> /MX80 mixtures hydrated with site water: initial dry density of (a) 1.45 Mg/m <sup>3</sup> and (b) 1.60 Mg/m <sup>3</sup> .....  | 142 |
| Figure 6-23 Variation of the applied vertical stress as function of the gallery's height, due to backfill's saturated unit weight. ....  | 144 |
| Figure 6-24 Calculated swelling potential mixtures as function of the gallery's height and the corresponding vertical stress for backfill composed of various CO <sub>x</sub> /MX80 mixtures emplaced at initial dry density of (a) 1.45 Mg/m <sup>3</sup> and (b) 1.60 Mg/m <sup>3</sup> . .... | 144 |
| Figure 6-25 Calculated displacement as function of the gallery's height and the corresponding vertical stress for backfill composed of various CO <sub>x</sub> /MX80 mixtures emplaced at initial dry density of (a) 1.45 Mg/m <sup>3</sup> and (b) 1.60 Mg/m <sup>3</sup> .....                 | 145 |
| Figure 6-26 Overall calculated displacement on gallery's vertical diameter of the studied CO <sub>x</sub> /MX80 backfill mixtures as function of MX80 content, for the investigated dry densities. ....  | 145 |
| Figure 7-1 Grain size distribution and presentation of the materials used on the hydro-mechanical study of pelletized materials.....   | 151 |
| Figure 7-2 CEA cell of 120 mm in internal diameter used for the swelling pressure measurements of the pelletized materials.....  | 154 |
| Figure 7-3 Preparation steps followed for the pelletized specimens. ....   | 154 |
| Figure 7-4 Photographs of the studied pelletized samples during preparation (left) and at the final preparation step (right): (a) Mixture 1 (70P-30WGS), (b) Mixture 2 (70P-30CP) and (c) Mixture 3 (70P-15CP-15WGS).....  | 157 |
| Figure 7-5 Experimental set-up used on swelling under constant volume tests on pelletized material.....  | 158 |
| Figure 7-6 Evolution of swelling pressure over time for Mixture 1 (16 mm, 10 mm and sand) prepared at initial dry density of $\rho_d = 1.60 \text{ Mg/m}^3$ and $\rho_d = 1.70 \text{ Mg/m}^3$ : (a) during the first 24 h of hydration and (b) until the end of the test. ....                  | 160 |
| Figure 7-7 Evolution of swelling pressure over time for Mixture 2 (16 mm, 10 mm and crushed pellets) prepared at initial dry density of $\rho_d = 1.64 \text{ Mg/m}^3$ .....   | 161 |
| Figure 7-8 Evolution of swelling pressure over time for Mixture 3 (16 mm, 10 mm and sand/crushed pellets) prepared at initial dry density of $\rho_d = 1.61 \text{ Mg/m}^3$ . ....   | 161 |
| Figure 7-9 Evolution of swelling pressure for all investigated pelletized mixtures, focusing on the materials composition.....   | 162 |
| Figure 7-10 Evolution of injected water volume over time for Mixture 1 (16 mm, 10 mm and sand) prepared at initial dry density of $\rho_d = 1.71 \text{ Mg/m}^3$ . ....  | 163 |

|  |     |
|--|-----|
| Figure 7-11 Evolution of injected water volume over time for Mixture 2 (16 mm, 10 mm and crushed pellets) prepared at initial dry density of $\rho_d = 1.64 \text{ Mg/m}^3$ : (a) during 24 h of injection and (b) until the end of the test. .... | 163 |
| Figure 7-12 Evolution of injected water volume over time for Mixture 3 (16 mm, 10 mm and sand/crushed pellets) prepared at initial dry density of $\rho_d = 1.61 \text{ Mg/m}^3$ . ....  | 164 |
| Figure 7-13 Variation of final swelling pressure with sand and clayey percentage contained in the pelletized mixture (mixture's initial dry density $\rho_d \approx 1.60 \text{ Mg/m}^3$ ). ....   | 165 |
| Figure 7-14 Specimens of Mixture 1 (16 mm, 10 mm and sand) prepared at initial dry density of $\rho_d = 1.60 \text{ Mg/m}^3$ (70P-30WGS-b) at the end of swelling pressure test (D=120 mm/H=50 mm). ....   | 166 |
| Figure 7-15 Specimens of Mixture 3 (16 mm, 10 mm, crushed pellets and sand) prepared at initial dry density of $\rho_d = 1.60 \text{ Mg/m}^3$ (70P-15CP-15WGS) at the end of swelling pressure and permeability test (D=120 mm/H=50 mm).. ....     | 167 |
| Figure 7-16 Specimens of Mixture 2 (16 mm, 10 mm, crushed pellets) prepared at initial dry density of $\rho_d = 1.60 \text{ Mg/m}^3$ (70P-30CP) at the end of swelling pressure and permeability test (D=120 mm/H=50 mm).....                      | 168 |
| Figure 7-17 Variation of saturated hydraulic conductivity with sand and clayey percentage contained in the pelletized mixture.....   | 169 |
| Figure 7-18 Swelling pressure and hydraulic conductivity developed by the investigated pelletized mixtures in relation to the sand content. ....   | 169 |
| Figure 7-19 Final swelling pressure for COx/MX80 powdered mixtures and pelletized sample composed of 30%MX80 (pellets and crushed pellets). ....   | 170 |
| Figure 7-20 Equivalent state of pellet dry density for pelletized mixtures containing sand as finer gains. ....  | 171 |
| Figure 7-21 Variation of void ratio as function of vertical pressure (in logarithmic scale) for sand and COx argillite. ....   | 172 |
| Figure 7-22 Swelling pressure developed by pelletized mixtures and powdered mixtures compacted at the equivalent pellet dry density.....   | 173 |
| Figure 7-23 Local heterogeneity of sand's distribution upon the materials emplacement....  | 174 |



# List of Notations

CP : Crushed pellets  
DEM : Discrete Element Method  
GSD : Grain Size Distribution  
HLW : High Level Waste  
ILW/ILW-LL : Intermediate-Level Long-lived Waste  
LVDT : Linear Variable Differential Transformer  
MIP : Mercury Intrusion Porosimetry  
NSCD : Non-Smooth-Contact Dynamics  
OCR : Over-consolidation ratio  
PGS : Poorly-graded sand  
PSD : Pore size distribution  
RH : Relative Humidity (%)  
SD : Standard Deviation (%)  
SEM : Scanning Electron Microscope  
SSA : Specific surface area  
WGS : Well-graded sand



# List of Symbols

- $\%d_i$  : Volumetric proportion of diameter of class  $i$   
 $\%d_{iN}$  : Proportion in number of diameter of class  $i$   
 $\Delta h$  : Hydraulic charge  
 $C_C$ : Compression index  
 $CC$  : Curvature coefficient  
 $C_S$ : Swelling index  
 $CU$  : Uniformity coefficient  
 $D$  : Specimen's diameter  
 $d_i$  : Diameter of particles of class  $i$   
 $d_{max}$  : Maximum diameter  
 $d_{med}$  : Medium diameter  
 $d_{min}$  : Minimum diameter  
 $e$  : Void ratio  
EPDD : Equivalent dry density of pellets  
 $g$  : Distance between pair of bodies  
 $h$  : Deposit height  
 $H_0$  : Specimen's initial height (before hydration)  
 $h_0$  : Initial (zero) height for specimen's preparation  
 $h_1$  : Specimen's height before compaction  
 $H_i$  : Specimen's height at each measurement of swelling potential tests  
 $H_{target}$  : Target specimen's height  
 $K_0$  : Coefficient of earth pressure at rest  
 $l_x, l_y, l_z$ : Cell dimensions in  $x, y, z$  direction  
 $M_{d\text{ pellets}}$  : Dry mass of pelletized material  
 $M_S$  : Mass of solid  
 $M_{sample}$  : Total mass of sample  
 $n$  : Porosity  
 $N_i$  : Number of spheres in class  $i$   
 $N_T$  : Total number of spheres  
 $Q$  : Average flow rate  
 $q$  : Grading parameter  
 $R_{COx}$  : argillite fraction inside mixture  
 $R_{MX80}$  : Bentonite fraction inside mixture  
 $R_N$  : Normal reaction force

$R_T$  : Tangential reaction force  
 $V_S$  : Total solid volume  
 $V_{\text{sand}}$  : Volume of sand  
 $V_T$  : Final volume of sample  
 $V_{S_i}$  : Total solid volume of all spheres of class i  
 $V_{S_{O_i}}$  : Solid volume of each sphere of class i  
 $w$  : Water content  
 $\alpha_i$  : Size ratio of diameter of class i  
 $A_{\text{sample}}$  : Specimen's cross-section  
 $\delta_{\text{req}}$  : Vertical displacement of piston  
 $\varepsilon_S$  : Swelling strain  
 $\mu$  : Friction coefficient  
 $\rho_{\text{sand}}$  : Apparent density of sand (dry)  
 $\rho_d^{\text{sphere}}$  : Sphere's dry density  
 $\rho_d^{\text{pellet}}$  : Intra-pellet dry density  
 $\rho_d$  : Dry density  
 $\rho_s^{\text{COx}}$  : argillite's solid particle density  
 $\rho_s^{\text{mix}}$  : Mixture's particle density  
 $\rho_s^{\text{MX80}}$  : Bentonite's solid particle density  
 $\varphi$  : Inter-particle friction angle





---

# Chapter 1 - Introduction

The issue of radioactive waste management has been raised since the advent of nuclear generated electricity. Thereafter, the deep geological isolation of waste has been considered as a reference solution (Andra 2013). Many countries around the world, such as France, Belgium, Germany, Sweden, Japan and Switzerland, examine clay or crystalline formations as potential host rocks for the waste storage, due to their beneficial characteristics (e.g. homogeneity, extremely low hydraulic conductivity, self-sealing potential and capacity for retardation of radionuclides) (Andra 2005, Gens 2019). Different design concepts have been worldwide proposed, all presenting a common basis: a multi-barrier system comprising an engineering barrier surrounded by the natural host rock. Waste treated according to their type, are isolated by using buffer, sealing and backfill materials to ensure their confinement (IAEA 2009). The following chapter focuses on the French geological disposal concept (Cigeo) and particularly on one of the backfill options which is currently considered. The objective of the present doctoral study and the adopted strategy are further addresses. The chapter is developed in the following main parts:

- 1.1 General context of deep geological disposal - Project Cigeo
- 1.2 Pelletized CO<sub>x</sub>/MX80 mixture as backfill
- 1.3 Objective and outline of the thesis

## 1.1 General context of deep geological disposal - Project Cigeo

In France, the national radioactive waste management agency (Andra) is in charge of the Industrial Centre for Geological Disposal “Cigéo” (Centre industriel de stockage géologique), designed to host the French High-Level Waste (HLW) and Intermediate-Level Long-lived Waste (ILW/ILW-LL), at approximately 500 m depth. It will be constructed at the mid-level of Callovo-Oxfordian (COx) claystone formation (thickness of ~140 m), located in the fringe of the Meuse and Haute-Marne departments, at the eastern boundary of Paris basin (Figure 1-1). The facility consists of two waste zones (HLW, ILW), developed in a complex network of drifts, shafts and ramps as part of the emplacement process (Figure 1-2). Similarly with other concepts, the operation safety relies initially on the waste disposal packages, the COx host-rock as natural barrier, as well as the closing structures as passive post-closure safety function system (Andra 2019).

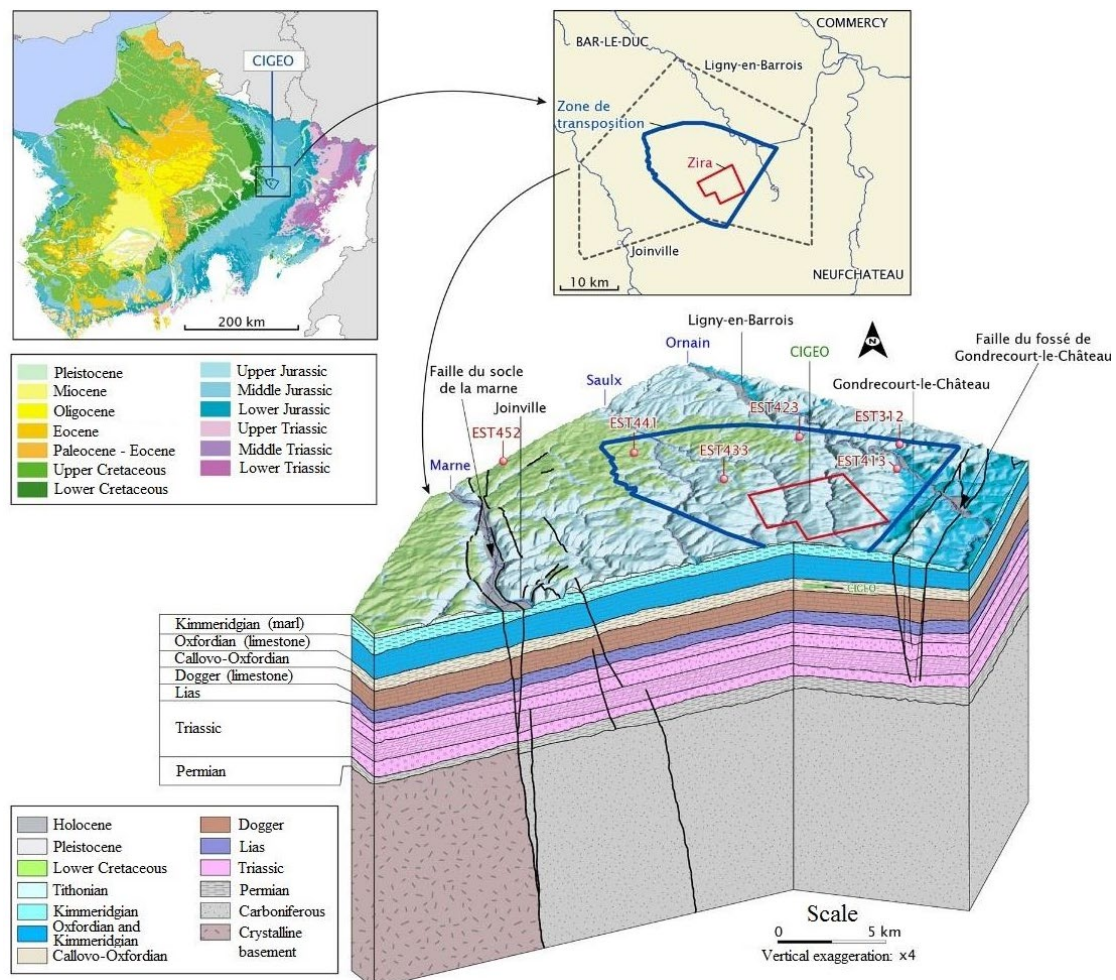
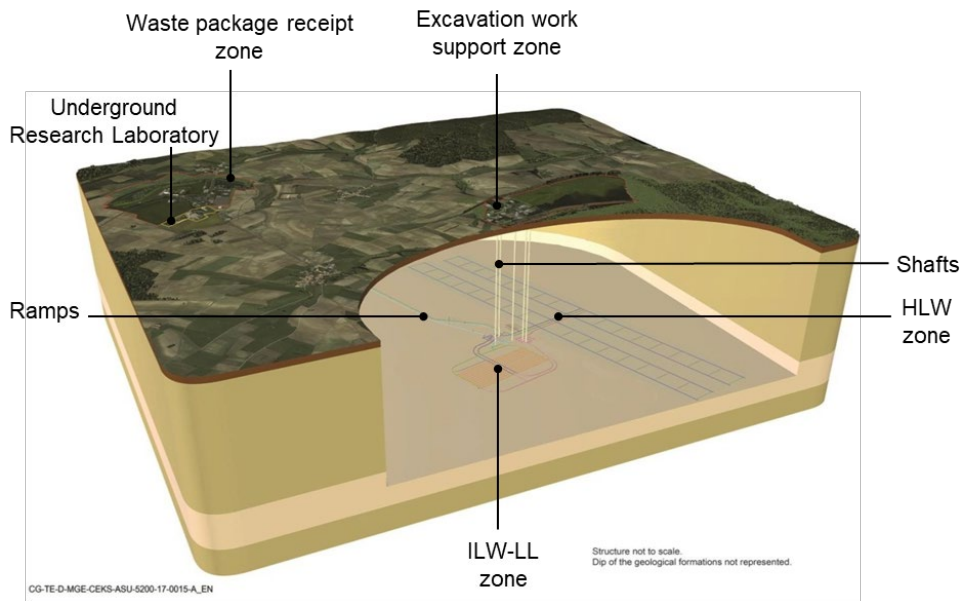
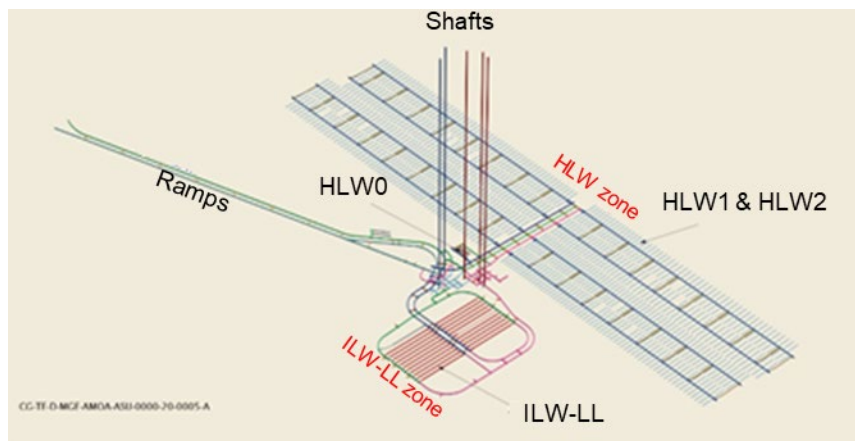


Figure 1-1 3D Geological diagram of the underground research laboratory location.



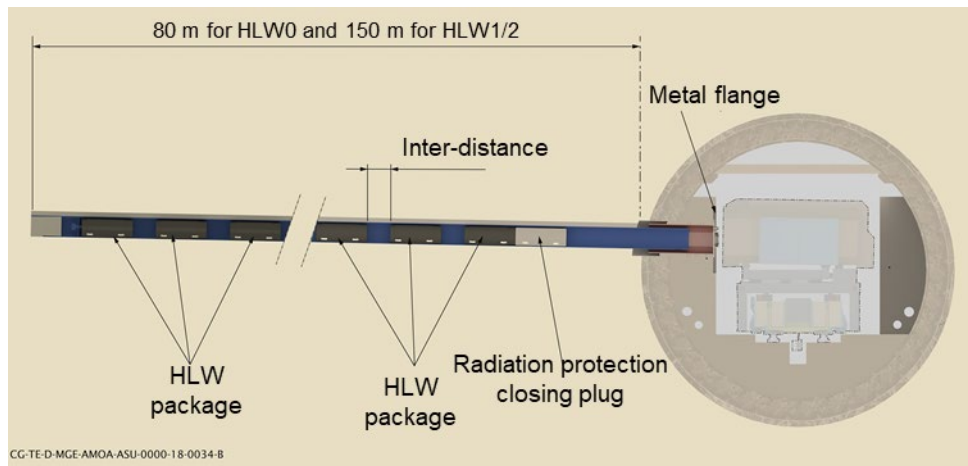
(a)



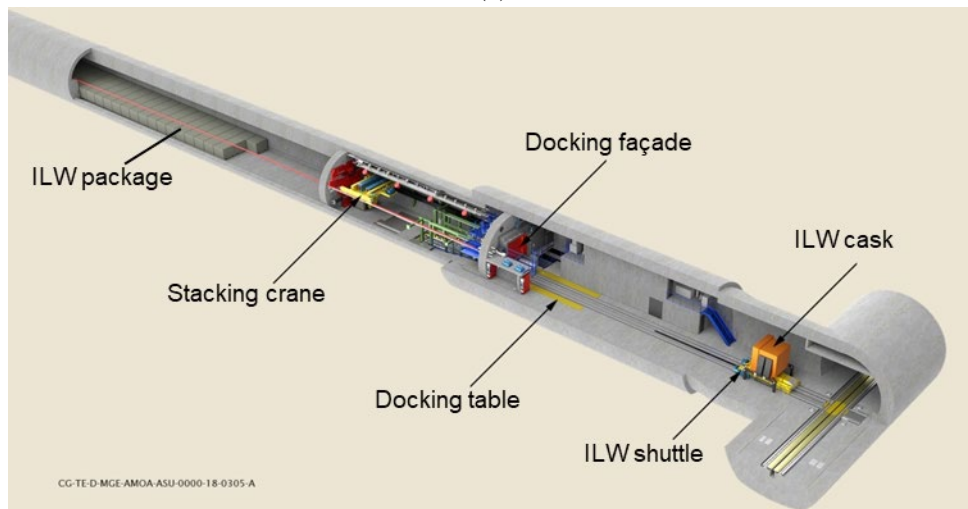
(b)

Figure 1-2 Illustration of (a) Cigeo underground facility and (b) basic engineering design stage on final phase (after Andra, 2016b).

HLW and ILW will be primarily placed into containers designed by materials capable to limit the radionuclide release. The waste containers are placed inside cells, located at horizontal underground elements. HLW are incorporated into a glass matrix and then poured into stainless steel packages, which are installed inside long micro-tunnels (Figure 1-3a). On the other hand, ILW are implemented in metal or concrete packages, stored in larger tunnels (Figure 1-3b). In both cases, the waste cells are served by access drifts.



(a)



(b)

Figure 1-3 Illustration of (a) HLW cell and (b) ILW cell in Cigeo disposal facility (concept in the beginning of the PhD study).

Cigéo's safety system relies principally on COx claystone as a natural barrier, but includes also structures as passive post-closure safety systems. When the disposal centre closes, the galleries will be backfilled and seals will be installed at specific locations to limit the water flow into the repository, contain the radioactivity and isolate the waste from humans/biosphere, by controlling aqueous and gaseous pathways. In particular, during the excavation phase, the so-called excavation damaged zone (EDZ) is produced around the drifts, generating pathways and therefore potential transport of nuclides (Armand et al. 2013). Additionally, groundwater coming from the host rock will gradually infiltrate the repository and saturate all the materials. In these conditions, closing structures are indicated and more precisely, the installation of seals and backfill material is planned. Clays (pure or with additives) and in particular swelling/expansive clays are widely used for this purposes, due to well-established characteristics developed upon water circulation: their swelling due to hydration results in filling of voids and reduction of permeability, creating therefore an

appropriate environment for the waste isolation (Komine and Ogata, 2003; Lloret et al., 2003; Imbert and Villar, 2006; Villar and Lloret, 2008; Baille et al., 2010). Each closure structure contributes uniquely on the safety system. According to design requirements (Andra, 2016a):

- (a) **Seals**, located in specific positions of the structure (ramps, shafts, drifts), behave as hydraulic barrier that opposes to water circulation inside the structure.
- (b) **Backfill** is emplaced in the remaining openings in order to limit the propagation of the EDZ around the drifts and further contribute to the sealing maintenance.

Figure 1-4 shows the installed seals and backfill in horizontal and vertical elements of the disposal system. Figure 1-5 presents more accurately the HLW and ILW cells at the end of the closing phase of Cigeo facility.

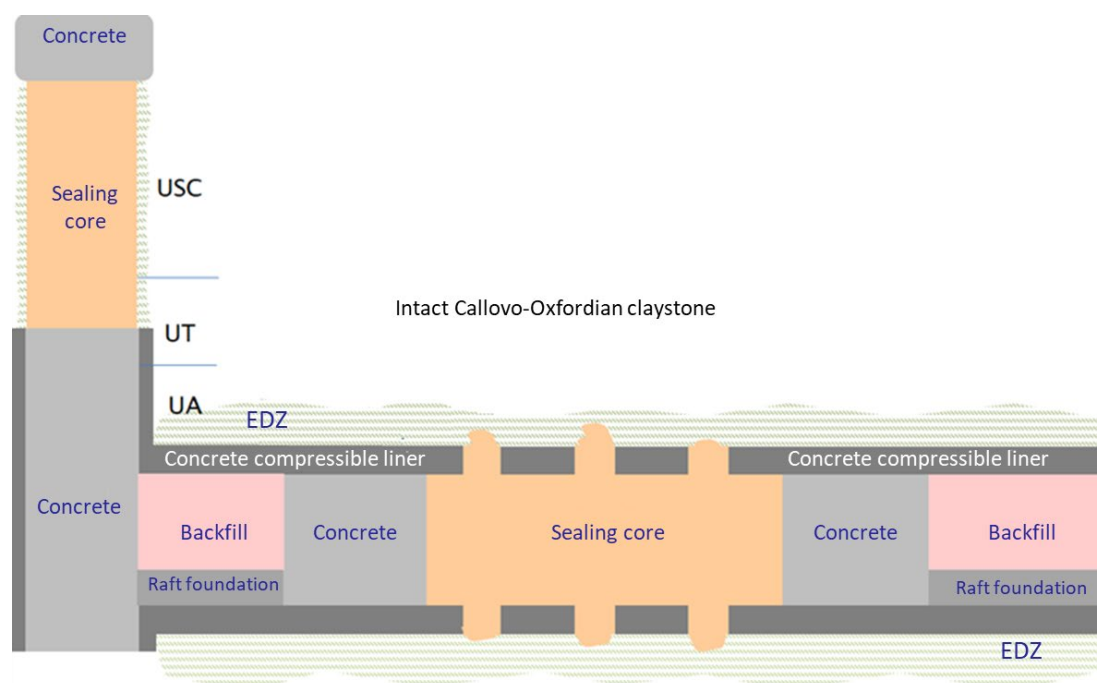
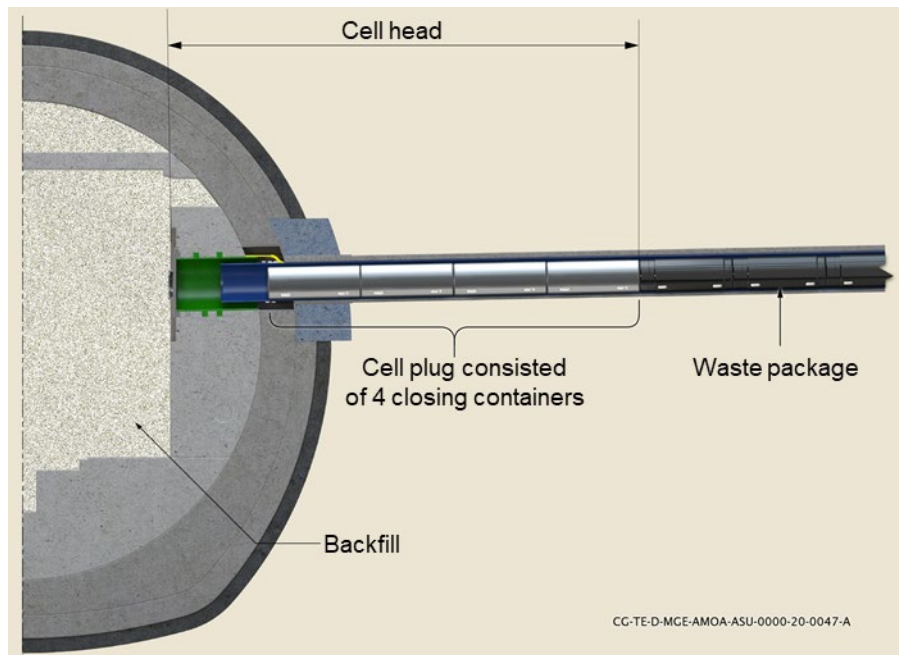


Figure 1-4 Schematic diagram for closing structures (seals, backfill) on horizontal and vertical configurations of Cigeo disposal system.

On the Cigeo project, seals are planned to be completely or partially composed of swelling clay materials (i.e. bentonite). On the other hand, the large quantity of the backfill necessary to fill the remaining openings and the chemical compatibility with the surrounding rock, proposes the re-use of the COx claystone that has been produced from the excavation, preferably mixed with a percentage of additive such as swelling clay. Andra is conducting a multi-criteria analysis taking into account the hydro-mechanical behaviour as well as the techno-economical aspect of different addition, treatment and setup process.



(a)



(b)

Figure 1-5 Illustration of (a) HLW cell and (b) ILW cell in Cigeo disposal facility on the closing phase (concept in the beginning of the PhD study).

Sealing and backfill materials will be placed at almost dry conditions and need to present an adequately dense state. Nonetheless, inevitable voids always exist inside the material and between the material and the gallery. At emplacement conditions, sealing and backfill absorb groundwater, swell and fill these technological voids. In the beginning, material's volume increases freely, filling the voids and as the available space is covered, swelling occurs under constant volume conditions. In parallel, degradation of concrete of the engineering barrier (liners along with drifts and ILW cells) produces alteration of groundwater's composition. Therefore, the alkaline perturbation on the installed materials consists another important aspect for investigation (Andra 2016a). At a longer time, when lining degradation and break-out will occur, the backfill's mechanical characteristics need to limit the concrete blocks movement.

In order to ensure the overall safety of the storage system, it is of high importance to develop a good understanding of the sealing/backfill materials involved throughout the repository life,

---

from a few hundred years to several thousand years as well as its long-term isolation performance.

## **1.2 Pelletized CO<sub>x</sub>/MX80 mixture as backfill**

It was already mentioned, that the role of backfill is to prevent possible propagation of the EDZ, in particular after linings rupture. In this concept, the backfill needs to present dry density as high as possible and adequate swelling behaviour to fill the technological voids.

The backfill's installation will be conducted in situ, using available technological means. In this context, different backfill solutions are studied alone or combined: pellets (i.e. highly compacted granules), pre-fabricated blocks, in-situ compaction. Since the early 2000s, pure bentonite pellets have been investigated for sealing purposes in the framework of radioactive waste disposal (Pasquiou, 2001; Pusch et al., 2003; Hoffmann et al., 2004). Many radioactive waste management agencies, including Andra in France, SKB in Sweden and Nagra in Switzerland, considered pelletized bentonite material in varied shapes due to their operation advantages (SKB 2011, Gatabin et al. 2014, Müller et al. 2017). Several experimental studies have focused on the analysis of bentonite granular pelletized mixtures (Van Geet et al., 2005; Imbert and Villar, 2006; Hoffmann et al., 2007; Molinero Guerra et al., 2019; Darde et al., 2020). Upon emplacement, the pelletized mixture is installed at almost dry conditions and behaves as a granular assembly. Even though the resulting porosity should be minimized as possible, inevitable voids will always exist. As long as hydration from the surrounding rock occurs, the pelletized mixture absorbs water and swells, filling up initial voids and leading to its gradual homogenization.

Currently, Andra examines the pelletized solution of a mixture containing excavated crushed CO<sub>x</sub> argillite, enriched with MX80 bentonite additive. The decision of reusing CO<sub>x</sub> takes into account the chemical compatibility between the host rock and the engineering barrier, the positive environmental impact of reusing the excavated host rock, as well as a more economical aspect for the design (Tang et al. 2011b). It was seen that remoulded CO<sub>x</sub> claystone compacted at high densities exhibits swelling characteristics, since it contains some swelling clay fraction (e.g. smectites) (Tang et al. 2011a, Tu 2011). However, bentonite addition as well-established swelling material is necessary to improve the hydro-mechanical response.

## **1.3 Objective and outline of the thesis**

Motivation for the present thesis is a first examination of the feasibility to implement a pelletized material constituted by CO<sub>x</sub> and bentonite additive, as well as the hydro-

---

mechanical response of the mixture at emplacement conditions. More precisely, the study includes the design, the fabrication and the analysis of the used granular mixture. In this context, the material had to initially be pelletized following semi-industrial criteria, by using COx argillite for the very first time. To our knowledge, no study has been carried out on the hydro-mechanical behaviour of COx/bentonite pellets.

More precisely, the objectives of this PhD highlight the following main aspects:

1. The determination of the selected pelletized mixture in terms of grain size distribution (GSD), which is carried out with the criterion of decreasing as possible the initial voids (i.e. maximising initial dry density) upon material installation. This state reflects the optimum conditions of implementation and therefore, the chosen GSD is referred hereafter as the optimum granulometry/GSD. In this concept, the investigated parameters are the GSD of the pelletized material and the achieved density state expressed in terms of dry density or porosity.
2. The COx/MX80 pellet fabrication. Pellets containing both argillite and bentonite are fabricated in the selected granulometry. Pellet production is examined in terms of intra-pellet density and pellet intactness.
3. The preliminary experimental characterisation of the hydro-mechanical response of various COx/MX80 pellets, by studying compacted powdered COx/MX80 mixtures. Therefore, swelling capacity at free and confiner volume conditions (i.e. swelling potential and swelling pressure) is studied.
4. The direct hydro-mechanical evaluation of the chosen pelletized assemblies. Pelletized mixtures with configurations proposed according to the GSD optimisation are studied. The swelling pressure and hydraulic conductivity are evaluated.

In order to address the different points, the research work has been divided in seven chapters.

*Chapter 2* presents the state of the art regarding the hydro-mechanical behaviour of remoulded swelling materials, beginning with the swelling response developed by crushed excavated COx argillite and extending to bentonite-based materials. The multi-scale mechanisms activated from interaction with water are addressed. The special features of pellets are examined, including their structure evolution from granular state until homogenisation. At the end, the strategy adopted to meet the study's objective is addressed.

*Chapter 3* aims to optimise the pellets assembly in terms of GSD, in order the emplacement of the granular material to result in densest packing as possible. A numerical approach based on the discrete element method is conducted, to select the used granulometry. Gravitational

---

deposits are performed to study the effect of grain sizes and the implementation protocol on the resulting packing density of bimodal and trimodal mixtures.

*Chapter 4*, following the results of Chapter 3, carries out the pellet fabrication on the optimum sizes. Before pelletization, the CO<sub>x</sub>/MX80 raw mixtures are initially studied upon uniaxial compression. The machine responsible for the pellet manufacturing and the necessary accessories are reconditioned and pellet production is studied in details.

In *Chapter 5*, the resulting packing density is evaluated experimentally for the optimum GSD defined by DEM. Gravitational deposits are conducted in similar conditions to numerical simulations. Additional finer materials are studied, focusing on the resulting density maximisation, while the density range of interest is assessed.

*Chapter 6* addresses a parametric study on the hydro-mechanical response of various CO<sub>x</sub>/MX80 powdered mixtures, primarily assessing the implement MX80 bentonite content. A series of experiments focuses on the physicochemical characterisation of the different mixtures, as well as on the swelling capacity under free and constant volume conditions. In the latter case, the swelling response of the pelletized material is studied through CO<sub>x</sub>/MX80 powdered material, compacted at densities belonging to the range of interest for this study.

*Chapter 7* examines the hydro-mechanical behaviour of the pelletized material at emplacement conditions. Several pelletized mixtures are tested, according to the optimum retained granulometry, which is finally containing also finer grains. Swelling pressure and saturated hydraulic conductivity are evaluated upon emplacement conditions, where no mechanical compaction is applied. The effect of finer grains types in the hydro-mechanical behaviour is discussed.

Finally, *Chapter 8* presents the outcomes and the main achievements of this study. Suggestions for future work are also provided.



---

## Chapter 2 - State of the art

The reused of COx argillite has been proposed as potential backfill solution for the French disposal facilities, due to some swelling capacity. Amongst others, the pelletized material is examined. In this chapter, a bibliographical review is conducted, in order to identify the essential parameters for the implementation of an argillite/bentonite pelletized material and define the adopted strategy. The swelling behaviour is studied on remoulded COx argillite as well as on bentonite-based materials, focusing also on the multi-scale interactions of smectites with aqueous solutions. The hydro-mechanical response of previously studied pellets for disposal systems is examined to demonstrate their features (e.g. fabrication, initial granular structure, homogenization upon saturation). The resulting packing state of dry granular materials is further discussed as a particular parameter of interest. The chapter is developed in the following main parts:

- 2.1 Introduction
- 2.2 Hydro-mechanical behaviour of remoulded COx argillite
- 2.3 Swelling clay presence in remoulded soil materials: Bentonite case
- 2.4 Implementation techniques of remoulded materials on radioactive waste disposal
- 2.5 Swelling clay pellets at disposal systems
- 2.6 Packing state of granular materials on emplacement conditions
- 2.7 Identification of needs and proposed strategy of the present PhD study

---

## 2.1 Introduction

Remoulded COx argillite has been studied as potential backfill material for the French disposal facility, due to its developed swelling characteristics and the advantageous reuse of the excavated material. The conducted studies were mainly focused on highly compacted materials, corresponding to the in-situ compaction implementation or the pre-fabricated block concepts (Tang et al. 2011a, Mohajerani et al. 2011, Zhang 2014, Cuisinier et al. 2014).

Pelletized material has been considered as an interesting alternative, because of operational convenience (Pasquiou, 2001; Pusch et al., 2003; Van Geet et al., 2005; Imbert and Villar, 2006; Hoffmann et al., 2007; Alonso et al., 2010; Molinero Guerra et al., 2018; Darde et al., 2020). Nonetheless, the available information concerning its hydro-mechanical behaviour includes only pellets composed of pure swelling clay (i.e. bentonite). On emplacement conditions the material behaves as a granular assembly, which is gradually homogenizing upon hydration. However, near saturation, the pelletized sample behaves similarly to the pre-compacted blocks (Imbert and Villar, 2006; Hoffmann et al., 2007; Karnland et al., 2008).

Clay swelling behaviour is known to originate from the important interactions between the clay mineral (i.e. smectite) and water, involving multi-scale mechanisms that are affected by several factors. An overview of the hydro-mechanical behaviour and in particular the swelling mechanism is presented, beginning with COx argillite and smectite-based materials implemented as engineering barriers. The bibliographical review further focuses on the characteristic features of pellets, including the evolution of their granular state to a homogenized saturated condition. At the end, the objectives and the strategy adopted by the present study are analysed.

## 2.2 Hydro-mechanical behaviour of remoulded COx argillite

As it was seen in section 1.1, the construction of the disposal facilities comprises a large network of tunnels, drifts and shafts, which produces large quantities of excavated argillite material. The reuse of the excavated COx has been proposed as a convenient backfill solution. In the following sessions, the hydro-mechanical response of remoulded COx argillite in terms of swelling capacity is presented.

### 2.2.1 Mineralogical composition of COx argillite

Callovo-Oxfordian argillite claystone constitutes a geological formation, divided vertically into three lithostratigraphic units (Armand et al. 2017). They are categorized (in base order), as:

- 
- Clay unit (UA), which comprises the 2/3 of total layer thickness. At the level of the URL (~490 m), it presents high clay fraction (40-60%).
  - Transition unit (UT), located between the clay and the silty-carbonate rich unit presenting high carbonate content (40-90%).
  - Silty-carbonate-rich unit (USC), a layer of around 20-30 m of thickness that presents more varied and heterogeneous mineral composition.

The mineralogical characterization of samples extracted from the URL level have shown a rather homogeneous composition formed by clay mineral (50-55%), carbonates (20-25%, mainly calcite and dolomite), tectosilicates (20%, mainly quartz and feldspar), together with subordinate pyrite and iron oxides (3%) (Robinet et al., 2012; Armand et al., 2014). Clay minerals presenting a fraction smaller than 2  $\mu\text{m}$ , consist principally of 55% illite-smectite interstratified minerals, 30% illite and 15% kaolinite and chlorite (Yven et al. 2007, Armand et al. 2014).

The analysis of CO<sub>x</sub>'s self-sealing of fractures at different scales revealed the importance of smectite on its behaviour (Andra 2016a). This feature, in combination with the chemical-mineralogical compatibility with the host rock as well as the environmental and techno-economic aspects introduced the idea of installing argillite to backfill the gallery remaining openings. Smectite presence inside the clay element (i.e. swelling clay mineral) is responsible for the sensitive behaviour upon water content variation, which is favourable for the pellets swelling behaviour.

### **2.2.2 Reminder of swelling mechanism in clays and experimental techniques for swelling capacity measurement at macroscopic scale**

The term “clay” is used to describe both size and mineral class, indicating in the first case the sizes finer than 2 or 5  $\mu\text{m}$  (depending on the engineering classification standards) and in the latter, the small particles presenting negative electrical charge, plasticity and high weathering resistance (Mitchell and Soga 2005).

The clay crystalline structure is composed of silicon tetrahedral sheets connected to aluminium/magnesium octahedral sheets (Figure 2-1). Depending on the sheets rearrangement, they are distinguished in two main categories:

- 1:1 or “TO” minerals (kaolinite, serpentine) consisting of alternating octahedral and tetrahedral sheets (silicon with oxygens) and

- 2:1 or “TOT” minerals (smectite, illite, chlorite, etc.) made of a central octahedral sheet between two tetrahedral silicon sheets (cations with hydroxyls or oxygens).

Each unit (1:1, 2:1) is known as laminae or layer, while stacks of them are forming the primary clay particles (Villar, 2002; Pusch and Yong, 2006). The aggregate is composed of the including clay particles (Figure 2-2). The complicated organization of clays gives place to the development of different level of structure (Gens and Alonso 1992).

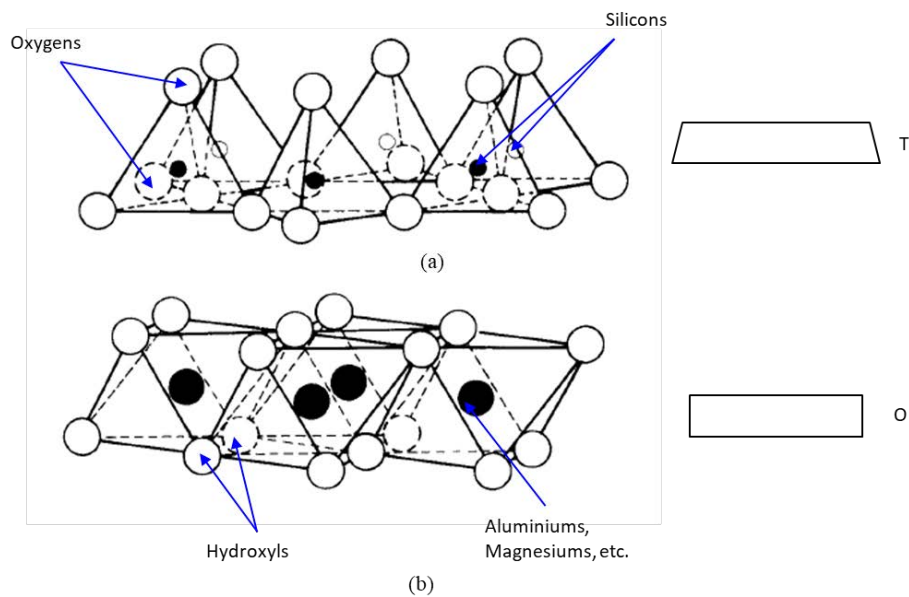


Figure 2-1 Sheet structure (left) and presentation (right) of (a) tetrahedral and (b) octahedral units (after Mitchell and Soga, 2005).

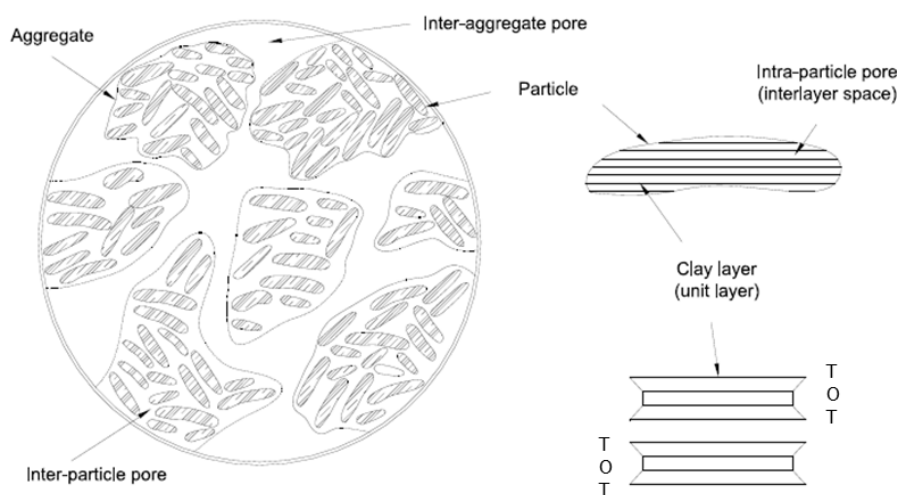


Figure 2-2 Schematic diagram of the organization of “TOT” clay mineral (after Jacinto et al., 2016).

Although inter-sheet bonds are very strong, the inter-layer bonding might be sufficiently weak to dictate their physical and chemical behaviour upon alteration of the environmental conditions. The isomorphous substitution provides clay particles with a net negative charge.

---

Cations are attracted and held between the layers and on the surfaces and edges of the particles in order to preserve electrical neutrality. Many of these cations are exchangeable, declaring clays as sensitive to water/humidity interaction. According to Mitchell and Soga, (2005) the following mechanisms are identified to explain the water absorption by clay minerals:

- Hydrogen bonding, which can be formed easily due to oxygens or hydroxyls presence on clays surfaces.
- Hydration of exchangeable cations, which is caused by the attraction of water molecules to the already attracted cations on the negatively charged clays surface.
- Attraction by osmosis, where the increased cation concentration as clay surface is approached, produces diffusion of water molecules with attempt to equalize concentrations.
- Dipole attraction, where similarly to the exchangeable cations, water dipoles are oriented toward the negatively charged clay surface to naturalize the charge.
- Attraction by London dispersion forces, where van der Waals attractive forces can bond water molecules to the clay surface.

On Table 2-1, basic characteristic of different clay minerals are presented. The cation exchange capacity (CEC) represents the amount of exchangeable cations found on materials surface and can be replaced by leaching with a solution containing other dissolved cations of higher replacing power than the adsorbed cation. The specific surface area (SSA) expresses the total surface area (interlayer surface and external surface of particles) per dry mass of clay. Both parameters are strongly related to the interaction of clay mineral with water and could be used to estimate the water absorption capacity of the soil material.

Unsaturated clays tend to absorb water, depending on their mineralogical characteristics. Water content increase may occur either by direct hydration with a polar liquid (specimen's soaking or infiltration) or through the vapour phase. In the first case, the material absorbs water until full saturation, without controlling the intermediate states. On the second case, soil's water content and consequently degree of saturation can be altered progressively, due to modification in relative humidity (RH). In that matter, the concept of soil suction is widely used to relate the imposed conditions of relative humidity (Kelvin's law) (Delage et al. 1998). In general, suction describes the water retention capacity of the unsaturated soils, expressing the ability to resist the water loss, when water passes from the liquid to vapor phase (Ridley 1993). In practice, as relative humidity becomes more significant (i.e. water content increase), soil total suction decreases.

Table 2-1 Summary of clay mineral characteristics (after Mitchell and Soga, 2005).

| Type | Clay mineral                | Inter-layer bond           | Basal Spacing (Å) | Cation Exchange Capacity (meq/100 g) | Specific Gravity (-) | Specific surface (m <sup>2</sup> /g)              |
|------|-----------------------------|----------------------------|-------------------|--------------------------------------|----------------------|---|
| 1:1  | Kaolinite                   | O-OH<br>Hydrogen<br>Strong | 7.2               | 3-15                                 | 2.60-2.68            | 10-20   |
| 2:1  | Montmorillonite (smectites) | O-O Very weak              | 9.6               | 80-150                               | 2.35-2.70            | 50-120 Primary*<br>700-840 Secondary <sup>‡</sup> |
|      | Illites                     | K ions; strong             | 10                | 10-40                                | 2.6-3.00             | 65-100  |
|      | Vermiculite                 | Weak                       | 10.5-14           | 100-150                              |                      | 40-80 Primary*<br>870 Secondary <sup>‡</sup>      |

\* surface area exclusive of interlayer zones

<sup>‡</sup> extended surfaced so that polar molecules can penetrate between layers

As Table 2-1 illustrated, smectites are clay minerals presenting crystalline structure of “2:1/TOT” units. The most common mineral of this group is montmorillonite and its unit layer structure is presented on Figure 2-3. By definition, smectites inter-layer bonding is caused by van der Waals forces and by cations exchange that balance charge deficiencies in the structure. These bonds are weak and easily separated by cleavage or adsorption of water or other polar liquids, giving their swelling/expansive behaviour (Bell 1993, Mitchell and Soga 2005).

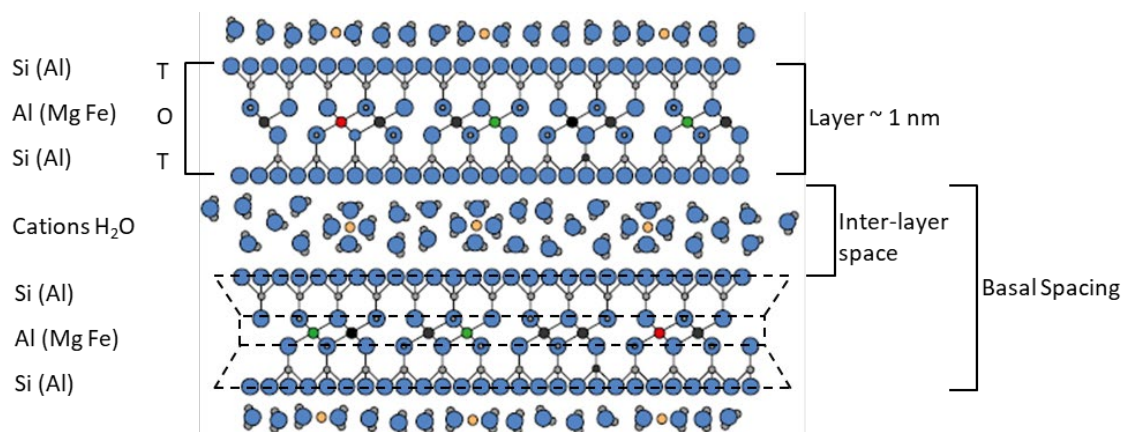


Figure 2-3 Schematic presentation of two montmorillonite unit layers with interlayer cations and water molecules (Karnland et al. 2006).

Their complex structure interacts with aqueous solutions or humid atmosphere, producing two types of swelling, the crystalline and the osmotic swelling (Norrish, 1954; Madsen and

---

Müller-Vonmoos, 1989). The case of montmorillonite is presented as characteristic example of smectite clays.

#### A. Crystalline swelling

In non-hydrated state, exchangeable cations are found in the layer surface of montmorillonites. Upon the beginning of hydration at low water contents, the first layers in clay surface are hydrated due to hydrogen bonds that are formed with water molecules (Norrish 1954). As water content increases, molecules insert into the interlayer space causing inter-layer widening, from 0.96 nm up to 2 nm (Figure 2-4) (Madsen and Müller-Vonmoos, 1989; Norrish, 1954; Saiyouri et al., 2004; Delage et al., 2006).

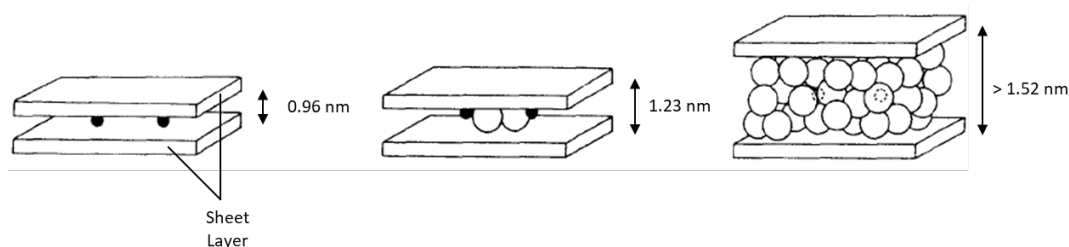


Figure 2-4 Inter-crystalline swelling on montmorillonite structure upon water adsorption (Kraehenbuehl et al. 1987).

The amount of water absorbed in the inter-layer spacing is indicated by the type of exchangeable cations available. For instance, according to Na-montmorillonite (MX80 bentonite) absorbs up to 4 layers of water compared to the Ca-montmorillonite (FoCa7) which increased the layer distance up to 3 water layers (Saiyouri et al., 2000, 2004; Laird, 2006; Villar et al., 2012). In parallel, subdivision clay particle is observed activating the double layer diffusion mechanism.

#### B. Osmotic swelling

It is based on the repulsion developed between electrical diffuse double layers, formed as hydrated cations are dissociated from clay units into the solution (Schanz and Tripathy 2009). In particular, part of the total charge is expressed on the external surface of quasicrystals, constituting the one half of the electric double layer (Figure 2-5). The other half is formed by the net positive charge of the aqueous solution close to the external surface, which is developed due to weak bonds of the exchangeable cations and the external surface as well as due to exchangeable cations diffusion towards regions of low concentration in the solution (Laird 2006). Contrary to crystalline mechanism, osmotic swelling applies on larger distances and is the swelling that is measured macroscopically in the laboratory (Madsen and Müller-

Vonmoos 1989). Nonetheless, Gouy-Chapman diffuse double-layer theory has been applied in order to calculate the developed swelling pressure for given properties of the clay, and fluid properties in a range of dry densities (Komine and Ogata 2003, Schanz and Tripathy 2009).

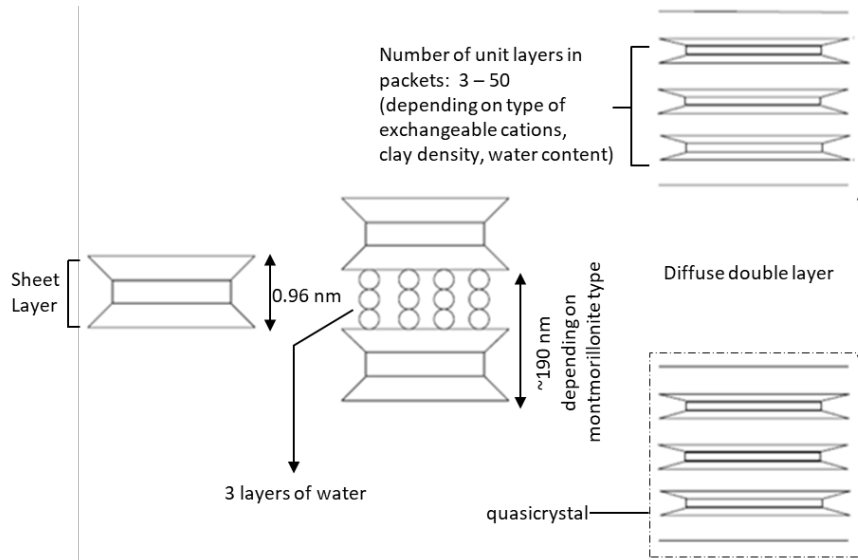


Figure 2-5 Schematic diagram of the unit layer arrangement upon double layer diffusion development (after Schanz and Tripathy, 2009).

The developed swelling impacts materials' mechanical properties. Depending on the volume conditions prevailing upon the hydration, swelling capacity is quantified by two parameters: swelling pressure and swelling potential. More specifically, swelling pressure is defined as the pressure required to prevent any volume increase (Sridharan et al. 1986, Madsen and Müller-Vonmoos 1989), whereas swelling potential expresses the magnitude of soil expansion for given initial conditions (Rao 2006). Stress and strain/deformation are the measured parameters in respect to each case (Komine and Ogata, 1994; Villar and Lloret, 2008; Wang et al., 2012; Cuisinier et al., 2014; Barast et al., 2017). The conventional oedometer has been the earliest mean used to determine the soil swelling performance, measuring either swelling pressure or swelling potential in different conditions.

Sridharan et al. (1986) reported three methods of determining swelling pressure. The specific methods and their corresponding stress paths are given (Figure 2-6):

- (a) Free swell and load (KLM), soil sample is subjected to hydration under a constant vertical load. As long as swelling strain is ceased, the specimen is consolidated until the initial volume is achieved. Swelling pressure is determined as  $\sigma_A$ .
- (b) Equilibrium void ratios for different consolidation loads (LN), where three or more identical samples are hydrated under different vertical loads (e.g.  $\sigma_1, \sigma_2, \sigma_3, \sigma_4$ ).

When sample's swelling or collapse is completed, the LN path is determined by the equilibrium states of the tested specimens. The intersection of the path with the initial volume condition points the swelling pressure as  $\sigma_B$ .

- (c) Constant volume (KO), where the pressure required to maintain the sample's original volume is measured ( $\sigma_C$ ). Constant volume conditions can be ensured either by gradually increasing the applied load in order to counterbalance the developed swelling (Sridharan et al., 1986; Al-Mhaidib, 1998; Wang et al., 2012) or by creating a constant-volume system that measures directly the developed stress by means of a pressure sensor (among others Kayabali and Demir, 2011; Saba et al., 2014a; Wang et al., 2012; Yigzaw et al., 2016).

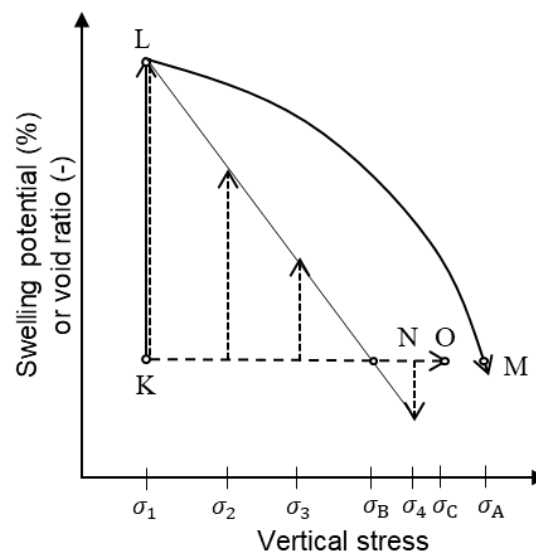


Figure 2-6 Experimental techniques for swelling pressure measurement (after Sridharan et al., 1986).

As Figure 2-6 implies, swelling pressure appear to depend on the experimental method and consequently on the followed stress path. Swell-consolidation test method normally results in higher swelling pressure values ( $\sigma_A$ ) than the direct measurement of pressure on constant volume conditions ( $\sigma_C$ ) (Tang et al. 2011a, Yigzaw et al. 2016). The difference is attributed to variations on hydration conditions (free or constrained) which lead to structure modification occurring during the free swell phase, as well as to the friction developed between specimen and oedometer cell during the consolidation stage (Tang et al. 2011a). On the other hand, when hydration occurs under an applied stress, swelling potential is partially inhibited according to the applied stress, resulting in lower swelling pressure (Hoffmann et al. 2007, Villar and Lloret 2008).

It should be noted that at gallery conditions inside the repository, the installed material initially swells until the available space is filled and swelling continues under constant volume condition, while gallery walls blocks the materials expansion.

### 2.2.3 Swelling capacity of remoulded COx argillite

As it was already evoked on section 2.2.1, smectite presence on COx mineralogy gives to argillite swelling characteristics. The reuse of the excavated rock indicates its crushing after being stored in muck piles in order to remove any local stress (Wang et al. 2013a, Andra 2016a). The way of processing COx after excavation (e.g. granulometry, water content) may influence the swelling capacity. Tang et al. (2011b) noticed that a finer COx product exhibited higher swelling properties than argillite crushed at coarser sizes, probably due to more available space for water penetration into the destructured illite-smectite minerals. Other experimental investigations showed a reduction of the developed swelling pressure when argillite presented higher initial water content (Tang et al. 2011a). The latter might be correlated to the reduction of water retention capacity when lower initial suction is observed, which is addressed in more details on section 2.3.

In the level of aggregates, Wang et al. (2013b) hydrated COx powder under free volume conditions. The developed strains measured by correlation of digital image of Scanning Electron Microscope (SEM) observations (Figure 2-7) presented a moderate swelling with a rather heterogeneity (ranging between 0.8-3.5%) which was probably related to the different types of mineral elements inside COx argillite. Similar remarks were reported by Tu (2011) in samples of low dry density.

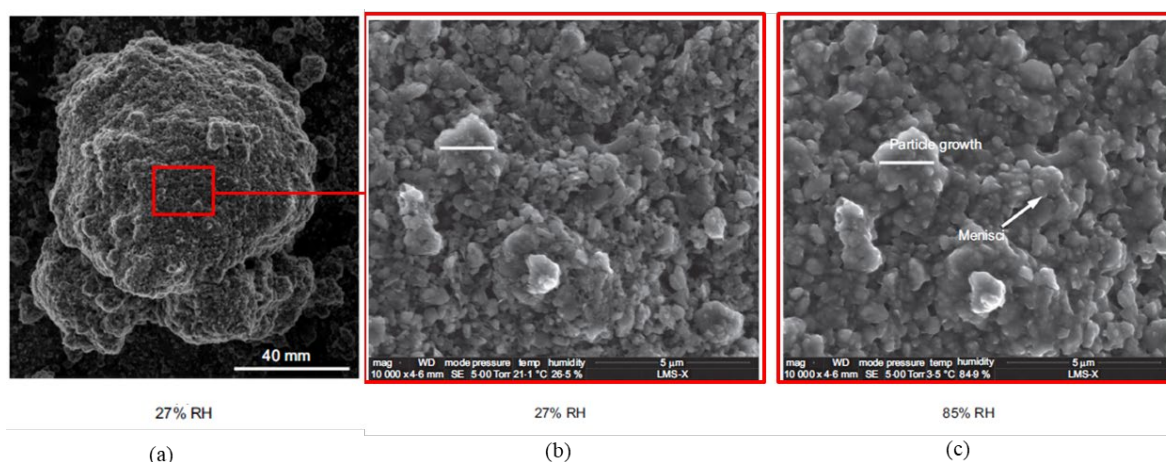


Figure 2-7 Micrographs of COx aggregates at (a) RH = 27% and (b) the enlarged domain outlined in red. (c) Hydrated aggregate at RH = 85% (Wang et al., 2013b).

Crushed excavated argillite compacted to high dry densities ranging between 1.60 Mg/m<sup>3</sup> and 2.00 Mg/m<sup>3</sup> has been hydro-mechanically investigated, simulating either the density state achieved by in-situ compaction or the densities of pre-compacted blocks (Tang et al., 2011a, 2011b; Cuisinier et al., 2014; Zhang, 2014; Zeng et al., 2019; Middelhoff et al., 2020). At this dense state, compacted COx presents swelling potential and pressure upon hydration.

Tang et al. (2011a) performed hydration on constant volume cells and observed the hydration path dependency of the developed swelling pressure (Figure 2-8). The swelling stress was gradually increased upon gradual suction decrease, whereas the direct hydration of the sample led to an instant augmentation of the swelling pressure, but in slightly lower values. A more homogeneous hydration could be achieved with suction-equilibrium process, where water absorption may initially occur on the intra-aggregate pore. In the case of direct hydration, water absorption commences in the inter-aggregate region, causing particles subdivision aggregate re-arrangement which induces small mechanical weakness and therefore the decrease of developed pressure. The swelling pressure ranged between 0.8 to 1.1 MPa for the highly compacted state of 2.0 Mg/m<sup>3</sup>.

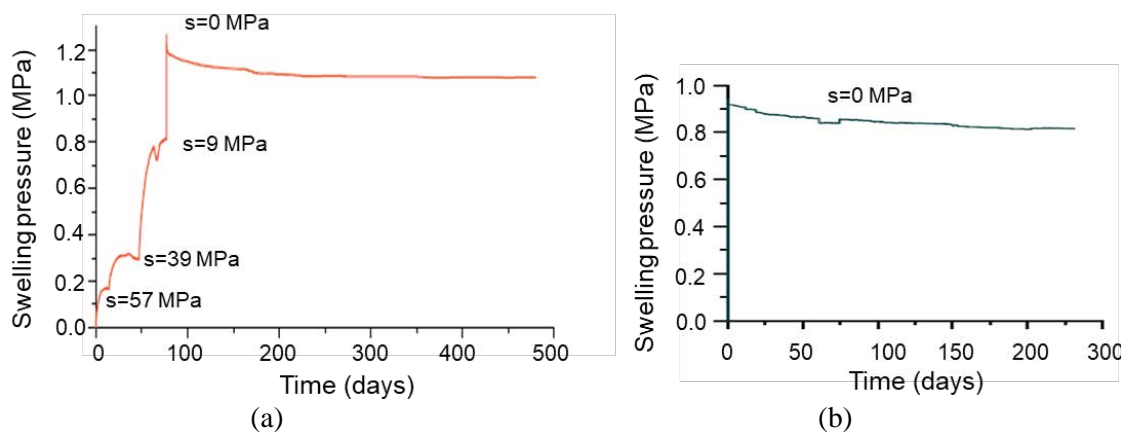


Figure 2-8 Evolution of swelling pressure at constant volume conditions on compacted COx argillite at initial dry density of 2 Mg/m<sup>3</sup>: (a) hydration with suction control and (b) direct hydration with distilled water (Tang et al. 2011a).

Another interesting point on the specific study was a stress history dependency observed on the hydro-mechanical response. In an adjusted method of constant volume conditions, COx samples were statically compacted until a vertical load (resulting in the desired density) and then unloaded at different initial vertical stresses ( $\sigma_v = 0.5$  MPa and  $\sigma_v = 7$  MPa), while hydration was imposed for fixed volume (Figure 2-9). Decrease of pressure was noticed for the higher initial applied stress (i.e.  $\sigma_v = 7$  MPa) and conversely swelling pressure was developed for the lower initial stress (i.e.  $\sigma_v = 0.5$  MPa). In fact, this behaviour can be correlated with the over-consolidation ratio (OCR) (i.e. the ratio of the maximum past consolidation effective stress to the present effective stress), where swelling capacity increases upon OCR increase (Dang 2007). According to information provided on the study of Tang et al. (2011a), OCR is calculated for the specific specimens at 4 and 74, for the sample hydrated under 7 MPa and 0.5 MPa respectively. The effect is explained in more details on section 2.3.4.2.

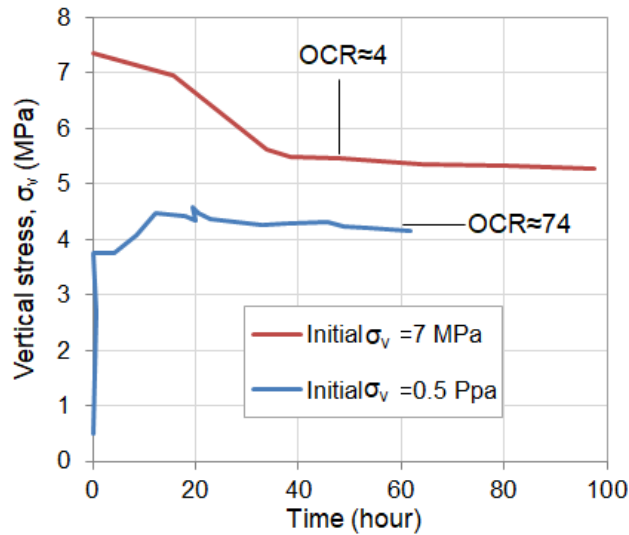


Figure 2-9 Evolution of swelling pressure of compacted COx argillite at adjusted constant volume conditions: different vertical stresses were applied before flooding under constant volume conditions (Tang et al. 2011a).

It is well established that swelling pressure is affected by the materials initial dry density, especially on pure swelling clays (Pusch, 1980; Villar and Lloret, 2008; Yigzaw et al., 2016). On Figure 2-10, a similar tendency is illustrated for COx argillite upon density variation (Zeng et al. 2019).

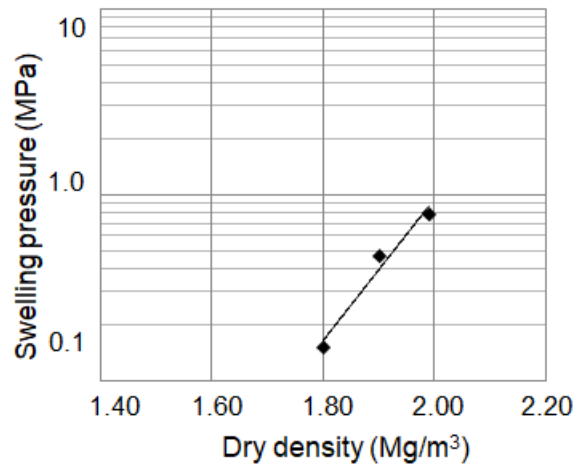


Figure 2-10 Swelling pressure of compacted COx argillite as function of sample's dry density (after Zeng et al., 2019).

## 2.2.4 Conclusions and necessity for supplementary swelling behaviour

Several experimental investigations illustrated the swelling ability of remoulded COx argillite. At loose state, heterogeneity on swelling potential was observed, probably due to the presence of other minerals inside argillite (quartz, calcite). At higher compacted states, this heterogeneity was not visible and COx's swelling capacity was influenced by the:

- 
- (a) initial dry density,
  - (b) applied hydration path and
  - (c) followed stress path.

For this domain of density (1.80-2.00 Mg/m<sup>3</sup>), the measured swelling pressure was ranging between 0.1 to 1 MPa. However, when pelletized materials have been investigated for different disposal concepts, lower resulted densities are expected upon their emplacement (Van Geet et al. 2005, Hoffmann et al. 2007, Dixon et al. 2011, Gatabin et al. 2014, Müller et al. 2017, Liu et al. 2019). For instance, “EB experiment” in Mont Terri URL and “FSS experiment” obtained dry densities of 1.36 and 1.50 Mg/m<sup>3</sup> respectively for granular materials composed of pure swelling clays (Mayor et al. 2005, Noiret et al. 2016).

As a consequence, it is evident that swelling clay additive in COx argillite is necessary in order to improve the swelling characteristics of a pelletized mixture. Bentonite - as a common swelling clay - is widely used as additive to govern the material’s swelling capacity. The hydro-mechanical behaviour of materials composed of soils and bentonite or pure bentonite will be later analysed in order to better understand the swelling behaviour.

### **2.3 Swelling clay presence in remoulded soil materials: Bentonite case**

Bentonite is the most common of smectites, containing high percentage of montmorillonite. It presents high number of unbalanced exchangeable cations and therefore exhibits high absorption capacity. Depending on the type of the dominant cation, there are different categories of bentonites, such as sodium (Na), calcium (Ca) and magnesium (Mg) bentonites. Montmorillonite presence in bentonite is the reason for the high swelling capacity and low hydraulic conductivity, e.g. lower than 10<sup>-11</sup> m/s according to Lee et al. (2001). In the following sections, the swelling behaviour will be analysed on bentonite-based materials, where the interactions upon hydration are more prominent and easier to investigate.

#### **2.3.1 Structure arrangement: pore families determination**

As it was already mentioned, clays present a multi-level structure (sheet, particle, aggregate). This complex unit gives place in porosity to be developed in different regions.

In the past years, microstructure studies focusing on the pore distribution of clays have been conducted using techniques such as Mercury Intrusion Porosimetry (MIP) and Scanning Electron Microscope (SEM) observations. In this context, studied specimens are freeze-dried in order to remove water without risking shrinkage caused by drying (Stoltz et al. 2012). Mercury - a non-wetting liquid - is inserted with pressure inside the sample, in order to

---

measure the volume of the soil pores. Assuming cylindrical pore configuration, the Laplace equation is considered to determine the pore entrance diameter from the intrusion pressure of mercury and define the pore size distribution (PSD) of the material (Romero et al., 1999; Delage et al., 2006; Tang et al., 2011a; Molinero-Guerra et al., 2019b). Similarly, SEM observations are used to directly identify and recognize the different pore families in soil samples (Romero, 2013; Seiphoori et al., 2014; Manca et al., 2015; Razakamanantsoa and Djeran-Maigre, 2016).

Different porosities are identified in different regions, depending on the referred scale (Villar 2002, Yven et al. 2007, Mohajerani et al. 2011). In particular,

- Pores with sizes smaller than 2 nm, are located in the inside the aggregate, in the inter-layer/inter-laminar space of minerals.
- Pores larger than 2 nm are located between particles and aggregates, and are classified as mesoporosity and macroporosity, depending on whether the diameter is below or above 50 nm.

In practice, these delimiting values are not definitive. Due to restrictions of the used techniques, inter-layer pores cannot be intruded during MIP tests and are not visible in the SEM observations (Seiphoori et al. 2014). Therefore, other values are usually used in order to distinguish micro and macroporosity (Delage et al. 2006, Romero et al. 2011). For compacted unsaturated soils, various levels of porosity have been established by many studies (Gens and Alonso, 1992; Delage et al., 2006; Tang et al., 2011a; Massat et al., 2016) and more precisely the observed voids are categorized as:

- planar inter-layer spaces between the clay layers inside the clay particles, interpreted as interlayer or intra-particle pores;
- small voids between clay particles inside the aggregates, interpreted as inter-particle or intra-aggregate pores;
- large voids between the aggregates made up of clay particles, interpreted as inter-aggregate pores.

The last two cases are those that are mainly investigated and are considered as microporosity and macroporosity respectively.

### **2.3.2 Pore structure at the as-compacted state**

The pore size distribution (PSD) of various bentonites and mixtures of soil/bentonite materials have been studied by the MIP technique, revealing a clear bimodal type of porosity

at the as-compacted state (Lloret et al., 2003; Lloret and Villar, 2007; Tu, 2011; Romero, 2013; Saba et al., 2014b; Seiphoori et al., 2014; Wang et al., 2014; Manca et al., 2015; Molinero Guerra et al., 2017). On Figure 2-11, this bimodal distribution of pores is illustrated for samples of pure MX80 bentonite, CO<sub>x</sub>/MX80 mixture (30/70) and sand/MX80 mixture (80/20) compacted at dry densities ranging between 1.80 and 2.00 Mg/m<sup>3</sup>. More precisely, for MX80 bentonite, peak in macroporosity is identified around 1.5 μm, whereas micropores are located at approximately 20 nm. Even at higher dry density (2.00 Mg/m<sup>3</sup>), slightly higher macrovoids (5 μm) are obtained when bentonite fraction decreases (30%MX80 mixed with 70% CO<sub>x</sub>). In lower bentonite fraction (20%MX80 mixed with 80% sand), larger micro and macrovoids are observed at 0.31 μm and 100 μm respectively. On sand/bentonite mixtures, a small shift in PSD in larger values is obtained more evident than in the case of argillite/bentonite mixtures. The remark coincides with observation of Saba et al., (2014b) for 35% sand/65%MX80 mixture.

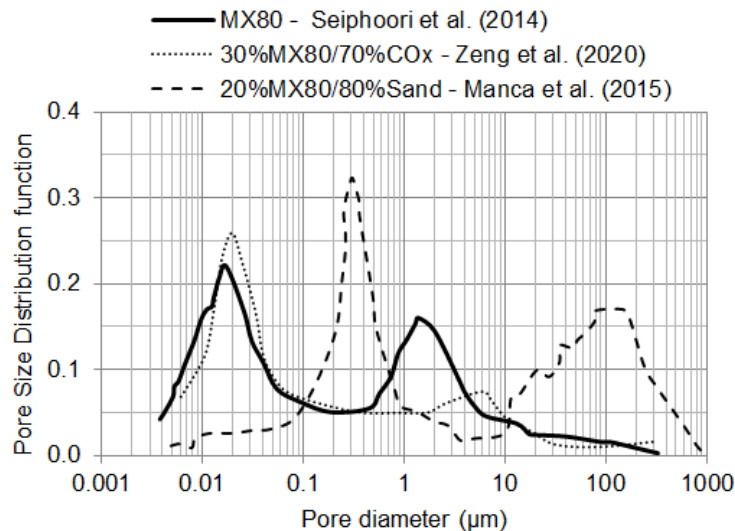


Figure 2-11 Pore size distribution of compacted MX80 bentonite ( $\rho_d = 1.8 \text{ Mg/m}^3$ ), CO<sub>x</sub>/MX80 ( $\rho_d = 2.0 \text{ Mg/m}^3$ ) and sand/MX80 mixture ( $\rho_d = 1.8 \text{ Mg/m}^3$ ) (Seiphoori et al. 2014, Manca et al. 2015, Zeng et al. 2020).

Several investigations have showed that fabric evolution of compacted soil materials is influenced by the compaction state (Gens and Alonso, 1992; Lloret et al., 2003; Lloret and Villar, 2007; Wang et al., 2013b; Sun et al., 2018). As Figure 2-12 illustrates, at mechanical loading, inter-aggregate porosity decreases, leaving the microstructural pore space largely unmodified (~20 nm). The effect can be easily visualized by observing data from electron microscopy in Figure 2-13, where the size of inter-granular pores is larger in the sample with smaller dry density.

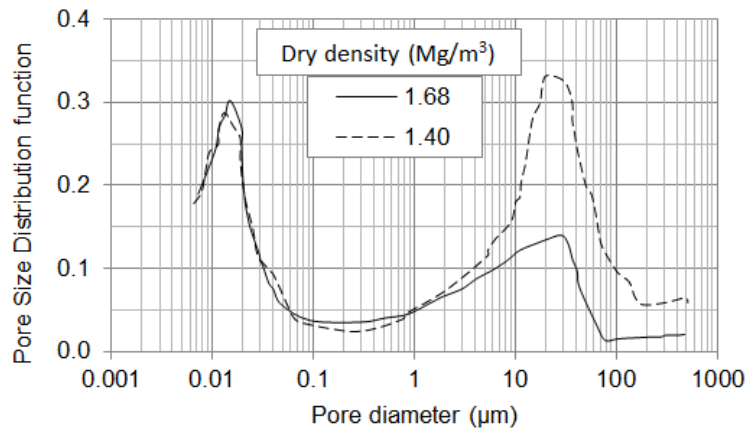


Figure 2-12 Pore size distribution of Febex bentonite compacted at different dry densities (Lloret and Villar 2007).

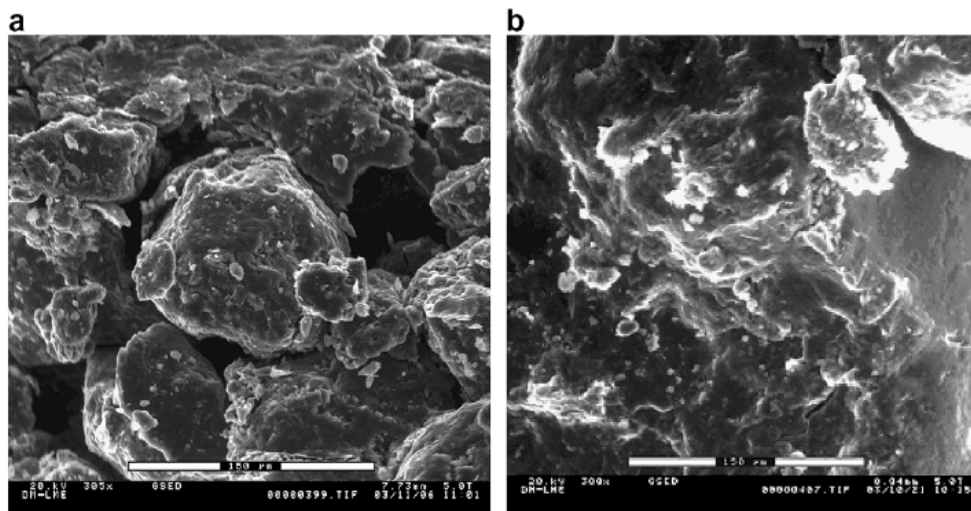


Figure 2-13 Micrographs of Febex bentonite compacted with hygroscopic water content at dry density of (a) 1.40 Mg/m<sup>3</sup> and (b) 1.65 Mg/m<sup>3</sup> (Lloret and Villar 2007).

### 2.3.3 Fabric evolution upon hydration path

Interactions between smectite clays and aqueous solutions or humidity activate swelling mechanisms in different levels. Clay fabric is sensitive to water content changes and important modifications on materials microstructure may occur upon suction decrease (Romero 2013). Similarly to section 2.3.1, the materials evolution from the as-compacted state to saturated conditions is observed.

Seiphoori et al. (2014) noticed that during isochoric hydration the bimodal pore distribution of compacted bentonite is gradually transmuted into monomodal (Figure 2-14a). The

macrovoids existing at the as-compacted state are reduced upon wetting with volume restriction. On contrary, the microporosity expands, without modifying the pore size. The same behaviour was reported in mixtures of bentonite mixed with other soil materials (Figure 2-14b). COx argillite flooded under constant volume conditions presented also an inter-aggregate pore decrease, while intra-aggregate pore were remained unaffected (Tang et al. 2011b). The evolution of inter-aggregate porosity is consistent with Massat et al. (2016) X-ray tomography scan, using aqueous solutions.

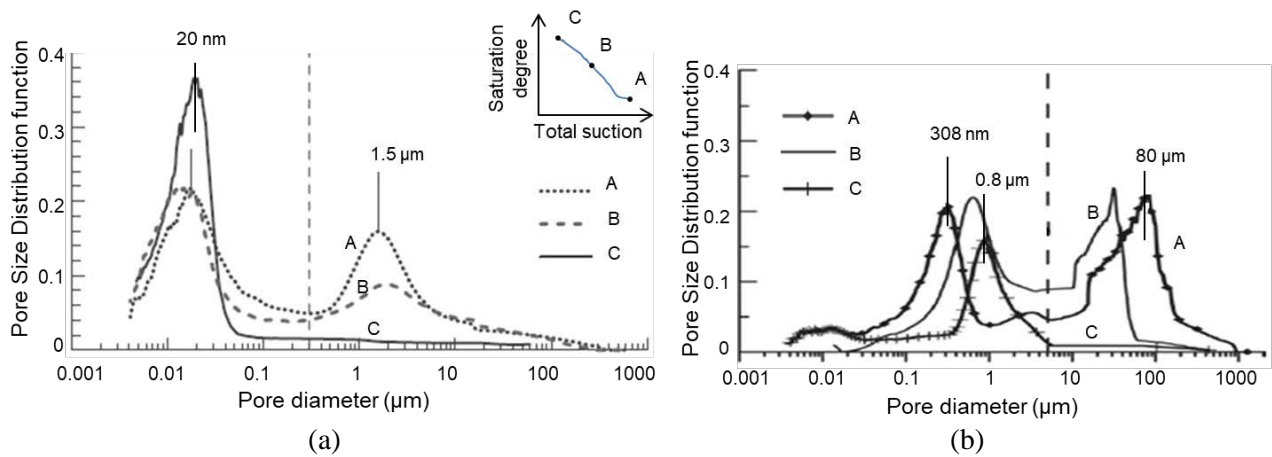


Figure 2-14 Evolution of pore size distribution of samples containing (a) MX80 bentonite (Seiphoori et al., 2014) and (b) Sand/MX80 mixture (Manca et al., 2015) during wetting at constant volume conditions.

On MX80 bentonite, dried after full saturation was reached, irreversible modification on the single PSD was observed, which was in accordance with a macroscopic irreversibility in material's water retention behaviour (Seiphoori et al., 2014).

At non-isochoric wetting (i.e. sample develops swelling strain), inter-aggregate pores reduce from 25 μm to approximately 1 μm is observed on Figure 2-15. However, a significant expansion is achieved (compared to constant volume conditions), since the material is able to swell. Similar observations were reported by Agus (2005) after absorption of water for a bentonite/sand mixture under unconfined conditions.

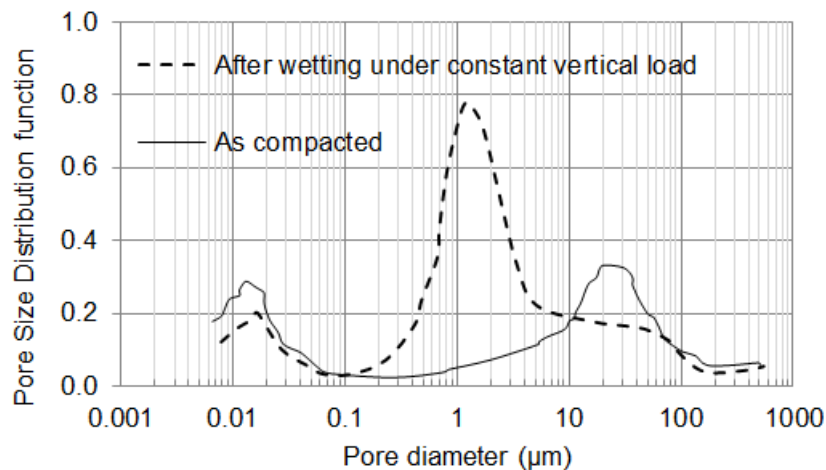


Figure 2-15 Pore size distribution of Febex bentonite samples at the as-compacted state ( $\rho_d=1.40 \text{ Mg/m}^3$ ) and after wetting at non-constant volume conditions (under constant vertical load) (Lloret and Villar 2007).

In general upon the hydration path, most of changes in microstructure occurred in macropores family (Wang et al. 2014).

### 2.3.4 Influential parameters of swelling behaviour

It was seen that in microscopic scale, clays containing smectites interact with water and reduce the macropores. At macroscopic scale, these interactions were presented for remoulded COx argillite (section 2.2.3). The limited swelling capacity necessitates the study of materials richer in smectite mineral, in order to better address the parameters governing the swelling response. Reasonably, these parameters are primarily related to the material's mineralogy and consequently to the mechanical loading prior to hydration, or the chemical and thermal conditions occurring during hydration. In the following sessions the impact of different parameters on swelling potential and swelling pressure is analysed.

#### 2.3.4.1 Smectite content

It has been underlined that smectite presence is responsible for the swelling response of the material. For instance, the developed swelling potential and pressure increases with increase of bentonite content in a bentonite/sand mixture (Figure 2-16). More time is necessary for samples to achieve stabilization for the measured value (Komine and Ogata, 2003, 1999; Muntohar, 2004; Karland et al., 2008). Even on pure bentonites, the expansive behaviour is influenced by the bentonite type. In general, Na bentonites exhibit higher swelling performance than Ca bentonite, a fact that is related to their cation exchangeable capacity and montmorillonite content (Komine and Ogata 1994, Di Maio et al. 2004, Wang et al. 2012).

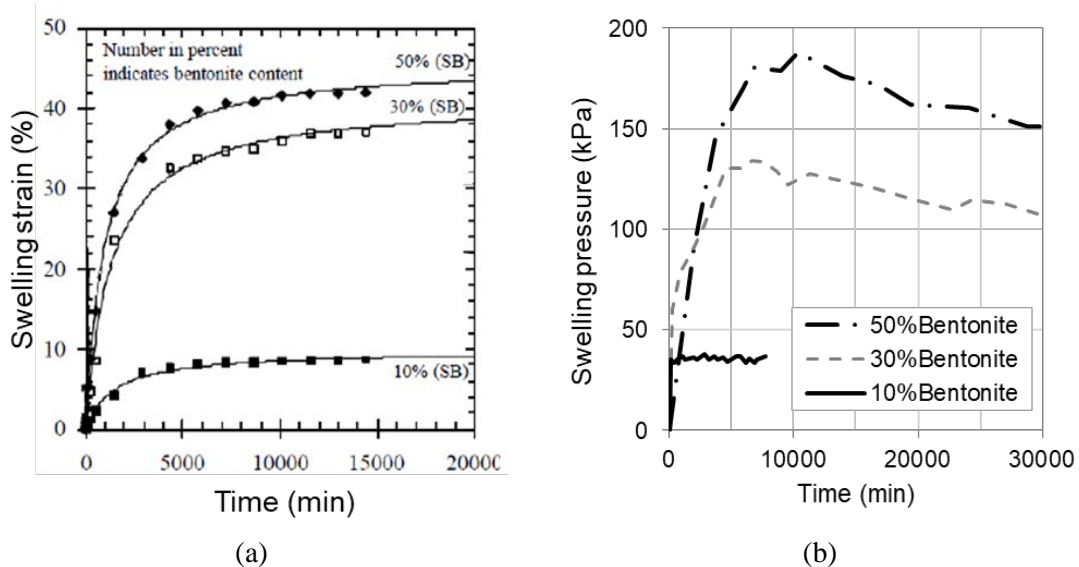


Figure 2-16 Bentonite/sand mixtures compacted at similar dry densities, in various fractions; results of (a) swelling potential (MX80/sand) and (b) swelling pressure (Kunigen-V1/sand) (after Muntohar, 2004 and Komine and Ogata 1999 respectively).

#### 2.3.4.2 Mechanical loading prior to hydration

On given smectite composition, the resulting packing density achieved before hydration has been established as a decisive parameter for the material's hydro-mechanical behaviour (Pusch, 1982; Karnland et al., 2008; Villar and Lloret, 2008; Manca et al., 2015; Yigzaw et al., 2016). Remoulded pre-compacted materials are emplaced inside the galleries, using different techniques (in-situ compaction, pellets or blocks). On each case, a mechanical load is applied during the material's preparation in order to achieve their target density. Depending on the imposed volume conditions (constant or non-confined volume), the final swelling capacity is affected by the initial dry density. According to Villar et al. (2012), lower initial voids provoke water absorption directly by the interlayer network, rather than the free pores.

Pure bentonites develop swelling pressure of several MPa (Imbert and Villar, 2006; Castellanos et al., 2008; Schanz and Tripathy, 2009; Baille et al., 2010; Seiphoori, 2014; Massat et al., 2016), whereas lower pressures are expected as smectite content decreases (Komine and Ogata 1999, Manca et al. 2015). In both cases, exponential relation between final pressure and dry density has been observed by several studies (Villar, 2005; Karnland et al., 2006; Hoffmann et al., 2007; Wang et al., 2012). Figure 2-17 demonstrates this relation on a semi-logarithmic scale (Y-axis) for a sand/bentonite mixture.

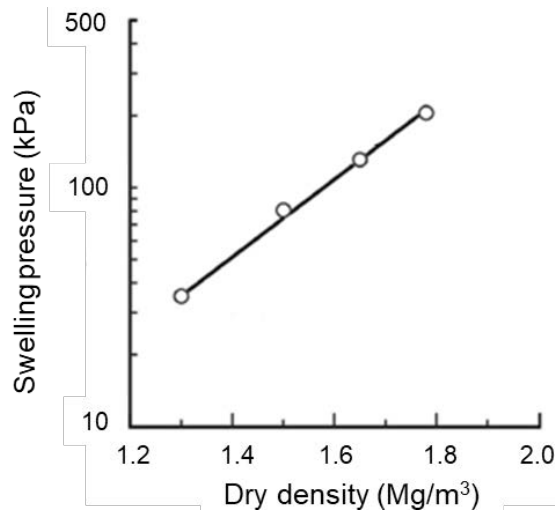


Figure 2-17 Final developed swelling pressure for sand/MX80 bentonite samples (80/20), prepared in different dry densities (Manca et al. 2015).

Likewise, the final swelling strain measured under low or high stress is affected by the material's compaction state (Komine and Ogata, 1994, 2003; Castellanos et al., 2008; Villar and Lloret, 2008; Manca et al., 2015). On Figure 2-18, strain developed under different stresses for loose and dense specimens is presented. Apart from the dry density effect, another parameter appears to influence the swelling potential. When higher stresses are applied upon hydration, the material may not be able to swell for a given density and collapse is obtained. In these cases, it is implied that the swelling capacity has been exceeded and the applied vertical stress is higher than the swelling pressure that would be developed at isochoric hydration conditions.

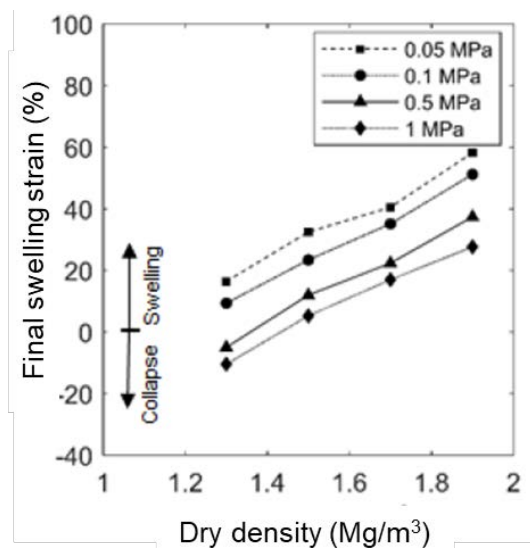


Figure 2-18 Final swelling potential for Febex bentonite samples prepared at different dry densities and hydrated under various vertical stresses (Hoffmann et al. 2005).

In order to better analyse these collapse phenomena during hydration at high stresses, it would be useful to correlate the initial density of compacted material with the subjected stress history. Over-consolidation ratio (OCR) constitutes an indicator of soil's stress history, defined as the ratio of the maximum past consolidation effective stress to the present effective stress ( $OCR = \frac{\sigma'_{v\ max}}{\sigma'_v}$ ) (Mitchell and Soga, 2005). It is evident that higher  $\sigma'_{v\ max}$  leads to more compacted materials. Dang (2007) performed a series of swelling under constant vertical stress tests, on compacted MX80 bentonite and observed OCR dependency. Normally consolidated samples (i.e. hydration under the maximum applied vertical stress upon compaction) presented collapse (Figure 2-19a), with settlement to decrease at higher dry densities (i.e. higher  $\sigma'_{v\ max}$ ). On the other hand, overconsolidated specimens (i.e. hydration under stress lower than the compaction stress) presented clear swelling (Figure 2-19b), with swelling to increase when specimens were unloaded at lower stresses. The later observation is consistent also with other studies (Broc et al. 1988, Villar and Lloret 2008, Castellanos et al. 2008), where the specimens details suggest that swelling occurred on wetting under stresses lower than the compaction stress.

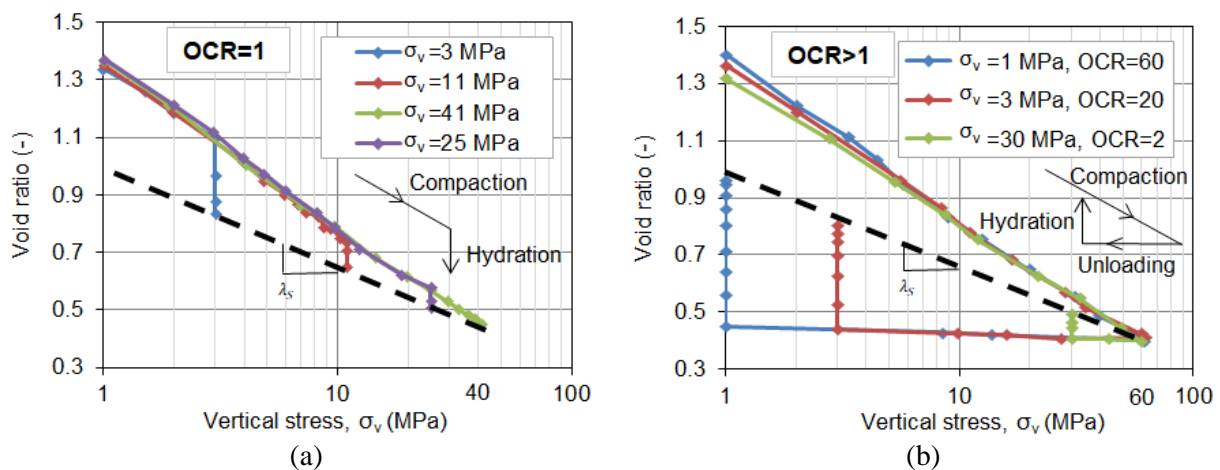


Figure 2-19 Swelling under constant vertical stress of MX80 bentonite, for (a) normally consolidated and (b) over-consolidated samples (Dang, 2007).

In a reverse process, swelling pressure can be determined by swelling under constant vertical stress tests, as it was seen in 2.2.2 for zero swelling strain. The effect of dry density on swelling pressure obtained by both methods is illustrated in Figure 2-20. A slight variation between the two methods is expected for higher densities (Hoffmann et al. 2007).

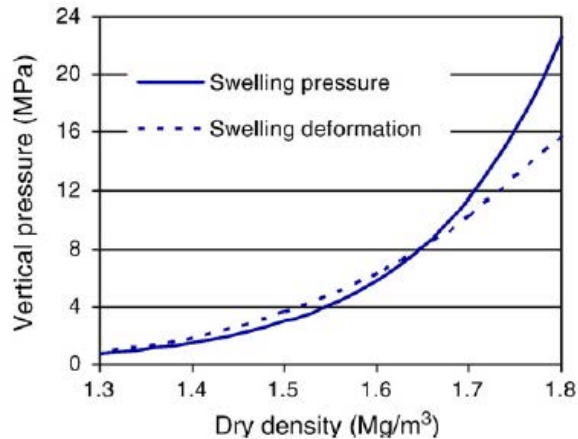


Figure 2-20 Swelling pressure obtained from swelling pressure tests and swelling under constant vertical stress tests (Villar and Lloret 2008).

### 2.3.4.3 Hydration path

Water content increase may occur by applying direct contact of material with water solutions (inundation or infiltration) or by increasing the RH conditions and consequently decreasing soil's suction. In the latter case, several experimental techniques are used to control suction depending on the applied suction range, such as the axis translation technique (Lloret et al. 2003, Hoffmann et al. 2007), the osmotic method (Yigzaw et al. 2016) and the vapour equilibrium technique (Tang et al. 2011a, Wang et al. 2012). Material's hydration using the vapor phase requires more time to reach equilibrium than the liquid phase. Here, the developed swelling pressure over time is discussed for each hydration method.

#### (a) Swelling pressure upon hydration

Since the early studies on compacted swelling clays for use in radioactive waste disposals, a non-monotonic swelling pressure development over time has been reported by many researchers (Pusch, 1982; Pasquiou, 2001; Imbert and Villar, 2006; Herbert et al., 2008; Baille et al., 2010; Seiphoori, 2014; Ye et al., 2014; Yigzaw et al., 2016), illustrated on Figure 2-21a. As it is shown, in the beginning of material's hydration, a rapid increase of swelling pressure is observed, followed by a decrease as water absorption continues. The pressure reduction is related to the collapse of aggregate (i.e. induced by subdivision) as their swelling caused the macroporosity filling (Massat et al. 2016). Nonetheless, this re-arrangement results in material's homogenisation and swelling increases again until reaching a stable value. On Figure 2-21b, similar trend has been reported also for bentonites mixed with other soils (e.g. sand or COx argillite) (Wang et al. 2012, Zhang and Kröhn 2019). Nonetheless, the material's initial conditions may affect this behaviour. For instance, Yigzaw et al. (2016) observed a less evident

behaviour for specimens of lower densities or Komine and Ogata (1994) obtained monotonic increase for samples of higher water contents.

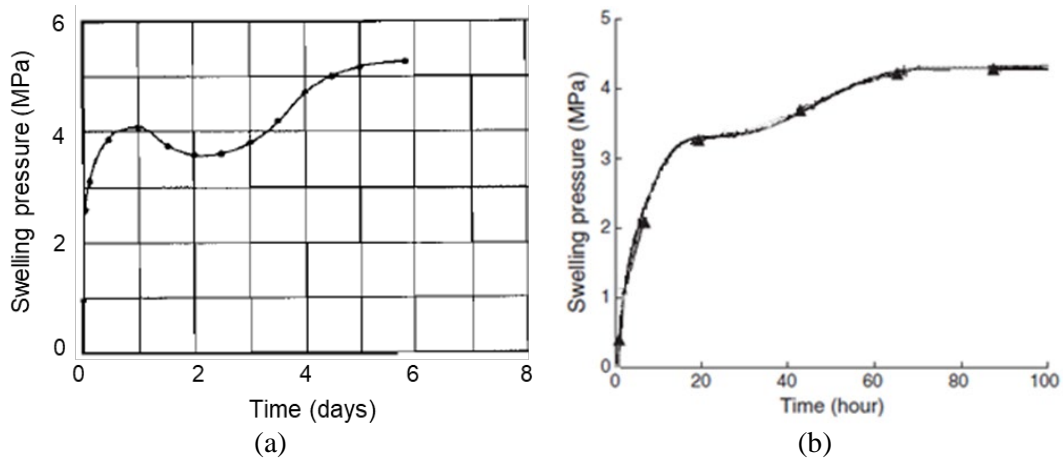


Figure 2-21 Swelling pressure development over time for (a) MX80 bentonite compacted at  $1.60 \text{ Mg/m}^3$  (Pusch 1982) and (b) MX80/COx mixture (70/30) compacted at initial dry density of  $1.70 \text{ Mg/m}^3$  (Wang et al. 2012).

(b) Swelling pressure upon suction decrease

On suction controlled tests, suction decrease is applied in steps using different techniques, while the developed swelling pressure is measured. Upon material's equilibration, lower suctions are subjected to the specimen (Zone I→Zone II of Figure 2-22). On the final step of zero suction (i.e. corresponding to full saturation-Zone III), direct hydration with water is used. In suction controlled conditions, swelling pressure evolution with time (Figure 2-22a) is less “smooth” compared to direct water hydration (Figure 2-21). Nonetheless, as Figure 2-22b better illustrates, the non-monotonic increase is similarly observed with the increase/decrease/increase pattern, characteristic of the inter-aggregate rearrangement during swelling (Lloret et al. 2003, Yigzaw et al. 2016). In general, hydration through vapour phase is a process that takes more time compared to liquid phase (Wang et al. 2012). In some studies on materials with lower smectite content, a small dependency of the final pressure to the applied hydration path was observed, without however presenting large differences (Tang et al. 2011a).

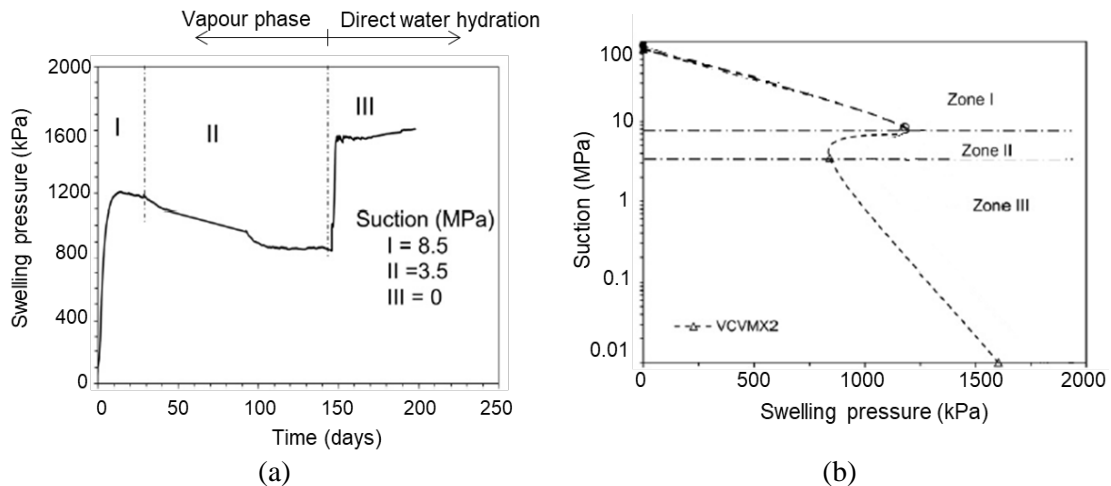


Figure 2-22 Swelling pressure of MX80 bentonite on suction controlled constant volume conditions  $\rho_d = 1.40 \text{ Mg/m}^3$ : Evolution (a) upon time and (b) upon suction decrease (Yigzaw et al. 2016).

At non-constant volume conditions, swelling potential is hyperbolically developed with time as Figure 2-16a already illustrated. No dependence of the final swelling strain on the followed hydration path (liquid or vapour hydration) has been reported. However, swelling potential increases with suction decrease (Yigzaw et al. 2016). Although, the effect of material's initial water content is relatively low, slight decrease might be observed for samples exhibiting higher moisture content, especially when they are hydrated under low applied vertical stresses (Lloret and Villar, 2007; Villar and Lloret, 2008; Lyu et al., 2015).

#### 2.3.4.4 Chemical interactions with infiltrated fluid

Swelling behaviour comes as result of the chemical interaction of clay surface with water molecules. The thickness of the diffuse double layer is dependent on the valence of the exchanged cations and the concentration of electrolyte. For example, the electrical double layer adjacent to the quasicrystal surface is compressed with increasing of NaCl concentration (Shirazi et al. 2011).

In engineering barrier conditions, backfill material is placed inside the galleries, gradually infiltrated by the groundwater. Concrete presence on the disposal structure additionally interacts with the groundwater, provoking a chemical modification and alternation of the pH conditions. Therefore, different chemical compositions of infiltrated solutions have been studied to determine the influence on material's swelling response.

As it was mentioned and also illustrated on Figure 2-23, the effect of fluid's salinity on the hydro-mechanical behaviour of bentonite-based materials shows in general, that increase of salinity and consequently solution's ionic strength, results in reduction of swelling capacity compared to pure water (Karland et al., 2006; Castellanos et al., 2008; Komine et al., 2009;

Shirazi et al., 2011). The effect has been similarly observed in materials with lower smectite content (Siddiqua et al., 2011; Mishra et al., 2009; Manca et al., 2015). Nonetheless, factors such as density state or experimental conditions may modify this effect. More precisely, for materials of higher densities, the influence of the wetting fluid at swelling pressure is less significant (Karnland et al. 2006, Komine et al. 2009, Siddiqua et al. 2011). Regarding the type of exchangeable cations, Ca-bentonites appear as less sensitive compared to Na-bentonites. At non-constant volume conditions, Castellanos et al. (2008) observed that the chemical impact is less significant at higher applied vertical stresses (Figure 2-23). Additionally, different studies reported that specimens hydrated with  $\text{CaCl}_2$  solutions present higher swelling capacity (potential and pressure) than those hydrated with NaCl solutions (Castellanos et al. 2008, Chen et al. 2018).

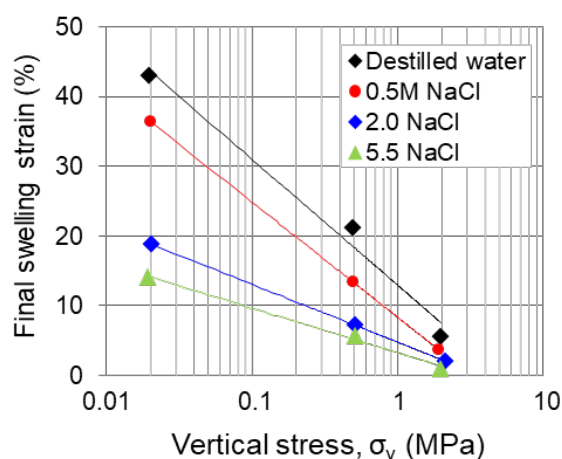


Figure 2-23 Final swelling strains of Febex bentonite, hydrated with different solutions under the different vertical stresses (Castellanos et al., 2008).

In the long-term of the disposal function, the liner of the drifts consisting of cementitious materials will produce alkaline fluids upon their chemical degradation. Past studies mainly on pure bentonites have shown that alkaline conditions could impact materials swelling response (Karnland et al. 2007, Herbert et al. 2008, Tu 2011, Ye et al. 2014). In that context, NaOH solutions are infiltrated in compacted samples, monitoring its effect on swelling pressure (Karnland et al. 2007, Ye et al. 2014). On Figure 2-24a, swelling pressure decrease is illustrated for pH increase on a Na-bentonite (GMZ01). In addition, X-ray diffractions conducted on compacted samples on Figure 2-24b revealed that higher pH increase the amount of dissolved montmorillonite (i.e. lower peak intensity). For natural MX80 bentonite, Karnland et al. (2007) reported decrease of swelling pressure at higher concentrations of NaOH solutions (0.3 M and 1.0 M corresponding at pH of 13.3 and 13.8), which was attributed to mineral modification (dissolution of silica) causing mass loss and density

reduction. Cuisinier et al. (2009) confirmed that Manois argillite with MX80 additive underwent dissolution processes induced by the high pH conditions.

The chemical impact has been also evaluated by studying the material's plasticity, where plasticity was reduced as solution's ionic concentration increases (Mishra et al. 2009, Shirazi et al. 2011, Zhang et al. 2012).

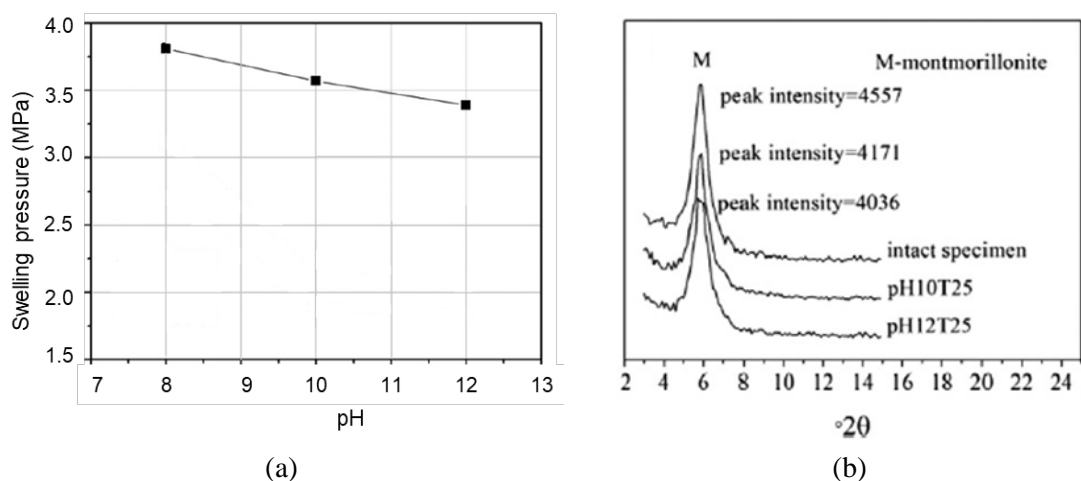


Figure 2-24 GMZ01 bentonite saturated with solutions of different pH: results of (a) swelling pressure measurements and (b) X-ray diffraction profiles of compacted samples (Ye et al. 2014).

#### 2.3.4.5 Temperature effect

According to several disposal concepts (e.g. SKB, Nagra), buffer material will be placed in contact with the waste containers, while heat release will occur from the radioactive waste decay. In that context, the effect of heating on swelling response has been addressed in previous studies (Robinet et al. 2003, Villar et al. 2010, Ye et al. 2014). As Figure 2-25 shows, swelling capacity can be reduced on temperature increase and as a consequence, higher hydraulic conductivity is observed.

However, it should be noted that in the French disposal system, backfill or sealing materials will not be in contact with waste packages and therefore the temperature effect is not considered.

#### 2.3.4.6 Conclusions

The macroscopic swelling capacity of bentonite-based materials was analysed considering different parameters. Besides the percentage of swelling clay (i.e. bentonite content) inside the hydrated material, “external” conditions are expected to govern the hydro-mechanical performance. The main obtained remarks are briefly summarised as follows:

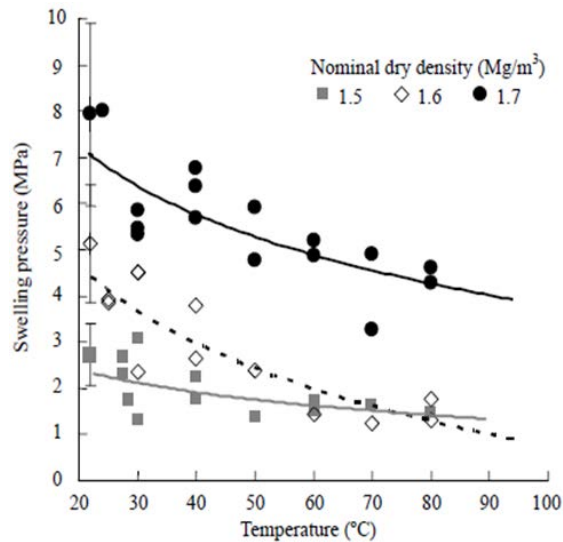


Figure 2-25 Effect of temperature on final swelling pressure of Febex bentonite compacted in different dry densities (Villar et al. 2010).

- More compacted materials before hydration increases the swelling response (e.g. exponential increase at constant volume conditions).
- A characteristic non-monotonic evolution of swelling pressure with time is developed, related to the collapse of macropores due to particles swelling.
- Direct water hydration accelerates the swelling pressure development in comparison to suction controlled conditions (i.e. vapour phase).
- The ionic strength of the infiltrated solution impacts materials swelling: the higher the ionic concentration, the lower the obtained swelling capacity.
- The higher temperatures occurring during hydration impact the swelling performance.

## 2.4 Implementation techniques of remoulded materials on radioactive waste disposal

Different concepts have been proposed to emplace the backfill material in the repository, according to the adopted configuration of the engineering barrier. In general, vertical shafts are more efficiently backfilled than horizontal tunnels, due to the gravity effect. During the last decades, several large-scale experiments have been carried out to investigate the implementation feasibility of backfill and sealing the disposal facilities by simulating the reality conditions. A small summary is presented below, focusing on the implementation form and the materials composition.

It has already been pointed out that sealing materials are mainly composed of swelling clays, whereas the supplementary role of backfill in the sealing elements, allows the reduction of the

swelling clay and gives the opportunity for reuse the excavated materials. In this framework, bentonite, excavated soils and sand have been studied in different forms over the years. According to the available techniques, these materials can be installed with different applications, such as in-situ compaction, bricks/blocks and pellets. In particular:

(a) In-situ compaction

On this concept, the material is compacted at its maximum density in the optimum water content. The objective is to achieve a compaction energy corresponding approximately to 95% of Standard Proctor energy by means of a compactor (Londe et al. 2008). Excavated material pure or with additive is compacted in thick inclined layers (Johannesson et al. 2007). Andra performed a drift backfilling demonstrator experiment, using pure excavated remolded COx and a mixture of COx/sand (33/67) (Remblayage de Richwiller”- 2004, in Figure 2-26), obtaining for both cases good contact between the backfill and the walls, except for the top of the drift (Andra 2016a).

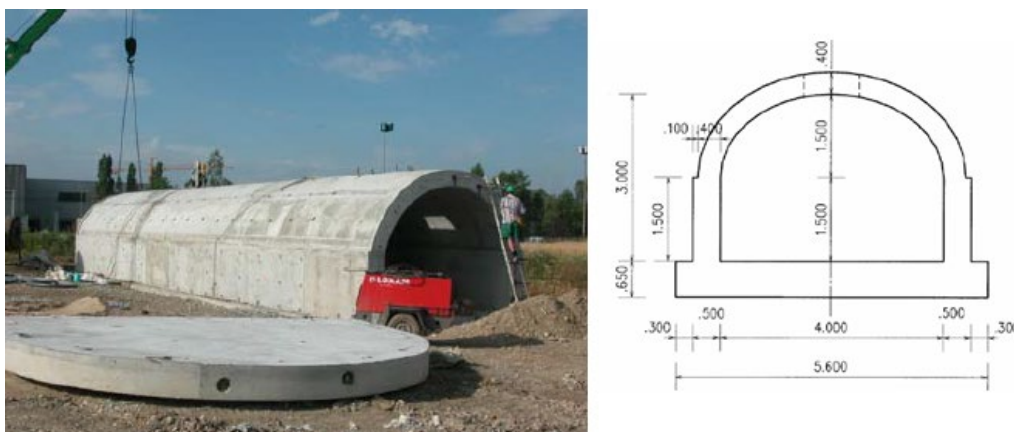


Figure 2-26 Presentation of Backfilling Demonstrator experiment (“Remblayage de Richwiller”- 2004) (Londe et al. 2008).

(b) Brick/blocks

Highly compacted material has been used as seal and buffer. In this case, the material can be compacted either on standard or more complicated shapes according to the desired filling volume. For instance, the Swiss and the Swedish disposal systems use bentonite blocks to support/surround the waste canisters (Mayor et al. 2005, Johannesson et al. 2007, Villar and Lloret 2007). On the other hand, in the French concept, Andra has examined the use of bentonite/sand bricks in order to construct the seals of Cigeo project in the framework of NSC experiment (Figure 2-27) (de la Vaissière et al. 2014).



Figure 2-27 Construction of seal walls of bentonite/sand (40/60) bricks inside the drift for the NSC experiment (de la Vaissière et al. 2014).

(c) Granular/pelletized material

Pelletized material presents the advantage of easily backfilling volumes of irregular shapes that can be found inside the galleries (Imbert and Villar 2006). Thus, bentonite pellets have been used to fill voids formed between bricks/blocks and the rock walls (Arvidsson et al. 2015). Additionally, the pelletized implementation technique requires almost no compression during its installation, in order to achieve a given average dry density.

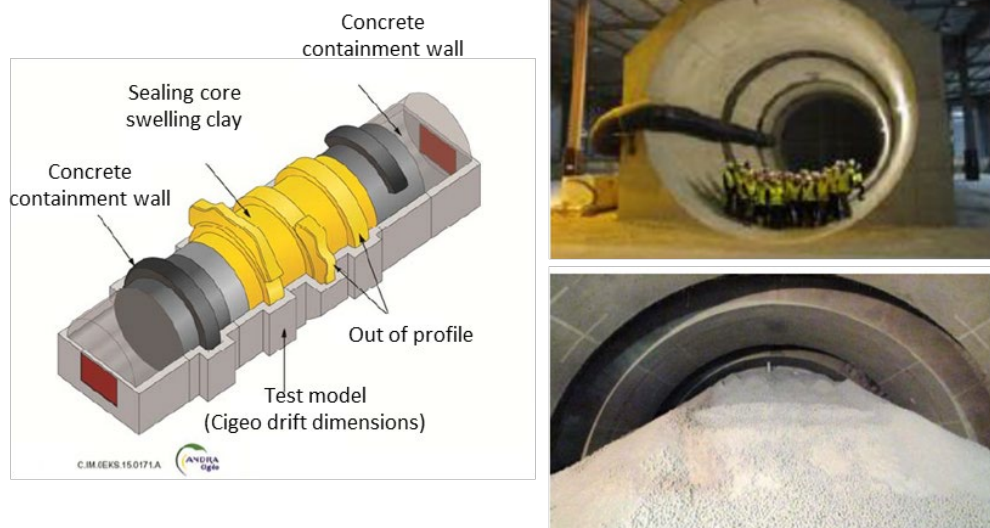


Figure 2-28 Design concept, construction and installation of pelletized swelling claycore seal during FSS experiment (Andra 2016a).

On large scale, Andra managed to successfully install a bentonite pellet/powder mixture (70/30) as seal in the Full-Scale Seal experiment (FSS) (Figure 2-28), inside

---

a 1:1 scale drift model (internal diameter of 7.6 m, 35.5 m long) (Noiret et al. 2016). A machine composed of two screw augers was specially designed and constructed to carry out the material installation. Pellet and powder material were conveyed via the screw auger and left to drop in the gallery under the gravity effect. A dry density of  $\sim 1.50 \text{ Mg/m}^3$  was obtained upon the emplacement without compaction, presenting slight variation between the top and the bottom of the drift.

Summarizing the abovementioned cases, it is clear, that remoulded COx has only been implemented using in-situ compaction. Pelletizing process has not been attempted on excavated argillite COx and no information is available until today regarding the feasibility of fabricating pellets containing COx.

## **2.5 Swelling clay pellets at disposal systems**

In the framework of radioactive disposal systems, swelling clay pellets made of bentonite have been investigated as backfill/sealing material since the early 2000s (Pasquiou, 2001; Pusch et al., 2003; Hoffmann et al., 2007), due to their implementation advantages, facilitation on technological void filling and their high density/suction (Alonso et al., 2010; Teodori et al., 2012; García-Siñeriz et al., 2015). Different terms have been used to describe these highly-compacted pre-fabricated granules of given shape (e.g. granular/granulated material, pelletized mixture, pellets). The following sections aim to present the state of the art considering the available pelletizing techniques and study the fabric evolution of pelletized materials from the initial to saturated state, as well as their hydro-mechanical response.

### **2.5.1 Pellet fabrication**

The process of pelletization has been firstly introduced by the pharmaceutical domain. In this framework, it is considered as a size-enlargement process applied to transform fine powders or particles of drugs into approximately spherical units, the so-called pellets (Hirjau et al. 2011). Different manufacturing procedures lead to different pelletizing techniques.

According to Lavanya et al. (2011) and Muley et al. (2016), the pelletizing methods can be summarized as:

1. Agitation, where fine particles are converted into pellets through liquid addition and continuous rolling/tumbling motion (balling process).
2. Compaction, where pressure is applied forcing particles to create pellets of defined shape and size. Depending on the mechanical means, two sub-methods are identified:
  - (a) Compression, when mixtures are compacted into pellets of defined dimensions

- 
- (b) Extrusion, where usually a wet initial mass is inserted inside a cylinder and then extruded. The material can be additionally rounded into spheres and a final drying is applied.
  3. Layering, that involves the deposition in layers of the raw material on a pre-formed nucleus.
  4. Globulation, where liquid materials are atomized into pellets via spray drying or spray congealing.

Similar with powders, soil materials have been transforming into pellets by applying compaction methods. Particularly, in the framework of nuclear waste disposal, pellets have been fabricated by extrusion (Johnsson and Sandén 2013, Marjavaara et al. 2013, Stastka and Smutek 2015), roller or uniaxial compression (Van Geet et al. 2005, Imbert and Villar 2006, Molinero Guerra et al. 2017, Stastka et al. 2019, Darde et al. 2020) as well as by crushing highly compacted material (Hoffmann et al. 2005, Karnland et al. 2008, Alonso et al. 2011, Seiphoori et al. 2014, Zhang et al. 2018). Examples of fabricated pellets resulting from the abovementioned techniques are illustrated on Figure 2-29 - Figure 2-31. It can be seen that their form depends on the geometries of the pellet machine (molds, dies) or the grinding procedure following the fabrication. It is evident that pellets present well-defined shape and size or wider grain sizes after being crushed.



Figure 2-29 Extruded pellets composed of IBECO bentonite (Johnsson and Sandén 2013).

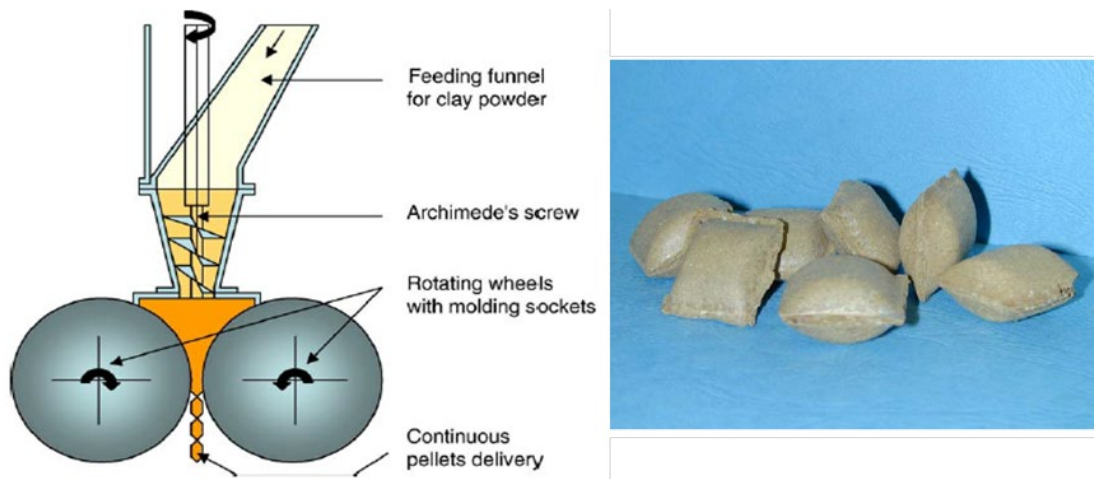


Figure 2-30 FoCa clay pellets fabricated by roller compaction (Imbert and Villar 2006).

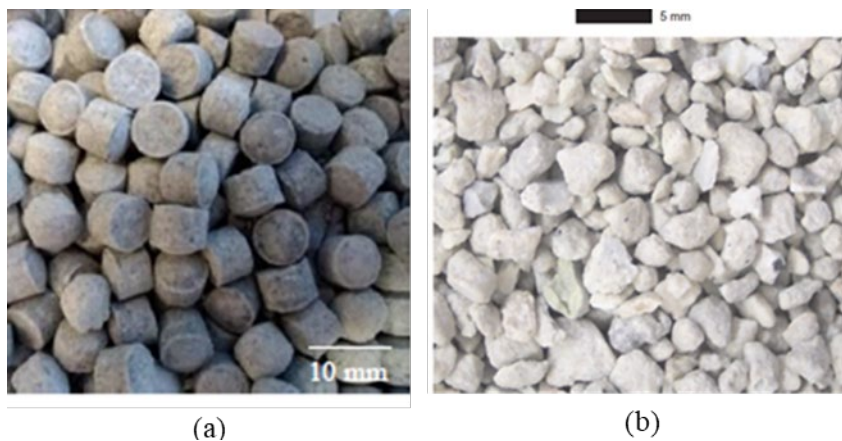


Figure 2-31 Pictures of bentonite pellets obtained (a) by compaction of MX80 bentonite and (b) by crushing highly compacted Febex bentonite (Dardé, 2019; Alonso et al., 2011).

### 2.5.2 Pelletized material at initial state

Low porosity and low water content (i.e. high suction) are typical features of pellets. Similarly with the compacted swelling clays, a single pellet exhibits an almost bimodal distribution of pores at non-hydrated conditions (Molinero-Guerra et al. 2019). As Figure 2-32 illustrates, macropores tend to disappear, due to high compaction and a clear peak is observed in micropore region inside the pellet around 13.3 nm (intra-pellet porosity). Similar observations were reported by Hoffmann et al., (2007, 2005) on Febex bentonite pellets. Seiphoori et al. (2014) obtained a single-modal PSD for MX80 grain, presenting micropores with very similar size (~12 nm). The difference in pore distribution was attributed to the different condition applied during manufacture processes (i.e. lower water content on pellets facilitates the formation of aggregates).

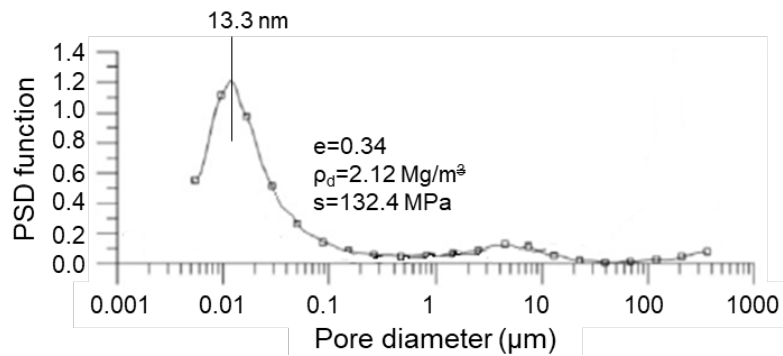


Figure 2-32 Pore size distribution of MX80 bentonite pellet at the initial state (Molinero-Guerra et al. 2019b).

A pelletized assembly is composed of pellet mixtures or mixtures of pellets with finer material (e.g. powder). Naturally, voids are created between these materials generating a new level of porosity. Hoffmann et al. (2007) investigated the pore distribution of mixtures of pellets in various density states (Figure 2-33). It was seen that the bimodal pore distribution was once again obtained. This time, an inter-pellet porosity was observed, more evident at mixtures of low density where no mechanical compaction was applied. In general, the smaller group of pores (micropores) remains essentially constant for all densities. In addition, similarly with compacted powders, density variation affects the macroporosity. Experimental data from Pasquiou (2001) on different-sized pellet mixtures showed that mixture's total porosity is attributed by 2/3 to the inter-pellet and by 1/3 to the intra-pellet porosity, verifying that at non-hydrated conditions, mixture's packing states is dictating by voids existing between pellets (macroporosity).

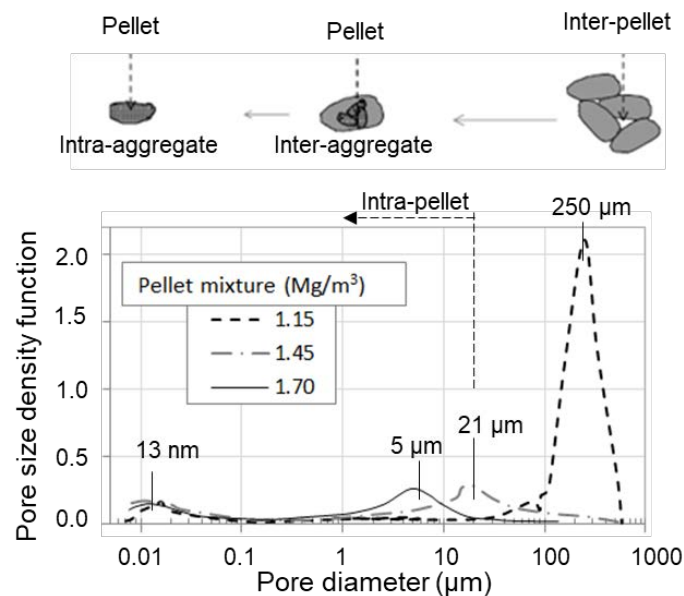


Figure 2-33 Pore size distribution of Febex bentonite pellet mixtures at different densities. Lowest density obtained by pluviation, higher densities by compaction (Hoffmann et al., 2007).

---

### 2.5.3 Evolution upon hydration and hydro-mechanical response

The pelletized assembly presents granular structure with distinct voids upon its emplacement (Figure 2-34). As material is hydrated, the mixture absorbs progressively water, leading to swelling. Van Geet et al. (2005) studied the evolution of materials structure by X-Ray tomography, in order to visualise the fabric modification. The investigated mixture was composed of FoCa clay pellets (Figure 2-31) and powder. Clear heterogeneities in density on the installation were measured (Figure 2-35). During hydration, swelling is initially observed on pellets due to their higher density and suction, whereas the low compaction of the FoCa powder results in macropores with negligible capillary suction. The pellet degradation due to swelling gives place to powder compaction, leading to a progressive homogenization of the material. Similar observations reported also by Molinero Guerra et al. (2018), where MX80 pellet/powder mixture lost its initial granular structure to reach a final homogeneous state after 100 days of hydration (Figure 2-36).

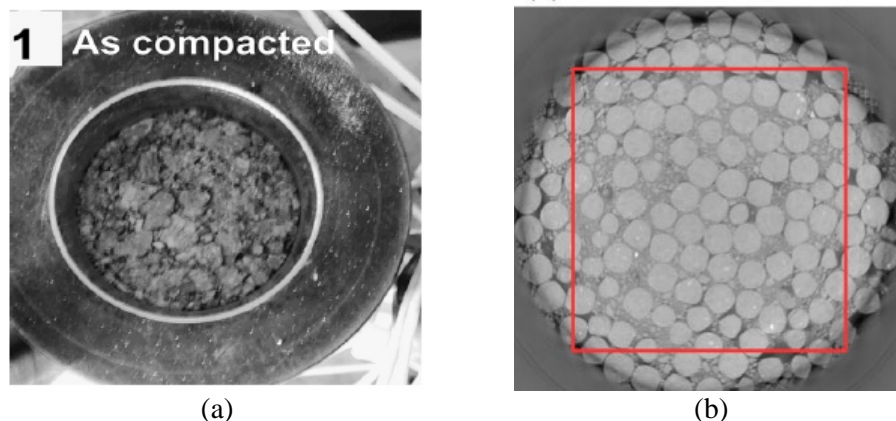


Figure 2-34 Granular structure and macrovoids of bentonite in: (a) pellets mixture (Hoffmann et al. 2007) and (b) pellet/powder (80/20) mixture at initial non-hydrated state (Molinero Guerra et al. 2017).

It should be mentioned that even in large-scale experiments, such as the “EB experiment” in the URL of Mont Terri (Switzerland), the bentonite barrier reached full saturation and the granular material appears to be homogeneous with no gaps. A relative variation of the final dry density obtained (1.12-1.48 Mg/m<sup>3</sup>) was probably caused by the initial segregation of the granular mixture upon emplacement as well as the initial “gravitational” distribution of water from the artificial hydration system (García-Siñeriz et al. 2015).

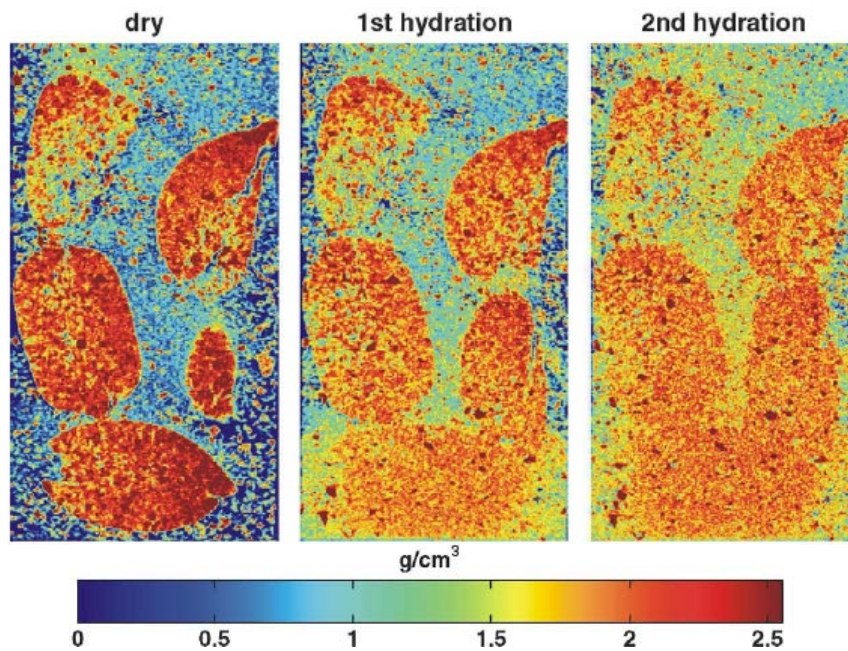


Figure 2-35 Visualization of density evolution on FoCa clay pellet/powder (50/50) mixture at initial state, after two weeks of hydration and 6 weeks of hydration (Van Geet et al. 2005).

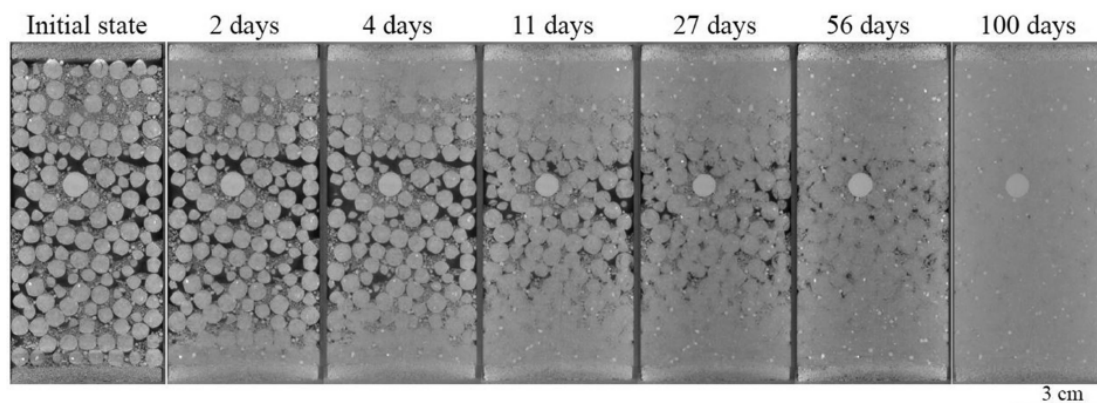


Figure 2-36 Evolution of the granular structure of a MX80 bentonite pellet/powder mixture during hydration (Molinero Guerra et al. 2018).

Apart from the evolution of the pelletized material's structure during hydration, interesting results regarding its hydro-mechanical response have been presented. Hoffmann et al. (2007) evidenced that the after a short initial phase of high permeability (i.e. high inter-pellet voids), the permeability was rapidly reduced and reached saturation, where it appeared as independent to material's form (bentonite pellets or bentonite powder). Contrariwise, the hydraulic behaviour was mainly controlled by the overall dry density of the sample rather than the initial grain size distribution (Figure 2-37). These remarks are in accordance with Karnland et al. (2008), where no significant difference was also shown between original bentonite and pelletized bentonite materials.

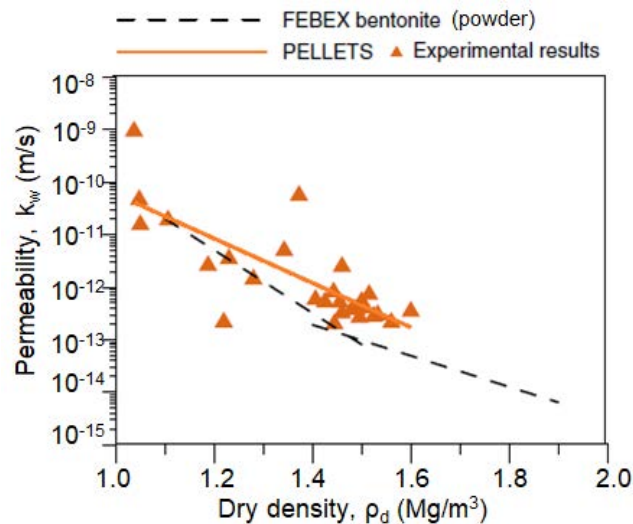


Figure 2-37 Saturated permeability of bentonite pellet mixtures prepared at different dry densities (Hoffmann et al., 2007).

Experimental studies on pelletized samples of different dimensions ( $D=120\text{mm}/H=50\text{mm}$  and  $D=35\text{mm}/H=10\text{mm}$ ), showed similar development of swelling pressure with the original non-pelletized material at common densities (Imbert and Villar 2006, Karnland et al. 2008). It can be evidenced from Figure 2-38, where the evolution of swelling pressure over time is presented for bentonite pellet/powder mixture (50/50) and powder. The typical development of swelling pressure with time is observed here similarly with compacted swelling clays (section 2.3.4.3). Pellets are the first hydrated due to their higher suction developing a rapid increase of swelling pressure. Pellets swelling causes loss of their initial structure and decrease of density (shown also in Figure 2-35), which activates collapse of macrostructure expressed by a decrease in strength. Upon the gradual homogenisation of the material, swelling predominates over the collapses and the final stage of swelling pressure is obtained. In addition, it was reported that minimum height of 50 mm needs to be formed in order to avoid misleading scale effects (Imbert and Villar 2006). It is worth noting that in both studies (Imbert and Villar 2006, Karnland et al. 2008), specimens containing pellets were statically compacted to achieve the desired densities. On the other hand, Dardé (2019) performed constant volume hydration on several MX80 bentonite pellet/powder mixtures ( $D=60\text{mm}/H=30\text{mm}$ ) with different densities ( $1.05\text{-}1.50\text{ Mg/m}^3$ ) without applying compaction. The final swelling pressures were compared with those estimated by Wang et al. (2012) for the same material. The obtained values were once again of the same magnitude for both pelletized and non-pelletized samples.

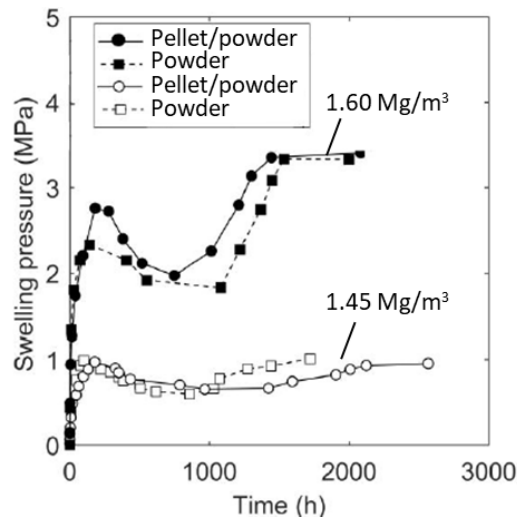


Figure 2-38 Evolution of swelling pressure of pelletized and non-pelletized material (FoCa bentonite) over time, for different dry densities (Imbert and Villar, 2006).

*Important remark*

It has been clearly pointed out that swelling response is governed principally by the material’s overall density (inter-pellet porosity). In addition, studies showed no significant impact of materials form (pelletized or powdered) on its response at saturation.

## 2.6 Packing state of granular materials on emplacement conditions

It was seen that at conditions prior to hydration, pellets assembly presents a granular state with clear inter-pellet voids (section 2.5.2). On the other hand, at hydration, the initial dry density governs the material’s hydro-mechanical behavior, since lower initial voids increase swelling pressure (2.5.3). Consequently, emplacement conditions and saturation are inextricably connected.

In an attempt to better understand the conditions affecting the packing state of a granular material, a bibliographical review is conducted to investigate the parameters influencing the compaction state, expressed either as resulting packing density or as porosity. For the present concept, it is of high importance to define that the conditions where voids are minimized and density is maximised are characterized as optimal.

At dry conditions, a granular medium presents an overall packing state, which could mainly be defined by factors such as the following:

- (a) density and shape of grains
- (b) grain size distribution (GSD)
- (c) surface characteristics (smooth or rough)
- (d) implementation protocol (e.g. vibration, compaction, etc.).

Clearly, the higher the intra-grain density, the more compacted the material's state. Nonetheless, a pelletized mixture's global density is governed by the inter-pellet pores (Figure 2-33) and therefore the density within a grain is not considered as influential parameter.

Pellets as artificial granules are formed and shaped according to the adopted manufacturing procedures. A common parameter to study the shape effect of particles is sphericity, which expresses the ratio of the surface area of a sphere with the same volume as the given particle to the surface area of the particle. Zou and Yu (1996) performed experiments on mono-sized spherical and non-spherical particles (e.g. disks and cylinders) that were deposited on cylindrical container at loose random packing. It was observed that as sphericity decreases (i.e. particles of less spherical shape), porosity increases and higher initial voids are measured (Figure 2-39a). Lower porosities are achieved after material's tapping, with still following very similar trend (Figure 2-39b). The behaviour was also reported on bimodal mixtures containing spherical and cylindrical components (Yu et al. 1992). Garitte et al. (2015) witnessed similar behaviour on rounded and elongated bentonite pellets and Cho et al. (2006) outlined decreases particle mobility on sands with irregular grains. It is believed the effect is related to a combination of facts connected to particle geometry, such as the bridges that are likely to be formed between the corners of angular parts, the developed inter-particle frictions and surface roughness.

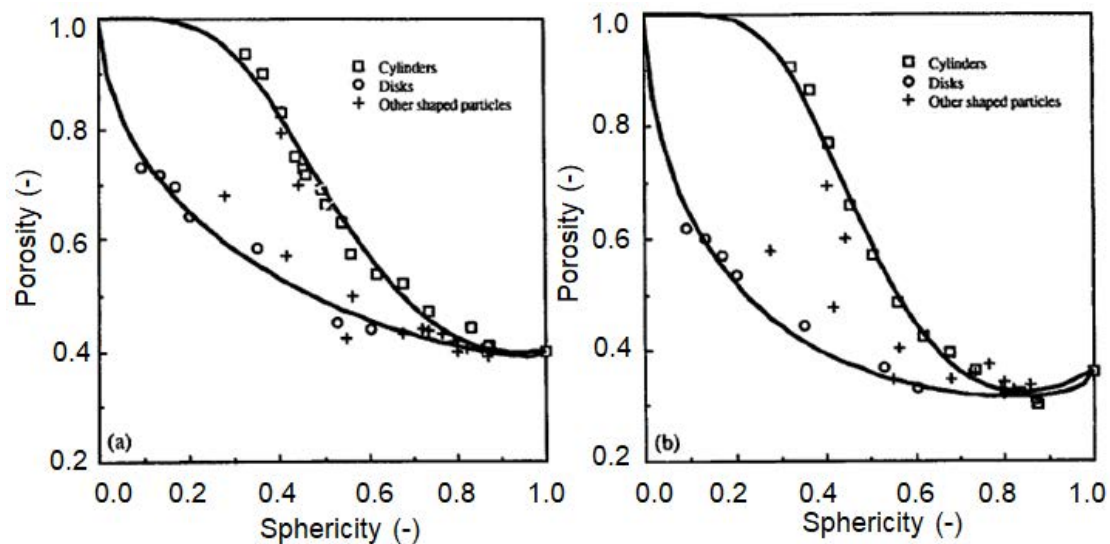


Figure 2-39 Evolution of porosity in relation to sphericity on mono-sized spherical and spherical particles: (a) at loose deposit and (b) after tapping (Zou and Yu 1996).

The concept of optimal packing density has been of interest to the research community for a few decades (Westman and Hugill, 1930; Standish and Borger, 1979; de Larrard, 1999). In terms of grain sizes, the aim of packing density concept focuses on achieving an “optimum grain size distribution” to reduce the inter-particle voids in a mixture, which eventually leads

to the most compacted state (Kumar and Santhanam 2003). There are models investigating the optimum GSD, which can be divided into two main categories:

- discrete models, where packing systems containing two or more discrete classes of particle sizes are considered and
- continuous models, assuming that all possible sizes are present in the granulometry.

The fundamental assumption of the discrete approach is that each particles class size will be packed to its maximum density in the available volume. Conversely, in continuous approach no gaps between the size classes are observed (i.e. discrete approach having adjacent size classes ratios that approach 1:1) (Mangulkar and Jamkar 2013).

Ideal size distribution curves are representative examples of the continuous models. According to this approach, the granular material follows granulometries of well-graded soils (Head 2006). Specific equations describe the PSD of the material by calculating the passing percentage,  $P(d_i)$  of the each diameter  $d_i$  used in the mixture. Table 2-2 summarizes the ideal curves as reported by Ghasemi (2017). Specimens prepared after ideal grading models have been used for multi-sized mixtures containing several size fractions (Hoffmann et al. 2005, Head 2006, Garitte et al. 2015, Zhang et al. 2018).

Table 2-2 Ideal grain size distribution curves resulting in optimum packing (Ghasemi 2017).

|                               |  |            |
|-------------------------------|--|------------|
| Fuller and Thompson (1907)    | $P(d_i) = \left(\frac{d_i}{d_{max}}\right)^q$              | $q = 0.5$  |
| Andreasen and Andersen (1930) |  | $q = 0.37$ |
| Funk and Dinger (1994)        | $P(d_i) = \frac{d_i^q - d_{min}^q}{d_{max}^q - d_{min}^q}$ | $q = 0.37$ |

$q$ : grading parameter

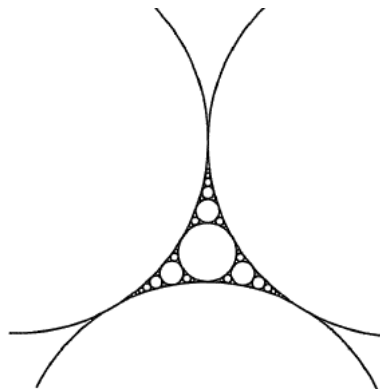


Figure 2-40 Packing of soil particles following idealized Fuller's curve (Head 2006).

Discrete models also investigate packing state as a function of the grain sizes in the mixture. Nonetheless, bimodal and trimodal mixtures are usually studied (Standish and Borger 1979, Standish and Collins 1983, Marshall and Dhir 1986, Pasquiou 2001, Gatabin et al. 2014). On Figure 2-41, the effect of particle's size fraction on bimodal samples, where packing density increases with increase of fractional solid volume of large particle until a certain value and then expands (Dodds 1980, Pasquiou 2001). In the case of ternary mixtures, Standish and Borger (1979) reported that lower porosities are likely to be obtained when the proportion of the smallest size component is intermediate in the mixture. Additionally, particle size ratio as important a factor influencing the resulting packing state (Yu et al. 1992, Zheng et al. 1995, Wiącek 2016). This parameter is defined as the ratio of an existing size in the mixture to the maximum used grain size and practically expresses the gradation of the granular material (i.e. lower size ratios result in larger ranges of particle sizes). In binary mixtures as size ratio decreases, the smaller particles can easily penetrate voids formed by larger particles, resulting in more compacted samples (Yu and Standish 1987).

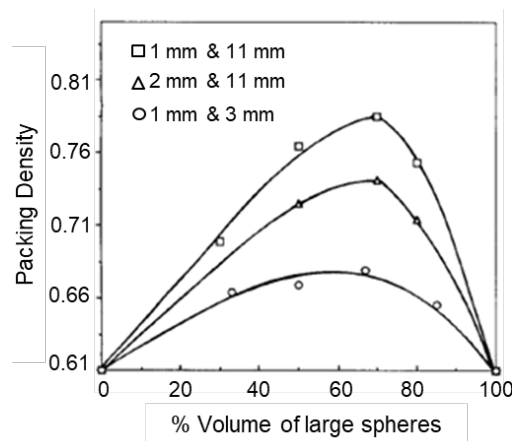


Figure 2-41 Effect of GSD on packing state on bimodal mixtures and (Yu et al. 1992).

From another point of view, particle size dictates the forces developed between particles and eventually their packing state. For instance in fine powders, electrostatic forces are more important than gravity and cohesion between particles is developed (Zou et al. 2011). Experimental studies on fine powders showed that increase of inter-grain cohesion leads to a reduction of packing density (Vandewalle et al. 2007). Nader et al. (2017) noted that an increase of intra-granular cohesion hinders material's compressibility on samples tested upon oedometric compression. On the other hand, coarse-sized spheres are considered as non-cohesive granular materials, where inter-particle friction can impact the resulting packing state. Material characteristics indicating smooth or rough surfaces, facilitate or hinder compaction respectively (Vandewalle et al. 2007, An et al. 2008). It is evident, because the inter-particle friction makes tends to prevent particles from sliding.

In the “final” stage of the material’s implementation, the adopted process will additionally impact the particle rearrangement. At gallery conditions, implementation can be considered as a dynamic process indicating by the available technological means. In smaller scale experimental studies have been conducted to investigate the impact of the applied implementation conditions on the resulting packing state. For instance, studies on monosized spheres under vibration show density dependence on the time and frequency of the vibrating process (An et al. 2008, 2009). More recently Liu et al. (2019) observed that denser samples are formed with vibration of mixtures made of different sizes on non-spherical particles. Nonetheless, after a certain time of vibration ( $t=180$  s) no variation of density was observed (Figure 2-42). Vaid and Negussey (1984) investigated the effect of drop height on pluviated natural sands, observing that void ratio decreased asymptotically as drop height was higher.

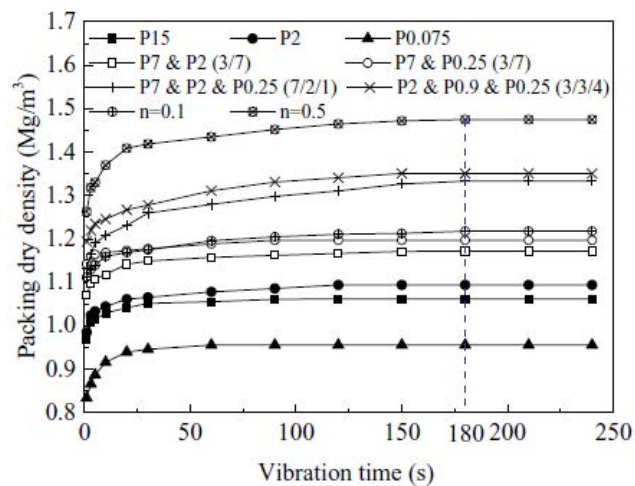


Figure 2-42 Effect of vibration time of specimens with different GSD on packing state (Liu et al. 2019).

## 2.7 Identification of needs and proposed strategy of the present PhD study

The previous literature review clarified that COx argillite is necessary to be enriched with bentonite additive in order to meet design requirements in swelling behaviour terms. Nonetheless, bentonite presence needs to be contained as minimum as possible to reduce cost and therefore 30% of bentonite was set as the highest target boundary for the backfill material.

Several parameters are affecting material’s final response. In accordance with the Cigeo requirements, as decisive factors are identified the following:

- Smecite content (i.e. bentonite content)
- Initial compaction state (i.e. dry density)

- 
- Infiltrated water chemistry (ground water and alkaline conditions).

One of the most interesting outcomes from the overview is that despite the clear initial granular state, pure bentonite pellet mixtures present similar hydro-mechanical response with the original “powdered” material for similar compaction states. Nonetheless, no available knowledge has been provided on swelling behaviour pelletized COx argillite (i.e. less expansive material). In this concept, the present study identifies the packing state of the pelletized granular material as the most significant design parameter. In that case, the studied pelletized material will be fabricated in order to result in the most compacted state, focusing especially on the granulometric characteristics and the implementation protocol for given pellet shape.

On this direction, the feasibility assessment the COx/MX80 pelletized mixture will be carried out, including its optimisation and hydro-mechanical characterisation of the material. Design requirements indicate always the MX80 minimization. Therefore the following experimental program is proposed:

- 1. Numerical study focusing on the optimisation of the used Grain Size Distribution of pellets**

In the beginning of the study, the granulometry of the pelletized assembly is optimised by the means of simulations using the Discrete Element Method (DEM). Different GSD (grain sizes and proportions) are tested and the optimal is selected in order to result in the most compacted state.

- 2. Pelletizing process and COx/MX80 pellet fabrication**

The initial powdered COx/MX80 mixtures are pelletized for the sizes selected by the DEM. The pelletization is carried out by means of tablet pellet machine in order to sufficiently produce pellet in semi-industrial scale.

- 3. Experimental study for maximising the resulting packing density**

The resulting density state is evaluated experimentally for the fabricated pellets. A series of supplementary tests in alternative granulometric configurations is conducted to maximise the mixtures density, defining the investigated density range.

- 4. Preliminary experimental characterization of COx/MX80 pellet mixtures from initial powdered material**

A parametric study on the hydro-mechanical swelling response of various COx/MX80 is conducted in order to characterize the material’s swelling capacity for the equivalent emplacement conditions (i.e. investigated density range). The effect of bentonite content, density state and water chemistry is examined.

---

## 5. Experimental study on CO<sub>x</sub>/MX80 pelletized form on the selected Grain Size Distribution

The experimental study on density maximisation allows us to define the final granulometry of the used material. Consequently, pelletized mixtures corresponding to the final GSD are hydro-mechanically tested, in order to evaluate the material's response in terms of swelling capacity and hydraulic conductivity on saturation.



---

## **Chapter 3 - Numerical study for optimisation of pellets assembly**

The objective of the chapter is to determine the granulometric distribution (GSD) of a pelletized assembly, leading to the most compacted packing state (i.e. optimal conditions). Numerical simulations following the discrete element method (DEM) are conducted. Gravitational deposits are carried out on bimodal and trimodal samples containing different sized spheres. The optimum GSD is selected and a parametric investigation examines the effect of the inter-particle friction and deposit height on the resulting packing dry density. The chapter is developed in the following main parts:

- 3.1 Introduction
- 3.2 Numerical approach: theoretical aspects and calculations
- 3.3 Bimodal and trimodal samples: Results, parametric study and discussion
- 3.4 Conclusions and optimum GSD obtained by DEM

---

### 3.1 Introduction

Dense packing state is an essential property of a pelletized assembly, planned to be used as backfill in radioactive waste disposal systems. Therefore, minimization of initial voids needs to be the criterion of the material's selection.

A brief literature review already proved that the investigation of packing state is a multi-parameter study. Experimental investigations on this direction can be an expensive and definitely a time-consuming process. Consequently, numerical simulations appear to increase in popularity for many researchers. Among other, the discrete element method (DEM) has been widely used to simulate the behaviour of granular media.

In that framework, the present study examines the resulting packing density of a pellet mixture by using numerical means. The primary objective is the identification of the granulometric conditions (grain sizes and proportions) that lead to the densest state without compaction. It is reminded that this state is defined as optimum and thus the granulometry is referred to as "optimum GSD".

In the following sections, numerical simulations using the DEM, examine the compactness of a pelletized mixture, by reproducing gravitational deposits of a dry granular material composed of spheres inside a cuboidal cell. In the beginning, granulometries obtained from past experimental studies are tested and compared with the present numerical results, evaluating the repeatability of the adopted process. Additional bimodal and trimodal mixtures compatible with specific criteria (e.g. pelletizing process, laboratory scale means) are tested and the optimum GSD is accordingly determined. The effect of implementation protocol (i.e. deposit height), as well as the material's surface characteristics (i.e. inter-particle friction) on the resulting density state are analysed, by conducting a parametric study on the optimum GSD.

### 3.2 Numerical approach: theoretical aspects and calculations

The compactness of a pelletized mixture is studied numerically by simulating the deposit of a sample containing spheres under the effect of gravity. The numerical experiment is conducted in 3D conditions. A sample of defined granulometry (grain sizes and volumetric proportions) is left to fall inside a cubical container of fixed dimensions and the resulted dry density is measured.

### 3.2.1 Numerical model

The open-source software LMGC<sup>90</sup> is used as the numerical tool for the present study. The Discrete Element Method uses the Non-Smooth Contact Dynamics (NSCD), suitable for rigid and/or deformable collections of bodies. The NSCD considers contact of impenetrable particles and dry friction between particles (Jean and Moreau 1992, Jean 1999). The problem is studied at two levels: movement equations of the particles expressed using global variables (kinematic variables) and the interactions between particles described using local variables (contact variables) (Nader et al. 2017).

The system identifies a unique pair of bodies formed by the candidate object  $O$  and the antagonist object  $O'$  (Figure 3-1), with  $g$  the distance between them ( $g \geq 0$ ). Once contact has been achieved, the normal reaction force  $R_N$  is activated following Signorini's contact law. Otherwise, the contact force disappears for positive distance  $g > 0$ . Coulomb's friction law is applied in the case of dry contact without cohesion between particles and is expressed by the tangential force  $R_T$  and sliding velocity  $U_T$ . Sliding movement is developed when  $R_T$  overcomes the product of friction coefficient  $\mu$  and normal reaction  $R_N$  ( $R_T = \mu \cdot R_N$ ).

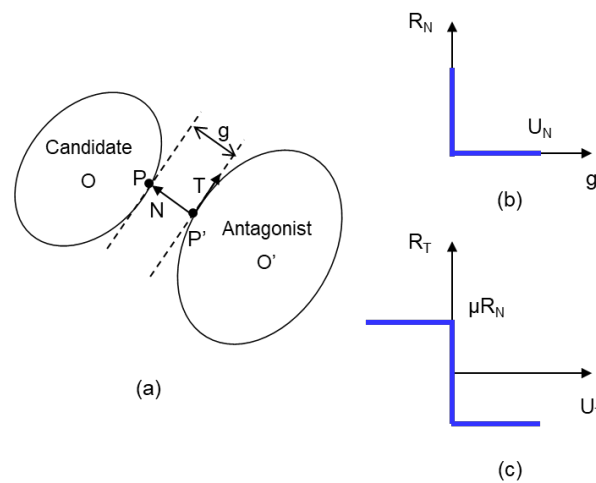


Figure 3-1 Non-Smooth Contact Dynamics: (a) Approach of contact on a binary body system, (b) Signorini unilateral contact law and (c) Coulomb law of dry friction (after Jean, 1999).

### 3.2.2 Simulation procedure

Numerical simulations are developed in two stages:

- (1) The sample is formed, by randomly generating rigid spherical particles of diameter  $d_i$  containing  $i$  classes, in given volumetric fractions ( $\%d_i$ ) within the planes of a cubic cell (Figure 3-2a). The cell dimensions are set ( $l_x = l_y = l_z = 10 \cdot d_{max}$ ) in an attempt

to decrease computational time without compromising the representative properties of the simulation. The sample presents an initially loose packing state, having a total height equal to 1.25 times larger than the cell. The cell lid is in contact with the highest sphere; it has a very low mass and enables the determination of the sample's volume. A sufficient number of spheres needs to be generated in order to fill this initial available space. The imposed deposit height,  $h$  and physical parameters, such as density and friction coefficient are defined upon the first step of simulation.

- (2) The sample is dropped under the gravity effect (Figure 3-2b). The spheres are free to fall and rearrange their positions, until their kinetic energy turns into zero. The sample's final height  $l'_z$  is determined by the position of the lid at the end of the deposit.

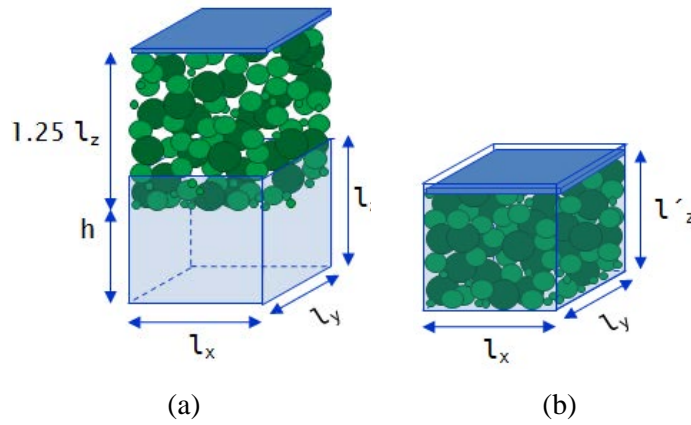


Figure 3-2 Schematic view of the numerical simulation: (a) sample generation and (b) sample deposit, for a given deposit height.

In the present numerical study, the GSD is expressed in volumetric fraction of each spherical diameter. Instead, the software implements the desired granulometry in proportions in numbers. Therefore, the following modifications were taking place for each tested sample containing  $i$  classes of grain sizes (i.e. for bimodal samples  $i=\text{max, min}$  and for trimodal samples  $i=\text{max, med, min}$ ). The volumetric proportion of class  $i$   $\%d_i$  is equal to:

$$\%d_i = \frac{VS_i}{V_S} = \frac{VS_{oi} \cdot N_i}{V_S} \quad (3.1)$$

where :

$VS_i$  is the total solid volume of all spheres of class  $i$ ,

$V_S$  is the total solid volume of the mixture,

$VS_{oi}$  is the solid volume of each sphere of class  $i$ ,

$N_i$  is the number of spheres in class  $i$ .

The proportion in number of spheres for each class  $i$  is calculated as:

$$\%d_{iN} = \frac{N_i}{N_T} \quad (3.2)$$

where :

$N_i$  is the number of spheres in class  $i$

$N_T$  is the total number of spheres.

From equation (3.1), it is evident that:

$$N_i = \frac{\%d_i \cdot V_S}{V_{SOi}} \quad (3.3)$$

and therefore

$$N_T = \sum \frac{\%d_i \cdot V_S}{V_{SOi}} \quad (3.4)$$

Consequently, the proportion in number of spheres of class  $i$   $\%d_{iN}$  is finally expressed as:

$$\%d_{iN} = \frac{\frac{\%d_i}{V_{SOi}}}{\sum \frac{\%d_i}{V_{SOi}}} \quad (3.5)$$

At the end of the deposit, the generated granulometry is evaluated.

Once the particles rearrangement is finalized, the final volume of the sample  $V_T$ , as well as the generated solid volume  $V_S$  are determined and the global results are obtained. On Figure 3-3, snapshots of the different steps of deposits are illustrated for a random tested mixture.

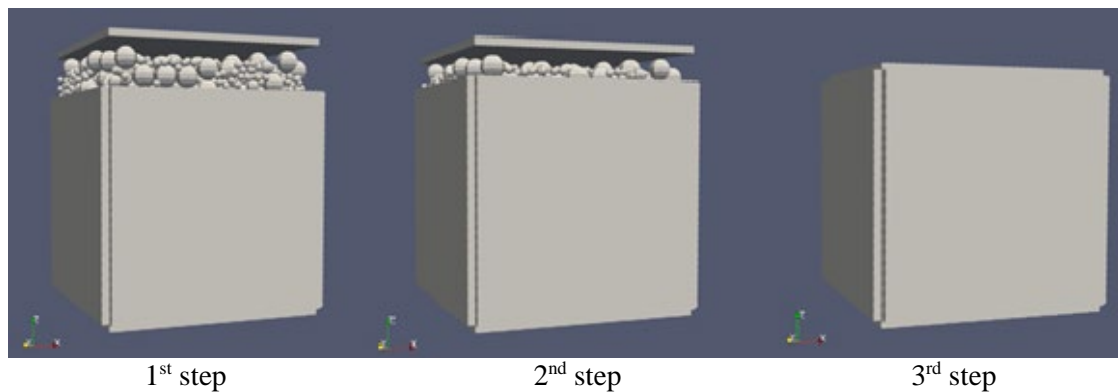


Figure 3-3 Snapshots during deposit of random granular mixture inside the cell using the LMGC<sup>90</sup> software: (a) the beginning of deposit, (b) during the deposit (c) at the final step of deposit.

However, bias might be introduced by the cell boundaries, since the calculations concern the fixed dimensions of the container. In an attempt to eliminate these edge effects and reduce the possible scale effect on the particles rearrangement, a fictional sphere is created, enclosing the sample. This fictional spherical boundary presents a diameter slightly lower than the height of the sample at the end of the deposit. The sample's total solid volume  $V_S$  and total volume  $V_T$  are calculated anew, considering at this step the particles inside the fictional sphere. Nonetheless, three cases corresponding to different boundary conditions are examined for the re-calculation of solid volume (Figure 3-4):

- $1^{st}$  case: spheres strictly contained inside the fictional boundary;
- $2^{nd}$  case: spheres intersecting the fictional boundary with centers located on the interior;
- $3^{rd}$  case: spheres intersecting the fictional boundary with centers located inside and outside the fictional boundary.

A series of numerical simulations showed that the variation of re-calculation cases from the global results was always lower for the  $2^{nd}$  case. In that case, the resulted packing state was denser than the overall global results. Thus, in an attempt to extrapolate the well-defined conditions of the fixed container to the in-situ gallery/infinite conditions, the  $2^{nd}$  case was selected for material compactness re-calculation. Therefore, the global results correspond to samples of small volume, whereas the re-calculated results refer to samples of larger scale.

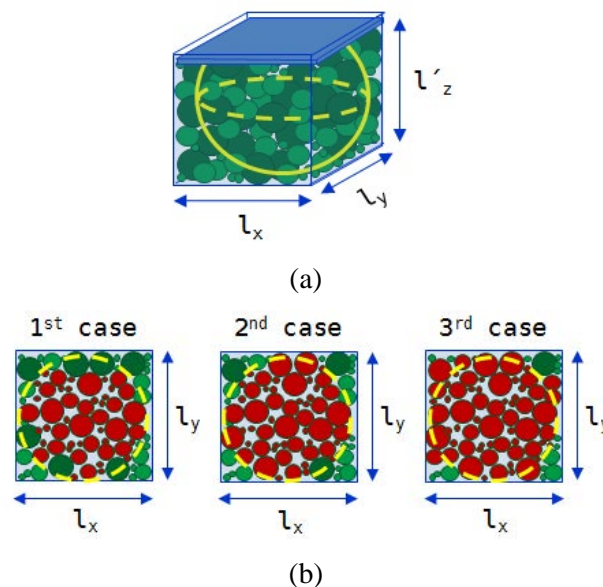


Figure 3-4 Determination of the final compaction state: (a) creation of fictional spherical boundary and (b) considered cases for solid volume calculation inside fictional boundary.

Compaction state can be evaluated using several properties, such as void ratio ( $e = V_V/V_S$ ), porosity ( $n = V_V/V_T$ ), compacity ( $e = V_S/V_T$ ). In the present study, the final compaction

---

state of the granular samples is examined in terms of dry density,  $\rho_d$ . The decision was based on the fact that the swelling capacity (which is investigated on the hydro-mechanical part of the study) is traditionally expressed by the dry density. It is calculated as:

$$\rho_d = \frac{M_S}{V_T} = \frac{\rho_d^{sphere} \cdot V_S}{V_T} \quad (3.6)$$

where  $M_S$  the solid mass,  $V_T$  the sample's total volume,  $\rho_d^{sphere}$  the dry density of each sphere, and  $V_S$  sample's solid volume. The numerical results presented and discussed later have been obtained from the global results (small scale), as well as the re-calculated results according to 2<sup>nd</sup> case (larger scale).

A relatively low but non-zero inter-particle friction coefficient ( $\mu = \tan 5^\circ \approx 0.09$ ) is set. The friction between grains and cell are always neglected. As a default case, the granular samples were left to fall from zero deposit height ( $h = 0$ ), expecting a lower packing density, in a way to decrease computational time and balance possible uncertainties caused by the low friction parameters. The density of all spheres  $\rho_d^{sphere}$  was considered equal to 2.0 Mg/m<sup>3</sup>, simulating the intra-pellet density.

### **3.3 Bimodal and trimodal samples: Results, parametric study and discussion**

#### **3.3.1 Sample's porosity found in literature**

The adopted model was initially evaluated by simulating granulometries matching Standish and Borger's (Standish and Borger 1979) experimental study, where various proportions of wooden spheres with diameters of 12.7 mm, 9.6 mm and 6 mm were mixed and their resultant porosity was reported. In the framework of the present study, five volumetric proportions of the same sphere sizes were randomly chosen to be tested by using the DEM numerical model. The implemented physical parameters were set as the default. At the end of simulation, the final GSD was evaluated. For each GSD, 10 complete simulations (generation and deposit) are conducted and the mean values are selected. The numerical results are listed on Table 3-1, presenting global and re-calculated porosity data. The experimental data measured by Standish and Borger (Standish and Borger 1979) are also given for comparison.

Firstly, low variation between the imposed and the generated GSD is observed with absolute errors lower than 2.6%, indicating a reliable method of GSD generation during simulations.

---

Global porosity presents lower Standard Deviation ( $SD \leq 0.15\%$ ) compared to re-calculated porosity ( $SD \leq 0.53\%$ ). Nonetheless, both methods give significantly repeatable results.

In Figure 3-5, numerical and experimental (literature) porosities are compared. A clear variation between the two methods is observed: for global results porosity is increased by 10.3% to 11.3% in comparison to re-calculated porosity. This behaviour was expected, since the porosity's re-calculation was attempted to simulate a greater scale, where voids due to edge effects are limited. On the other hand, experimental results seem to be better described by re-calculated porosity (absolute error  $\leq 5.5\%$ ) than global porosity (absolute error  $\leq 10.4\%$ ). Nonetheless, the errors can be attributed to several factors such as the cell's shape or the mechanical procedure (free fall in simulations instead of vibration of the sample in the experimental process of Standish and Borger, 1979).

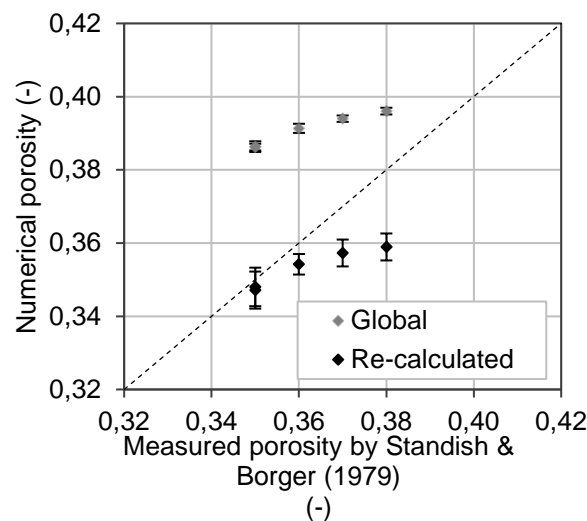


Figure 3-5 Comparison of experimentally measured porosity (Standish and Borger, 1979) and numerical porosity obtained by global and re-calculated results (present study).

Table 3-1 Results of considered cases of spherical particles with diameters of 12.7 mm, 9.6 mm and 6 mm: experimental data reported by Standish and Borger (1979) compared with global and re-calculated porosities of present study.

| Experimental data* |                                   |             |             |                       | Numerical results‡               |             |             |                      |             |             |                          |        |              |                                 |        |               |
|--------------------|-----------------------------------|-------------|-------------|-----------------------|----------------------------------|-------------|-------------|----------------------|-------------|-------------|--------------------------|--------|--------------|---------------------------------|--------|---------------|
|                    |                                   |             |             |                       | Generated volumetric proportions |             |             |                      |             |             | Global Results           |        |              | Re-calculated results           |        |               |
| Case               | Considered volumetric proportions |             |             | Measured porosity (-) | Mean                             |             |             | Absolute Error (%) § |             |             | Mean global porosity (-) | SD (%) | Error (%) §§ | Mean re-calculated porosity (-) | SD (%) | Error (%) §§§ |
|                    | % $d_{max}$                       | % $d_{med}$ | % $d_{min}$ |                       | % $d_{max}$                      | % $d_{med}$ | % $d_{min}$ | % $d_{max}$          | % $d_{med}$ | % $d_{min}$ |                          |        |              |                                 |        |               |
| 1                  | 60                                | 5           | 35          | 0.350                 | 59.6                             | 5.1         | 35.4        | 0.7                  | 1.4         | 1.0         | 0.386                    | 0.09   | -10.3        | 0.348                           | 0.53   | 0.6           |
| 2                  | 70                                | -           | 30          | 0.350                 | 69.7                             | -           | 30.3        | 0.4                  | -           | 0.9         | 0.386                    | 0.15   | -10.4        | 0.347                           | 0.51   | 0.8           |
| 3                  | 45                                | 25          | 30          | 0.360                 | 44.9                             | 25.3        | 29.8        | 0.3                  | 1.3         | 0.6         | 0.391                    | 0.12   | -8.70        | 0.354                           | 0.28   | 1.6           |
| 4                  | 40                                | 35          | 25          | 0.370                 | 40.7                             | 34.9        | 24.4        | 1.8                  | 0.2         | 2.6         | 0.394                    | 0.09   | -6.50        | 0.357                           | 0.37   | 3.4           |
| 5                  | 40                                | 40          | 20          | 0.380                 | 39.9                             | 40.1        | 20.1        | 0.4                  | 0.2         | 0.3         | 0.396                    | 0.09   | -4.20        | 0.359                           | 0.37   | 5.5           |

\* measured by Standish and Borger (1979)

‡ simulations performed in present study (10 simulations for each case)

§ error in relation to the target experimental proportion

§§ error between measured and numerical porosities

SD: Standard Deviation

### 3.3.2 Resulting packing density of pelletized samples

The ultimate objective of the present study is to determine the optimum GSD of a pelletized material and identify the maximum obtained density. In order to advance in this direction, trimodal and bimodal samples containing different sized spheres are tested. The resulting packing dry density is examined in terms of particle sizes (diameters) and volumetric proportions. The tested spherical sizes are compatible with the pelletizing process as well as the available laboratory measurement tools. Table 3-2 summarizes the geometrical parameters (diameters and size ratios) of the tested bimodal and trimodal mixtures. It presents also the maximum and minimum number of generated spheres reported for each tested sample. The impact of volumetric proportions  $\%d_i$  and the size ratio  $\alpha_i$  on the densest state is later assessed. As it was already been mentioned, upon simulations steps, the total number of generated spheres is analysed, to verify if an adequate quantity of particles is produced to fill the cell's initial space (i.e. before deposit). It can be seen on the table that it varied approximately from 1900 to 45500 spheres for all conducted simulations on trimodal and bimodal mixtures. This number is affected by the imposed sizes (and consequently size ratios), as well as the volumetric proportions. It is evident that when wider grain size is used (i.e. smaller size ratio), a greater number of particles is expected to be produced. On the other hand, for a given tested sample, this number can be used as a first indicator of the material's porosity (i.e. the higher the solid volume for a relatively similar initial volume, the lower the porosity is resulted).

#### 3.3.2.1 Bimodal samples

Six different bimodal samples (Table 3-2) mixed in four volumetric proportions (50-50, 60-40, 70-30, 80-20) are generated. The results of the obtained dry density are illustrated on Figure 3-6, presented in terms of global and re-calculated results. In both cases, a non-monotonic relation between dry density and volumetric percentage of maximum diameter is observed. The dry density increases to reach a peak, then it decreases. The behaviour is in agreement with previous experimental (Yu et al. 1992, Pasquiou 2001, Xu et al. 2019) and analytical studies (Dodds 1980, Yu and Standish 1987, Liu and Ha 2002). A common pattern is observed: the maximum resultant density for each tested grain size is expected when the proportion of large diameter is between 60% and 70% of total volume, revealing an optimal range of volumetric proportion for bimodal samples (i.e. proportion where the maximum packing density is obtained). However, bimodal samples of 12-7 mm, 16-10 mm and 10-7 mm are not significantly influenced by volumetric fraction variation. The maximum obtained

density was observed for mixtures containing spheres of 12 mm and 3 mm (global density of 1.39 Mg/m<sup>3</sup> and re-calculated density of 1.46 Mg/m<sup>3</sup>).

Table 3-2 Geometrical parameters of the tested bimodal and trimodal samples.

| Bimodal samples |                             |  |                                     |                                     |
|-----------------|-----------------------------|--|-------------------------------------|-------------------------------------|
| No sample       | $d_{max} - d_{min}$<br>(mm) | $\alpha_{max} - \alpha_{min}$ *<br>(-) | Minimum number of generated spheres | Maximum number of generated spheres |
| 1               | 16 - 10                     | 1.0 - 0.63                             | <b>1890</b>                         | 3053                                |
| 2               | 12 - 7                      | 1.0 - 0.58                             | 2159                                | 3573                                |
| 3               | 12 - 4                      | 1.0 - 0.33                             | 7319                                | 17303                               |
| 4               | 12 - 3                      | 1.0 - 0.25                             | 16346                               | 42255                               |
| 5               | 10 - 7                      | 1.0 - 0.70                             | 1631                                | 2338                                |
| 6               | 10 - 4                      | 1.0 - 0.40                             | 5016                                | 9709                                |

| Trimodal samples |                                       |   |                                     |                                     |
|------------------|---------------------------------------|---|-------------------------------------|-------------------------------------|
| No sample        | $d_{max} - d_{med} - d_{min}$<br>(mm) | $\alpha_{max} - \alpha_{med} - \alpha_{min}$ *<br>(-) | Minimum number of generated spheres | Maximum number of generated spheres |
| 1                | 20 - 10 - 5                           | 1.0 - 0.50 - 0.25                                     | 9127                                | 42647                               |
| 2                | 16 - 10 - 4                           | 1.0 - 0.63 - 0.25                                     | 6574                                | 41632                               |
| 3                | 12 - 7 - 4                            | 1.0 - 0.58 - 0.33                                     | 5014                                | 19605                               |
| 4                | 12 - 4 - 3                            | 1.0 - 0.33 - 0.25                                     | 12542                               | <b>45508</b>                        |

\* size ratio  $\alpha_i = d_i / d_{max}$  with  $i = \text{max, med, min}$

In order to further evaluate this behaviour, the impact of the selected sphere sizes on the achieved dry density is studied in Figure 3-7, where the maximum obtained density is plotted as function of size ratio  $\alpha_{min}$ . The usual variation between global and re-calculated results is observed: 5%-10% higher compaction state is obtained by eliminating the edge effects. The effect of size ratio is universal for both cases: the more significant the size difference of the selected diameters is (i.e. lower size ratio), the lower the observed voids are and a better compactness is exhibited. Additionally, when size ratio becomes higher than 0.6 the effect is reduced. Wiącek (2016) also reported that if the size ratio is larger than a certain value, the packing state does not reach a maximum upon variation of volumetric fractions. In fact, the smaller diameters can more easily penetrate the voids formed by the large particles and result into a more compacted state. Consequently, when spheres with similar sizes are mixed, the impact on the achieved density becomes less visible.

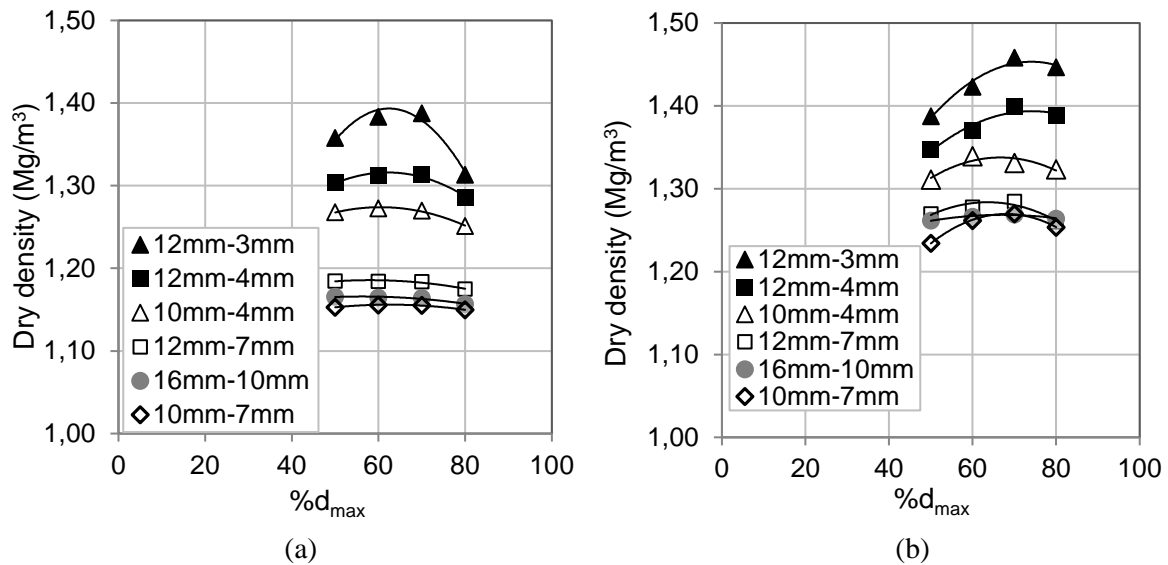


Figure 3-6 Achieved dry density of tested bimodal samples in relation to volumetric proportion of maximum sphere on each sample: (a) global results and (b) results after re-calculation.

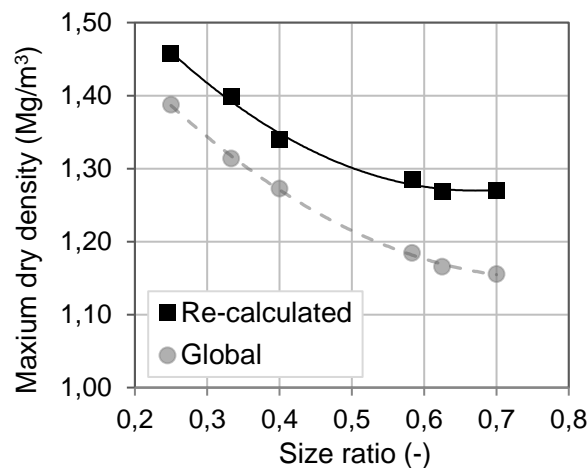


Figure 3-7 Effect of size ratio on the highest achieved dry density of bimodal tested samples: (a) global results and (b) results after re-calculation.

### 3.3.2.2 Trimodal samples

As the number of the sizes in a mixture increases, the study of the optimal packing state in terms of granulometry becomes more complex. Consequently, the investigation of the optimum GSD in the ternary pelletized mixtures raised the question of the tested volumetric proportion selection. In order to better focus on proportions able to decrease voids, an initial literature study aimed at investigating percentages that minimized the porosity independently from the used particle size. Proportions in past experimental studies that resulted in lowest porosities are considered (Westman and Hugill 1930, Standish and Borger 1979, Gatabin et al. 2014). Nonetheless, additional proportions are also generated. In total, 17 proportions are studied for each tested grain size.

The numerical results in terms of global and re-calculated density are presented in details in Table 3-3 for trimodal samples deposits with default parameters ( $h = 0$ ,  $\mu = \tan 5^\circ = 0.09$ ). Each line represents the imposed volumetric proportions that correspond to each component of trimodal sample. Their resulting dry density is marked in the gray area. For each sample, the two highest density values are highlighted. Apart from the chosen literature proportions (60-5-35, 70-10-20 and 60-20-20), the proportion of 60-10-30 is amongst the cases where the densest states are obtained. However, the volumetric proportion resulting in the densest mixtures for each tested sample does not necessarily coincide for both methods of compactness calculation, but insignificant differences are observed. In particular, for mixtures containing spheres with diameters of:

- (a) 20, 10 and 5 mm, the maximum, global density ( $1.38 \text{ Mg/m}^3$ ) is obtained for volumetric proportions of 60, 10 and 30% respectively, whereas maximum re-calculated density ( $1.45 \text{ Mg/m}^3$ ) is obtained for the proportions of 70, 10 and 20% respectively;
- (b) 16, 10 and 4 mm, the maximum global density ( $1.38 \text{ Mg/m}^3$ ) is observed for volumetric proportions of 60, 5 and 35% as well as for 60, 10 and 30% respectively, whereas the maximum re-calculated density ( $1.44 \text{ Mg/m}^3$ ) is obtained for the proportions of 60, 10 and 30% respectively;
- (c) 12, 7 and 4 mm, the maximum global density ( $1.32 \text{ Mg/m}^3$ ) and the maximum re-calculated density ( $1.40 \text{ Mg/m}^3$ ) is obtained for volumetric proportions of 60, 5 and 35% respectively;
- (d) 12, 4 and 3 mm, the maximum, global density ( $1.39 \text{ Mg/m}^3$ ) is obtained for volumetric proportions of 60, 5 and 35% respectively, whereas maximum re-calculated density ( $1.45 \text{ Mg/m}^3$ ) is obtained for the proportions of 70,10 and 20% respectively.

Figure 3-8 illustrates the results of the achieved global and re-calculated dry density as a function of the proportion of the three components,  $d_{max}$ ,  $d_{med}$  and  $d_{min}$ . Their influence on the compaction state is not homogeneous. The maximum and minimum diameters  $d_{max}$  and  $d_{min}$  respectively appear to exhibit an optimum value (Figure 3-8 a, c, d, f). On the contrary, volumetric fraction of the medium diameter  $d_{med}$  presents a more linear relation with the compaction state. The more important the presence of  $d_{med}$  the more voids are obtained. In order to minimize the voids, a general rule could be concluded, the presence of the largest particle should be the most significant, whereas the intermediate-sized particles should be the least present in the mixture. Besides, in the idealized particle rearrangement (i.e. densest possible packing state), the large particles are in contact with each other, whereas the

intermediate-sized particles need to be enough to occupy the voids between the largest without holding them apart (Head 2006). As a consequence, it appears that the most compacted state is achieved when 60-70% of the maximum diameter is mixed with 5-10% of medium diameter and 20-35% of the minimum diameter. Similar observations were reported by Liu et al. (2019).

The impact of the size ratio on the densest state is examined in Figure 3-9. For trimodal specimens, size ratio is expressed by the two variables,  $\alpha_{med}$  and  $\alpha_{min}$  for the medium and minimum tested diameter respectively. A less clear influence for the ternary mixtures compared to binary samples is observed, for the studied range. Generally, increase of size ratio hinders the compactness of the granular sample. The behaviour is more prominent in the case of  $\alpha_{min}$ . Furthermore, samples with an identical size ratio of minimum diameter ( $\alpha_{min} = 0.25$ ) lead to significantly similar particle rearrangement.

It is clear, that trimodal samples of 20-10-5 mm, 12-4-3 mm and 16-10-4 mm result in higher packing state than mixtures of 12-7-4 mm, due to their greater difference of the mixed grain sizes. Furthermore, the highest resulting density for those cases presents low variations for both methods of density calculation (1.38-1.39 Mg/m<sup>3</sup> and 1.44-1.45 Mg/m<sup>3</sup>).

Table 3-3 Results of (a) global density and (b) re-calculated density for trimodal tested samples (the two highest values of density are highlighted with red and black bold letters).

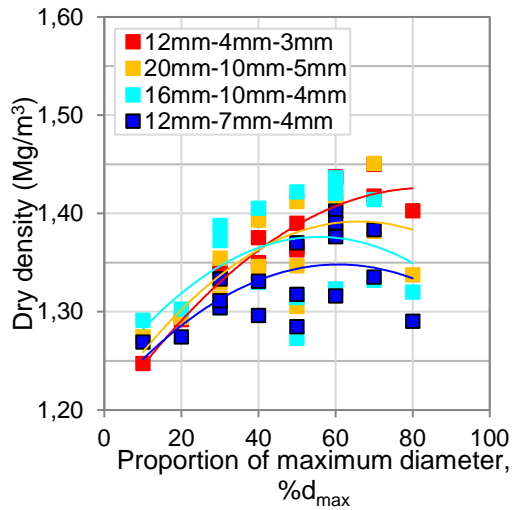
| (a)            | Volumetric proportions |             |             | Diameters of spheres<br>$d_{max} - d_{med} - d_{min}$ (mm) |             |             |             |
|----------------|------------------------|-------------|-------------|--|-------------|-------------|-------------|
|                |                        |             |             | 20-10-5  | 16-10-4     | 12-7-4      | 12-4-3      |
| Case           | $\%d_{max}$            | $\%d_{med}$ | $\%d_{min}$ | Dry density (Mg/m <sup>3</sup> )                           |             |             |             |
| 1*             | 60                     | 5           | 35          | <b>1.37</b>  | <b>1.38</b> | <b>1.32</b> | <b>1.39</b> |
| 2 <sup>‡</sup> | 70                     | 10          | 20          | 1.36   | <b>1.35</b> | 1.30        | <b>1.38</b> |
| 3 <sup>§</sup> | 60                     | 20          | 20          | 1.35   | <b>1.35</b> | 1.30        | 1.37        |
| 4              | 80                     | 10          | 10          | 1.25   | 1.24        | 1.25        | 1.30        |
| 5              | 70                     | 20          | 10          | 1.30   | 1.26        | 1.25        | 1.36        |
| 6              | 60                     | 30          | 10          | 1.31   | 1.26        | 1.26        | 1.35        |
| 7              | 60                     | 10          | 30          | <b>1.38</b>  | <b>1.38</b> | <b>1.31</b> | <b>1.38</b> |
| 8              | 50                     | 45          | 5           | 1.31   | 1.23        | 1.23        | 1.33        |
| 9              | 50                     | 40          | 10          | 1.29   | 1.27        | 1.25        | 1.33        |
| 10             | 50                     | 20          | 30          | 1.35   | 1.37        | 1.30        | 1.36        |
| 11             | 40                     | 50          | 10          | 1.28   | 1.26        | 1.25        | 1.31        |
| 12             | 40                     | 30          | 30          | 1.34   | 1.35        | 1.29        | 1.33        |
| 13             | 30                     | 60          | 10          | 1.27   | 1.26        | 1.24        | 1.28        |
| 14             | 30                     | 30          | 40          | 1.31   | 1.34        | 1.27        | 1.31        |
| 15             | 30                     | 20          | 50          | 1.31   | 1.33        | 1.27        | 1.31        |
| 16             | 20                     | 70          | 10          | 1.25   | 1.25        | 1.23        | 1.26        |
| 17             | 10                     | 80          | 10          | 1.23   | 1.24        | 1.22        | 1.23        |

| (b)            | Volumetric proportions |             |             | Diameters of spheres<br>$d_{max} - d_{med} - d_{min}$ (mm) |             |             |             |
|----------------|------------------------|-------------|-------------|--|-------------|-------------|-------------|
|                |                        |             |             | 20-10-5  | 16-10-4     | 12-7-4      | 12-4-3      |
| Case           | $\%d_{max}$            | $\%d_{med}$ | $\%d_{min}$ | Dry density (Mg/m <sup>3</sup> )                           |             |             |             |
| 1*             | 60                     | 5           | 35          | <b>1.42</b>  | <b>1.43</b> | <b>1.40</b> | <b>1.44</b> |
| 2 <sup>‡</sup> | 70                     | 10          | 20          | <b>1.45</b>  | 1.41        | 1.38        | <b>1.45</b> |
| 3 <sup>§</sup> | 60                     | 20          | 20          | <b>1.42</b>  | 1.42        | <b>1.39</b> | 1.41        |
| 4              | 80                     | 10          | 10          | 1.34   | 1.32        | 1.29        | 1.40        |
| 5              | 70                     | 20          | 10          | 1.38   | 1.33        | 1.34        | 1.42        |
| 6              | 60                     | 30          | 10          | 1.38   | 1.32        | 1.32        | 1.38        |
| 7              | 60                     | 10          | 30          | 1.41   | <b>1.44</b> | 1.38        | <b>1.44</b> |
| 8              | 50                     | 45          | 5           | 1.31   | 1.27        | 1.28        | 1.37        |
| 9              | 50                     | 40          | 10          | 1.35   | 1.31        | 1.32        | 1.36        |
| 10             | 50                     | 20          | 30          | 1.41   | 1.42        | 1.37        | 1.39        |
| 11             | 40                     | 50          | 10          | 1.35   | 1.33        | 1.30        | 1.35        |
| 12             | 40                     | 30          | 30          | 1.39   | 1.41        | 1.33        | 1.38        |
| 13             | 30                     | 60          | 10          | 1.31   | 1.30        | 1.30        | 1.31        |
| 14             | 30                     | 30          | 40          | 1.35   | 1.39        | 1.33        | 1.34        |
| 15             | 30                     | 20          | 50          | 1.33   | 1.37        | 1.31        | 1.34        |
| 16             | 20                     | 70          | 10          | 1.29   | 1.30        | 1.27        | 1.29        |
| 17             | 10                     | 80          | 10          | 1.27   | 1.29        | 1.27        | 1.25        |

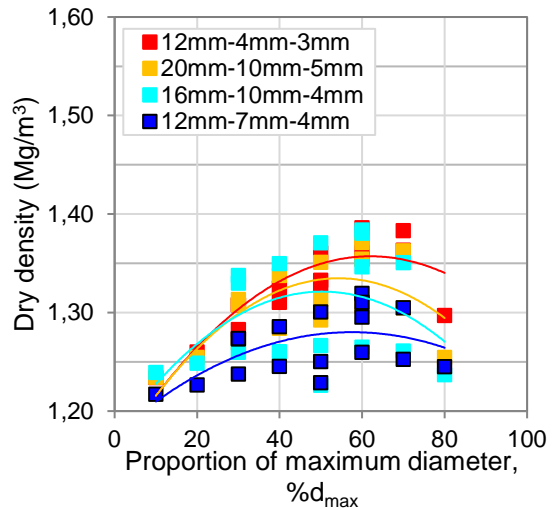
\* Westman and Hugill, 1930

<sup>‡</sup> Marshall and Dhir, 1986

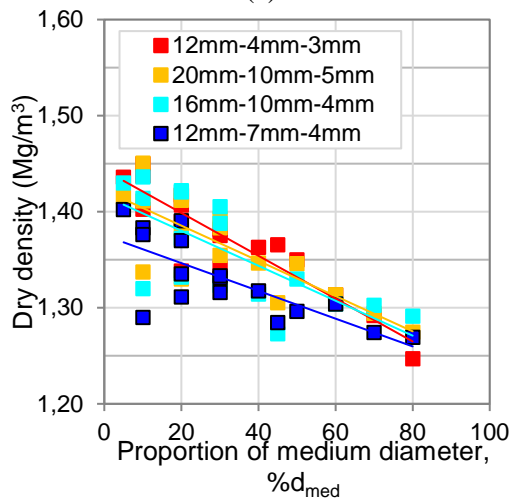
<sup>§</sup> Gatabin et al., 2014



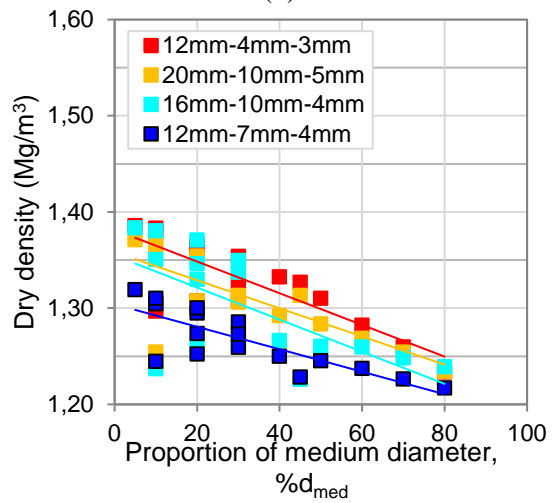
(a)



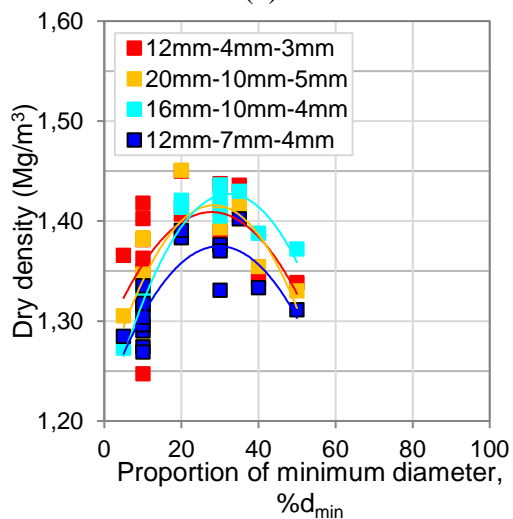
(d)



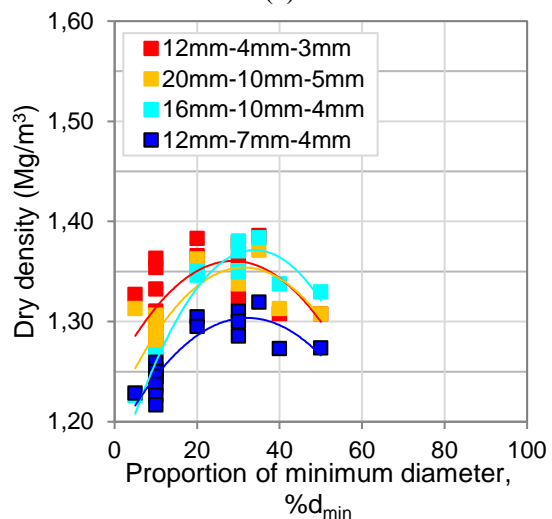
(b)



(e)



(c)



(f)

Figure 3-8 Trimodal tested samples: global dry density in relation to volumetric proportion of (a) maximum, (b) medium and (c) minimum diameter and re-calculated dry density in relation to volumetric proportion of (d) maximum, (d) medium and (f) minimum diameter.

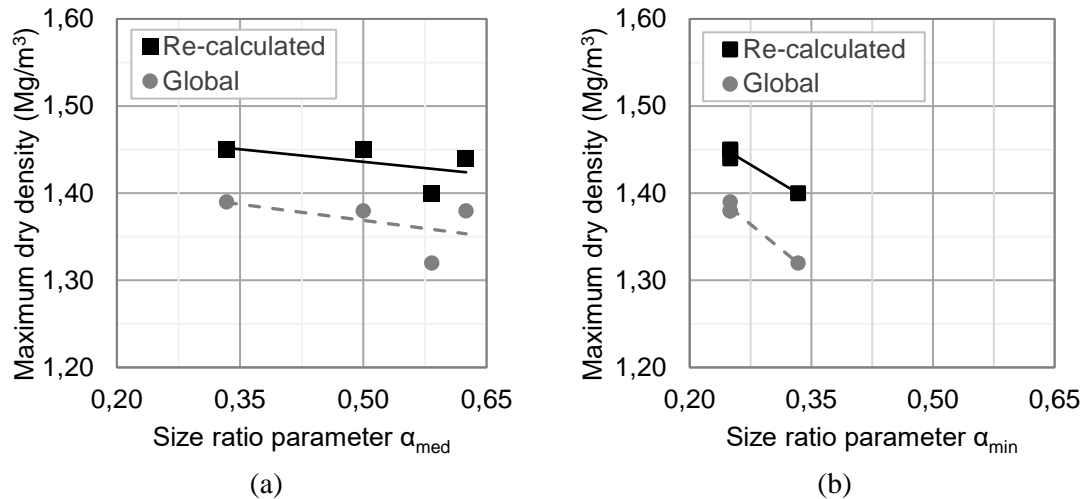


Figure 3-9 Effect of size ratio of (a) medium diameter and (b) minimum diameter on the highest achieved density of trimodal tested samples.

### 3.3.2.3 Discussion on bimodal versus trimodal samples

A comparison in maximum density between bimodal and trimodal samples allows to evaluate the impact of component number on the packing state. Bimodal and trimodal samples presenting identical “extreme” sizes  $d_{max}$  and  $d_{min}$  (12-7-4 mm and 12-4 mm, 12-4-3 mm and 12-3 mm) are compared in Figure 3-10, where only the maximum obtained dry density is illustrated for each case. In other words, mixing only the maximum and minimum diameter could lead to similar compaction state with three-component samples containing maximum, medium and minimum diameters.

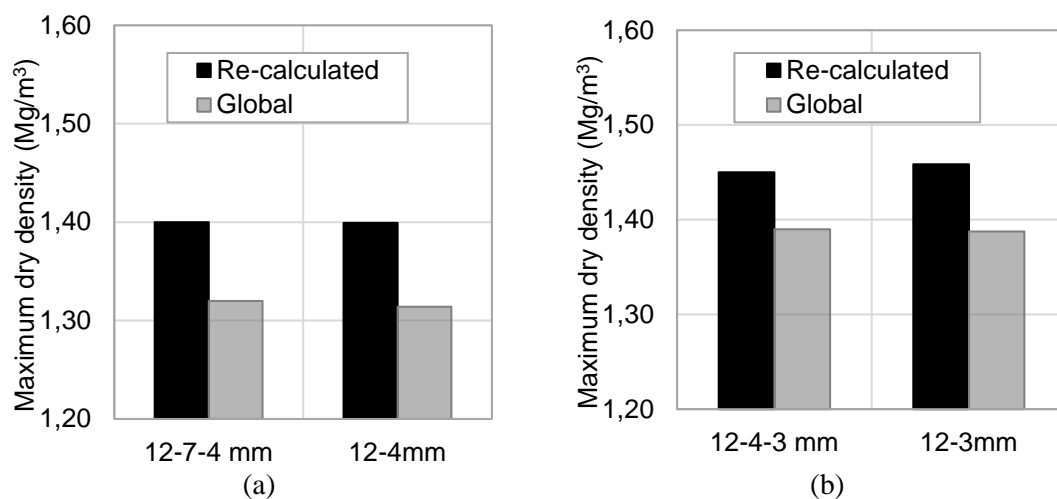


Figure 3-10 Comparison of maximum obtained density for bimodal and trimodal samples with identical maximum and minimum diameters: (a) 12-7-4 mm 12-4 mm and (b) 12-4-3 mm and 12-3 mm.

Obtained results for trimodal mixtures reported that the presence of medium size should be the least important component in order to increase the material’s compactness and that the size ratio of medium size is not a significantly influential parameter. Therefore, if the medium

diameter is eliminated (i.e. case that can reduce the cost of the mixture's fabrication and set-up), a similar state of compaction can be achieved with the two extreme particle sizes, but clearly in different proportions.

#### 3.3.2.4 Parametric study on optimum DEM Grain Size Distribution

In the framework of the present study, the optimum GSD is selected in order to reach the highest possible dry density. The chosen granulometry will be later fabricated. Therefore, the final selection of the grain sizes needs to be absolutely compatible with the pellet machine capacity. Based on results presented in Table 3-2, the mixture containing spheres of 16 mm, 10 mm and 4 mm gave one of the highest reported dry densities. The specific sizes were found to be more suitable for the pelletization and were chosen as the optimum sizes. Regarding the optimum proportions, re-calculated density attempts to better simulate the emplacement on large scale. Consequently, the optimum GSD is selected consisting of spheres of 16, 10 and 4 mm in proportions of 60, 10 and 30% respectively. A parametric study was conducted in order to examine the effect of the surface characteristics and the deposit height on the density of the chosen optimum GSD. The effect of deposit height on the compaction state of the granular material was studied by increasing its value, while inter-particle friction was set as default ( $\mu = \tan 5^\circ = 0.09$ ). The sample was left to fall from different heights equal to 0,  $l_z$ ,  $2l_z$ ,  $5l_z$  and  $9.4l_z$  corresponding to values of 0, 0.16, 0.32, 0.80 and 1.5 m. Increase of deposit height on larger values was avoided, because it could increase the risk of possible pellet breakage.

On Figure 3-11, the results of the resulting dry density in relation to the drop height are presented as determined by the two methods. For certain cases, multiple simulations were conducted and the mean obtained density is presented; the obtained variation is illustrated by error bars. The compactness is clearly improved as the drop height increases. Higher drop heights correspond to higher imposed kinetic energies of the particles and therefore allowing a better rearrangement of their position. Density increases non-linearly with deposit height for the tested range, as Vaid and Negussey (1984) also concluded. Zhang et al. (2001) observed that after a certain value ( $h=1.5$  m) no significant impact on the packing of monosized samples was reported. In addition, it can be seen that the increase of deposit height decreases the difference between global and re-calculated results and for heights around 0.80 m, an inverse behaviour is observed. As it was mentioned on section 3.3.1, the density variation of multiple simulations is lower for global method compared to re-calculated data. In the present results, this variation appears to be more intense, as drop height becomes more significant (e.g.  $h=0.80$  m) and therefore, this reversed behaviour is obtained.

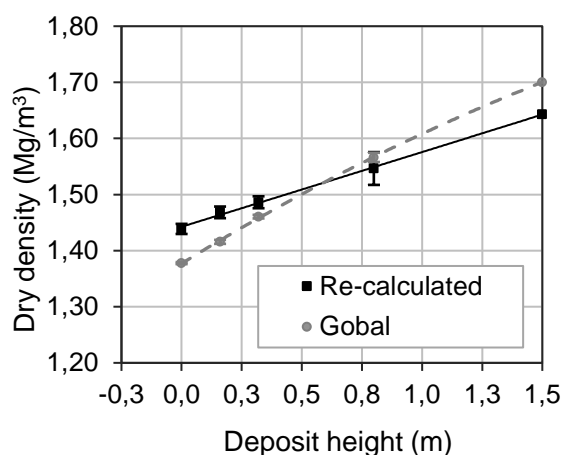


Figure 3-11 Influence of deposit height on the dry density of the chosen optimum GSD (16, 10 and 4 mm in 60, 10 and 30% respectively).

Inter-particle friction coefficient  $\mu$  was varied from 0 to 0.84 representing surfaces going from smooth to rough, while deposit height was kept constant ( $h = 0$  or  $0.160$  m). The results are presented in Figure 3-12 for the two density calculation methods. Increase of friction hinders the re-arrangement of the specimen resulting in lower degree of compactness. The increase of inter-particle friction coefficient  $\mu$  up to 0.84 ( $\varphi = 40^\circ$ ) resulted in 10% decrease of the density comparing to particles with smooth spherical surfaces. In previous studies (Silbert et al. 2002, Vandewalle et al. 2007, Rosato et al. 2010) a non-linear relation was also observed with a lower variation of packing density beyond friction coefficient  $\mu$  of 1 ( $\varphi = 45^\circ$ ). Nonetheless, the impact of deposit height on the packing state decreases as inter-particle friction increases. For the re-calculated results (Figure 3-12b) that consider a larger scale, the effect of deposit height is not significant when  $\mu > 0.2$ . On larger scale, the kinetic energy imposed by the deposit height increase might be absorbed, whereas its effect on smaller scales (e.g. cell conditions) could significantly modify the local particle rearrangement.

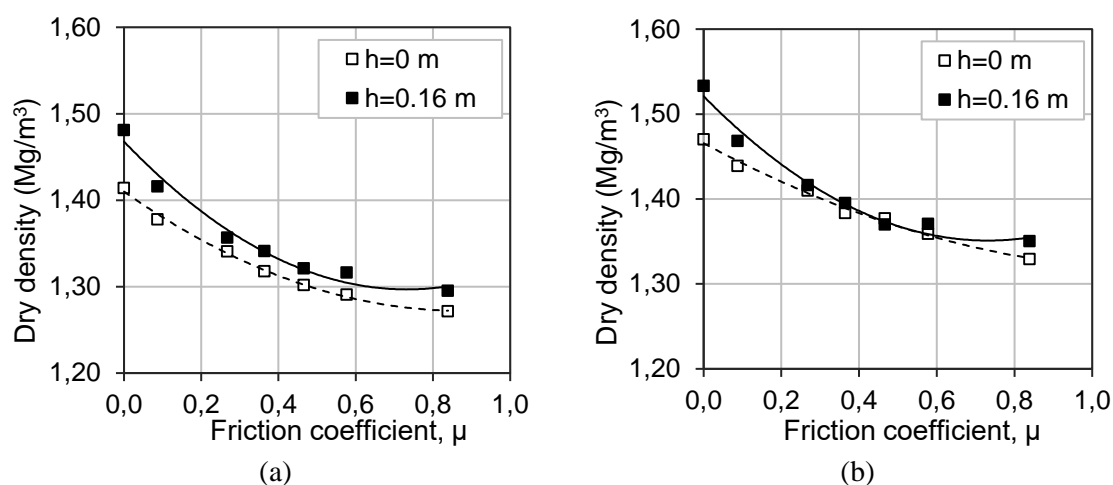


Figure 3-12 Influence of friction coefficient on the achieved dry density for the chosen optimum GSD (16, 10 and 4 mm in 60, 10 and 30% respectively) deposited from 0 and 0.160 m: (a) global and (b) re-calculated results.

### 3.4 Conclusions and optimum GSD obtained by DEM

The optimum granulometry of a mixture containing pellets was optimised, in order to exhibit the maximum resulting density. DEM simulations were used to define the GSD of the granular material. The influence of size ratio, inter-particle friction and deposit height were assessed.

In this context, gravitational deposits of bimodal and trimodal samples were carried out, proposing two methods for the resulting density calculation: global and re-calculated data to correspond on samples of small scale and larger scale respectively. The different methods revealed a clear impact of the boundaries on the packing state. However, in both cases, the model exhibited high repeatability in terms of generated GSD and packing state. Therefore, conclusions can be drawn independently about density method calculation.

- For bimodal samples, maximum density was observed for volumetric fractions of maximum diameter of 60-70%. Higher maximum density was obtained as the size ratio  $\alpha_{min}$  decreased, while for  $\alpha_{min}$  higher than 0.6, the resulting density was less affected.
  - For ternary samples, the densest state was presented when the following proportions criteria were fulfilled:  $\%d_{max} > \%d_{min} > \%d_{med}$ . For constant size ratio  $\alpha_{min}$ , low variation on the maximum dry density was obtained (<1%). Lower voids are observed with the decrease of the minimum particle size, due to the efficient penetration of smaller grains in voids created by larger grains.
  - Maximum obtained density is independent to intermediate diameter. More precisely, bimodal and trimodal configurations with common  $d_{max}$  and  $d_{min}$  present the same packing state, in evidently different volumetric proportions.
  - Density improvement is observed with increase of deposit height; higher imposed kinetic energy resulted in better particle rearrangement.
  - Inter-particle friction increase hinders particle sliding and rearrangement in a more compacted state. A non-linear relation obtained with weakened friction effect for friction coefficients higher than 0.6.
- ✓ As optimum DEM granulometry, the sizes of 16-10-4 mm in proportions of 60%-10%-30% were selected. They led to one of the highest re-calculated densities (absolute error 0.7% from the maximum observed density value) and they were considered more compatible with pelletizing means.

The next step includes the further experimental verification of the specific configuration in order to counterbalance encountered limitations of the numerical model (e.g. in term of code, use of finer material, or alternative filling protocols).

## Chapter 4 - Pelletizing process

The present chapter focuses on the pellet fabrication at semi-industrial conditions of CO<sub>x</sub>/MX80 mixtures in the optimum diameters (16 mm, 10 mm, 4 mm). In this context, the raw soil mixtures are initially studied upon uniaxial compression tests, matching the applied pelletizing technique. The adopted pellet machine is reconditioned to carry out the pellet fabrication. The process of pelletization is optimised to overcome the encountered issues, examining several parameters. CO<sub>x</sub>/MX80 pellets are manufactured for the first time. The chapter is developed in the following main parts:

- 4.1 Introduction
- 4.2 Studied soil materials: physical parameters
- 4.3 Pellet machine and fabricated accessories
- 4.4 Optimisation of CO<sub>x</sub>/MX80 pellet production: Influential factors
- 4.5 Conclusions

## 4.1 Introduction

In the pharmaceutical domain and more precisely in powder industry, compression method is one of the main pelletization techniques. Considering soil a mineral powder, this technique is adopted to fabricate pellets of soil materials. The initial raw material is inserted on the pellet machine, which compacts and forms the pellet at the target size. The resulting shape depends on the geometries of the machine (i.e. moulds, dies), while pellet production might be affected by the raw material's initial state (e.g. mineralogy, water content, granulometry).

As it has been underlined, the adopted strategy included the fabrication of pellets containing COx argillite and MX80 bentonite, compacted at sizes defined by the preliminary DEM investigation (Chapter 3). In the present study, the applied pelletizing technique is based on the material's uniaxial compression inside moulds of the target sizes. The fabricated pellets must present dry density of approximately 2.0 Mg/m<sup>3</sup> and intact form. In this context, pellets of 16 mm, 10 mm and 4 mm in diameter were selected for fabrication. It is reminded that MX80 pellets have already been fabricated and studied in past studies (e.g. Seiphoori et al., 2014; Molinero Guerra et al., 2017; Darde et al., 2018). However, no available information on the feasibility of COx pelletization is available.

The present chapter deals with the issue of pelletization as addressed for the needs of our study. In the beginning, the raw materials are characterized using basic soil index properties before being processed, focusing also in soils compressibility (section 4.2). In parallel, the used tablet press machine is reconditioned and the necessary accessories are designed and fabricated in order to produce 16 mm, 10 mm and 4 mm sized pellets (section 4.3). Pellet production is analysed by identifying and investigating influential factors (section 4.4).

## 4.2 Studied soil materials: physical parameters

Mixtures of Callovo-Oxfordian (COx) argillite and MX80 bentonite in different fractions were studied. COx argillite claystone was excavated from Andra's Underground Research Laboratory (URL) and subsequently crushed. It is reminded that COx presents a rather homogeneous composition (20% tectosilicates, 20-25% carbonates and 50-55% clay minerals) (Armand et al. 2013). MX80 is a commercial sodium bentonite from Wyoming (USA), containing 80% smectites and other non-clay minerals (Molinero Guerra et al. 2017).

Both materials present maximum grain size  $d_{max}$  of 2 mm at the as-received condition. The materials GSD obtained by the dry sieving method is presented on Figure 4-1. It is shown that MX80 contains grains up to 200  $\mu$ m, whereas on COx argillite includes about 30% of grains smaller than 200  $\mu$ m. Table 4-1 presents details concerning the granulometry of the two

materials. The particle density of COx and MX80 were considered as 2.70 Mg/m<sup>3</sup> and 2.78 Mg/m<sup>3</sup> respectively (Zhang and Kröhn 2019)

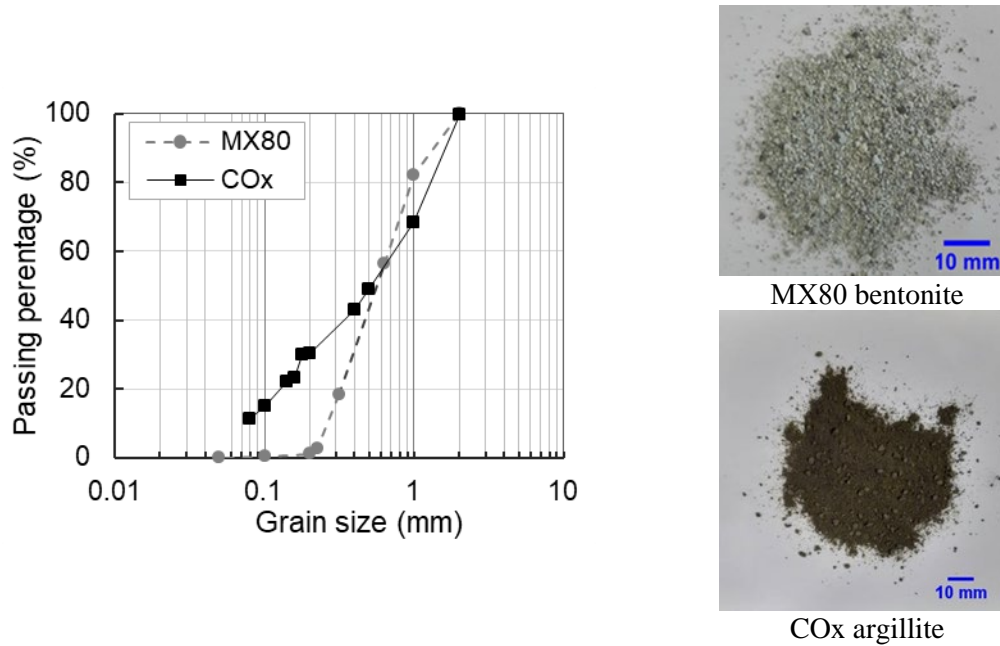


Figure 4-1 The grain size distribution and photographs of the studied materials at reception conditions.

Table 4-1 Details regarding the grain size distribution of COx and MX80 soil materials.

| Material | $d_{max}$<br>(mm) | $d_{10}$<br>(mm) | $d_{60}$<br>(mm) | $CU$ | $CC$ |
|----------|-------------------|------------------|------------------|------|------|
| COx      | 2.0               | 0.08             | 0.71             | 9.47 | 0.68 |
| MX80     |                   | 0.21             | 0.61             | 2.90 | 1.25 |

Table 4-2 summarises the physical and chemical properties of the studied materials. The natural water content at reception conditions was measured 6.2% for argillite and 12.5% for bentonite. All parameters were determined by using demineralized water. The liquid limit ( $LL$ ), plastic limit ( $PL$ ) and  $MBV$  values (Methylene blue adsorption capacity) were determined following the French Standards (AFNOR 1993, 1995, 1998). Specific Surface Area ( $SSA$ ) was estimated from  $MBV$  (Unikowski 1982). Free swelling index ( $FSI$ ) was determined following the (AFNOR 2002), where two grams of dried powdered clay ( $d < 160 \mu\text{m}$ ) are progressively poured into a graduated cylinder, containing 100 ml of aqueous solution. The volume of swollen clay in the cylinder is measured after 24 h. The pH and electrical conductivity values were obtained at the end of the  $FSI$  test using demineralized water.

Clear differences in plasticity index, swelling capacity and specific surface are obtained between the soil materials. The observations are consistent with their mineralogical

differences. MX80 is an expansive clay with high smectite content exhibiting high specific surface area and therefore more sensitive to interaction with water. Similar values were also reported by previous researchers regarding the *FSI* and *MBV* values (Seiphoori et al., 2014; Barast et al., 2017; Davies et al., 2017).

Table 4-2 Physical and chemical characteristics of the studied materials.

| Material | <i>w</i><br>(%) | <i>LL</i><br>(%) | <i>PL</i><br>(%) | <i>MBV</i><br>(g/100g) | <i>SSA</i><br>(m <sup>2</sup> /g) | <i>FSI</i><br>(cm <sup>3</sup> /2g) | <i>pH</i> | <i>EC</i><br>(mS/cm) |
|----------|-----------------|------------------|------------------|------------------------|-----------------------------------|-------------------------------------|-----------|----------------------|
| COx      | 6.2             | 47               | 21               | 3.3                    | 70                                | 4                                   | 9.1       | 0.159                |
| MX80     | 12.5            | 465              | 57               | 25                     | 523                               | 30                                  | 9.7       | 1.143                |

*w*: water content

*LL*: Liquid Limit obtained from Atterberg limits

*PL*: Plastic Limit obtained from Atterberg limits

*MBV*: Methylene Blue adsorption capacity Value

*SSA*: Specific Surface Area

*FSI*: Free Swelling Index

*EC*: Electrical Conductivity

For further evaluation of the materials interaction with water, the absorption capacity for argillite and bentonite were measured according to the French standard (AFNOR 2002). The testing method requires 1 g of dry clayey material (<160µm) poured inside a specific device, which consists of a saturated porous plate connected to a horizontal graduated cylinder, while the volume of the absorbed water is measured. The test conditions are able to control low suction phenomena (Razakamanantsoa et al. 2012). The recorded volume over time is illustrated at Figure 4-2. MX80 clearly absorbs almost 6 times more water than COx. The result is in accordance with the *SSA* values of each material; the higher the specific surface, the more water molecules can be absorbed.

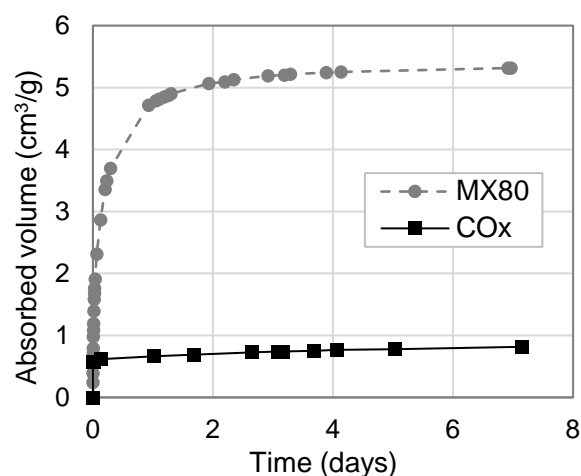


Figure 4-2 Water absorption test results on COx argillite and MX80 bentonite using demineralized water.

#### 4.2.1 Parametric study of COx/MX80 mixtures: characterisation and compressibility

Mixtures containing COx argillite and MX80 bentonite are studied in different proportions (in total mass). The maximum imposed bentonite content is set at 40% to match the design requirements, dictating the minimization as possible of MX80 presence.

In the following sections, the effect of bentonite addition on mixture properties is studied. Plasticity index (Atterberg limits) and *FSI* values were determined. Additionally, materials compressibility is analysed by performing confined uniaxial compression tests up to a compaction state corresponding the target intra-pellet density ( $\rho_{d\text{ pellet}} = 2.0 \text{ Mg/m}^3$ ).

##### 4.2.1.1 Index properties

In the present experimental study, the liquid limit test was determined following the rolled thread method (AFNOR 1993), whereas plastic limit was evaluated by using the penetrometer (AFNOR 1995). The *FSI* was measured after 24 h of posing 2 g of material inside the aqueous solution. The studied COx/MX80 mixtures were expressed as function of MX80 content (in total mass) in the mixture. Here, demineralized water was used as reference solution.

The results of liquid limit and plastic limit are presented on Figure 4-3 for the different investigated COx/MX80 mixtures. Both parameters increase as bentonite content becomes more significant. In particular, an exponential increase of liquid limit with MX80 content is observed. The impact of MX80 addition follows linear relation with the plastic limit, showing a less pronounced effect. The outcome actually is correlated with the mixture's higher absorption capacity as MX80 is more significant. Similar observations have been reported by Zhang et al. (2012) on different mixtures of GMZ bentonite and sand.

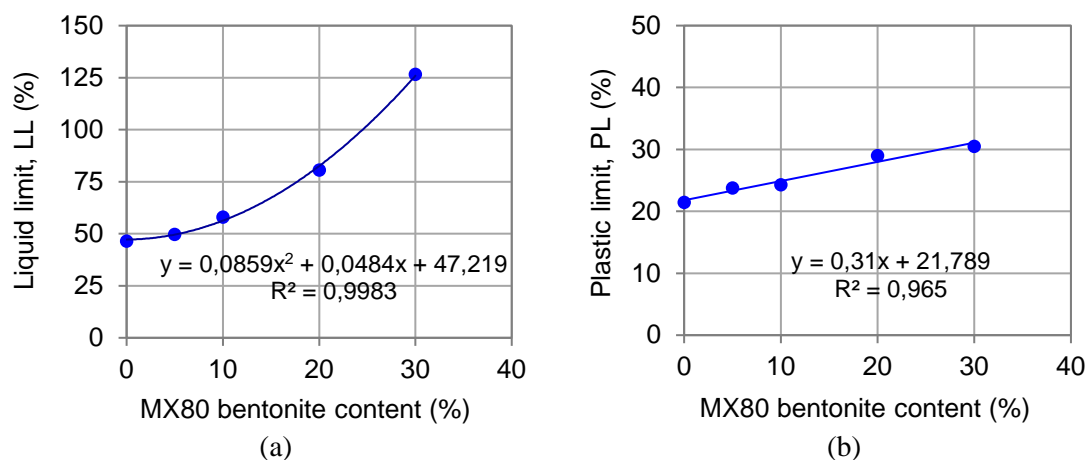


Figure 4-3 Evolution of: (a) liquid limit and (b) plastic limit in relation to bentonite content for COx/MX80 mixtures.

On Figure 4-4, the obtained values of Atterberg limits are plotted on the plasticity chart. Clearly, a gradual increase of plasticity is noted with bentonite addition. Pure COx argillite is medium plasticity clay, COx containing 5 to 10% MX80 exhibits high plasticity and mixtures with 20%MX80 belongs to the region of very high plasticity. Mixtures containing more than 30% of MX80 bentonite are clays of extremely high plasticity. The observed relation with bentonite content anticipates an initial indication on the swelling capacity. In that direction, the results of FSI tests are presenting on Figure 4-5. As it was expected, swelling capacity is improved with bentonite addition in the mixture. Nonetheless, it remains relatively low (e.g. lower than 6 for  $MX80 \leq 30\%$ ).

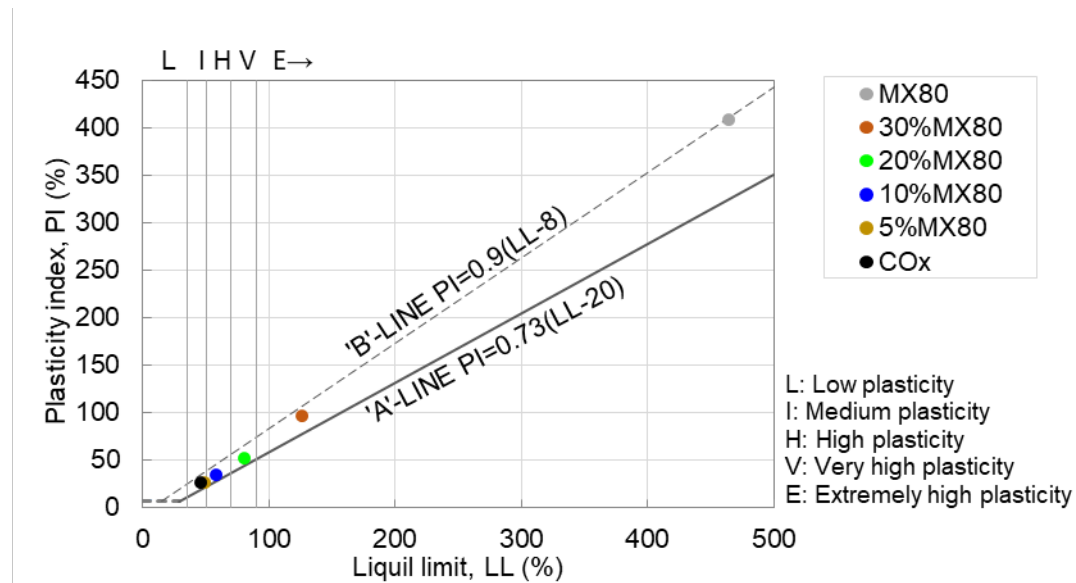


Figure 4-4 Plasticity chart for the different materials.

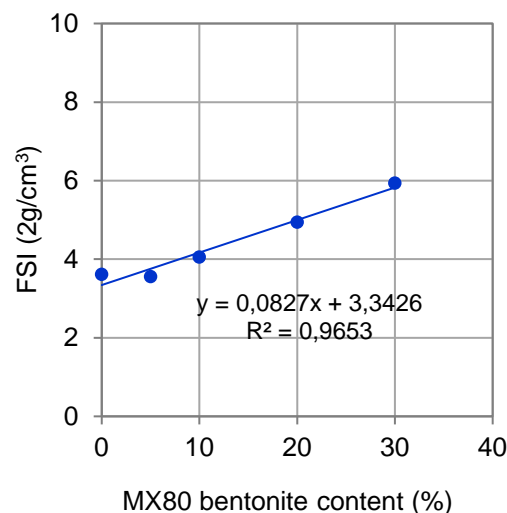


Figure 4-5 Free swelling index in relation to bentonite content for COx/MX80 mixtures.

#### 4.2.1.2 Confined uniaxial oedometric compression tests

A series of uniaxial compression tests were conducted on CO<sub>x</sub>/MX80 mixtures ( $\leq 40\%$ MX80). The objective of the experimental work was to evaluate the material's behaviour during the pelletizing process and to possibly identify conditions favouring the pelletization.

In this direction, powdered mixtures were statically compacted using an oedometric apparatus (Figure 4-6). The device consists of a metallic frame, divided in two parts: the cylindrical cell of internal diameter  $D=40$  mm containing the specimen and a piston located in the bottom of the cell, through which the vertical stress is applied. The cell receives the remoulded soil material and screws are fixed in the upper part to ensure its confinement. Porous disks are placed on specimen's parallel sides. The remaining space between the cell's lower part and the piston is filled with water (water chamber) and the water-tightness between the specimen and the chamber are guaranteed by O-rings installed on the piston's wall. A hydraulic pump (maximum applied pressure 60 MPa) is connected to the oedometer and applies the vertical stress by injecting water to the water chamber with a constant pressure. A pressure sensor located on the cell's body allows the measurement of the radial stresses. The sample's unloading is carried out by carefully open the outlet valve on the bottom of water chamber, for water drainage. The sample's displacement is monitored by means of a displacement transducer. During the experiments, the upper outlets remain.

The adopted experimental protocol instructs a soil sample of initial height of 40 mm, to be statically compacted to dry density of 2.0 Mg/m<sup>3</sup> (i.e. corresponding to the desired intra-pellet dry density). On Table 4-3, the experimental program is presented. Firstly, the mixtures at the water content of reception were tested by studying the pure effect of MX80 addition. The influence of higher water contents as well as the impact of the compaction velocity (i.e. displacement rate) on the compressibility was also investigated.

The particle density of each mixture was obtained as weighed average of the particle densities of CO<sub>x</sub> argillite and MX80 bentonite as follows:

$$\rho_{s,mix} = \frac{1}{\frac{R_{COx}}{\rho_s^{COx}} + \frac{R_{MX80}}{\rho_s^{MX80}}} \quad (4.1)$$

where  $\rho_s^{COx}$  is the CO<sub>x</sub> argillite's solid particle density equal to 2.70 Mg/m<sup>3</sup>,

$\rho_s^{MX80}$  is the MX80 bentonite's solid particle density equal to 2.78 Mg/m<sup>3</sup>,

$R_{COx}$  is the CO<sub>x</sub> argillite fraction inside the mixture (dimensionless),

$R_{MX80}$  is the MX80 bentonite fraction inside the mixture (dimensionless).

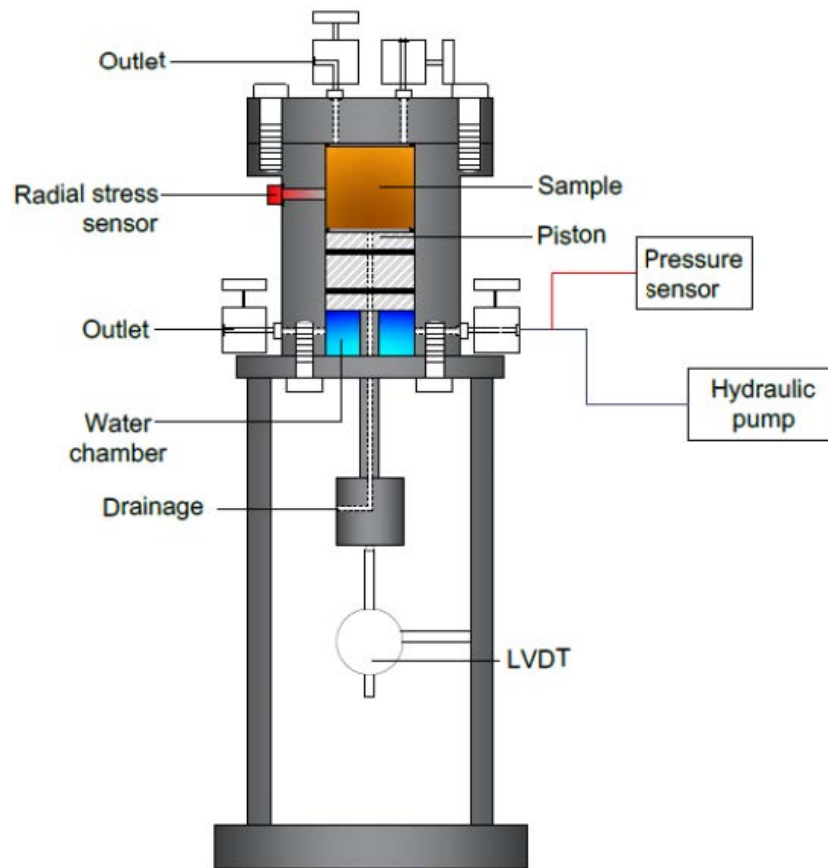


Figure 4-6 Schematic representation of the oedometric apparatus used for the uniaxial compression tests.

Table 4-3 Experimental program followed at uniaxial compression tests.

| N° Test series | MX80 content (%)  | Initial water content $w$ (%)      | Displacement rate (mm/min) | Investigated parameter |
|----------------|-------------------|------------------------------------|----------------------------|------------------------|
| 1              | 0, 10, 20, 30, 40 | 5.9~8.20<br>(reception conditions) | 0.40                       | MX80 bentonite content |
| 2              | 10, 20, 30, 40    | 10<br>15                           | 0.40                       | Water content          |
| 3              | 10, 20, 30, 40    | 15                                 | 0.04<br>0.85               | Displacement rate      |

### Effect of MX80 bentonite content (reception conditions)

The results of compression tests for the studied CO<sub>x</sub>/MX80 mixtures at the reception (almost dry) conditions are presented on Figure 4-7, in terms of void ratio and dry density on semi-logarithmic scale. The observed variations in the water content are attributed to the different initial water contents of CO<sub>x</sub> and MX80 upon the reception. An almost linear relation is observed between void ratio and the applied effective vertical stress in logarithmic scale. The addition of MX80 bentonite introduces more initial voids and thus higher pressure needs to be applied as bentonite content increases. Pure CO<sub>x</sub> was additionally compacted to evaluate this observation regarding the introduced voids by the bentonite. The results showed that it indeed CO<sub>x</sub> presents higher initial dry density, as well as slightly higher compressibility than the CO<sub>x</sub>/MX80 mixtures.

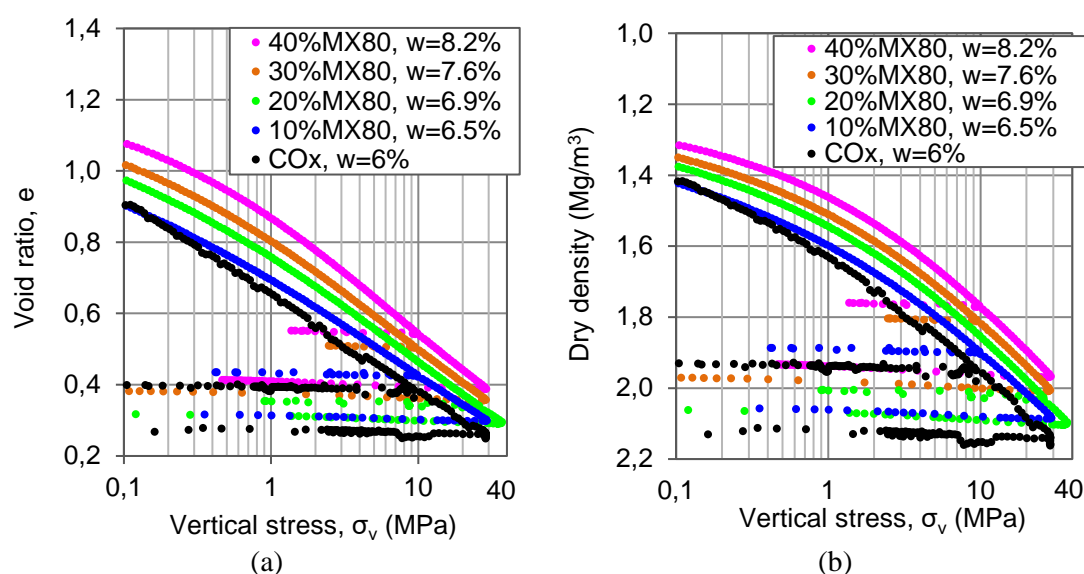


Figure 4-7 Results of uniaxial compression tests at CO<sub>x</sub> and CO<sub>x</sub>/MX80 at initial water content conditions as function of vertical pressure (in logarithmic scale): (a) void ratio and (b) dry density.

The compression index  $C_c$  and swelling index  $C_s$  were determined for the studied CO<sub>x</sub>/MX80 mixtures as the slope of  $e-\log\sigma_v$  curve on the loading and unloading path respectively. On Figure 4-8, the results are presented in relation to the imposed bentonite content. The low variations are evident ( $SD_{C_c} = 1.2\%$ ,  $SD_{C_s} = 0.3$ ), suggesting that compressibility is mainly governed by the CO<sub>x</sub> argillite. Therefore, average values are proposed for both parameters ( $C_c=0.26$ ,  $C_s=0.009$ ).

The evolution of the radial stress  $\sigma'_h$  with the applied vertical stress  $\sigma'_v$  is presented on Figure 4-9. A typical path is observed during loading/unloading/reloading conditions (Mayne and Kulhawy, 1982; Robinet et al., 2003; Mitchell and Soga, 2005). On the normally consolidated conditions, the virgin loading is obtained. On the unloading path (passing to

over-consolidation state), the horizontal stress does not decrease on the same rate as the vertical. The material's reloading leads to further increase of radial stress and eventually following the virgin loading path. However, no significant effect of MX80 additive is detected on this condition. The coefficient of earth pressure at rest  $K_0$  ( $\sigma'_h/\sigma'_v$ ) was determined for the loading path of each mixture (Figure 4-10). A small variation is observed (SD=1.3%), therefore, an average value of 0.43 was selected.

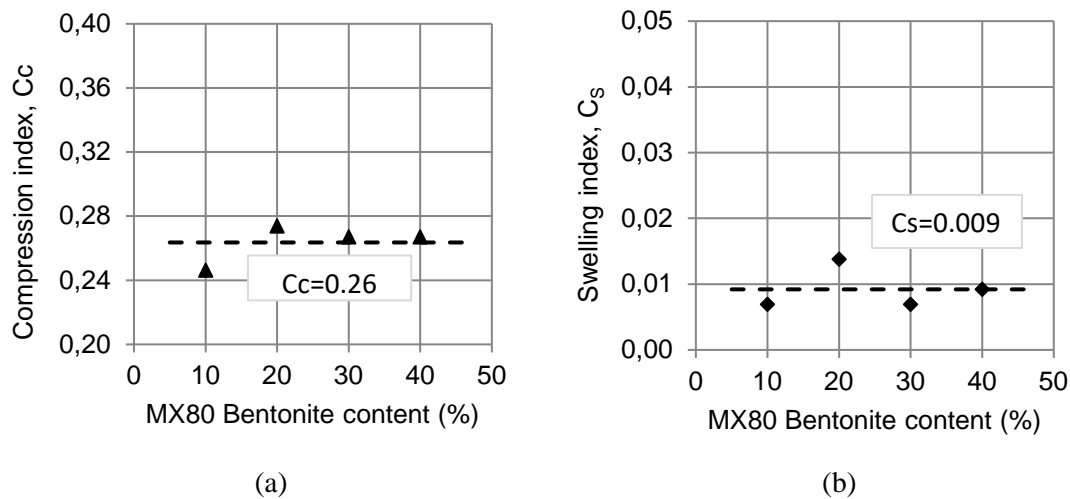


Figure 4-8 Variation of (a) compression and (b) swelling index for COx/MX80 mixtures, in relation to MX80 content.

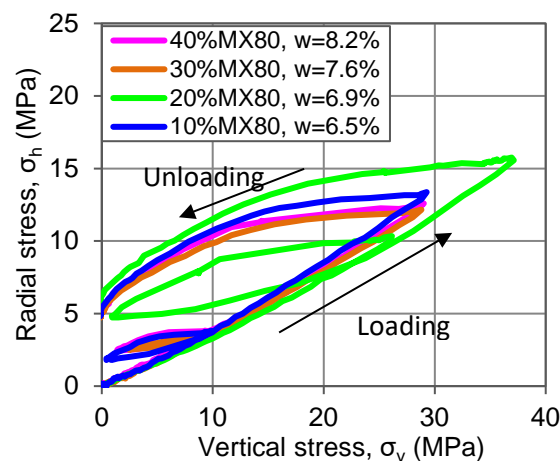


Figure 4-9 Variation on radial stresses with the applied vertical stress during the loading and unloading paths of compression tests on COx/MX80 at their initial conditions.

On Figure 4-11, the different compacted COx/MX80 mixtures at their reception water content conditions are presented after the uniaxial compression tests. The bentonite addition is visible on every specimen.

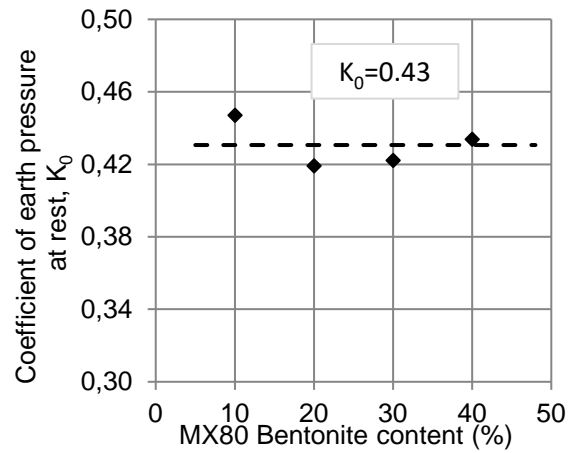


Figure 4-10 Variation of coefficient of earth pressure at rest for CO<sub>x</sub>/MX80 mixtures, in relation to MX80 content.

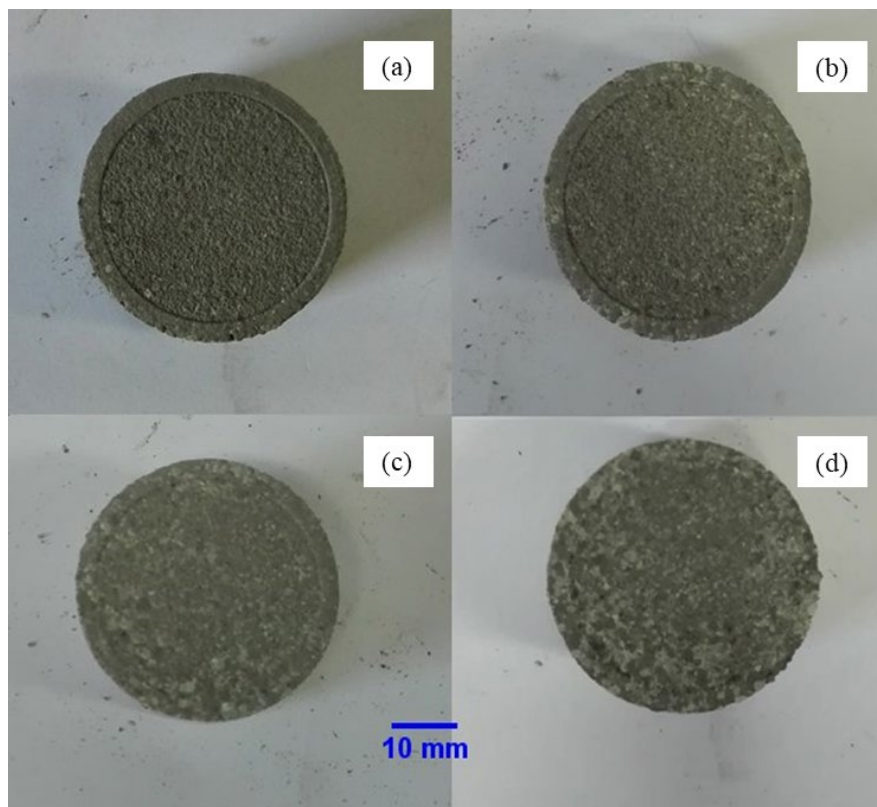


Figure 4-11 Compacted CO<sub>x</sub>/MX80 mixture at reception conditions, at the end of uniaxial compression tests, containing (a) 10%MX80, (b) 20%MX80, (c) 30%MX80 and (d) 40%MX80.

## Effect of water content

It is known that water content increase up to an optimum value, can improve soil's compaction characteristics. In this context, water was added in COx/MX80 mixtures and the impact on their compaction was evaluated by performing uniaxial compression tests. COx and MX80 were homogeneously mixed in desired proportions and they were humidified by using demineralised water in vapour form. The samples were kept in hermetic chambers for 24 h to achieve homogenous hydration. Similar to the experimental protocol followed at the reception conditions, two cycles of loading/unloading were carried out: loading up to 10 MPa with unloading and then reloading until 2.0 Mg/m<sup>3</sup> of dry density were obtained (~ 30 MPa). Radial stresses were monitored.

The test results are presented on Figure 4-12, illustrating also the water content conditions as measured at the end of each test. It is clear that water content increase, leads to higher initial void. In fact, it was observed that the water addition modified the mixture's initial granulometry. Since the material was no longer dry, water presence caused cohesion development and the particles formed larger grains, which resulted in looser state upon preparation. Nonetheless, for applied stresses higher than 1 MPa, compressibility significantly improves when more water is used. For water contents in the magnitude of 15%, the linear relation of void ratio with vertical stress is affected ( $\sigma_v \geq 10$  MPa) and the material is not further compressed. It might be attributed to pore-pressure developed due to the water presence, which hinders compaction. Tang et al. (2009) analysed this "S-shaped" compression curve ( $e - \log \sigma_v$ ) similarly appearing at high stresses. It was observed more frequently when the soil plasticity and/or the initial water content are high, since the mechanism of capillary water flow becomes dominant. According the present experimental results, the non-linear part is less prominent when bentonite content increases, probably because the free water is absorbed by the interlayer in this case. This behaviour shows that finally increase of water content more than 15% does not facilitate the material's compaction at high densities.

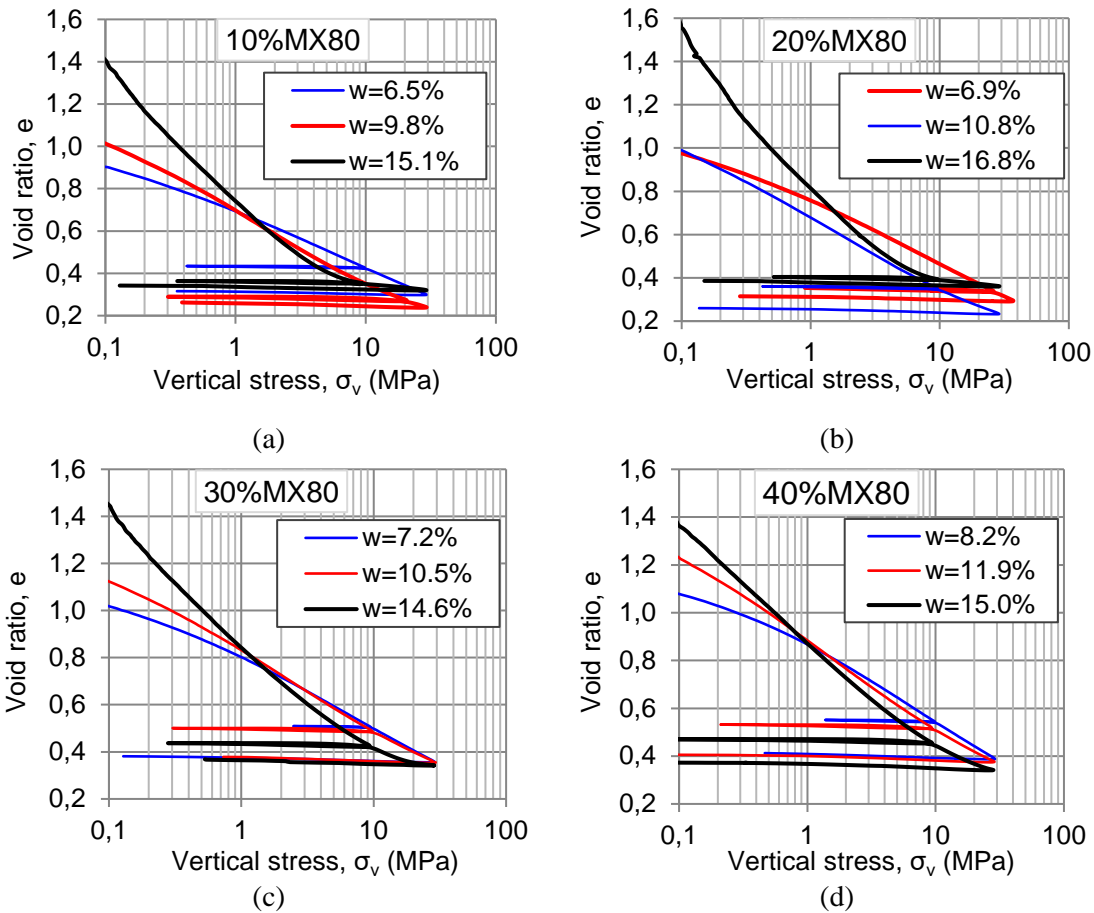


Figure 4-12 Evolution of void ratio with the applied vertical stress (in logarithmic scale) for different water content conditions of COx/MX80 mixtures containing: (a) 10%, (b) 20%, (c) 30% and (d) 40% of MX80.

Figure 4-13 illustrates the evolution of radial stresses during the materials compression for the varied COx/MX80 mixtures prepared at different water contents. Increase of water content results in more rapid development of the radial stress. The coefficient of earth pressure at rest  $K_0$  ( $\sigma'_h/\sigma'_v$ ) was determined for the loading path of each mixture prepared at different water content (Figure 4-14). The same effect of water content is observed. For all COx/MX80 samples, a linear increase of  $K_0$  is obtained at higher water content.

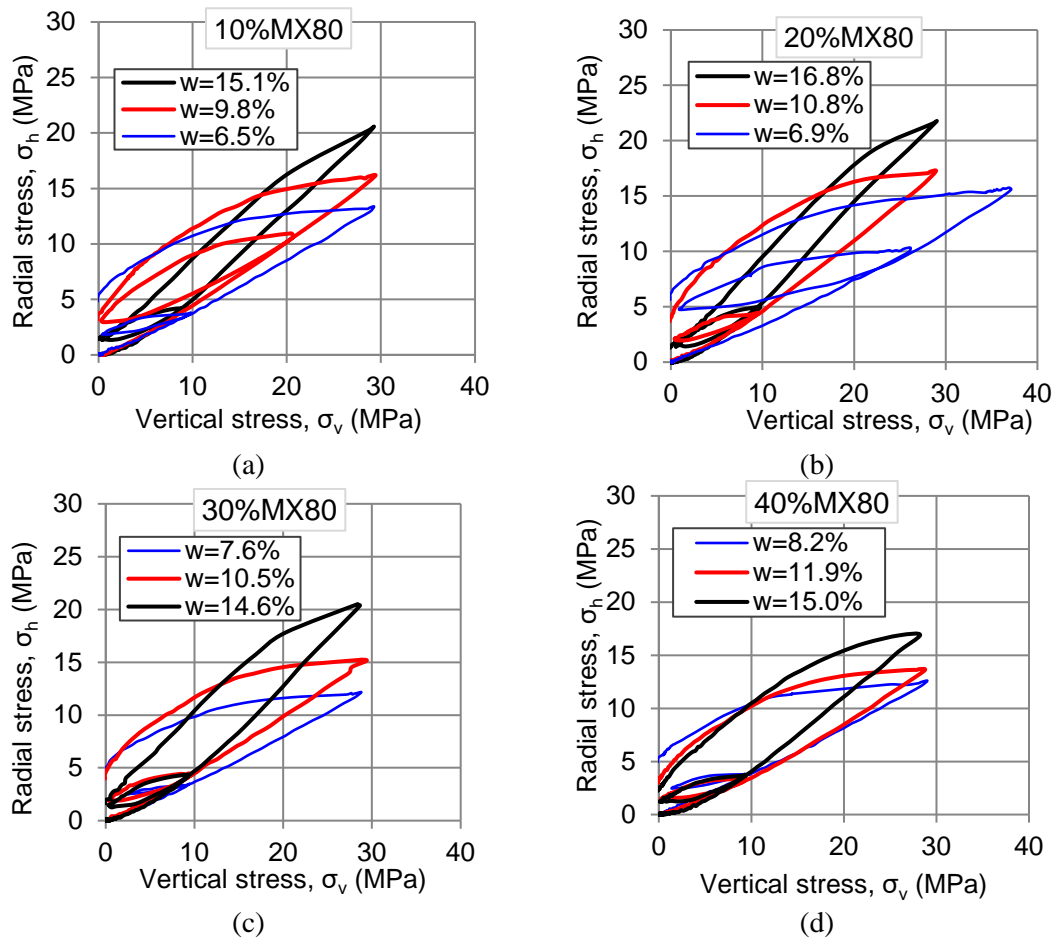


Figure 4-13 Evolution radial stress with the applied vertical stress for different water content conditions of COx/MX80 mixtures containing: (a) 10%, (b) 20%, (c) 30% and (d) 40% of MX80.

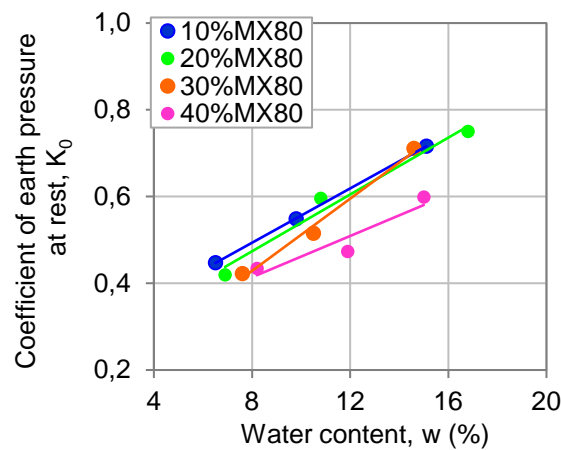


Figure 4-14 Variation of coefficient of earth pressure at rest for various COx/MX80 mixtures, in relation to imposed water content.

## Effect of displacement rate

The abovementioned results indicated that capillarity water flow is developed at water contents close to 15% that hinders the material's compaction at high stresses. In order to evaluate if this response could be affected by the imposed compaction velocities, different displacement rates were applied on the investigated mixtures of COx argillite and MX80 bentonite. Apart from the default displacement rate of 0.4 mm/min, higher (0.85 mm/min) and lower (0.04mm/min) compression velocities were also imposed. One loading/unloading cycle was carried out on every test. The obtained results in terms of void ratio are presented on Figure 4-15. The impact of water content on the linear relation  $e - \log \sigma_v$  is observed independently to the imposed displacement rate after the application of 10 MPa.

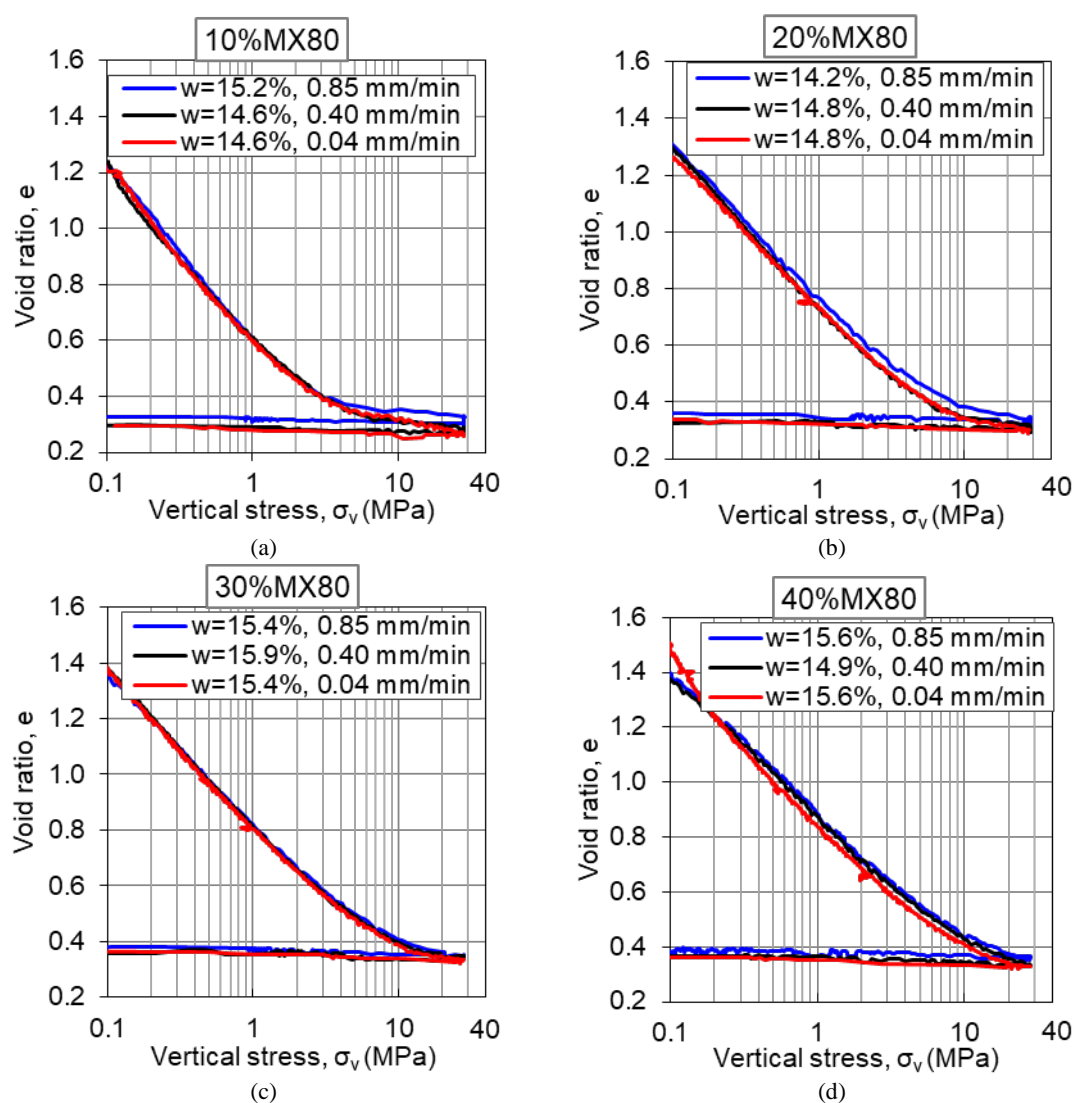


Figure 4-15 Evolution of void ratio with the applied vertical stress (in logarithmic scale) for different displacement rates (0.04-0.40-0.85 mm/min) of COx/MX80 mixtures with water content of ~ 15%, containing: (a) 10%, (b) 20%, (c) 30% and (d) 40% of MX80.

On Figure 4-16, the maximum obtained dry density is plotted as function of the applied displacement rate. An influence of the applied compaction velocity on the achieved density is observed for all the tested mixtures. Indeed, compaction carried out on lower displacement rates could slightly improve the achieved density. However, the effect of the imposed compaction velocity decreases with the increase of MX80, since the free water could be absorbed by the interlayer.

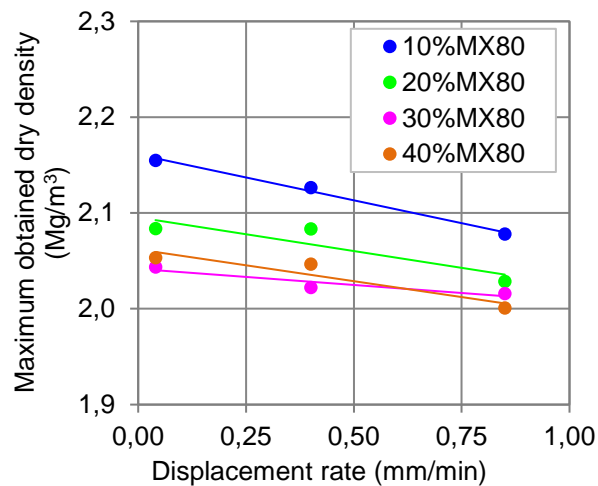


Figure 4-16 Maximum obtained dry density as function of the applied displacement rate for different CO<sub>x</sub>/MX80 mixtures.

Upon pellet fabrication, the raw material is compressed by the pellet machine, which operates at with high velocities (even than 0.85 mm/min). Taking into consideration the results of uniaxial compression tests and this technical parameter, the potential increase of water content (i.e. intended to improve the material's compressibility) will eventually hinder the fabrication of pellets and therefore is not suggested.

### 4.3 Pellet machine and fabricated accessories

In the framework of the present study, the fabrication of pellets containing mixtures of CO<sub>x</sub> argillite and MX80 bentonite is proceed. The pelletizing technique is based on the material's uniaxial compression inside moulds of target sizes, until an approximate dry density of 2.0 Mg/m<sup>3</sup> is achieved. Following the preliminary study of material's compression (section 4.2.1.2), the actual pelletization is carried out. Pellets of quasi-spherical shape with diameters of 16 mm, 10 mm and 4 mm are selected for fabrication as instructed by the numerical study of Chapter 3. The target shape of the fabricated pellets is illustrated on Figure 4-17.

A Frogerais 1B tablet press machine was reconditioned for the needs of the present project (Figure 4-18a). A motor drives a pulley on the axis of the crankshaft via a belt. Closer to the metallic frame, a second pulley is activated by the transfer of the belt. The movement triggers

two pistons in the upper and bottom part of the metallic frame, responsible for the material's compaction. In the central part of the frame, a matrix is fixed containing the cell-moulds of cylindrical cross-section (Figure 4-18b). The upper and lower pistons are equipped with cylindrical punch tools presenting curvature at each ending with suitable size to pass through the mould (Figure 4-18c). According to the manufacture process, the pellet total height (as well as the lines intersecting the pellet edges and passing through the pellet center) have length were very close to the value of the pellet diameter.

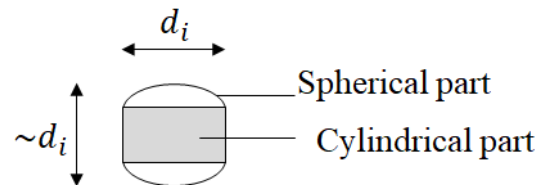


Figure 4-17 Target pellet shape.

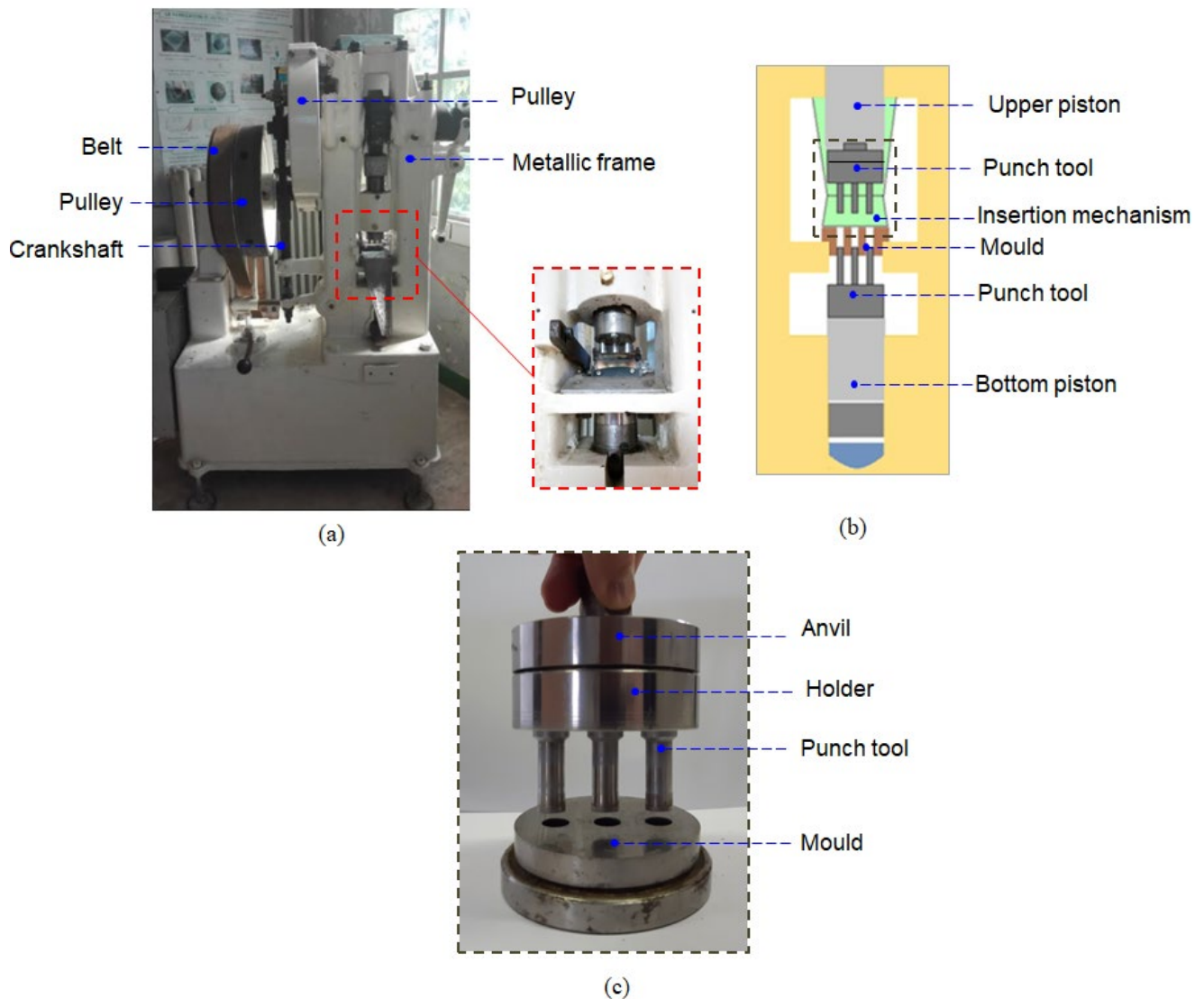


Figure 4-18 (a) Frogerais 1B tablet press machine used on the present study, and detailed description of (b) the machine's metallic frame and (c) part of mould and punch tools.

An automatic mechanism located in the back part of the machine, inserts the raw powdered material into the moulds through a funnel. The downward movement of the upper piston to a fixed position compresses the material to the desired shape. After the completion of its movement, it ascends automatically and the lower piston moves, upwards traversing the mould's height in order to eject the fabricated pellet. The next movement of the inserting mechanism pushes away the pellet and marks the beginning of the next pelletizing cycle. Along this process, the inserted soil mixture undergoes a rapid loading/unloading cycle with very high displacement rate.

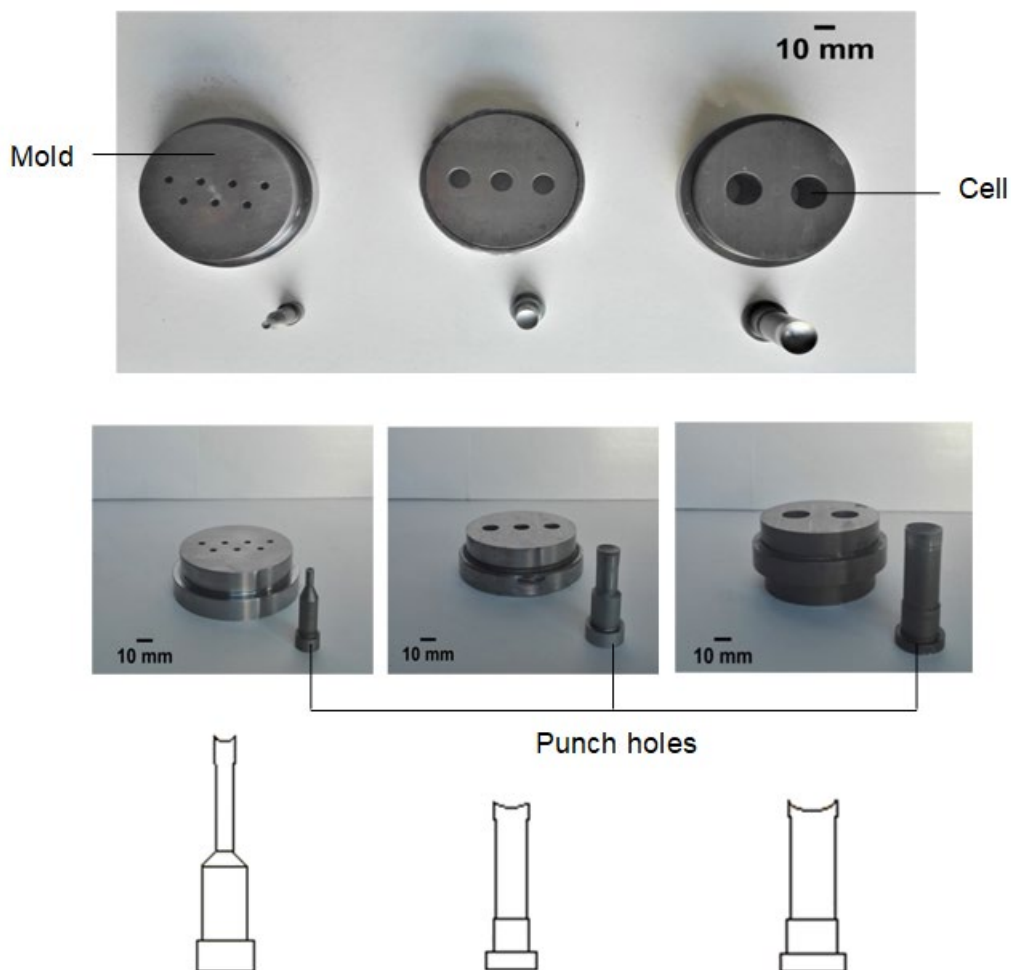


Figure 4-19 Fabrication of accessories for target sizes (4 mm, 10 mm and 16 mm): moulds and punch tools.

The mould is responsible for shaping the pellet's cylindrical part, whereas the punch tool forms the spherical parts upon compaction (Figure 4-19). As the illustration of Figure 4-19 shows, the cylindrical punch tool presents a relatively varying cross-section. The essential accessories were designed and manufactured for the desired pellet sizes. More precisely, for each target size, the mould equipped with an appropriate number of cells and two pairs of punch tools with the corresponding number are designed. In order to accelerate the produced

quantity, the number of cells on each mould is maximised, taking in account the available geometry of the mould. Therefore, for the fabrication of the diameter of 4 mm, 10 mm and 16 mm, seven (7), three (3) and two (2) cells were designed. More details are presenting on the Appendix A.

#### **4.4 Optimisation of CO<sub>x</sub>/MX80 pellet production: Influential factors**

In general, pelletizing process can be considered successful, when intact pellets of high density are easily fabricated. Therefore, the parameter of high production at long-term (e.g. 200-300 kg) should be additionally taking into consideration, even at the semi-industrial scale.

In the beginning of the pelleting process, it was seen that the pelletization of pure MX80 bentonite was carried out successfully without difficulties. On the other hand, CO<sub>x</sub>/MX80 pellet fabrication was proven to be a complicated challenge, where several parameters had to be assessed in order to overcome the encountered problems. The difficulties when CO<sub>x</sub> was inserted in the pellet machine were related to the machine blockage or pellet damage. Pellets were considered damaged upon the unloading process, when they presented decohesion or a missing spherical part (e.g. due to material's attachment on the upper punch hole). Therefore, the entire manufacturing process was examined, taking into consideration the characteristics of the fabricated accessories, as well as the materials initial state. Pellet intactness was evaluated by calculating the damaged pellets' percentage measured on 10 kg of produced material, using the sieving method. The process is divided in two main categories, which are related with:

- parameters that lead the fabrication of a CO<sub>x</sub>/MX80 pellet, such as material and geometry comprising the fabricated accessories, and
- the inserted material's initial state (e.g. water content, granulometry, etc.).

##### **4.4.1 Realisation of pellet fabrication**

In the present context, objective factors had to be defined, in order to achieve fabrication of CO<sub>x</sub>/MX80 pellets.

###### **1. Metallurgy of the fabricated accessories**

Moulds and punch tools were assessed, after machine blockage was observed for the first time. A visual evaluation revealed numerous scratches in the punch surfaces (Figure 4-20), which was causing fine particles to be inserted in different parts. Therefore, the nature of the accessories had to be modified. Another type of steel, in

particular high-speed steel containing cobalt was selected, additionally treated to avoid corrosion. That metallurgical type was proven as suitable for production of large amount of pellets. Nonetheless, currently (after the production of almost 50 kg of pellets), rupture occurred at the end of the punch tool (Figure 4-21), proposing a new material modification, by using high hardness steel of high corrosion resistance.

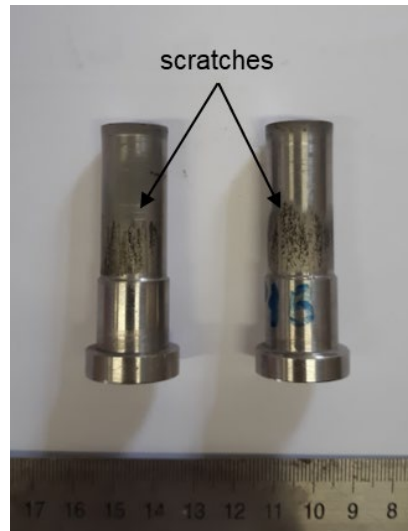


Figure 4-20 Scratches observed in the first type of fabricated punch tools.

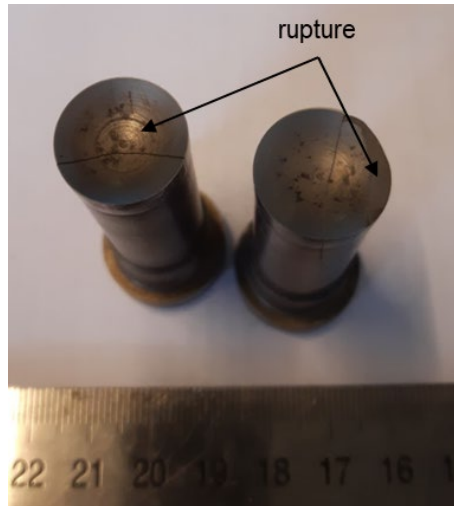


Figure 4-21 Rupture of punch tool's ending occurred after the fabrication of approximately 50 kg of pellets.

## 2. Geometrical characteristic of accessories

The geometry of the punch tool had to be adjusted, without however losing the curvature at its ending that provides the pellet with the spherical upper and bottom part. Firstly, the cross-section of the punch tool cylinder had to be modified, by

reducing gradually its width, in order to allow fine particles release and avoid any breakage. The effect is more visible on the detail illustrated on Figure 4-19. Nonetheless, material attachment on the upper punch was observed upon the pellet de-compaction, risking its intactness (Figure 4-22). Therefore, it was suggested that the high volume of spherical part hindered pelletization. Therefore, the endings were modified to exhibit lower curvature radius in order the spherical part to present a volume equal of approximately 10% of the total pellet volume.



Figure 4-22 Observed soil attachment to the punch tool with the initial curvature.

The approach of implementing the pellet fabrication is summarised on Figure 4-23.

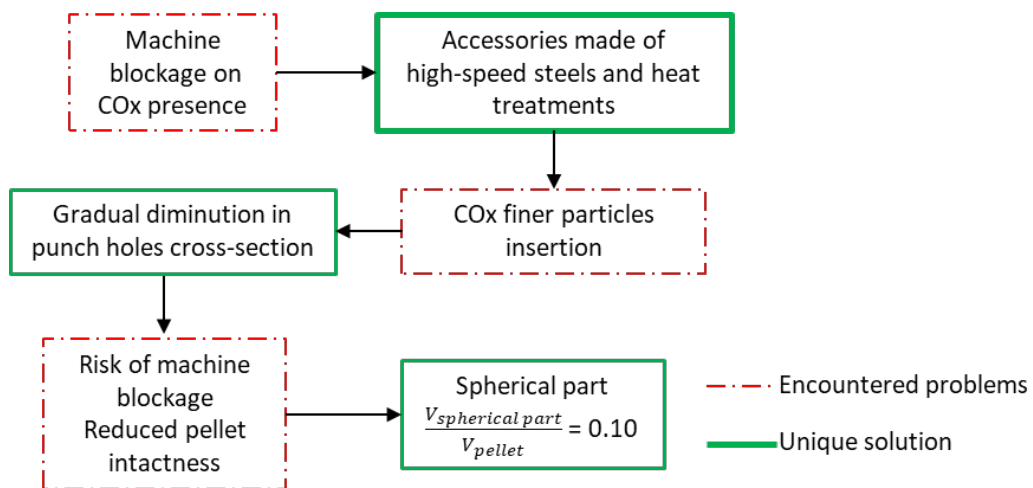


Figure 4-23 Schematic presentation of the adopted approach for realisation of pellet fabrication.

#### 4.4.2 Optimisation of pellet production

Once the CO<sub>x</sub>/MX80 pellet fabrication could be actually carried out, the pellet production was studied. In the following sessions, an analysis on factors affecting pellet production is presented. For each encountered problem, either a unique solution was suggested or a parameter was proposed for optimisation.

##### 1. CO<sub>x</sub>'s argillite initial state

As it has been mentioned, CO<sub>x</sub> presence obstructed the pelletizing process due to finer particles that risked blocking the machine. Two alternative solutions were explored in order to overcome this obstacle.

In the beginning, the initial granulometry of CO<sub>x</sub> was modified in order to decrease fines and approach a similar GSD of that of MX80 bentonite. Thus, the content in 200 μm sized grains was gradually decreased by sieving the argillite material, while the effect on pellet intactness was examined. The results are presented on Figure 4-24a. It is clear, that 10% of grains finer than 200 μm should be contained. This adjustment is hereafter referred as modified CO<sub>x</sub> granulometry.

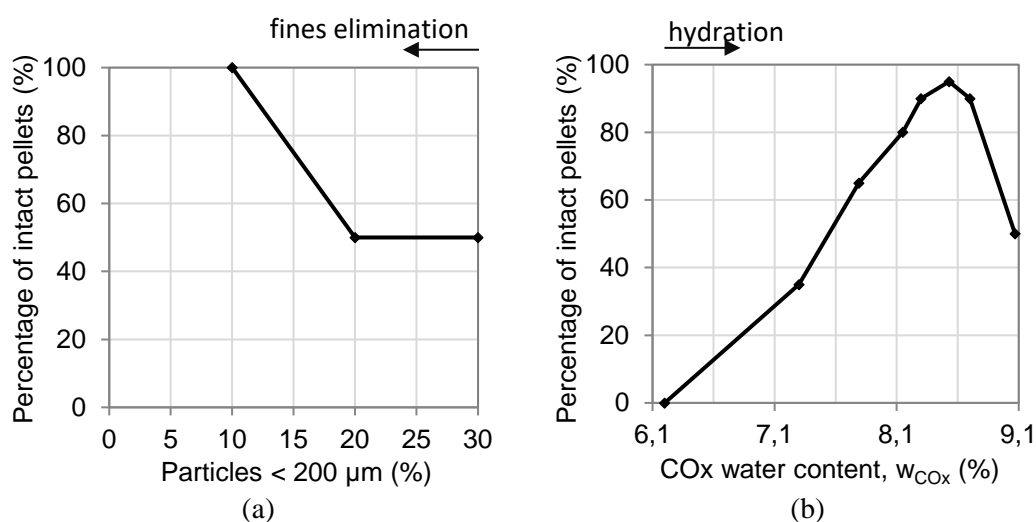


Figure 4-24 Effect of CO<sub>x</sub> argillite's initial state on pellet production: (a) percentage of particles finer than 200 μm, (b) water content.

Nonetheless, modifying the argillite's GSD does not facilitate a pellet production at a more industrial scale, due to time consuming material processing. Therefore, CO<sub>x</sub> progressive hydration was proposed in order to increase the cohesion of inserted material and prevent fines from interfering pelletization. The observed results are presented on Figure 4-24b. The damaged pellets are decreasing with increase of CO<sub>x</sub>'s water content. After an optimum value corresponding at w<sub>CO<sub>x</sub></sub>=8.53%, further

hydration hinders pellet production. Consequently, this water content value is suggested if no alternation in granulometry is required.

## 2. CO<sub>x</sub>/MX80 mixtures water content

In the case of the modified CO<sub>x</sub> granulometry, the effect of formed CO<sub>x</sub>/MX80 water content studied. Argillite and bentonite were firstly mixed and their water content was later varied (Figure 4-25). The conditions were applied by either hydrating or drying of the prepared CO<sub>x</sub>/MX80 mixtures. Mixture's drying caused pellet de-cohesion. On the contrary, CO<sub>x</sub>/MX80 mixture's hydration up to 12.8% resulted in attachment of upper spherical part on the surface. Finally, water content at the as-received state presented high pelletizing performance.

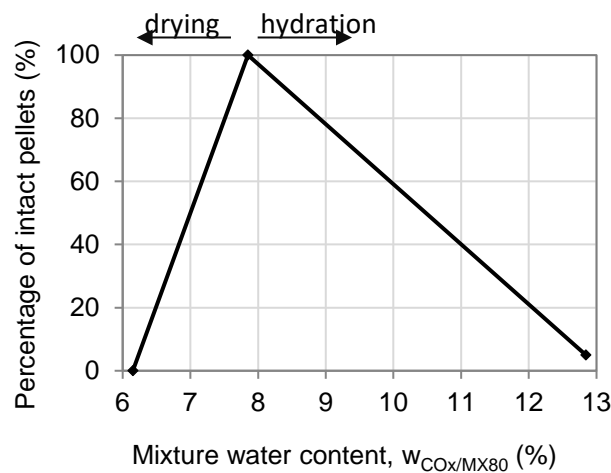


Figure 4-25 Effect of initial CO<sub>x</sub>/MX80 mixture's water content on pellet production using the modified CO<sub>x</sub> granulometry.

## 3. Mass proportion of CO<sub>x</sub>/MX80 mixture

An investigation of the mixtures composition on pelletization was conducted by compacting different CO<sub>x</sub>/MX80 mixtures using the modified CO<sub>x</sub> granulometry (Figure 4-26). A gradual impact is observed when bentonite content is reduced. Although mixture contain 40% of MX80 was compacted successfully, ease in compaction is decreased for further reduction of MX80 content. The observation is in agreement with the noted initial difficulty in pelletization of CO<sub>x</sub>/MX80 instead of pure bentonite material. Although material's composition is defined by the hydro-mechanical response of CO<sub>x</sub>/MX80 mixture, a successful pelletizing process should focus on fabrication in complete CO<sub>x</sub>/MX80 fractions. Therefore, 5% diminution of target intra-pellet density is proposed in order to achieve an easier two-component mixture pelletization.

Figure 4-27 summarises the adopted approach to improve the pelletizing process, by illustrating the encountered problems and the proposed solutions. In that framework, the chosen pellet sizes were successfully fabricated, presenting on Figure 4-28. It should be mentioned that these quasi-spherical shaped pellets (i.e. pellet diameter is very close in size with the pellet height) present sphericity that varies insignificantly from 0.90 to 0.97 (contrary to 1, for a perfect sphere). Pellets of 16 and 10 mm in diameter were produced by COx/MX80 mixtures in various fractions. However, pellets with 4 mm diameters were fabricated only for pure MX80 bentonite, because a good mixture distribution could not be assured due to the small pellet size and the granulometry of the materials ( $d_{max} \leq 2$  mm). Nonetheless, the material's composition inside the pellets is possible to be adapted in order the overall MX80 presence to be close to 30%. The obtained intra-pellet dry density was determined by immersing a pellet covered in paraffin inside demineralized water. A minimum dry density of  $1.95 \text{ Mg/m}^3$  is assured.

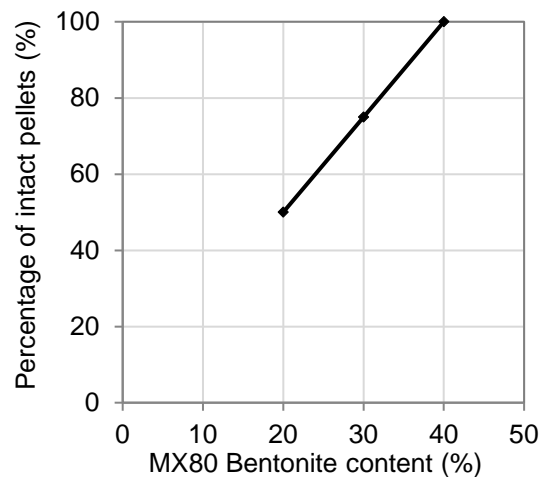


Figure 4-26 Effect of COx/MX80 mixture's composition on pellet production using the modified COx granulometry.

The approach followed for optimising the pellet production is summarised on Figure 4-27. Detailed information for the conducted work is presented on the Appendix B.

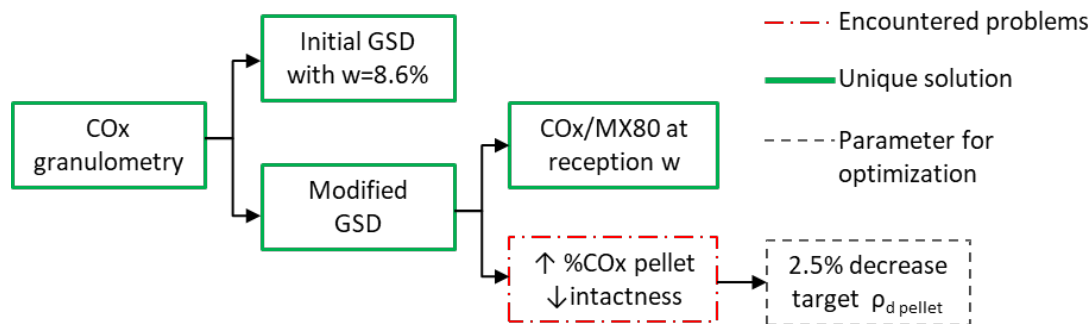


Figure 4-27 Schematic presentation of the adopted approach for optimisation of pellet production.

## 4.5 Conclusions

The pelletizing process was investigated for the studied CO<sub>x</sub>/MX80 mixtures ( $\leq 40\%$ MX80), by initially characterising their physical parameters and their compressibility, as well as by carrying out the actual pellet fabrication for the sizes previously defined by the numerical study (16 mm, 10 mm, 4 mm).

The initial characterisation demonstrated a clear difference on the materials physical parameters: CO<sub>x</sub> argillite is a medium plasticity clay with significantly lower absorption capacity than the MX80 bentonite of extremely high plasticity. The effect of bentonite content followed the expected trend for the CO<sub>x</sub>/MX80 mixtures: MX80 addition on CO<sub>x</sub> increases mixture's plasticity, while free swelling capacity becomes more significant.

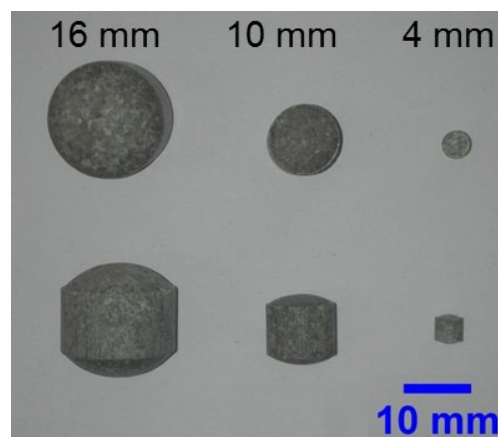


Figure 4-28 Fabricated pellets with diameter of 16 mm and 10 mm (CO<sub>x</sub>/MX80 mixture) and 4 mm (pure MX80)

Uniaxial compression tests ( $D=40$  mm,  $H=40$  mm) attempted to primarily evaluate the materials behaviour upon the pelletizing process (target dry density of  $2.0$  Mg/m<sup>3</sup>). At compression with low imposed velocities, the following remarks can be outlined:

- Compressibility is not influenced by bentonite content: vertical and radial stress development does not significantly vary on bentonite addition. However, MX80 inserts initial voids and therefore higher vertical stress is necessary to achieve the desired density state.
- Water content increase can improve material's compressibility at lower stresses. For higher water content ( $\sim 15\%$ ), capillarity water flow is more significant, opposing compaction at higher stresses. This behaviour is also observed when displacement rate decreases.

Pelletization was conducted by a tablet press machine, reconditioned for the needs of the present study. The pellet machine compacts the raw materials at high compaction velocities,

producing quasi-spherical pellets. The necessary accessories (moulds, punch tools) were fabricated for the target sizes (16 mm, 10 mm, 4 mm). The CO<sub>x</sub>/MX80 mixtures first pelletization was proven as a challenging procedure. It needs to be noted that the high compaction velocity of real pelletization conditions in combination with the slightly different configuration (i.e. perfect cylindrical specimen of uniaxial compression tests and quasi-spherical pellets) did not allowed a clear correlation between pelletization and uniaxial compression tests. More precisely, the uniaxial compression tests showed that CO<sub>x</sub> results in lower initial voids and compaction at the target intra-pellet density (displacement rate  $\leq 0.85$  mm/min) could be carried out at lower applied stresses (i.e. easier). On the other hand, the CO<sub>x</sub> argillite presence on the inserted material significantly hindered the procedure. Therefore, the process was optimised, taking into consideration the encountered problems. A series of actions were undertaken concerning the fabricated machine accessories and the state of the inserted powdered material:

- Punch tools and moulds were fabricated from materials capable to successfully compact mixtures containing CO<sub>x</sub> argillite, while a calibration of their resulting geometry (edge and spherical height) was necessary.
- Regarding the inserted CO<sub>x</sub>/MX80 mixtures, two possible solutions were proposed. Decrease of CO<sub>x</sub> fine content facilitated the fabrication of intact pellets. In that case, the natural resulted CO<sub>x</sub>/MX80 water content was optimal for high pellet production. On the other hand, a slight increase of original CO<sub>x</sub> water content appeared as sufficient solution for a successful industrial pellet production.
- In general, CO<sub>x</sub> addition was a limiting factor for pellet realization. Therefore, an insignificant reduction of intra-pellet density was proposed to achieve intact pellet fabrication.

# **Chapter 5 - Experimental optimisation of the resulting packing density of pellets assembly**

The objective of the chapter is to determine experimentally the resulting packing state of the pelletized assembly, in the direction of its maximisation. The fabricated pellet sizes (16 mm, 10 mm, 4 mm) are studied by means of gravitational deposits on conditions similar to the numerical study. The presence of finer grains inside the mixture is examined, by using sandy materials. The effect of implementation protocol on the material's compactness is assessed. The granulometric configuration leading to the maximum resulting packing density is finally selected for the pelletized material. The chapter is developed in the following main parts:

- 5.1 Introduction
- 5.2 Studied materials and experimental set-up
- 5.3 Results and discussions
- 5.4 Conclusions and optimised resulting packing density

## 5.1 Introduction

In Chapter 3, the numerical approach on the optimum GSD suggested the pelletized material to be composed of pellets with 16 mm, 10 mm and 4 mm in diameter mixed in proportions of 60%, 10% and 30%, in order to obtain the maximum resulting packing dry density. In Chapter 4, the pellet sizes were successfully fabricated (Figure 4-28), presenting quasi-spherical form, consisting of a central cylindrical part of the given diameter and two spherical elements located on the top and bottom part.

Following the adopted strategy of the study, the next objective is twofold. The present experimental analysis initially aims to evaluate the actual resulting density state for the fabricated pelletized material. The secondary objective focuses on the investigation of additional conditions that maximise the resulting packing density (optimisation). In the latter, alternative granulometric configurations containing finer grains are examined. Different implementation protocols as well as alternative proportions are tested.

In this chapter, the optimisation of the resulting density is analysed for the pellet assembly, in order to maximise as possible the packing state. The experiments are conducted on a medium scale, very similar to that one followed in the numerical simulations. On section 5.2, the studied materials, the experimental set-up as well as the followed program are summarised. The experimental data are directly compared with the numerical DEM results on section 5.3.1.2. A series of supplementary tests is conducted to investigate in more details the conditions maximising the density state (section 5.3.2). Finally, the investigated density range for the pelletized assembly is defined.

## 5.2 Studied materials and experimental set-up

Fabricated pellets of 16 mm, 10 mm and 4 mm in diameter were used to evaluate the emplaced dry density. Details about their composition, water content and measured intra-pellet dry density are presented on Table 5-1. An average dry density of  $2.0 \text{ Mg/m}^3 (\pm 0.05)$  is obtained, as measured by immersing a pellet covered with paraffin inside demineralized water.

The impact of finer grains ( $d \leq 2 \text{ mm}$ ) inside the pelletized mixture was examined by testing two types of dry commercial sands. The sandy materials presented different granulometry; a well-graded sand (WGS) and a uniform/poorly graded sand (PGS) were used. The PGS was resulted from sieving of the WGS. Figure 5-1 illustrates the grain size distribution of the sandy materials as well as the investigated pellets. It is observed that both sands have maximum diameter,  $d_{max}$  of 2 mm. Nonetheless, PGS contains grains with diameters up to

600  $\mu\text{m}$ , while WGS contains finer grains with diameters up to 80  $\mu\text{m}$ . Details of the uniformity coefficient ( $CU$ ) and curvature coefficient ( $CC$ ) of the two sands are presented on Table 5-2. Even though WGS does not meet the exact criteria of the Unified Soil Classification System for well-graded sands ( $CU \geq 6$  and  $1 \leq CC \leq 3$ ), it is known that a higher  $CU$  parameter implies wider sized particles and thus is considered as well-graded.

Table 5-1 Details of studied pelletized materials.

| Pellet diameter $d_i$ (mm) | Contained materials        | Water content, $w$ (%) | Intra-pellet dry density, $\rho_{d \text{ pellet}}$ ( $\text{Mg}/\text{m}^3$ ) |
|----------------------------|----------------------------|------------------------|--|
| 16                         | Argilite/Bentonite (60/40) | 6.5                    | 1.94   |
| 10                         | Argilite/Bentonite (60/40) | 6.3                    | 2.05   |
| 4                          | Bentonite                  | 11.9                   | 2.00   |

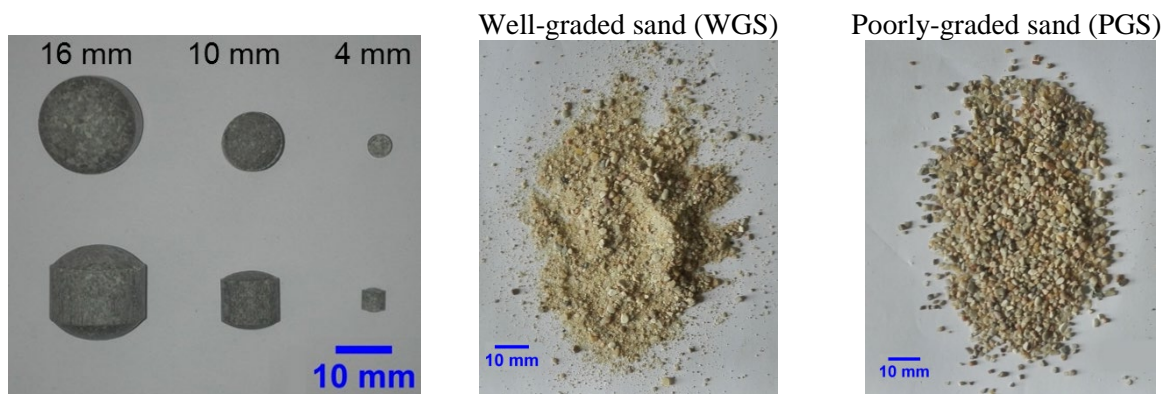
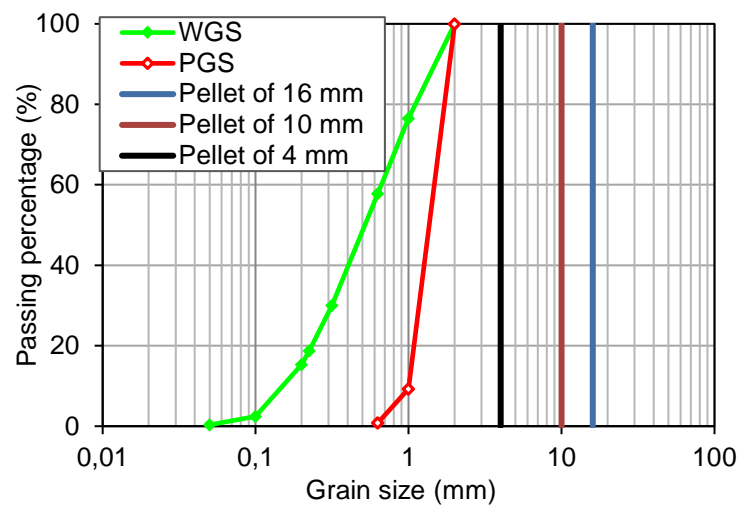


Figure 5-1 Granulometry and pictures of materials used for the experimental study of density maximisation.

Table 5-2 Granulometric details of studied sandy materials.

| Material | $d_{max}$<br>(mm) | $d_{10}$<br>(mm) | $d_{60}$<br>(mm) | $CU$ | $CC$ |
|----------|-------------------|------------------|------------------|------|------|
| WGS      | 2.0               | 0.12             | 0.61             | 5.1  | 1.2  |
| PGS      |                   | 1.00             | 1.20             | 1.2  | 1.0  |

The resulting packing density was measured experimentally by means of two transparent containers. A cubic Plexiglas cell (Figure 5-2a) is used with internal dimensions of 0.160 m in length and width ( $l_x = l_y = 10 \cdot d_{max}$ ) and height ( $l_z$ ) of 0.180 m. The maximum total volume corresponds at 0.005 m<sup>3</sup>. Additionally, a cylindrical container (Figure 5-2b) with diameter equal to  $D \approx 0.155$  m was adopted. The sample's height never exceeded the variation spotted in the cylinder's cross-section and thus the available height was  $H \approx 0.165$  m. The maximum total volume corresponds at 0.003 m<sup>3</sup>. Thus, the possible effect of cell's form on the resulting packing state was assessed.

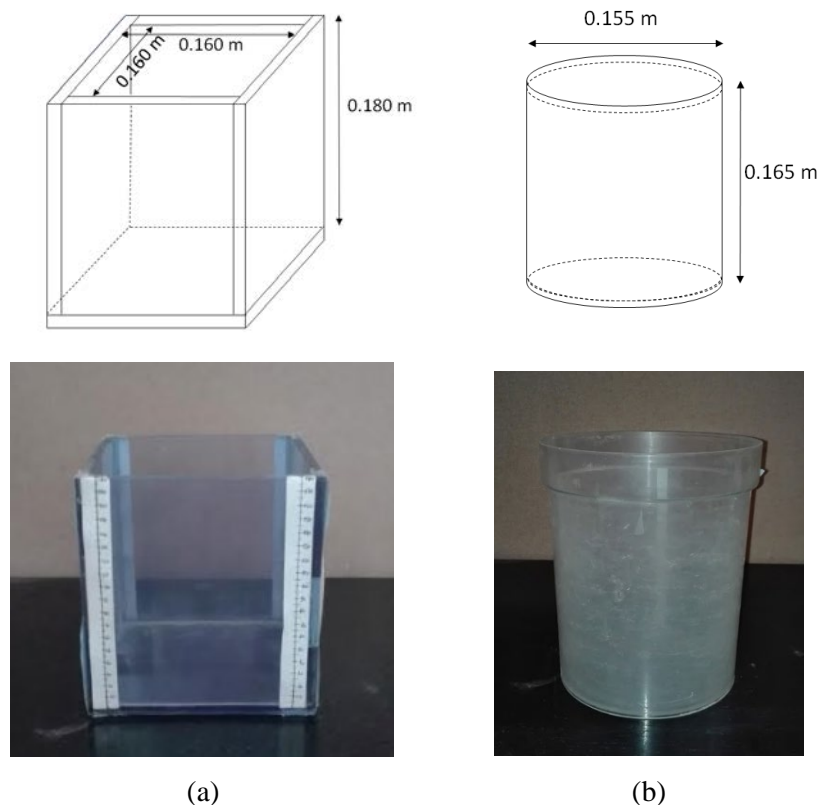


Figure 5-2 Transparent cells used for the density measurement of the pelletized mixture: (a) cubic and (b) cylindrical container.

Different implementation protocols for the samples deposit were applied. The imposed GSD (pellets, pellets and sand) is prepared by two methods:

- by **blending** the desired proportions of grain sizes and directly deposited them inside the used cell (deposit from the cell's height)
- by **layering** the desired proportions; each layer is prepared by placing the diameters in the corresponding proportions in order of size ( $d_{max} \rightarrow d_{med} \rightarrow d_{min}$ ).

In both protocols, the material's deposit takes place a position equal to the cell's height. In general, the final specimen height was ranging between 0.150 m to 0.180 m.

Contrary to DEM simulations where GSDs are generated in volumetric proportions, the experimental study deals with proportions of total mass. Since the dry intra-pellet density was commonly considered as  $2.0 \text{ Mg/m}^3$ , proportions coincide. In the experiments, the final mass and volume are measured at the end of the deposit and the bulk density is calculated. Specimen's water content is determined and the achieved dry density is reported.

On Table 5-3, the followed experimental program is summarised. For each case, at least two tests were conducted and the average value was obtained. It can be seen that the effect of different parameters on the dry density is studied. Apart from the assessment of the optimum GSD defined by DEM, conclusions regarding the implementation protocol, the cell's form, the type of finer grains as well as the proportions of finer grains in the mixtures can be driven for different types of mixtures (i.e. bimodal, trimodal, multimodal).

## 5.3 Results and discussions

In the following sections, the results of the tested mixtures are presenting.

### 5.3.1 Evaluation of optimum pelletized DEM Grain Size Distribution

The resulting dry density of the optimum GSD obtained by DEM is determined (i.e. pellets of 16, 10 and 4 mm in mass proportions of 60%, 10% and 30% respectively). As in the numerical experiment, the pelletized materials is deposited inside a cubic cell (Figure 5-2a) using the blending and layering method.

Table 5-3 Experimental program followed on density optimisation tests.

| Tested sample | Mixture type | Tested grain diameters, $d_i$                                | Tested proportions, % $d_i$            | Cell's form         | Implementation protocol |
|---------------|--------------|--|--|---------------------|-------------------------|
| 16- 4         | Bimodal      | 16 mm- 4 mm  | 70- 30                                 | Cubic/Cylindrical   | Layering                |
| 16-10- 4*     | Trimodal     | 16 mm- 10 mm- 4 mm   | 60- 10- 30                             | Cubic               | Layering / Blending     |
| 16-10-WGS     |              | 16 mm- 10 mm- $80\mu\text{m} \leq d \leq 2 \text{ mm}$       | 60- 10- 30                             | Cubic / Cylindrical | Layering                |
| 16- 4-WGS     |              | 16 mm- 4 mm- $80\mu\text{m} \leq d \leq 2 \text{ mm}$        | 60- 10- 30<br>60- 20- 20<br>70- 10- 20 | Cubic / Cylindrical | Layering                |
| 16- 4-PGS     |              | 16 mm- 4 mm- $600\mu\text{m} \leq d \leq 2 \text{ mm}$       | 60- 10- 30<br>60- 20- 20<br>70- 10- 20 | Cubic / Cylindrical | Layering                |
| 16-10-4-WGS   | Multimodal   | 16 mm- 10 mm- 4 mm, $80\mu\text{m} \leq d \leq 2 \text{ mm}$ | 42- 7- 21- 30                          | Cubic / Cylindrical | Layering                |

\* optimum GSD defined by DEM  
WGS: Well-graded sand  
PGS: Poorly-graded sand

### 5.3.1.1 Resulting packing density

The experimental results of dry density for the chosen optimum GSD is presented in Figure 5-3. A clear impact of the implementation method on mixture's packing state is observed: layering method results in 5% higher density compared to the blending method. The effect can be spotted also on Figure 5-4, where the two deposited samples are illustrated. Higher voids between the pelletized particles and the cell are observed when material is implemented by the blending method. On the other hand, mixtures prepared in layers, result in a more homogeneous distribution of the materials and the “wall effects” are less significant.

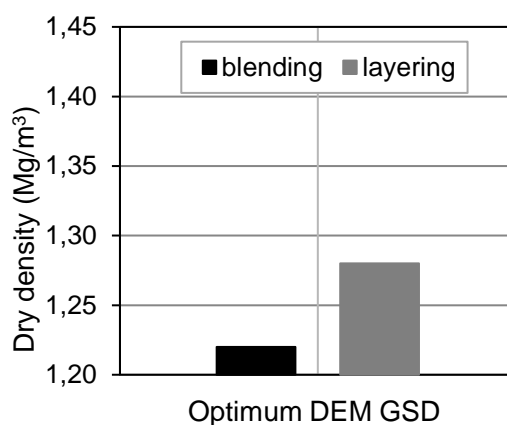


Figure 5-3 Experimental results of the resulting dry density for the optimum GSD defined by DEM (16mm-10mm-4mm in 60%-10%-30%) prepared by blending and layering methods.

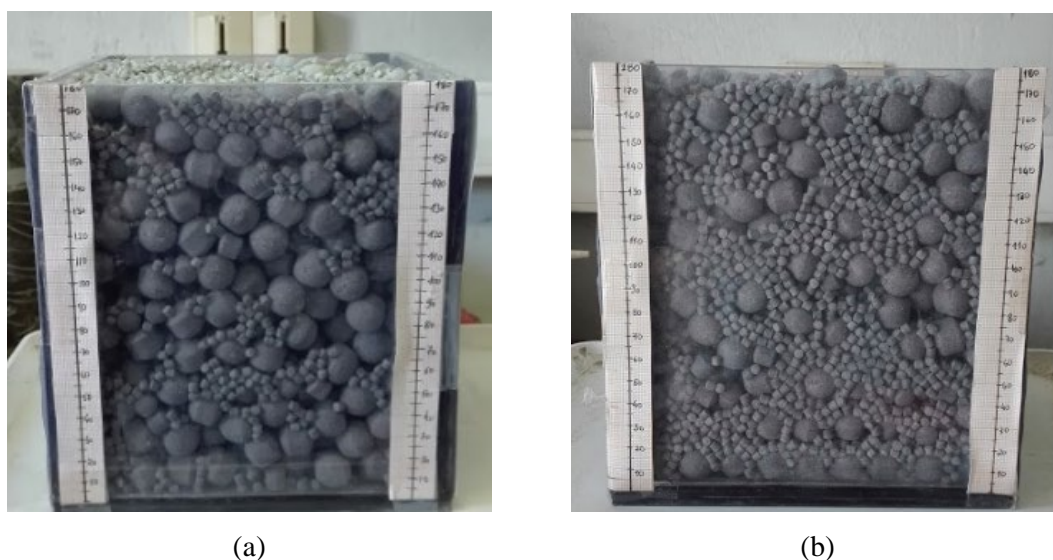


Figure 5-4 Presentation of the pelletized DEM granulometry deposited inside the cubic cell by (a) blending and (b) layering method.

The reported behaviour is in agreement with previous experimental work conducted by Gatabin et al. (2014). It can be attributed to the interactions between the particles and the cell. In fact when the sample is left to fall inside the container, the particles/cell planes interaction

are not negligible and the effect of friction between particles and cell are more significant, compared to samples prepared in layers. Therefore, blending method does not facilitated dense packing conditions.

### 5.3.1.2 Discussion on experimental and numerical results

Following the experimental evaluation of the optimum GSD's resulting dry density, a comparison with the equivalent numerical results was conducted. Therefore, the experimental measurements (Figure 5-4) are correlated with the numerical density obtained by the global results, since in these cases the actual size of the cell is considered (numerical and experimental container with very similar dimensions). The comparison is presented on Figure 5-5. The DEM parametric study conducted for different friction coefficients and deposit heights is plotted with the values of experimental results of blending and layering method. A discussion focuses on similarities and differences between numerical simulations and experiments.

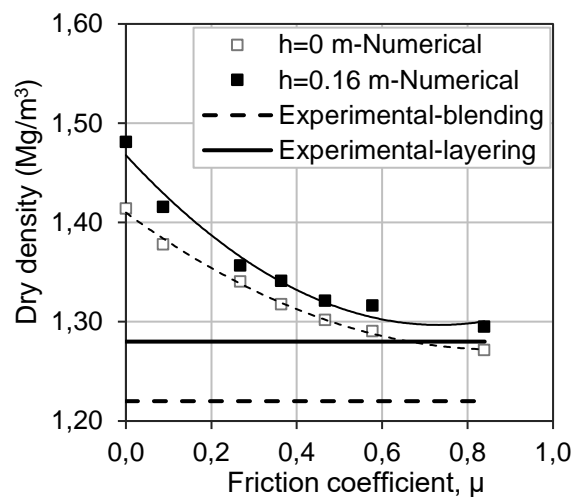


Figure 5-5 Comparison between numerical global density (for deposit height of 0 and 0.16 m) and experimental density obtained by two methods.

The fabricated pellets used for the experiments present quasi-spherical shape, in contrast to the perfectly spherical geometry of particles generated in DEM simulations. According to previous studies (Zou and Yu 1996, Cho et al. 2006), decrease in particle's sphericity as well as shape irregularities hinder particle rearrangement and increase initial porosity. Thus, the actual resulting compaction state in the experiments might be less dense than the numerical simulations. However, the present study shows that samples prepared in layers exhibit lower variations with global numerical results for inter-particle friction coefficient  $\mu \geq 0.58$  ( $\varphi = 30^\circ$ ), regardless of the imposed deposit height. It should be reminded that on numerical simulations, friction between particles and the cell was considered zero. Therefore, the layering

protocol (i.e. interactions with cell planes are reduced) agrees better with numerical results. In other numerical studies using the DEM, inter-particle friction coefficient,  $\mu$  ranging between 0.20 and 0.32 was used as input for numerical simulations on granular materials simulating glass and steel beads or clay pellets (Adema et al. 2009, Yi et al. 2011, Wiącek 2016, Darde et al. 2020). Nonetheless, it was not clear, if these parameters were previously determined experimentally. In general inter-particle friction can be a challenging parameter to determine, as it is influenced by factors such as grain size or material (Farhat et al. 1996, Marigo and Stitt 2015, Hyodo et al. 2018, Wei et al. 2020). Hence, “indirect calibration” has been used in order to correlate a measured bulk property (e.g. packing density, distribution of particle or angle of repose) with a matching numerical result after varying a set of input parameters (Al-Hashemi and Al-Amoudi 2018).

In this framework, the angle of repose (i.e. the maximum angle where a material stays barely stable) was proven to be a useful tool to evaluate the inter-particle friction. Terzaghi (1943) reported that angle of repose is approximately equal to the angle of internal friction of a sand in the loosest state. Even though these two angles are considered identical only at specific assumptions, it has been seen that increase in sliding friction coefficient or internal friction angle, increases the angle of repose (Zhou et al. 2002, Ghazavi et al. 2008, Coetzee 2016) and therefore it can be used as an indicator of friction coefficient. In the present study, the angle formed by a pile of pelletized mixture of the optimum DEM GSD was evaluated. The sample of pellets with 16 mm, 10 mm and 4 mm was left to fall from a height approximately equal to 0.150 m on a plastic surface (3 deposits in total). The measurement of the repose angle was carried out by analysing photographs of the resulted heap. Figure 5-6, illustrates a typical pellet pile. The resulting angle of repose ranges between  $25.7^\circ$  to  $34.2^\circ$ . Deganutti et al. (2011) reported a repose angle between  $30.9^\circ$  and  $35^\circ$  for rounded river gravel with grain sizes ranging for 31.5 mm to 4 mm.



Figure 5-6 Photograph of experimental pellet pile formed by the optimum DEM GSD.

### 5.3.2 Supplementary experimental study on density maximisation

The experimental study on the optimum GSD as defined by DEM simulations showed that dry packing density up to  $1.28 \text{ Mg/m}^3$  is achieved for a sample prepared in layers of the desired granulometry. Therefore, a series of supplementary experiments was conducted to further investigate the granulometric conditions maximising the resulting density.

The presence of finer material was assessed by testing two sandy materials, well-graded sand (WG-S) and poorly-graded sand (PGS) (Figure 5-1). Samples were prepared in layers, since it appeared that higher densities could be achieved (Figure 5-3). Both cubic and cylindrical cells were used (Figure 5-2).

Different types of pelletized mixtures containing two, three and four components were tested in order to further identify the conditions resulting in the densest state of compaction. The produced proportions were selected according to DEM results on bimodal and trimodal samples that led to the densest states. In particular, the investigated proportions (in total mass) were:

- For **bimodal** samples,  $d_{max} - d_{min}$  in 70-30%.
- For **trimodal** samples,  $d_{max} - d_{med} - d_{min}$  in 60-10-30%, 60-20-20% and 70-10-20%.
- For **multimodal** samples with four components,  $d_{max} - d_{med} - d_{min} - \text{finer}$  in 42-7-21-30%. The specific proportions were chosen in order for finer grains to correspond to 30% of the total mass, while the diameters  $d_{max} - d_{med} - d_{min}$  to be distributed at 60-10-30% of the mass.

The detailed summary of the testing program was already presented on Table 5-3.

The experimental data of the resulting packing density are analysed hereafter, for the different mixture types as well as the effect of finer grains proportion.

#### 5.3.2.1 Resulting packing density for different mixture types

Figure 5-7 illustrates the results obtained from the different tested samples, using the cylindrical and cubic container. On the figure, the mixture types and the material component (fabricated pellets and sands) are also given. In this section, the generated proportions correspond to 70-30% for bimodal samples, to 60-10-30% for trimodal samples and 42-7-21-30% for samples containing four grain sizes. The analysis is categorised according to different parameters.

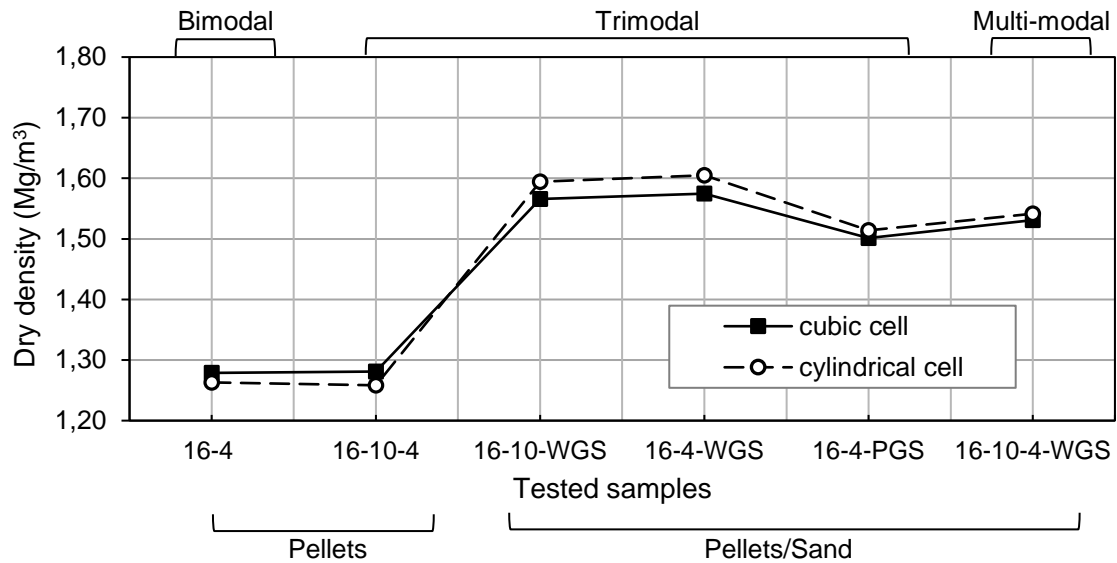


Figure 5-7 Experimental dry density of different mixture types for density optimisation.

### Cell form

It appears that cell type and size does not affect the mixture's final packing state, since no significant difference of the achieved density is observed for the tested GSD prepared in layers in cubic or cylindrical cells ( $SD < 2\%$ ). Both containers presented volumes of the same magnitude ( $0.003 \sim 0.005 \text{ m}^3$ ) and therefore the wall effects may behave in a similar manner.

### Bimodal versus trimodal samples

A comparison between bimodal and/or trimodal samples with identical maximum and minimum diameters is possible. In particular, the samples of 16-4 and 16-10-WG-S were compared to the samples of 16-10-4 and 16-4-WGS respectively. It is evident that in both cases, the resulting dry density is clearly independent to the existence of an intermediate diameter, implying that if the extreme diameters are constant the packing state does not vary. The same conclusion was also reported in the numerical approach on Figure 3-10, reinforcing the argument that the most influential factor in terms of grain sizes is the size ratio  $\alpha$ . As size ratio decreases, better particle rearrangement is achieved and higher density can be obtained.

### Finer grains presence

A clear effect of the finer grains granulometry was established. In the case of PGS with the smallest grains of about  $600 \mu\text{m}$ , the achieved dry density was at  $1.50 \text{ Mg/m}^3$ . On the contrary, the WGS sand with finer grains up to  $80 \mu\text{m}$  increased the resulting packing density to  $1.60 \text{ Mg/m}^3$ .

## **Multimodal mixture**

On the other hand, adding a fourth component and keeping the presence of the finer grains at 30% of the total mass does not facilitate the increase of resulting packing state. Since the samples were prepared in consecutive layers, it was seen that the sand grains could not penetrate voids formed by the 4 mm pellets.

To sum up, the maximum dry density as obtained from the present experimental study was reported by two trimodal samples: 16 mm, 10 mm and well-graded sand or 16 mm, 4 mm and well-graded sand, both prepared in layers in proportions of 60%, 10% and 30% of total mass.

### **5.3.2.2 Effect of the proportions of finer grains**

On 5.3.2.1, it was seen that mixtures composed of pellets and well-graded sand are necessary to result in dry densities higher than  $1.50 \text{ Mg/m}^3$ . It is reminded that the pelletized assembly is selected in order to present the maximum possible packing density. Nonetheless, the granular configuration needs to present a target hydro-mechanical response, i.e. high swelling capacity and low hydraulic conductivity. Sands presence might interfere with the resulting permeability. Thus, the effect of the reduction of its proportion on the packing state should be investigated.

In this context, alternative proportions were studied for trimodal mixtures containing pellets of 16 mm, 10 mm and well-graded (WGS) and 16 mm, 10 mm and poorly-graded (PGS). The tested proportions were the 60-10-30%, 60-20-20% and 70-10-20%, respectful to the decrease of finer grains proportion.

The results are presented on Figure 5-8. For all tested proportions, the resulting packing state of the well-graded sand is constantly higher than the poorly-graded sand. The difference is reduced finer grains consist the 20% of mixture's total mass. It is observed that for both types of sandy materials, the dry density of the mixture is lower than  $1.50 \text{ Mg/m}^3$  when the proportion of finer grains is less than 30%. Nonetheless, the effect is less prominent for the case of the poorly-graded sand. It appears that the proportion of 60-10-30% behaves as optimum in both samples.

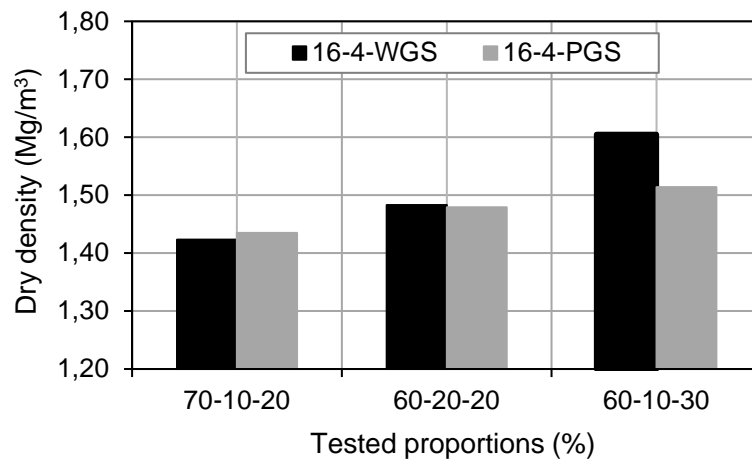


Figure 5-8 Effect of finer grains proportion on the resulting dry density (WGS: well-graded sand, PGS: poorly-graded sand).

#### 5.4 Conclusions and optimised resulting packing density

The experimental optimisation of the resulting packing density was studied after the optimisation of the GSD proposed by the numerical DEM simulations (16 mm, 10 mm and 4 mm in 60, 10 and 30%). In that framework, the resulting dry density of the abovementioned configuration was measured. Furthermore, finer grain sizes (poorly-graded and well-graded sands with  $d \leq 2$  mm) were tested as components in several combinations, in order to improve the dry density of the used pelletized material. The possible reduction of sand's presence inside the mixture was examined by testing alternative proportions. The experimental program investigated also the effect of “external” conditions such as the effect of implementation protocol (layering, blending) and the cell's form on the achieved state of compaction of a granular material.

A detailed discussion on the obtained experimental results as well as the numerical results obtained on Chapter 3, allowed addressing the following conclusions:

- Implementation protocol affected the resulting dry density. Layering method led to higher density than blending deposits, since the particles of samples prepared in layers present lower interactions with the boundaries of the used cell.
- The geometry of the cell did not behave as influential parameter of the resulting packing state, if the available volume is very similar.
- The dry packing density obtained from the optimum DEM granulometry was not sufficiently high ( $\sim 1.30$  Mg/m<sup>3</sup>).
- The resulting density of the optimum DEM granulometry prepared by layering coincides with global numerical results, due to similar boundary conditions (cell scale, sample/cell interactions). Comparison between numerical and experimental data led to

inter-particle friction coefficient estimation for the fabricated pellets (approximately  $\mu=0.6$ , friction angle of  $30^\circ$ ). The value was in agreement with the repose angle measurement.

- Both numerical and experimental results showed that the intermediate diameter  $d_{med}$  is independent to the maximum obtained density. Bimodal and/or trimodal configurations with common  $d_{max}$  and  $d_{min}$  present the same packing state.
- Configurations containing finer grain components ( $d \leq 2$  mm) proved that a wide range of fines (WGS) was necessary to improve the resulting packing density (1.45-1.60 Mg/m<sup>3</sup>).
- The alternative proportions produced for the trimodal mixtures containing finer grains validated the percentages of 60-10-30% as optimum proportions.
- The maximum dry density (1.60 Mg/m<sup>3</sup>) was reported by two trimodal samples presented on Figure 5-9: 16 mm, 4 mm and well-graded sand or 16 mm, 10 mm and well-graded sand, prepared in layers of proportions of 60%, 10% and 30% in total mass.

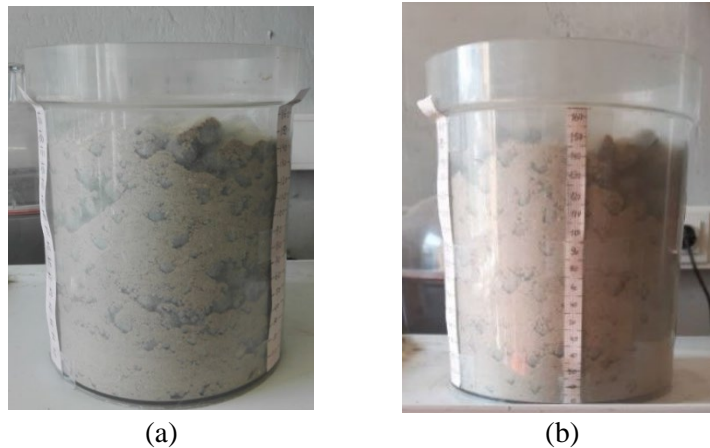


Figure 5-9 Pictures of the two mixtures reported the highest resulting dry density deposited on cylindrical cell: (a) 16 mm, 4 mm and well-graded sand (60%, 10% and 30%) and (b) 16 mm, 10mm and well-graded sand (60%, 10% and 30%).

Considering the abovementioned remarks, two key-decisions are taken:

- ✓ The adequate investigated density range is defined to be around 1.45-1.60 Mg/m<sup>3</sup>, with  $\rho_d = 1.60$  Mg/m<sup>3</sup> marked as the optimum density.
- ✓ Since the fabrication of pellets of 4 mm is more complicated (only pellets of pure MX80 were fabricated, time-consuming production), the retained GSD is finally optimised as the trimodal sample of 16 mm, 10 mm and well-graded sand (i.e. finer grain component) prepared in layers of proportions of 60%, 10% and 30% in total mass.

# **Chapter 6 - Hydro-mechanical parametric study of CO<sub>x</sub>/MX80 pelletized material from compacted CO<sub>x</sub>/MX80 powdered mixtures**

On this chapter, the hydro-mechanical behaviour of the pelletized material is indirectly evaluated via the hydro-mechanical analysis of various CO<sub>x</sub>/MX80 powdered mixtures, for the expected resulting packing dry densities. Basic physicochemical properties, as well as the swelling capacity in constant and non-constant volume conditions are examined. The parametric investigation focuses on the effect of the MX80 bentonite content, the initial dry density and the infiltrated solution on the response of the studied materials. A preliminary estimation of the swelling capacity of different CO<sub>x</sub>/MX80 backfill is applied to determine the optimised bentonite content range of interest. The chapter is developed in the following main parts:

- 6.1 Introduction
- 6.2 Tested materials and infiltrated fluids used in the experiments
- 6.3 Experimental methods and program
- 6.4 Experimental results
- 6.5 Discussion

## 6.1 Introduction

The swelling capacity of a pellets assembly material of various CO<sub>x</sub>/MX80 mixtures is indirectly investigated by studying the swelling response of CO<sub>x</sub>/MX80 powdered mixtures. The criteria of the followed strategy were set based on previous experimental evidence, which indicated the common swelling response of pelletized assemblies with compacted powders, if both exhibit the same dry density (Imbert and Villar, 2006; Hoffmann et al., 2007; Karnland et al., 2008). In this context a parametric experimental study is conducted on various CO<sub>x</sub>/MX80 powdered mixtures to evaluate their hydro-mechanical response on conditions corresponding to the design.

The present experimental program was developed as a result of observations presented on previous chapters. On Chapter 5, the experimental study on the density optimisation for a pelletized assembly, recognized as the adequate investigated density range to vary between 1.45 and 1.60 Mg/m<sup>3</sup>, with  $\rho_d = 1.60 \text{ Mg/m}^3$  marked as the optimum density. Therefore, the swelling capacity of the compacted CO<sub>x</sub>/MX80 mixtures is tested for these equivalent dry densities. The addition of well-graded sand as a finer component was proposed in order to maximise as possible the packing state (section 5.3.2.2). In addition, the modification of CO<sub>x</sub>'s initial granulometry was suggested as alternative solution that facilitates the pelletizing process (section 4.4). Moreover, the design requirements mark the effect of water chemistry (groundwater and groundwater altered by the concrete structural elements) as a parameter of investigation.

In this chapter, different CO<sub>x</sub>/MX80 mixtures ( $\leq 40\% \text{MX80}$ ) are studied upon hydration with demineralised water and the synthetic aqueous solutions of site and cementitious water. The effect of bentonite content inside the mixture, as well as the hydration solution's chemical impact is examined by testing the mixture physicochemical properties (plasticity index, free swelling capacity, compaction characteristics) on section 6.4.1. The swelling capacity of compacted mixtures is studied under constant vertical stress and constant volume conditions, determining the swelling potential (section 6.4.2) and swelling pressure (section 6.4.3) respectively. On section 6.5, the obtained results are analysed, combining the used experimental methods, while a preliminary evaluation of various CO<sub>x</sub>/MX80 backfill materials on the gallery conditions was attempted. The main outcomes of the hydro-mechanical parametric study are outlined on section 6.6.

## 6.2 Tested materials and infiltrated fluids used in the experiments

The hydro-mechanical response of mixtures containing various materials was investigated. In the beginning, mixtures of COx argillite and MX80 bentonite at the reception conditions were used. Furthermore, as it was instructed in section 4.4, the modification of COx argillite's initial granulometry was carried out by Euro-Geomat Consulting, to facilitate the pelletizing process. The modification concerned the reduction of the COx particles finer than 200  $\mu\text{m}$ . Modified COx was also tested in some experiments. In parallel, the use of the well-graded sand (WGS) proposed on Chapter 5. Therefore, its impact on the COx/MX80 mixture was examined.

The studied materials are presented on Figure 6-1. COx argillite at reception conditions is hereafter noted as COx-D<sub>orig</sub>, whereas the modified granulometry is referred to as COx-D<sub>mod</sub>. In all studied mixtures, the imposed bentonite content did not exceed 40% of the mixture's total mass.

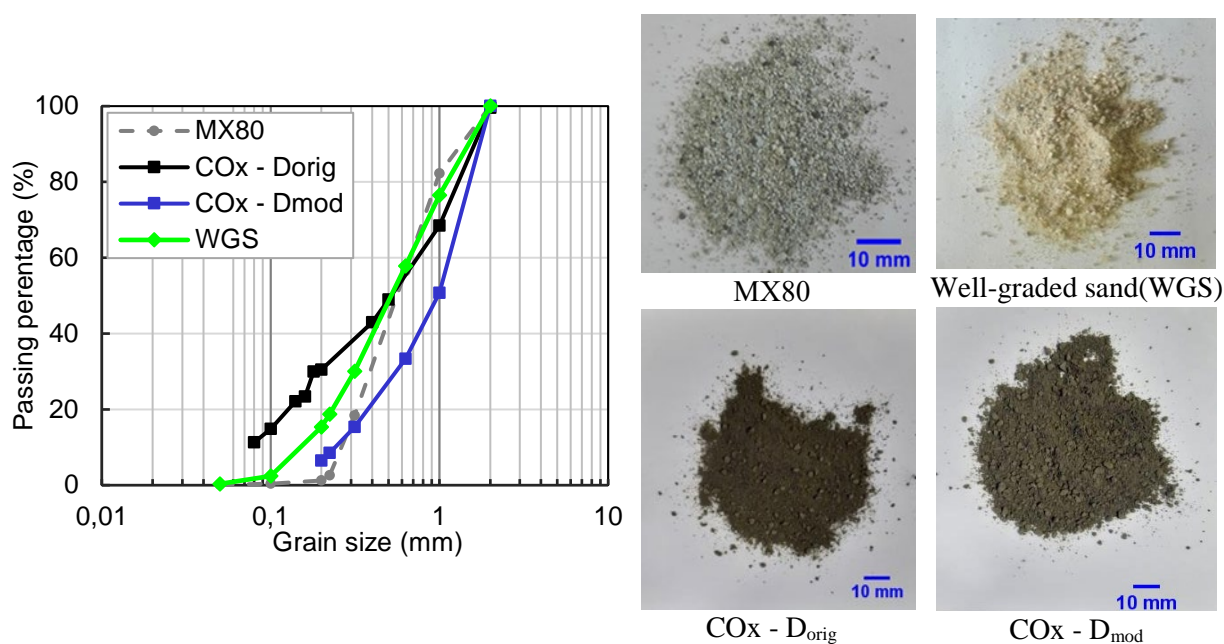


Figure 6-1 Grain size distribution and presentation of the materials used on the hydro-mechanical study of powdered mixtures.

The conducted experimental work is primarily focused on the effect of bentonite content and mixture's dry density on the hydro-mechanical response. Nonetheless, according to the repository conditions, the installed materials are saturated directly from the water of the surrounding host rock as well as the groundwater passing through the concrete liners. On section 2.3.4, it was underlined that the interaction of the bentonite-based materials with water is strongly influenced by the infiltrated water's chemistry. Therefore, the chemical impact of the infiltrated fluid was also evaluated.

In this framework, different types of infiltrated fluids were used, according to the design conditions (i.e. Bure's groundwater, alkaline perturbation). Tests were conducted by using demineralised water (DW) as reference, as well as two synthetic fluids, site (SW) and cementitious (CW) water. Table 6-1 presents the receipts used for the synthetic solution preparation according to Andra's indications, whereas Table 6-2 illustrated the ionic concentration. The characteristics of the different infiltrated fluids used upon the experimentation are summarised on Table 6-3. It can be seen that cementitious water present alkaline conditions, while the ionic strength of the two synthetic solution does not significantly alter.

Table 6-1 Receipt for the preparation of synthetic waters.

| Component<br>(g/L) | NaCl  | KCl   | NaHCO <sub>3</sub> | CaSO <sub>4</sub> .2H <sub>2</sub> O | MgSO <sub>4</sub> .7H <sub>2</sub> O | CaCl <sub>2</sub> .2H <sub>2</sub> O | Na <sub>2</sub> SO <sub>4</sub> | Ca(OH) <sub>2</sub> |
|--------------------|-------|-------|--------------------|--------------------------------------|--------------------------------------|--------------------------------------|---------------------------------|---------------------|
| SW                 | 1.950 | 0.035 | 0.130              | 0.630                                | 1.020                                | 0.080                                | 0.700                           | -                   |
| CW                 | 1.286 | 0.596 | -                  | -                                    | -                                    | -                                    | -                               | 1.408               |

SW: Site water, CW: Cementitious water

Table 6-2 Ionic concentration of synthetic waters.

| Component<br>(mmol/L) | Na <sup>+</sup> | Cl <sup>-</sup> | K <sup>+</sup> | HCO <sub>3</sub> <sup>-</sup> | Mg <sup>2+</sup> | SO <sub>4</sub> <sup>2-</sup> | Ca <sup>2+</sup> | OH <sup>-</sup> |
|-----------------------|-----------------|-----------------|----------------|-------------------------------|------------------|-------------------------------|------------------|-----------------|
| SW                    | 44.8            | 34.9            | 0.5            | 1.5                           | 4.1              | 12.7                          | 4.2              | -               |
| CW                    | 22.0            | 30.0            | 8.0            | -                             | -                | -                             | 19.0             | 38.0            |

SW: Site water, CW: Cementitious water

Table 6-3 Properties of infiltrated fluids used in the experiments.

| Component<br>(g/L) | pH   | Electrical<br>conductivity, <i>EC</i><br>(μS/cm) | Ionic strength, <i>I</i><br>(mmol/L) |
|--------------------|------|--|--------------------------------------|
| DW                 | 6.1  | 3.5  | -                                    |
| SW                 | 7.9  | 547  | 83                                   |
| CW                 | 12.8 | 10800  | 87                                   |

DW: Demineralised water, SW: Site water, CW: Cementitious water

### 6.3 Experimental methods and program

Different types of tests were used to assess the hydro-mechanical response on various CO<sub>x</sub>/MX80 mixtures. The objective of the tests was to analyse the impact of the bentonite content, the initial compaction state and the chemistry of the infiltrated fluid on the materials behaviour. The experimental program was a parametric study focusing on the:

- (i) **Physicochemical properties** of CO<sub>x</sub>/MX80 mixtures, in particular plasticity index, free swelling capacity and dynamic compaction characteristics.
- (ii) **Swelling capacity**, expressed in constant vertical stress conditions (swelling potential) and constant volume conditions (swelling pressure).

It is reminded that the conducted series of tests on powdered material constitutes a preliminary characterisation on the response of a pelletized material composed of different mixtures. Hence, the time-consuming pellet fabrication of different mixtures as well as their longer testing time was avoided.

#### 6.3.1 Physicochemical properties

In the first experimental part, the physicochemical properties of various CO<sub>x</sub>/MX80 samples were studied by following conventional soil testing methods. The purpose of these tests was to evaluate the impact of the used hydration solution and the bentonite addition on CO<sub>x</sub>/MX80 mixtures basic properties, such as plasticity index, swelling capacity and compaction, by measuring the corresponding known index properties. Therefore, the values of Atterberg limits (AFNOR, 1993, 1995), Free Swelling Index (AFNOR 2002) and the optimum compaction conditions (AFNOR 2014) were measured according to French Standards. Atterberg limits and FSI tests were performed by using demineralized, site and cementitious water. The dynamic compaction characteristics were determined by the Standard Proctor tests, where approximately 2 kg of the material at their reception conditions was prepared. Mixtures hydration was conducted by spraying the proper amount of water (corresponding to the target water content) on CO<sub>x</sub> argillite and then adding the necessary MX80 bentonite on the hydrated material. The decision focused on avoiding the immediate swelling of bentonite, which would prevent a homogeneous mixing process. The mixtures were stored in hermetic plastic bags at least 12 h. Site water and cementitious water were used.

### 6.3.2 Swelling capacity of compacted powdered samples

Swelling capacity was determined at isochoric and free-volume conditions (i.e. swelling pressure and swelling potential respectively), using oedometric cells with diameter  $D=40$  mm. The cells included a piston and two porous disks to sandwich the soil specimens. Mixtures containing COx/MX80 were studied, with bentonite content not exceed 40% of the mixtures total mass. In the following sections, the adopted experimental protocol is described.

#### 6.3.2.1 Samples preparation

The remoulded tested soil mixtures were compacted by means of a manual hydraulic press at the target dry densities. The following protocol was adopted for specimens prepared for swelling under constant vertical stress tests and swelling pressure tests.

According to the process, a predefined mass of COx/MX80 mixtures ( $M_{sample}$ ) was prepared, by carefully mixing the corresponding quantities of materials according to the imposed mixture fraction. Figure 6-2 illustrates the steps followed to achieve the desired compaction of the specimens. The initial “zero” height,  $h_0$  which included the two porous disks, two filter papers and the piston was measured using a caliper. The prepared mass of the mixture was poured inside the cell and the new non-compacted specimen height was determined ( $h_1$ ).

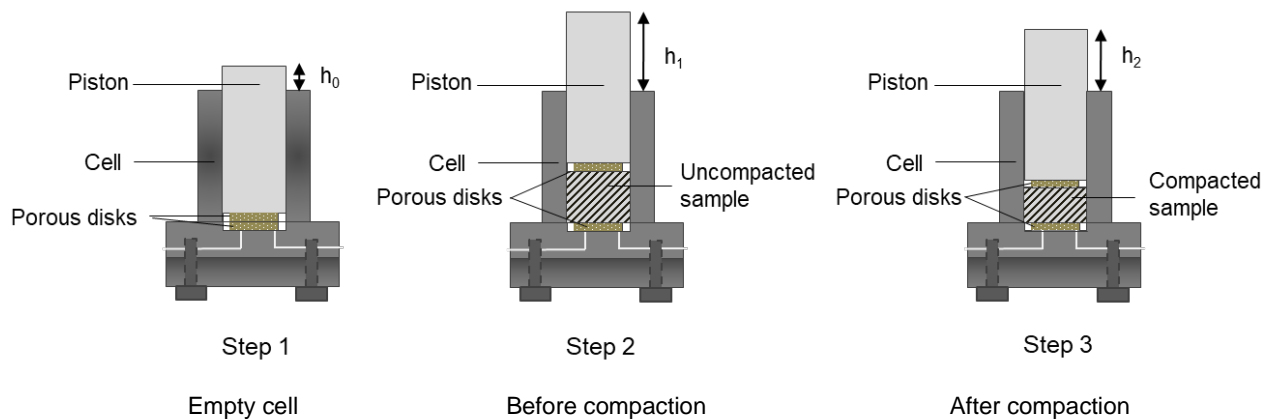


Figure 6-2 Specimens compaction steps.

The target height of the specimen ( $H_{target}$ ) was calculated as follows:

$$H_{target} = \frac{M_{sample}}{A_{sample} \cdot (1 + w) \cdot \rho_d} \quad (6.1)$$

where  $M_{sample}$  is the samples total mass,

$A_{sample}$  is the cross-sectional area of the specimen

$w$  is the sample's water content (measured before the test)

$\rho_d$  is the target dry density.

The vertical displacement of the piston required to obtain the target height ( $\delta_{req}$ ) corresponding to the desired dry density was calculated as:

$$\delta_{req} = h_1 - h_0 - H_{target} \quad (6.2)$$

Once the sample was placed on the press, a vertical load was gradually applied and the required displacement was imposed while monitoring the displacement of the piston by a dial gauge. After the material's compaction, the sample's height was measured ( $H_0 = h_2 - h_0$ ), corresponding to the specimen initial height prior to hydration. An equivalent mixture of identical composition was also prepared, in order to precisely determine the water content of the sample (oven drying at 105°C for 24 hours). The sample's initial dry density  $\rho_d$  was finally measured. Details on the tested specimens are given below.

### 6.3.2.2 Swelling under constant vertical stress

The swelling potential of the material was determined under constant vertical stress conditions. After its compaction at the target dry density, the oedometric cell was placed on the swelling under constant vertical stress system illustrated on Figure 6-3. The lower applied vertical stress corresponded to the piston (6 kPa). For higher applied stresses ( $\sigma_v=52$  kPa and 100 kPa), additional loads were placed. Once the stress was applied to the sample, the material was directly hydrated from the bottom part. The displacement developed by the specimen was monitored by means of a dial gauge.

Deminerised (DW), site (SW) and cementitious water (CW) were used to hydrate the samples. In the case of DW and SW, the cell is connected to a graduated bottle of Mariott which is used to apply the constant hydraulic charge. When CW is infiltrated to the sample, a different hydration system was developed in house, to prevent the contact of the alkaline solution with the atmosphere and avoid carbonation. Therefore, the reservoir was filled with water under void and afterwards helium was injected to the system. Constant hydraulic charge of 40 cm, was applied, corresponding to injection pressure of 4 kPa (hydraulic gradient  $i \approx 20$ ).

The test was considered finished when the deformation of the sample was stable. At the end of the tests samples were completely saturated and the final water content was measured. The swelling potential  $\varepsilon_s$  (%) was considered as the developed swelling strain and it was calculated as:

$$\varepsilon_s = \frac{H_i - H_0}{H_0} \quad (6.3)$$

where  $H_i$  is the specimen's height at each measurement and  $H_0$  corresponds to the initial specimen height.

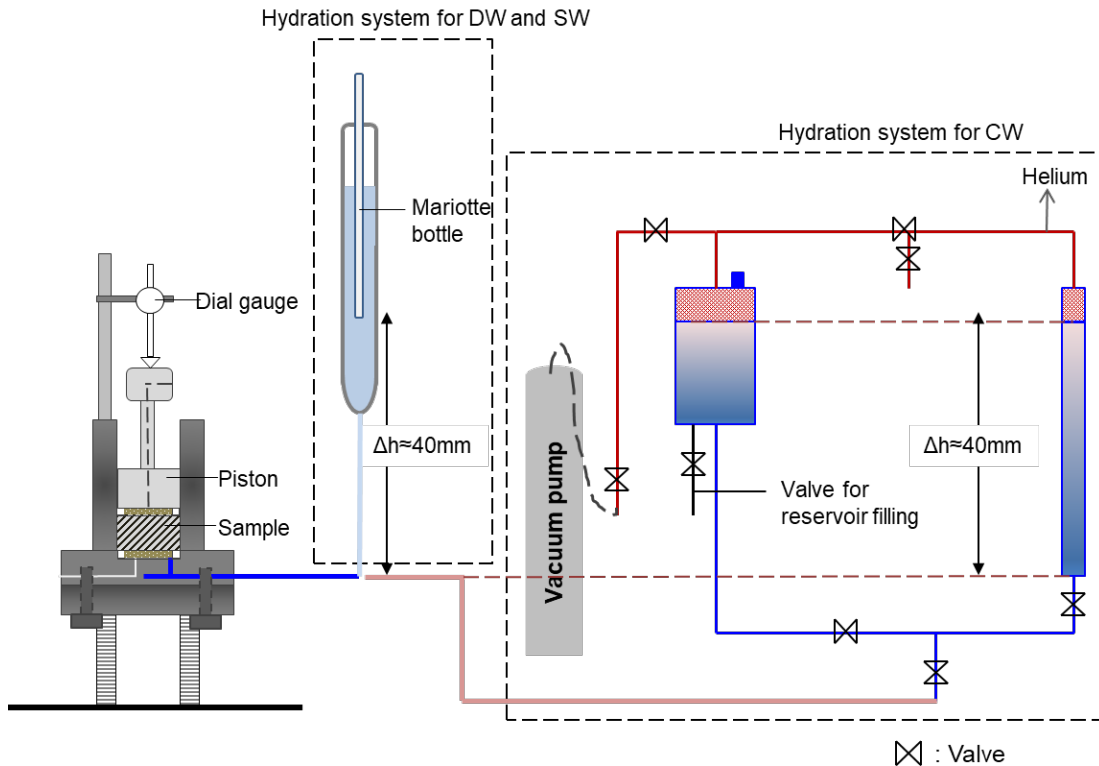


Figure 6-3 Experimental system used on swelling under constant vertical stress tests.

Specimens with total mass of  $\sim 50$  g and height of  $\sim 20$  mm were prepared for testing ( $D=40$  mm,  $H \approx 20$  mm). Various mixtures of CO<sub>x</sub> argillite and MX80 bentonite at the original conditions of reception were studied, exhibiting bentonite proportions of 10%, 20%, 30% and 40%. The samples were compacted at 1.45 and 1.60 Mg/m<sup>3</sup>, corresponding at the dry density over the range of interest for this study. Stresses of 6, 52 and 100 kPa were applied during hydration. Details are presented on Table 6-4 (Test series 1-4). A possible influence of CO<sub>x</sub>'s granulometry modification was also examined (Table 6-4, Test series 5-8). In addition, the addition of sand on CO<sub>x</sub>/MX80 was evaluated (Table 6-4, Test series 9-12). The tested proportions were selected to correspond at a pelletized assembly containing 60% pellets of 16mm (CO<sub>x</sub>/MX80), 10% pellets of 10 mm (CO<sub>x</sub>/MX80) and 30% sand (WGS) as paragraph 5.3.2 suggested.

Table 6-4 Details of the experimental program of the conducted swelling under constant vertical stress tests.

| Test series | COx granulometry   | MX80 content (%) | Sand content (%) | Initial dry density, $\rho_d$ (Mg/m <sup>3</sup> ) | Initial water content, $w$ (%) | Applied stress, $\sigma_v$ (kPa) | Infiltrated fluid | Comments |
|-------------|--------------------|------------------|------------------|--|--------------------------------|----------------------------------|-------------------|----------|
| 1           | $D_{orig}^*$       | 10               | -                | 1.45, 1.60   | 6.0 ~ 6.4                      | 6                                | DW, SW, CW        | 12 tests |
|             |                    |                  |                  |  |                                | 52                               | SW                |          |
|             |                    |                  |                  |  |                                | 100                              | SW, CW            |          |
| 2           |                    | 20               | -                |  | 6.4 ~ 7.1                      | 6                                | DW, SW, CW        | 12 tests |
|             |                    |                  |                  |  |                                | 52                               | SW                |          |
|             |                    |                  |                  |  |                                | 100                              | SW, CW            |          |
| 3           |                    | 30               | -                |  | 7.1 ~ 8.2                      | 6, 100                           | DW, SW, CW        | 12 tests |
|             |                    |                  |                  |  |                                | 52                               | SW                |          |
|             |                    |                  |                  |  |                                | 100                              | SW, CW            |          |
| 4           |                    | 40               | -                |  | 7.9 ~ 8.2                      | 6, 100                           | DW, SW, CW        | 12 tests |
|             |                    |                  |                  |  |                                | 52                               | SW                |          |
|             |                    |                  |                  |  |                                | 100                              | SW, CW            |          |
| 5           | $D_{mod}^\ddagger$ | 10               | -                | 1.60   | 6.1                            | 6                                | SW                | 4 tests  |
| 6           |                    | 20               | -                |  | 6.9                            |                                  |                   |          |
| 7           |                    | 30               | -                |  | 7.6                            |                                  |                   |          |
| 8           |                    | 40               | -                |  | 8.3                            |                                  |                   |          |
| 9           | $D_{mod}^\ddagger$ | 34               | 30               | 1.60   | 4.4                            | 6                                | SW                | 4 tests  |
| 10          |                    | 28               | 30               |  | 5.0                            |                                  |                   |          |
| 11          |                    | 21               | 30               |  | 5.5                            |                                  |                   |          |
| 12          |                    | 14               | 30               |  | 6.1                            |                                  |                   |          |

\* Original COx granulometry

‡ Modified COx granulometry

### 6.3.2.3 Swelling under constant volume conditions

The swelling pressure developed under constant volume was measured by developing the system presenting on Figure 6-4. In the case of swelling pressure tests, the cell and the porous plates had been previously placed on the hydraulic press and a high load had been applied, to ensure the contact of the parts, assuring the rigidity during the swelling tests (constant volume). Then, the specimen was prepared as described on section 6.3.2.1. After the compaction of the sample at the target dry density, the oedometric cell was placed on the designed device consisting of a metallic frame. A force sensor was positioned on the piston to measure the developed pressure and a large screw was fixed in order to prevent the axial displacement upon wetting. The screw was reinforced by using a “pre-stressed” spring to minimise as possible the system’s deformability. During the experiment, the displacement of the piston was monitored by a displacement transducer.

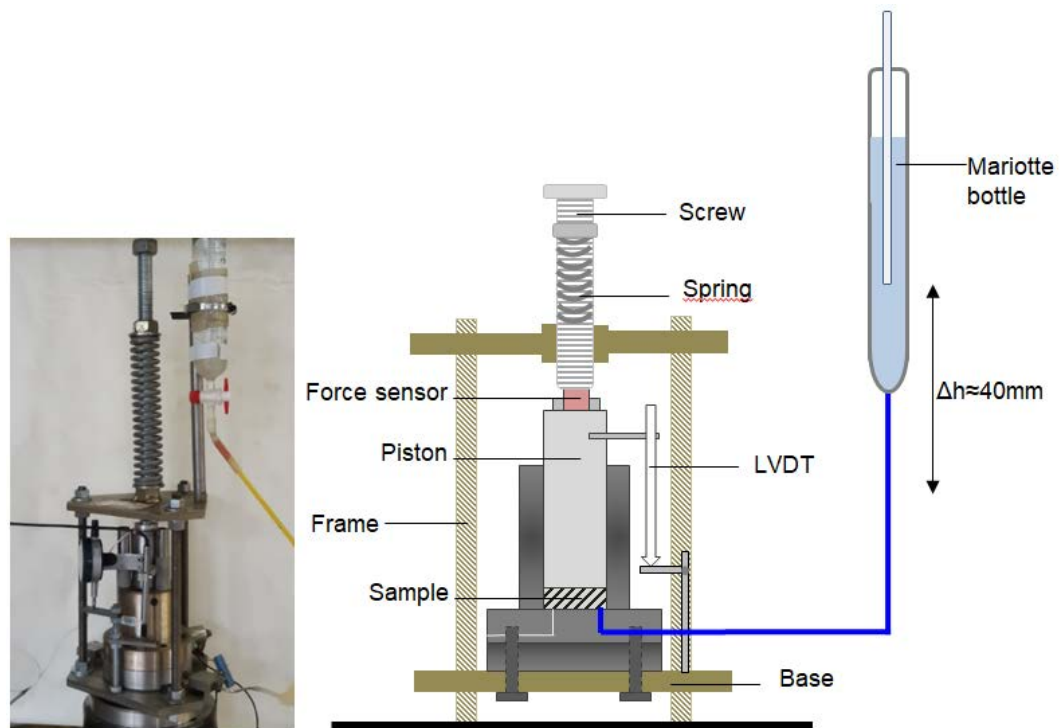


Figure 6-4 Experimental system used on swelling under constant volume tests.

In the beginning, an initial vertical stress of 90 kPa was applied to establish a good contact between the different parts. The swelling pressure was considered as the “clear” stress developed during the specimen’s wetting. Site water (SW) was used to hydrate the samples. The cell was connected to a graduated bottle of Mariotte, used to apply constant hydraulic charge of 40 cm, corresponding to injection pressure of 4 kPa (hydraulic gradient  $i \approx 40$ ). The test was considered finished when the developed swelling pressure was stable. At the end of the tests samples were saturated and the final water content was measured. The recorded displacements were ranging between 0.002 mm to 0.05 mm ( $\varepsilon_s = 0.01\% \sim 0.4\%$ ).

Specimens with total mass of  $\sim 25$  g and height of  $\sim 11$  mm were prepared for testing ( $D=40$  mm,  $H \approx 11$  mm). Various mixtures of COx argillite and MX80 bentonite at the original conditions of reception were studied having bentonite proportions of 10%, 20%, 30% and 40%. The samples were compacted at 1.45 and 1.60 Mg/m<sup>3</sup>, corresponding at the investigated density range. Details are presented on Table 6-5 (Test series 1-4). In addition, the effect of water content on the swelling pressure was studied. Therefore, a supplementary series of tests were conducted on COx/MX80 specimens prepared at higher water contents corresponding to the optimum compaction conditions (Table 6-5, Test series 5-8). The selected values of water content are related to the results which are later presented on Figure 5-8.

Table 6-5 Details of the experimental program of the conducted swelling pressure tests.

| Test series | COx granulometry    | MX80 content (%) | Initial dry density, $\rho_d$ (Mg/m <sup>3</sup> ) | Initial water content, $w$ (%) | Infiltrated fluid | Comments |
|-------------|---------------------|------------------|--|--------------------------------|-------------------|----------|
| 1           | D <sub>orig</sub> * | 10               | 1.45, 1.60   | 6.7                            | SW                | 8 tests  |
| 2           |                     | 20               |  | 7.3 ~ 7.5                      |                   |          |
| 3           |                     | 30               |  | 8.1 ~ 8.5                      |                   |          |
| 4           |                     | 40               |  | 7.5 ~ 8.5                      |                   |          |
| 5           | D <sub>orig</sub> * | 10               | 1.60   | ~18                            | SW                | 4 tests  |
| 6           |                     | 20               |  | ~22                            |                   |          |
| 7           |                     | 30               |  | ~25                            |                   |          |
| 8           |                     | 40               |  | ~25                            |                   |          |

\* Original COx granulometry

## 6.4 Experimental results

The following sections address the result of the conducted experimental study.

### 6.4.1 Physicochemical properties

The evolution of the Atterberg limits for various COx/MX80 mixtures wetted with demineralised, site and cementitious water are presented on Figure 6-5. For all solutions, both parameters increase while more bentonite added in the mixture. Synthetic waters exhibit similar behaviour with pure water: liquid limit presents non-linear increase with MX80 content (2<sup>nd</sup> degree polynomial is suggested), while plastic limit increases almost linearly on MX80 addition (i.e. less pronounced increase). In every case, high regression parameter ( $R^2 > 0.96$ ) was obtained. It is evident that the influence of the used fluid is more important for the values of  $LL$ . A decrease in plasticity index is observed when synthetic waters are used. The difference is more visible with MX80 additions, which increases smectite presence and consequently the sensibility to water chemistry. A comparison between site and cementitious water does not present a clear behaviour, especially in the case of liquid limit. It appears that COx/MX80 mixtures prepared with CW might present slightly higher plasticity than those prepared with SW. It is reminded that even the pH conditions differ between the two synthetic solutions ( $pH_{sw}=7.9$ ,  $pH_{cw}=12.8$ ), the ionic strength is very close (Table 6-3).

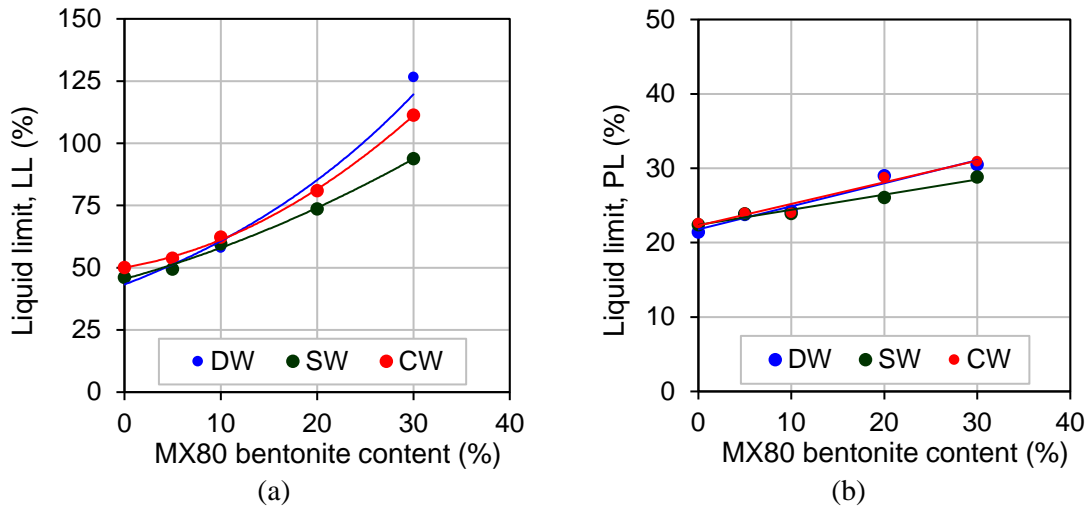


Figure 6-5 Effect of infiltrated solution on (a) liquid limit and (b) plastic limit in relation to bentonite content for COx/MX80 mixtures.

Similar observations are concluded from *FSI* measurements, illustrated on Figure 6-6. As expected, free swelling capacity increases with bentonite content for all types of fluids. In all cases *FSI* remains relatively low ( $FSI < 6 \text{ g/cm}^3$ ). Synthetic solutions appear to present relatively lower values compared to demineralised water. The effect is expected due to salinity exhibited by the synthetic waters. Here, the comparison between site and cementitious water shows that the alkaline solution resulted in decrease of swelling capacity that site water, especially for  $MX80 < 20\%$ .

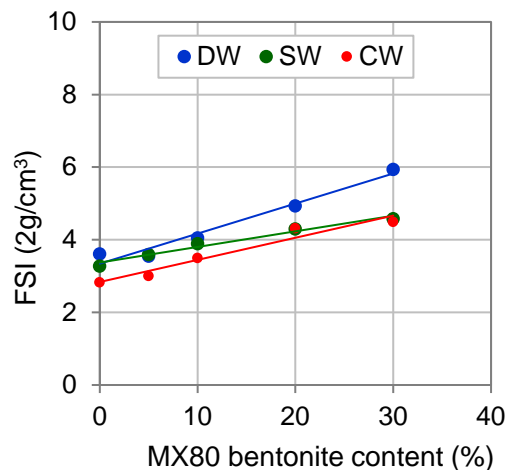


Figure 6-6 Results of Free Swelling capacity index.

The dynamic compaction properties of different COx/MX80 mixtures were determined using the Standard Proctor testing method. The obtained results for mixtures wetted with site and cementitious water are given on Figure 6-7. A clear behaviour in material's compaction is observed for both fluids: the higher the presence of bentonite in the mixture, the lower the

maximum dry density is achieved. Additionally, the optimum water content appears to be shifted on higher values. This tendency is caused due to bentonite's swelling upon hydration. Swelling of bentonite particles means that more volume is occupied by bentonite in the sample and lower compaction can be obtained for the same compaction energy. The remark is consistent with observations reported on the static uniaxial compression tests examining the water content effect in the present study (section 4.2.1.2). Past researcher have also observed similar results (de Magistris et al. 1998, Chalermyanont and Arrykul 2005, Ito and Komine 2008, Shariatmadari et al. 2011).

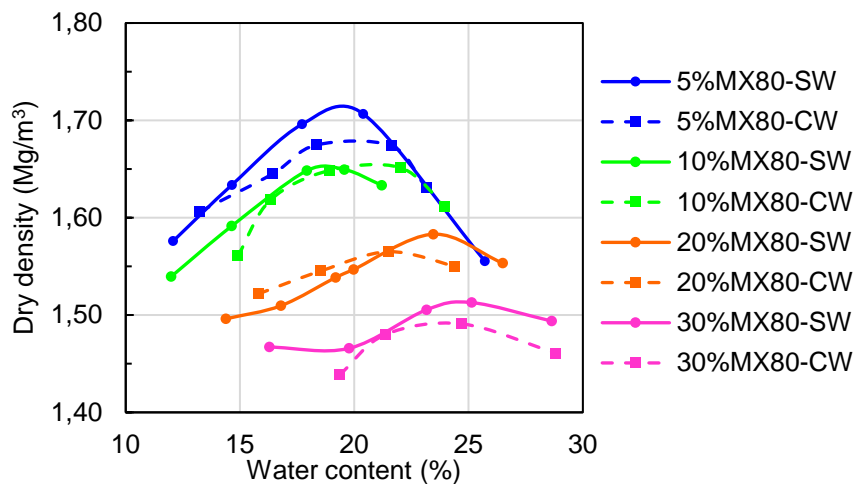


Figure 6-7 Results of standard Proctor tests on COx/MX80 mixtures prepared with site and cementitious water.

The optimum compaction properties can be used as an additional “indirect” method to evaluate the mixtures swelling capacity. Figure 6-8 presents more clearly the effect of bentonite content for the investigated COx/MX80 mixtures in terms of optimum dry density and water content. Samples prepared with site water could be compacted at higher dry densities than cementitious water, implying that the mixtures wetted with the alkaline solution had swollen more than those wetted with site water. This effect does similarly apply to the optimum water content values. For the studied COx/MX80 mixtures, when:

- MX80 ≤ 10%, optimum water of 18-20% was obtained
- MX80 = 20%, optimum water of 22-24% was obtained
- MX80 = 30%, optimum water of approximately 25% was obtained.

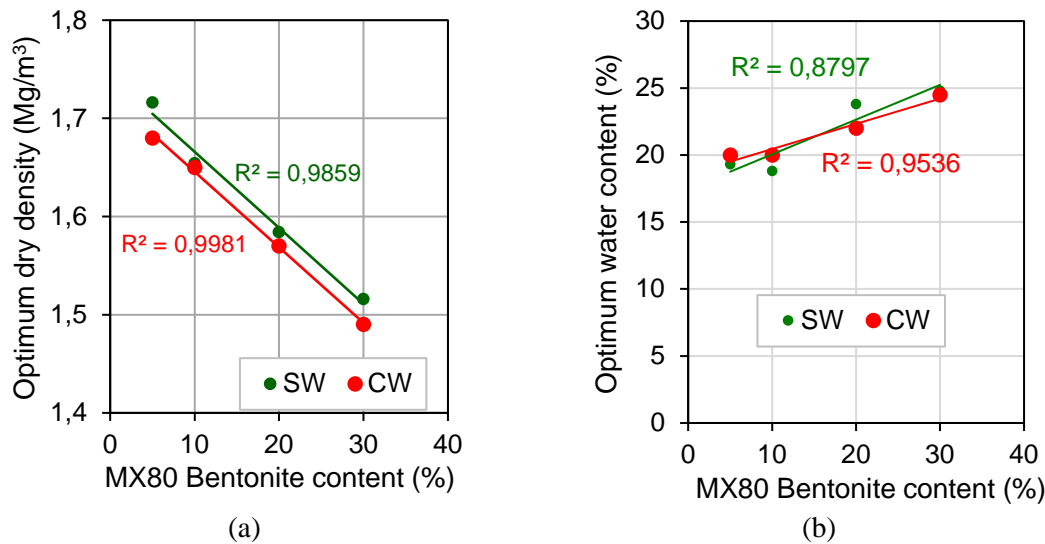


Figure 6-8 Evolution of (a) optimum dry density and (b) optimum water content, with MX80 bentonite content on COx/MX80 wetted with site and cementitious water.

#### 6.4.2 Swelling potential

Observations concerning the swelling potential of COx/MX80 are presented, as obtained by the swelling under constant vertical stress tests.

In the beginning, the obtained swelling strain of the studied mixtures prepared with the material at the original COx granulometry (COx- $D_{orig}$ ) using site (SW) and cementitious water (CW) are presented on Figure 6-9, Figure 6-10, Figure 6-11 and Figure 6-12. The results are given for the different dry densities and applied stresses.

As expected, a universal behaviour concerning the vertical stress was obtained for all tested mixtures: as the applied vertical load increases, the materials swelling potential reduces (Komine and Ogata 1994, Dang 2007, Hoffmann et al. 2007, Villar and Lloret 2008, Castellanos et al. 2008). Typical hyperbolic development of the swelling strain over time was obtained (Komine and Ogata 1994, 1999). In some cases, collapse was observed when samples were hydrated under application of  $\sigma_v = 100$  kPa, indicating that the applied stress overcomes the developed swelling pressure for the given dry density. On the other hand, more time needed for stabilization of the measured strain, as the bentonite content increased and/or as the vertical stress decreased.

### COx/MX80 mixtures with 10%MX80

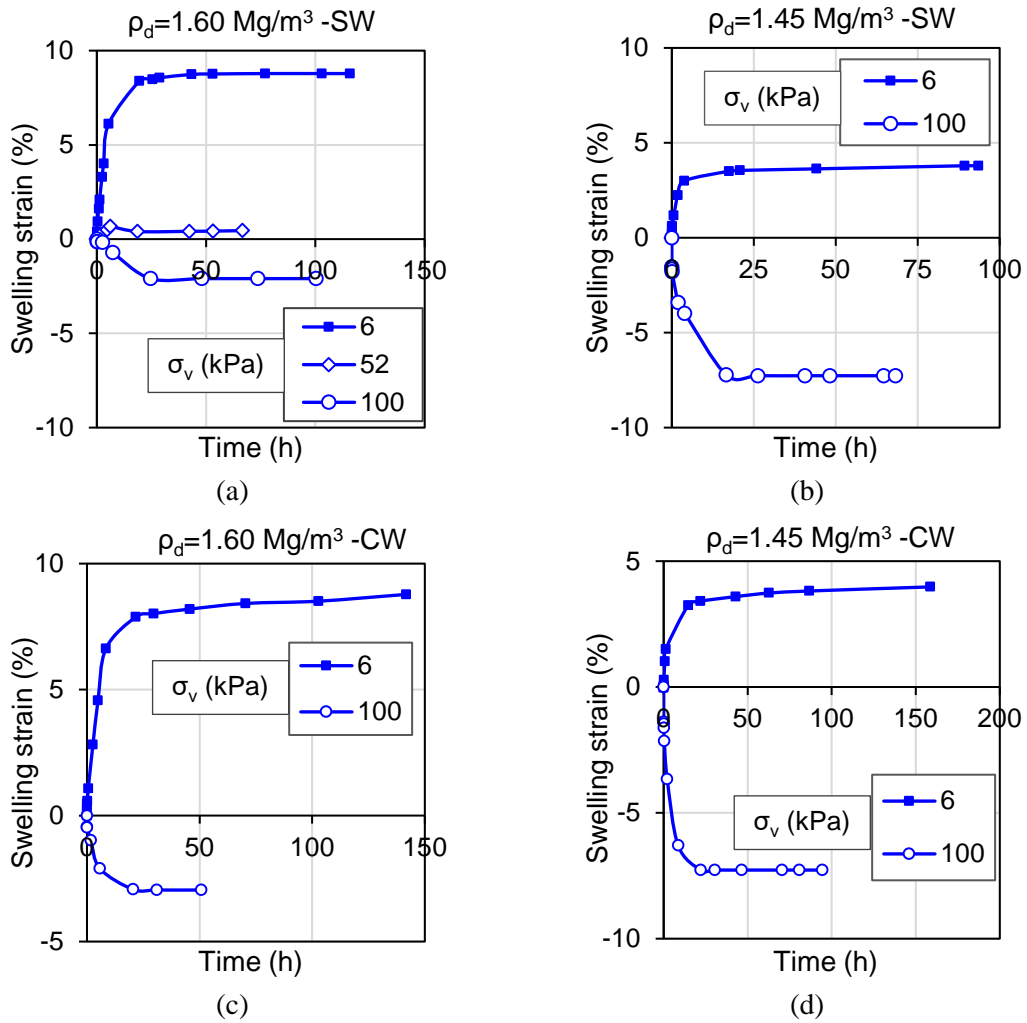


Figure 6-9 Results of swelling potential tests under different vertical stresses on COx/MX80 mixture containing 10%MX80: (a)  $\rho_d = 1.60 \text{ Mg/m}^3$  hydrated with site water, (b)  $\rho_d = 1.45 \text{ Mg/m}^3$  hydrated with site water, (c)  $\rho_d = 1.60 \text{ Mg/m}^3$  hydrated with cementitious water, (d)  $\rho_d = 1.45 \text{ Mg/m}^3$  hydrated with cementitious water.

COx/MX80 mixtures with 20%MX80

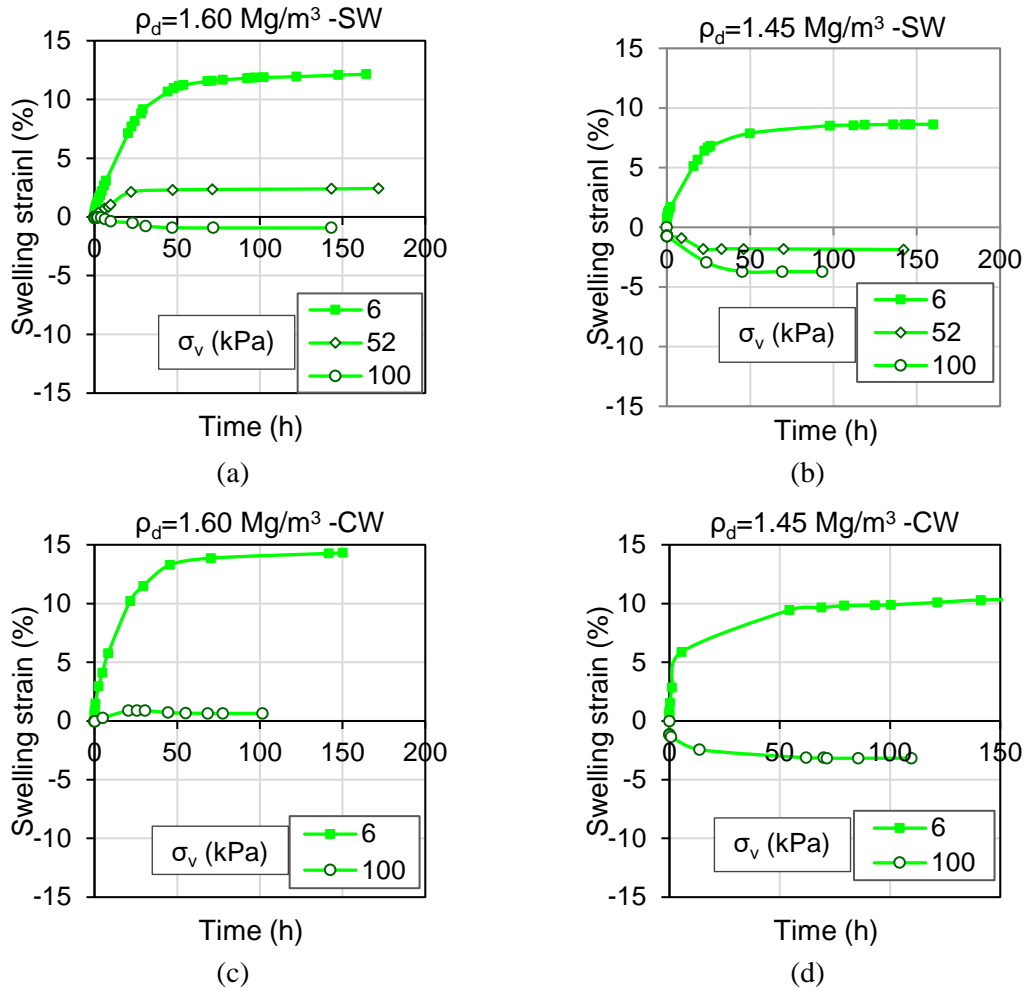


Figure 6-10 Results of swelling potential tests under different vertical stresses on COx/MX80 mixture containing 20%MX80: (a)  $\rho_d = 1.60 \text{ Mg/m}^3$  hydrated with site water, (b)  $\rho_d = 1.45 \text{ Mg/m}^3$  hydrated with site water, (c)  $\rho_d = 1.60 \text{ Mg/m}^3$  hydrated with cementitious water, (d)  $\rho_d = 1.45 \text{ Mg/m}^3$  hydrated with cementitious water.

COx/MX80 mixtures with 30%MX80

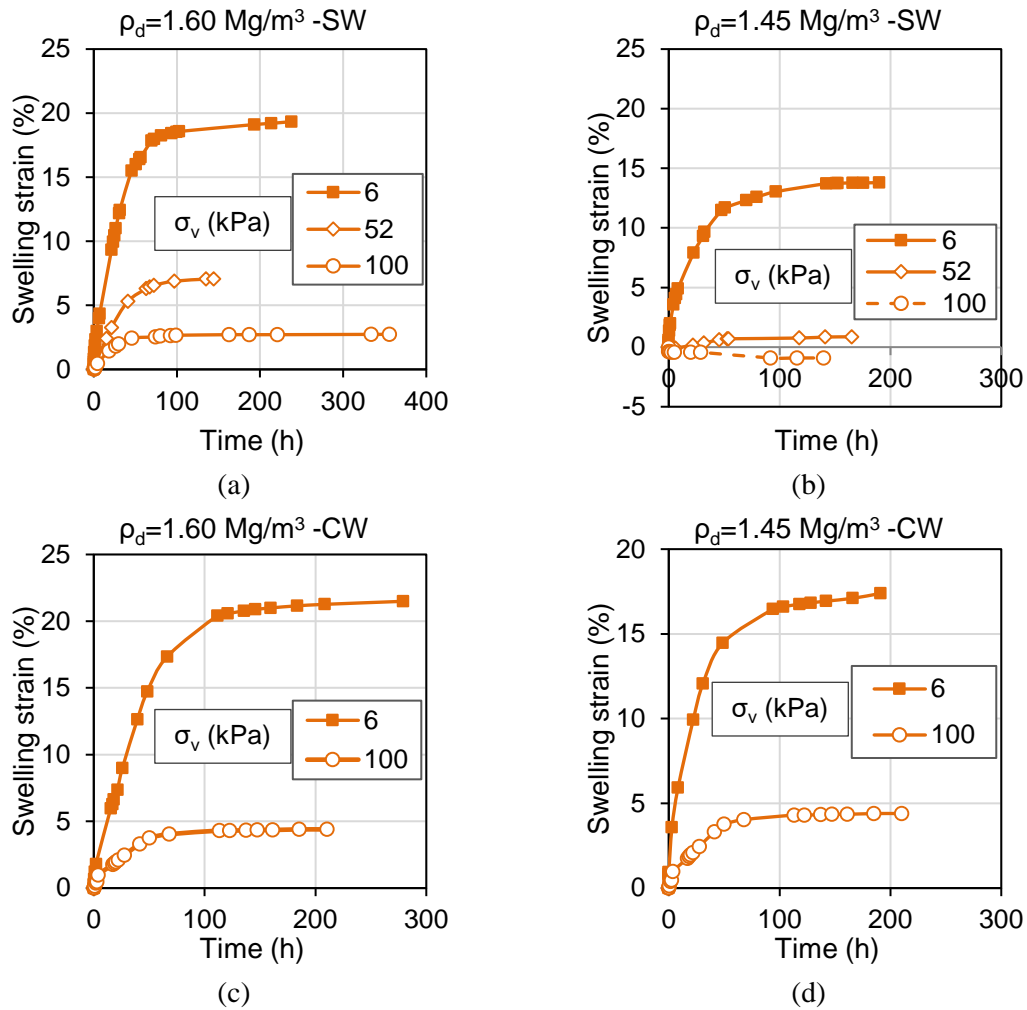


Figure 6-11 Results of swelling potential tests under different vertical stresses on COx/MX80 mixture containing 30%MX80: (a)  $\rho_d = 1.60 \text{ Mg/m}^3$  hydrated with site water, (b)  $\rho_d = 1.45 \text{ Mg/m}^3$  hydrated with site water, (c)  $\rho_d = 1.60 \text{ Mg/m}^3$  hydrated with cementitious water, (d)  $\rho_d = 1.45 \text{ Mg/m}^3$  hydrated with cementitious water.

### COx/MX80 mixtures with 40%MX80

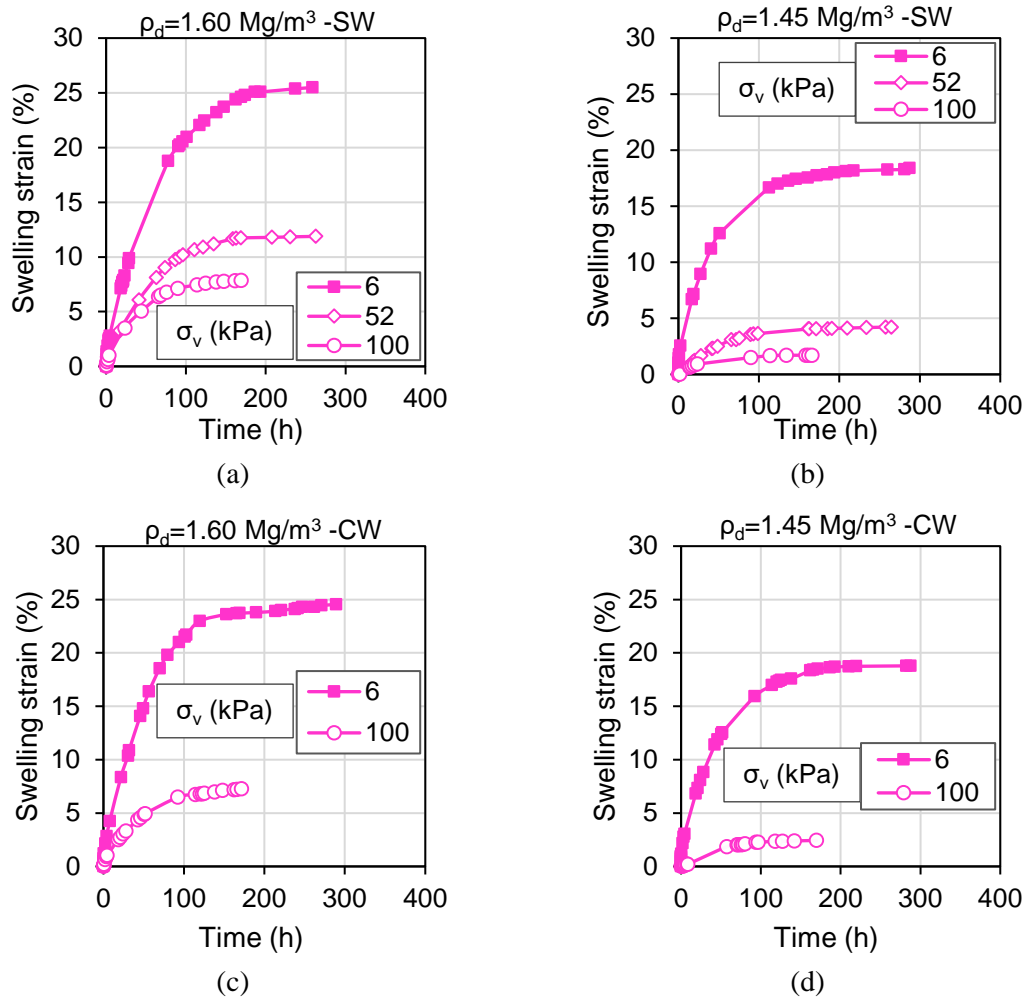


Figure 6-12 Results of swelling potential tests under different vertical stresses on COx/MX80 mixture containing 40%MX80: (a)  $\rho_d = 1.60 \text{ Mg/m}^3$  hydrated with site water, (b)  $\rho_d = 1.45 \text{ Mg/m}^3$  hydrated with site water, (c)  $\rho_d = 1.60 \text{ Mg/m}^3$  hydrated with cementitious water, (d)  $\rho_d = 1.45 \text{ Mg/m}^3$  hydrated with cementitious water.

In order to better analyse the materials swelling potential (i.e. final swelling strain), the results are presented on Figure 6-13 as function of the MX80 content. The initial dry density and the infiltrated liquids are also illustrated (demineralised, site, cementitious water). A linear increase of the swelling potential upon bentonite addition was observed for the tested CO<sub>x</sub>/MX80 mixtures (MX80 ≤ 40%) independent to the applied vertical stress. The well-established role of initial dry density was reported: higher density state gave higher swelling potential. Swelling capacity was clearly higher when DW was infiltrated the specimens. Similarly to the physicochemical properties, the observed chemical impact becomes more significant, when the mixtures containing more MX80. On the other hand, the variation of the swelling is considered insignificant between site and cementitious water, especially for the higher dry density ( $\rho_d = 1.60 \text{ Mg/m}^3$ ) or applied stress ( $\sigma_v = 100 \text{ kPa}$ ).

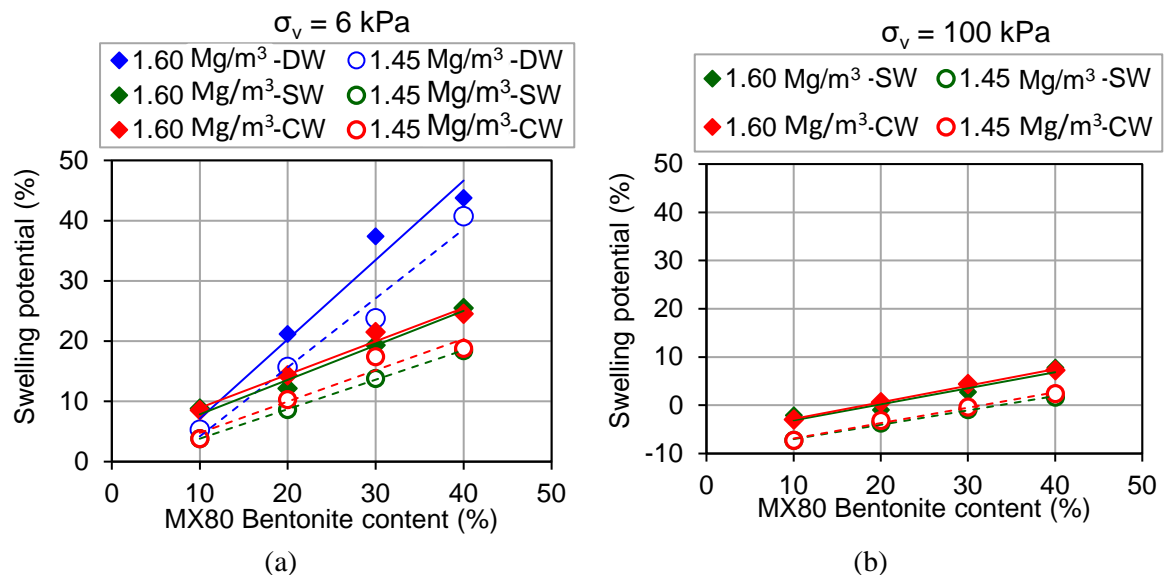


Figure 6-13 Evolution of CO<sub>x</sub>/MX80 mixtures obtained swelling potential with bentonite content for different initial dry densities and infiltrated fluid: (a) under 6 kPa and (b) under 100 kPa.

Figure 6-14a presents the development in swelling strain of pure CO<sub>x</sub>/MX80 mixtures prepared with the modified CO<sub>x</sub> granulometry (CO<sub>x</sub>-D<sub>mod</sub>). The addition of 30% sand inside the mixtures is examined on Figure 6-14b. The usual hyperbolic swelling strain evolution is obtained with time for the CO<sub>x</sub>/MX80 mixtures (Figure 6-14a), while on CO<sub>x</sub>/MX80/sand mixtures strain rapidly increased and then follows an almost linear relation. Bentonite effect is reported on both cases. Lower swelling seems to be obtained by the CO<sub>x</sub>/MX80/sand samples. It is reminded that the highest implemented MX80 content on those mixtures is lower than 40%MX80. This parameter is better analysed below. It needs to be underlined that in the case of CO<sub>x</sub>/MX80/sand mixtures, specimens appeared to be very quickly saturated. The swelling strain kinetics also suggests. Therefore, it was highlighted that if sand is used as component of the backfill, the resulting hydraulic conductivity must be assessed.

The effect of MX80 bentonite on the resulting swelling is examined for all tested samples of identical dry density, hydrated under common vertical stress. Therefore, Figure 6-15 presents the developed swelling potential under  $\sigma_v = 6$  kPa for the different mixtures compacted at  $\rho_d = 1.60$  Mg/m<sup>3</sup>. A common behaviour without clear variations is obtained for all studied mixtures. The results show that the eliminations of COx finer grains ( $\leq 200\mu\text{m}$ ) did not cause any impact on the reported swelling potential. Similar remarks can be concluded for the presence of sand inside the COx/MX80 mixture. The experimental data suggest the swelling behaviour is exclusively obtained due to bentonite presence, while COx argillite does not contribute in swelling for this density range ( $\rho_d \leq 1.60$  Mg/m<sup>3</sup>).

Table 6-6 summarises the final swelling strain recorded from all the tested mixtures.

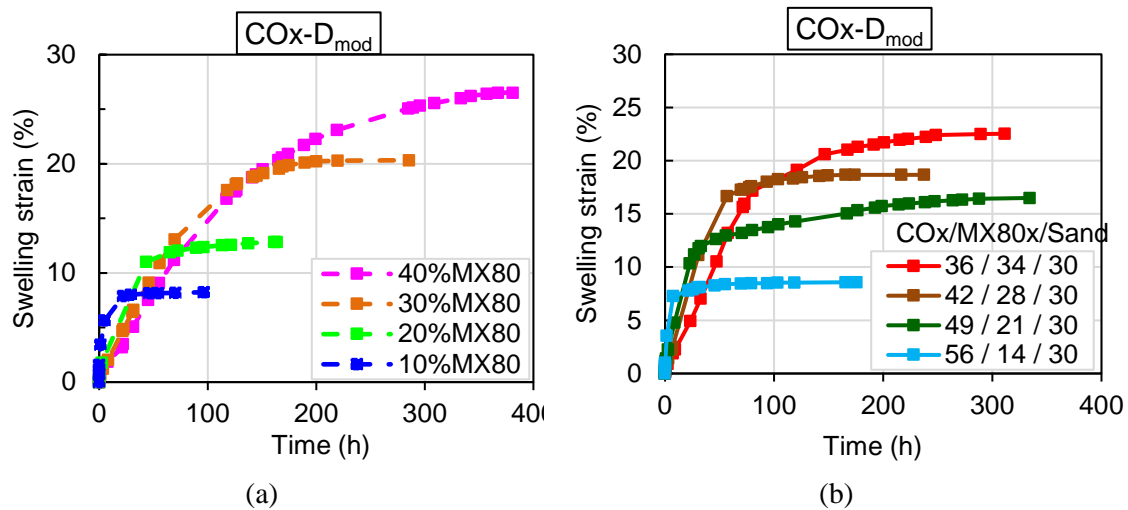


Figure 6-14 Results of swelling potential tests under  $\sigma_v = 6$  kPa using site water, on samples with initial dry density of  $\rho_d = 1.60$  Mg/m<sup>3</sup> prepared with the modified COx granulometry: (a) COx/MX80 mixtures and (b) COx/MX80/sand mixtures.

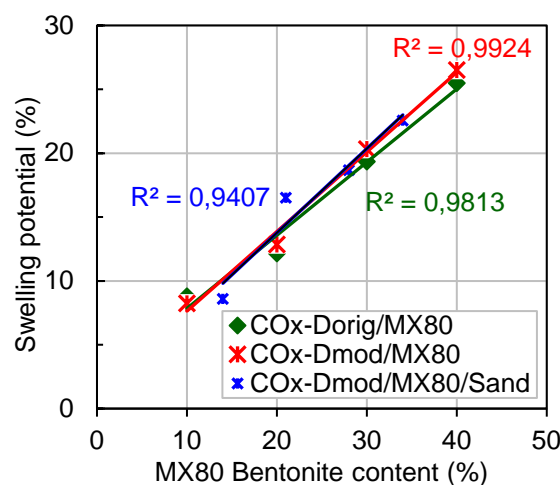


Figure 6-15 Evolution of swelling potential obtained for COx/MX80 mixtures of original granulometry, COx/MX80 mixtures with modified granulometry and COx/MX80/sand mixtures, under  $\sigma_v = 6$  kPa using site water ( $\rho_d = 1.60$  Mg/m<sup>3</sup>).

Table 6-6 Summary of final results for all swelling potential tests.

| COx                 | %MX80 | %Sand | Initial dry density,<br>$\rho_d$ (Mg/m <sup>3</sup> ) | Swelling potential (%) |       |       |                     |                      |       |
|---------------------|-------|-------|---|------------------------|-------|-------|---------------------|----------------------|-------|
|                     |       |       |   | $\sigma_v = 6$ kPa     |       |       | $\sigma_v = 52$ kPa | $\sigma_v = 100$ kPa |       |
|                     |       |       |   | DW                     | SW    | CW    | SW                  | SW                   | CW    |
| D <sub>orig</sub> * | 10    | -     | 1.46 ± 0.002  | 5.26                   | 3.79  | 3.81  | -3.62               | -7.27                | -7.27 |
|                     |       | -     | 1.61 ± 0.004  | 5.25                   | 8.78  | 8.51  | 0.45                | -2.10                | -2.95 |
|                     | 20    | -     | 1.45 ± 0.009  | 15.70                  | 8.64  | 10.30 | -1.86               | -3.71                | -3.17 |
|                     |       | -     | 1.59 ± 0.003  | 21.15                  | 12.14 | 14.31 | 2.43                | -0.94                | 0.65  |
|                     | 30    | -     | 1.45 ± 0.002  | 23.80                  | 13.80 | 17.39 | 0.87                | -0.91                | -0.37 |
|                     |       | -     | 1.60 ± 0.001  | 37.40                  | 19.34 | 21.49 | 7.04                | 2.73                 | 4.40  |
|                     | 40    | -     | 1.46 ± 0.004  | 40.75                  | 18.39 | 18.79 | 4.22                | 1.71                 | 2.43  |
|                     |       | -     | 1.60 ± 0.006  | 43.75                  | 25.48 | 24.53 | 11.88               | 7.77                 | 7.26  |
| D <sub>mod</sub> †  | 10    | -     | 1.60  | 8.23                   |       |       |                     |                      |       |
|                     | 20    | -     | 1.59  | 12.85                  |       |       |                     |                      |       |
|                     | 30    | -     | 1.59  | 20.33                  |       |       |                     |                      |       |
|                     | 40    | -     | 1.60  | 26.52                  |       |       |                     |                      |       |
| D <sub>mod</sub> †  | 14    | 30    | 1.60  | 8.57                   |       |       |                     |                      |       |
|                     | 21    | 30    | 1.61  | 16.50                  |       |       |                     |                      |       |
|                     | 28    | 30    | 1.61  | 18.67                  |       |       |                     |                      |       |
|                     | 34    | 30    | 1.61  | 22.54                  |       |       |                     |                      |       |

\* Original COx granulometry

† Modified COx granulometry

### 6.4.3 Swelling pressure

The swelling pressure developed by the studied COx/MX80 mixtures was tested at constant volume conditions. Figure 6-16 presents the results of COx/MX80 samples containing 10%, 20%, 30% and 40% of bentonite compacted at dry densities of 1.45 and 1.60 Mg/m<sup>3</sup>. The mixtures are prepared by using the soil materials at their reception conditions (water content, granulometry). The final values of swelling pressure are illustrated for each sample. They were determined as the average value after pressure stabilization (> 100 h). In some cases, more than one test was carried out to verify the repeatability of the process and an average value was obtained.

All tested samples presented a characteristic swelling pressure development. The stress was rapidly increased upon wetting until a maximum value. Then, it decreased reaching stabilization. The difference between maximum and final swelling pressure ( $P_{smax}/P_{sfinal}$ ) is less significant as the bentonite percentage increases inside the mixture. The peak has also been reported by previous studied on swelling clay-based materials (e.g. Komine and Ogata, 1994;

Pusch, 1982; Saba et al., 2014a). The behaviour has been connected to the macropores, which is more significant at the low dry densities (i.e. higher macroporosity) and collapse as saturation progresses (Lloret and Villar 2007). The results suggest that macroporosity increases at lower bentonite contents. Similar to the results of swelling potential tests, more time was necessary to reach stabilization with higher bentonite content. Permeability decreases with bentonite addition and more time is needed for the material to process to full saturation (Tu, 2011; Akgün and Koçkar, 2018; Kohno et al., 2018).

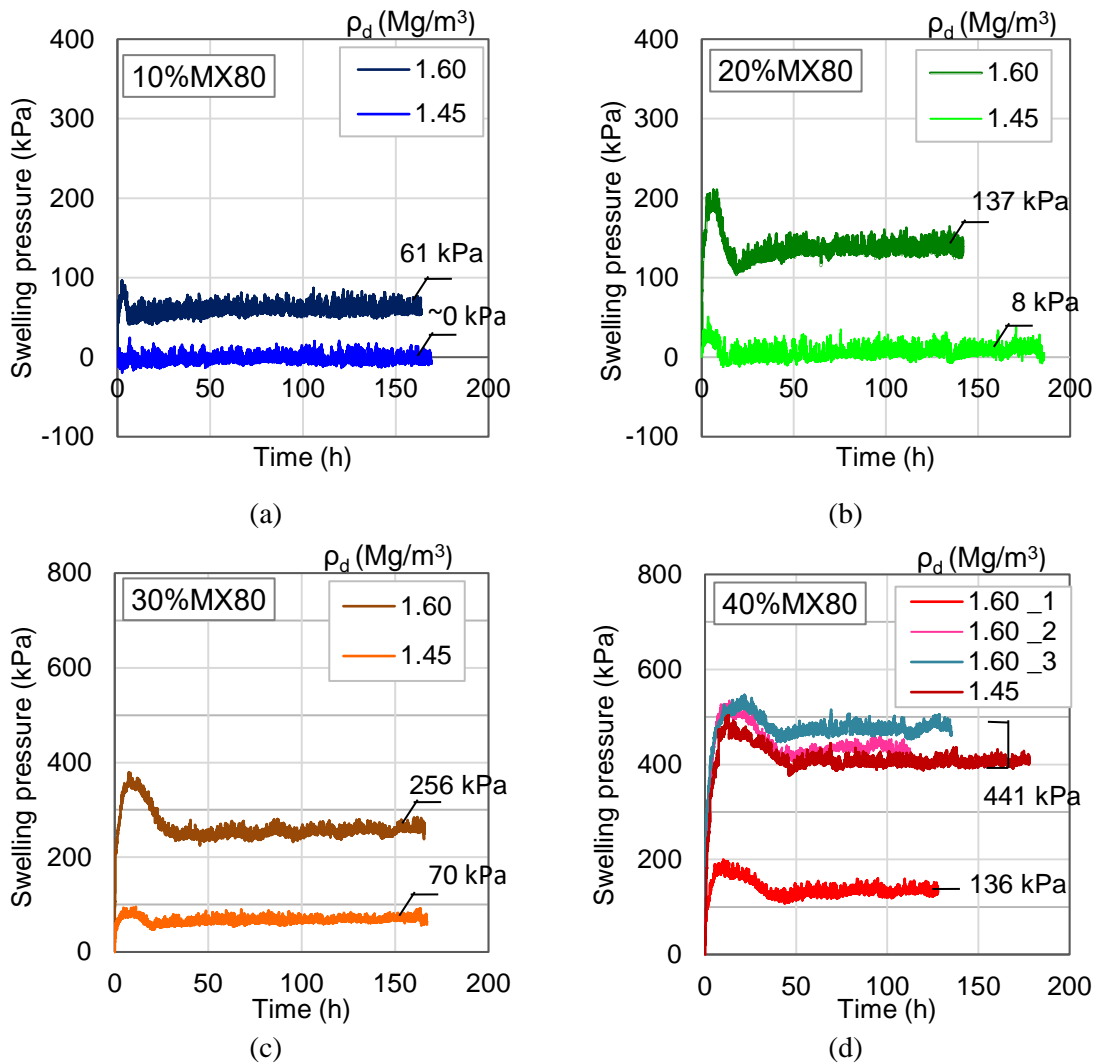


Figure 6-16 Evolution of swelling pressure with time for samples compacted at initial dry density of  $\rho_d = 1.45 \text{ Mg/m}^3$  and  $\rho_d = 1.60 \text{ Mg/m}^3$ : COx/MX80 mixtures containing (a) 10%, (b) 20%, (c) 30% and (d) 40% of MX80.

On Figure 6-17, the effect of bentonite content and dry density is examined for the tested COx/MX80 mixtures. Swelling pressure follows non-linear increase with the imposed bentonite percentage, while the effect is more notable for higher dry densities. For both cases, polynomial relation of 2<sup>nd</sup> degree is suggested, presenting high correlation ( $R^2 > 0.98$ ). It is evident that

COx/MX80 mixture at lower bentonite content  $\leq 20\%$  and dry density of  $1.45 \text{ Mg/m}^3$  practically exhibit no swelling pressure.

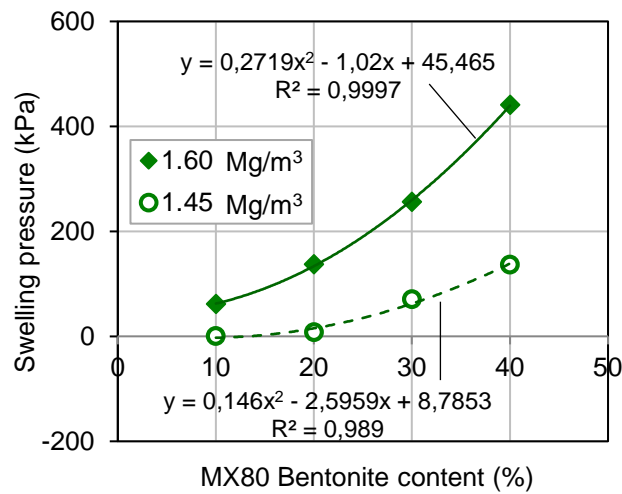


Figure 6-17 Influence of MX80 bentonite content on final swelling pressure of COx/MX80 mixtures compacted at different initial dry densities.

The influence of water content on the swelling capacity was evaluated, by performing constant volume tests on COx/MX80 mixtures prepared on the “optimum” water content and compacted at dry density of  $1.60 \text{ Mg/m}^3$ . The selected water content values corresponded on those resulted from the normal Proctor tests (Figure 6-8b). The obtained results are illustrated on Figure 6-18, together with those obtained from the reception water content.

A clear impact of water content on the swelling pressure kinetics is observed. When COx/MX80 mixtures were prepared at the optimum water content conditions, the pressure resulted from the materials hydration increases until it reaches stabilization. No collapse of macropores is noticed. The remark is in agreement with Komine and Ogata (1994) on swelling pressure tests on Kunigel bentonite prepared at higher water contents. Since specimens of higher initial water content are more wetted in the beginning of the experiment, bentonite particles are partially swollen. Therefore, mechanical collapse was not observed upon further hydration.

A slight effect of the initial water content conditions on the final swelling pressure is presented on Figure 6-19 for the different tested COx/MX80 mixtures compacted at the same dry density. The impact increases as bentonite content is more significant. When low bentonite is imposed on COx argillite the effect of water content becomes insignificant. The results show the sensibility of bentonites hydro-mechanical behaviour on interaction with water. When the material is pre-wetted, swelling capacity decreases.

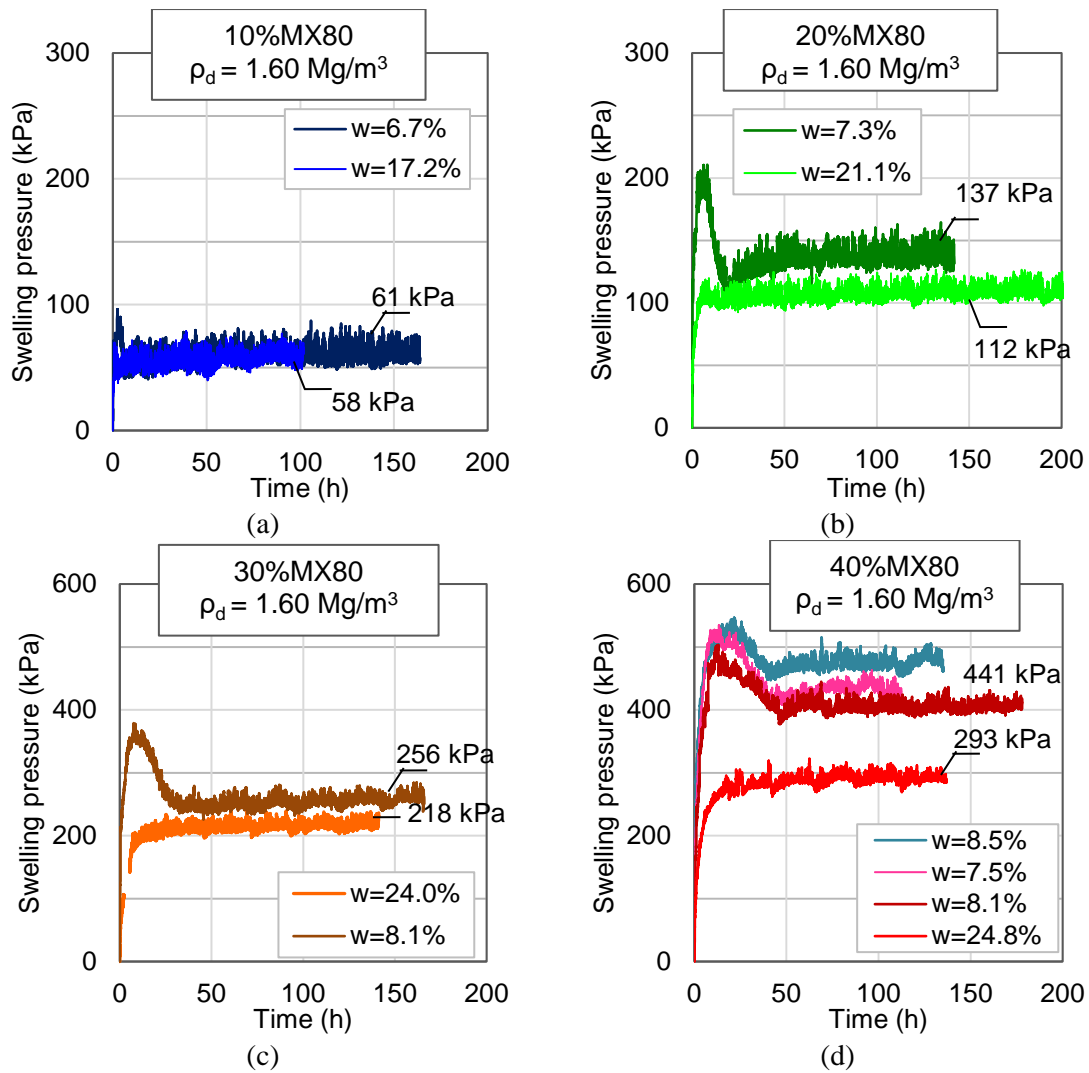


Figure 6-18 Evolution of swelling pressure with time for samples compacted at initial dry density of  $\rho_d = 1.60 \text{ Mg/m}^3$  with water content of reception and optimum water content: COx/MX80 mixtures containing (a) 10%, (b) 20%, (c) 30% and (d) 40% of MX80.

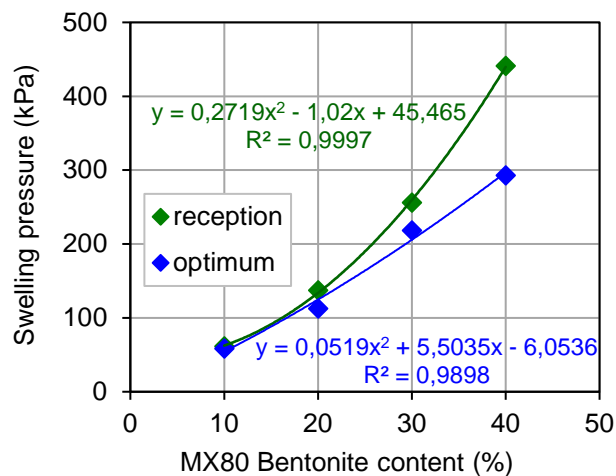


Figure 6-19 Influence of MX80 bentonite content on final swelling pressure of COx/MX80 mixtures compacted at initial dry density  $\rho_d = 1.60 \text{ Mg/m}^3$  at water content of reception and optimum water content conditions.

Table 6-7 summarises the results of swelling pressure tests obtained for all the tested mixtures.

Table 6-7 Summary of final results for all swelling pressure tests.

| COx                 | %MX80 | Initial water content, $w$ (%) | Initial dry density, $\rho_d$ (Mg/m <sup>3</sup> ) | Maximum swelling pressure (kPa) | Final swelling pressure (kPa) |
|---------------------|-------|--------------------------------|--|---------------------------------|-------------------------------|
| D <sub>orig</sub> * | 10    | 6.7                            | 1.61   | 96.3                            | 61.3                          |
|                     |       | 17.2                           | 1.59   | 79.0                            | 58.3                          |
|                     |       | 6.7                            | 1.46   | 20.7                            | 0.0                           |
|                     | 20    | 7.3                            | 1.60   | 210.6                           | 137.6                         |
|                     |       | 21.1                           | 1.60   | 128.0                           | 110.6                         |
|                     |       | 7.5                            | 1.45   | 37.6                            | 6.8                           |
|                     | 30    | 8.1                            | 1.59   | 378.9                           | 254.8                         |
|                     |       | 24.0                           | 1.62   | 241.7                           | 218.1                         |
|                     |       | 8.5                            | 1.45   | 92.0                            | 68.7                          |
|                     | 40    | 8.6                            | 1.60   | 508.0                           | 440.8                         |
|                     |       | 24.8                           | 1.60   | 322.8                           | 292.9                         |
|                     |       |                                | 7.9  | 1.46                            | 160.0                         |

\* Original COx granulometry

## 6.5 Discussion

The experimental results are further discussed for the different studied parameters.

### 6.5.1 Chemical effect of infiltrated solutions on swelling capacity

Pure demineralised water and synthetic solutions of site and cementitious water were used to determine the physicochemical properties of various COx/MX80 mixtures, as well as the swelling potential of compacted samples.

As expected, hydration with pure water resulted in the highest swelling potential and plasticity index (Figure 6-5, Figure 6-6, Figure 6-13). The effect is more intense at higher bentonite contents. It has already been seen on previous experimental studies that swelling capacity decreases with solutions of higher ionic strength (Herbert et al. 2008, Shirazi et al. 2011).

Nonetheless, for the implemented test duration (of maximum 12 days) no clear conclusions can be drawn about the variation between the effect of site and cementitious water on the hydro-mechanical behaviour. The results of swelling potential tests of compacted COx/MX80 samples imply that cementitious water lead to higher swelling than site water, only on lower dry densities and applied vertical stresses. The variation on physical properties is not homogeneous. No significant impact of the alkaline solution is observed compared to the groundwater (site

water). In general, the two synthetic solutions present similar ionic strength and therefore the effect is considered insignificant.

### **6.5.2 Effect of initial dry density on swelling capacity**

The effect of the compaction state was analysed by studying at confined and non-confined volume conditions the swelling response of CO<sub>x</sub>/MX80 mixtures compacted at different dry densities. The powdered material was compacted at the density range that the pelletized backfill is expected to present ( $\rho_d = 1.45\text{-}1.60 \text{ Mg/m}^3$ ).

As expected, both parameters of swelling pressure and swelling potential were improved upon density increase. The behaviour is well-reported on pure bentonites and on swelling-clay based materials. More precisely, swelling potential increases linearly with the imposed dry density under a given applied stress (Hoffmann et al., 2007; Villar and Lloret, 2008; Manca et al., 2015). On the other hand, swelling pressure presents exponential increase (e.g. Pusch, 1982; Seiphoori, 2014; Yigzaw et al., 2016; Zeng et al., 2019). The results obtained from the swelling under constant vertical stress and under constant volume tests are presented on Figure 6-20 and Figure 6-21, for the investigated density range. Since only two initial densities were tested, it is not accurate to suggest a mathematical relation for the developed swelling capacity with the material's initial dry density. Therefore, the presented trendlines were plotted only to simply visualise the density effect. They were based on the previously mentioned relation of each parameter with density (i.e. linear for swelling potential, exponential for swelling pressure).

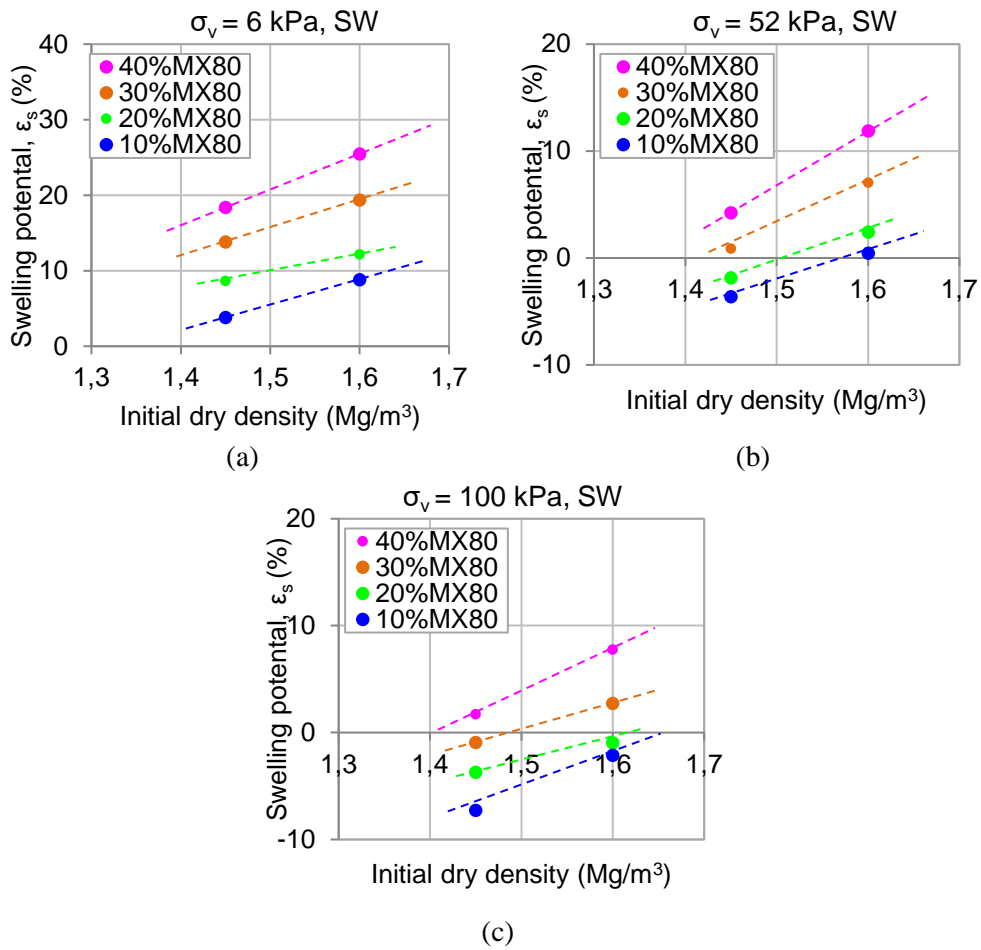


Figure 6-20 Evolution of swelling potential with initial dry density for various COx/MX80 mixtures: applied vertical stress of (a)  $\sigma_v = 6 \text{ kPa}$ , (b)  $\sigma_v = 52 \text{ kPa}$  and (c)  $\sigma_v = 100 \text{ kPa}$  (hydration with SW).

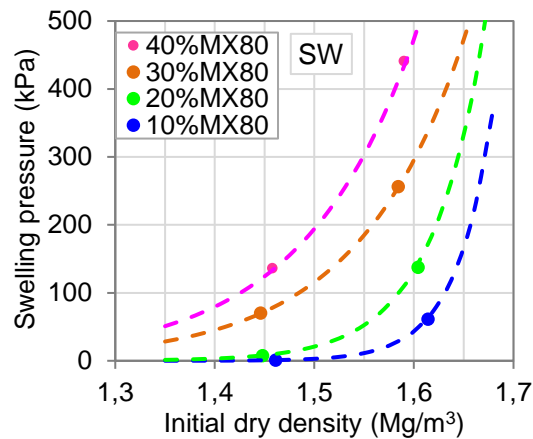


Figure 6-21 Evolution of swelling pressure with initial dry density for various COx/MX80 mixtures (hydration with SW).

### 6.5.3 Preliminary estimation of backfill's swelling capacity

The swelling response of a pelletized backfill composed of COx/MX80 mixtures was estimated for the in-situ gallery conditions, by exploiting the experimental results of the swelling potential tests (section 6.4.2). The calculations were based on the hypothesis of homogeneous distribution of the material's dry density, from installation to saturation conditions. As a reminder, the experimental work on the "expected" overall dry density of the pelletized sample showed a density range of interest between 1.45 and 1.60 Mg/m<sup>3</sup>. Only hydration with site water was considered.

On Figure 6-22, the swelling potential as function of the applied vertical stress for the investigated COx/MX80 mixtures compacted at different dry densities is presented as obtained from the experimental study. A clear logarithmic decrease of the obtained swelling strain is observed upon the stress increment. The remarks are in agreement with previous observations on swelling clays (Hoffmann et al., 2007; Castellanos et al., 2008; Villar and Lloret, 2008).

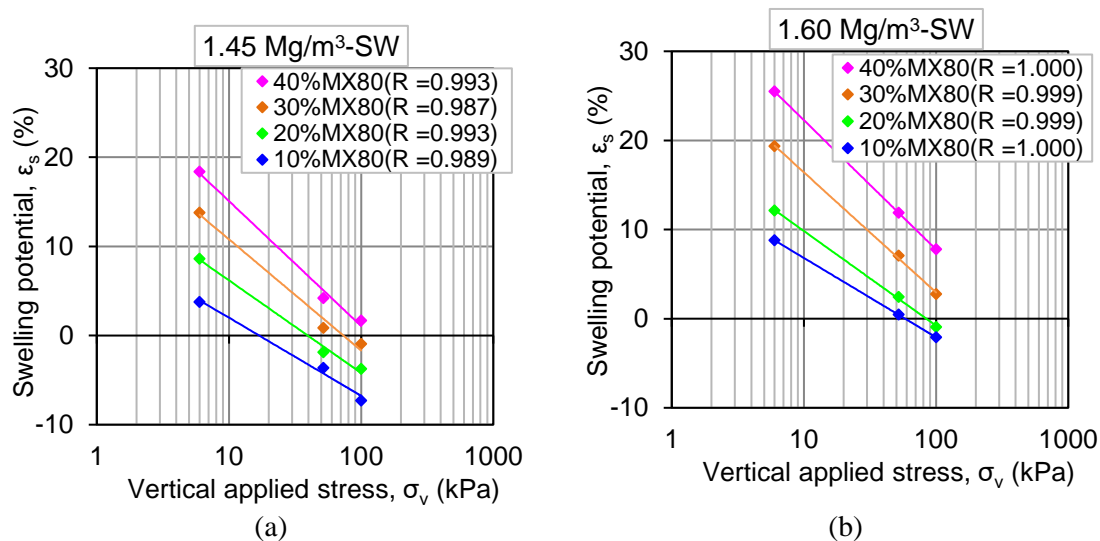


Figure 6-22 Influence of the applied vertical stress on the developed swelling potential of COx/MX80 mixtures hydrated with site water: initial dry density of (a) 1.45 Mg/m<sup>3</sup> and (b) 1.60 Mg/m<sup>3</sup>.

According to the design, the pelletized backfill material will be installed in horizontal galleries with diameter of approximately 8 m, exhibiting its overall dry density (1.45-1.60 Mg/m<sup>3</sup>). Granular rearrangement under such height may cause an evolution of the initial (setup) dry density. While infiltration of site water begins, the material swells under the effect of stresses applied due to backfill's unit weight. As long as void recovery has been achieved, the material continues swelling under constant volume conditions (fixed gallery limits).

It was observed that depending on the applied stresses, the material could either swell or collapse (Figure 6-22). Therefore, an estimation of the backfill's "self-sealing" ability (i.e. clear swelling potential) on saturated conditions is carried out for the backfill's unit weight. In practice, the present analysis aims to predict whether overall swelling or overall collapse will occur at gallery conditions for various CO<sub>x</sub>/MX80 mixtures.

It is known that the applied total vertical stress (in kPa) due to soil's unit weight can be determined according to the gallery's height as following:

$$\sigma_v = \gamma \cdot z \quad (6.4)$$

where  $z$  is the depth in m and  $\gamma$  is the unit weight of the soil material in kN/m<sup>3</sup>. The developed swelling potential follows a logarithmic relation with the applied stress for a given dry density and is calculated as:

$$\varepsilon_s = a \cdot \ln \sigma_v + b \quad (6.5)$$

where  $a$  and  $b$  is unique parameter for each CO<sub>x</sub>/MX80 mixture as on obtained from Figure 6-22 and are presented on Table 6-8.

Table 6-8 Curve fitting parameters calculated from the swelling potential tests.

| MX80 bentonite content (%) | Initial dry density, $\rho_d = 1.45 \text{ Mg/m}^3$ |       | Initial dry density, $\rho_d = 1.60 \text{ Mg/m}^3$ |       |
|----------------------------|---|-------|---|-------|
|                            | $a$   | $b$   | $a$   | $b$   |
| 10                         | -3.81   | 10.77 | -3.87   | 15.74 |
| 20                         | -4.51   | 16.57 | -4.61   | 20.45 |
| 30                         | -5.42   | 2327  | -5.85   | 29.88 |
| 40                         | -6.09   | 29.11 | -6.30   | 36.76 |

In the present study, the gallery's height was ranging from 0 to 8 m, while homogeneous distribution of saturated unit weight within the gallery was considered (i.e. 19.1 kN/m<sup>3</sup> and 20.1 kN/m<sup>3</sup> for initial dry density of 1.45 Mg/m<sup>3</sup> and 1.60 Mg/m<sup>3</sup> respectively). Thus, the swelling potential can be calculated as function of gallery's height, for the maximum applied stress conditions, as Figure 6-23 illustrates.

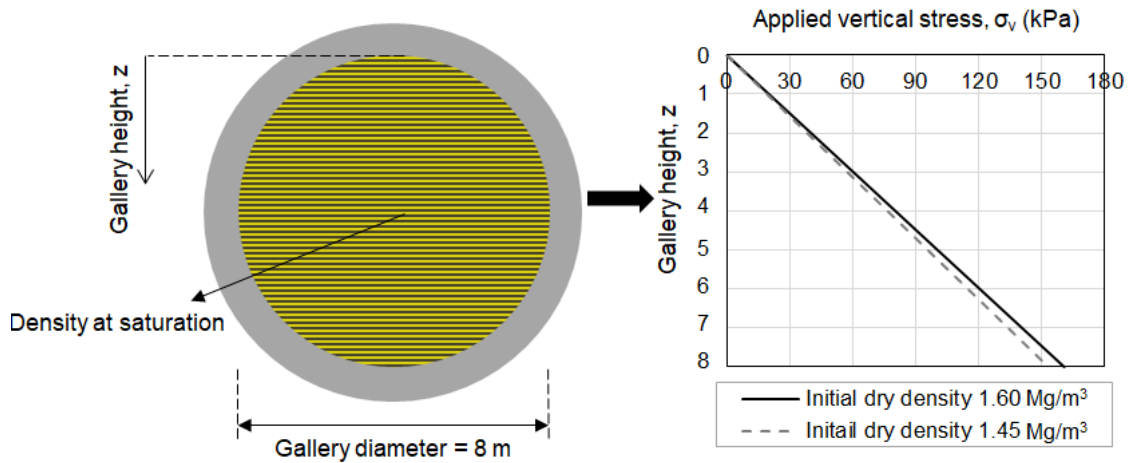


Figure 6-23 Variation of the applied total vertical stress as function of the gallery's height, due to backfill's saturated unit weight.

The results of the swelling potential calculations are presented on Figure 6-24 for various COx/MX80 emplaced at initial dry densities of 1.45 Mg/m<sup>3</sup> and 1.60 Mg/m<sup>3</sup>. The corresponding analytically calculated displacements were determined as illustrated in Figure 6-25. In both parameters, two zones of hydro-mechanical response are identified: the backfill located in the upper part of the gallery presents swelling, whereas the lower part presents collapse.

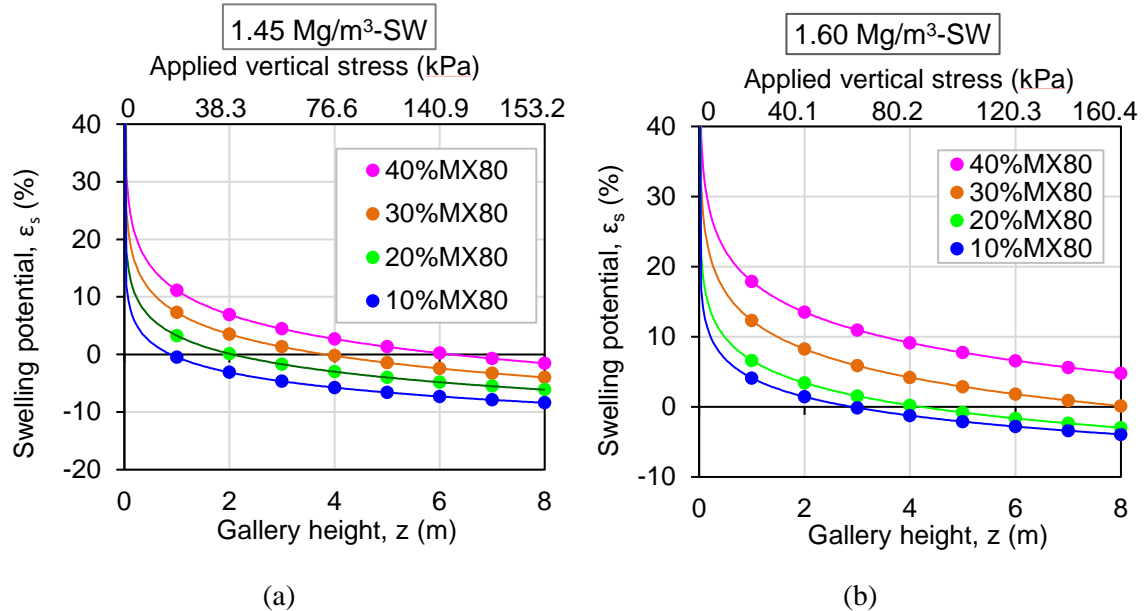


Figure 6-24 Calculated swelling potential mixtures as function of the gallery's height and the corresponding vertical stress for backfill composed of various COx/MX80 mixtures emplaced at initial dry density of (a) 1.45 Mg/m<sup>3</sup> and (b) 1.60 Mg/m<sup>3</sup>.

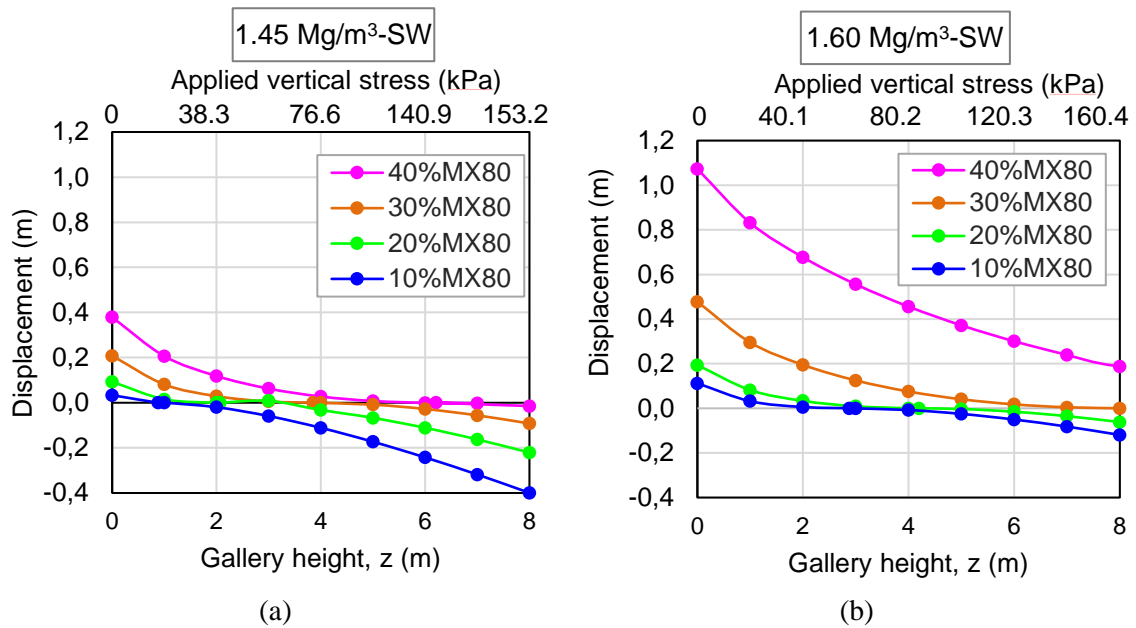


Figure 6-25 Calculated displacement as function of the gallery's height and the corresponding vertical stress for backfill composed of various COx/MX80 mixtures emplaced at initial dry density of (a) 1.45 Mg/m<sup>3</sup> and (b) 1.60 Mg/m<sup>3</sup>.

In order to conclude on the material's overall behaviour, the average displacements over the entire height of the gallery are determined on Figure 6-26. It can be observed that for the density range of interest, mainly COx/MX80 mixtures containing bentonite between 30% and 40% can be used in order to obtain a swelling behaviour. Nonetheless, a next step after the optimization/characterization of the optimal pellets solution would be the hydro-mechanical modelling of a full scale drift filling, taking into account the real set up and phase sequences.

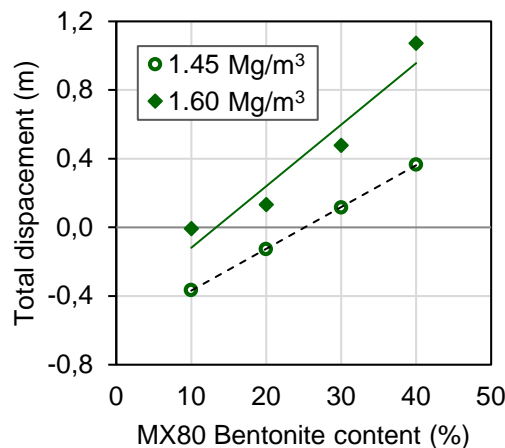


Figure 6-26 Overall calculated displacement on gallery's vertical diameter of the studied COx/MX80 backfill mixtures as function of MX80 content, for the investigated dry densities.

## 6.6 Conclusions

The hydro-mechanical behaviour of various COx/MX80 mixtures in powder was used in order to evaluate the hydro-mechanical response of COx/MX80 pellets assembly. The study was conducted on the equivalent density range, expected to be presented by the pelletized backfill material according to previous experiments (1.45-1.60 Mg/m<sup>3</sup>). The physicochemical properties and the swelling capacity of the investigated mixtures were examined. For all tests, bentonite fraction did not exceed 40% of the mixtures total mass.

The effect of the bentonite content, the infiltrated solution's chemistry, as well as the initial dry density on the hydro-mechanical response was assessed. In some cases, apart from the COx argillite and MX80 bentonite at the received conditions, the effect of COx's granulometry modification and sand's presence was studied. The main observations are summarised below.

The parametric study on the COx/MX80 mixtures physicochemical characteristics showed that:

- Plasticity (Atterberg limits) and free swelling capacity (FSI) increase with the increment of bentonite content introduced in the mixture, independently to the hydration solution. Bentonite addition is related with increase of clays specific surface area and therefore more water is absorbed, resulting in swelling. On the hand, the swelling increases bentonite's particles and therefore it hinders its compaction; the optimum dry density decreases as MX80 content is more important.
- Synthetic solutions (i.e. site water and cementitious water) result in decrease of swelling, compared to pure water, since salt presence impacts the materials swelling capacity. Cementitious water appeared to impact less significantly, but the overall results consider this difference as insignificant, probably because both solutions present very similar ionic strength.

The parametric study on the compacted COx/MX80 mixtures swelling capacity (i.e. swelling potential and swelling pressure) demonstrated that:

- The variation of swelling pressure and swelling potential was determined for the dry density range of interest for this study. The usual increase of swelling capacity was observed upon density increase from 1.45 to 1.60 Mg/m<sup>3</sup>.
- Swelling potential followed a linear increase upon bentonite addition. On the other hand, swelling pressure increased non-linearly with bentonite content and the effect was more significant for the higher densities.

- Swelling potential tests showed that the impact of CO<sub>x</sub>'s granulometry modification or the sand's presence inside the mixture was not important, while no pronounced effect of the alkaline solution was recorded.
- Swelling under constant volume conditions illustrated the increase/decrease/stabilized development of swelling pressure, which was more evident when MX80 content and initial dry density was decreased. The behaviour implies more important macroporosity with decrease of bentonite even for the same density. The kinetics was no more observed on the CO<sub>x</sub>/MX80 mixtures prepared at water contents corresponding to the optimum water content conditions, where the material presents lower initial suction. A slight effect of the initial water content conditions on the final pressure was obtained, especially for the higher bentonite content.
- The logarithmic relation of the obtained swelling potential with the applied vertical stress was determined from the data of the swelling under constant stress condition for all investigated CO<sub>x</sub>/MX80 hydrated with site water. They were used to preliminarily analyse the swelling capacity of backfill emplaced at gallery conditions. The method was carried out for the stress applied due to material's unit weight at saturation with the gallery's height (0 to 8 m), considering homogeneous density distribution. The calculations showed that for the density range of interest, mainly CO<sub>x</sub>/MX80 mixtures with bentonite contain between 30% and 40% are proposed in order to obtain swelling behaviour.



# **Chapter 7 - Hydro-mechanical study of CO<sub>x</sub>/MX80 pelletized materials**

On the present chapter, the hydro-mechanical behaviour of CO<sub>x</sub>/MX80 pelletized materials is directly evaluated upon emplacement condition (i.e. no compaction applied upon preparation). Swelling pressure development is measured at constant volume conditions and hydraulic conductivity is evaluated on saturation. Several pelletized mixtures are formed, according to the optimum retained granulometry selected on Chapter 5. In particular, samples composed of 16 mm pellets, 10 mm pellets and finer grains are prepared by layering proportions of 60%, 10% and 30% of the total mass. The used finer grains are either sandy material and/or crushed pellets, both presenting a wide range of grain sizes in order to achieve the desired high dry density for the mixture. The chapter is developed in the following main parts:

- 7.1 Introduction
- 7.2 Tested materials and infiltrated fluids used in the experiments
- 7.3 Experimental method and set-up
- 7.4 Experimental results
- 7.5 Discussion

## 7.1 Introduction

The hydro-mechanical behaviour of a pelletized assembly composed of COx/MX80 mixture is studied on constant volume conditions. The swelling pressure of the pelletized backfill is investigated upon its emplacement conditions, where the material is implemented without the application of mechanical compaction. In this concept, pelletized mixtures composed of different materials are tested to assess the swelling capacity and hydraulic performance.

On Chapter 5, the experimental study on the pelletized mixture's density optimisation marked the dry density of  $1.60 \text{ Mg/m}^3$  as the optimum achieved value. The specific conditions could be obtained by mixing pellets of 16 mm, 10 mm and a well-graded finer component ( $d \leq 2\text{mm}$ ), in proportions of 60%, 10% and 30% (section 5.3.2.2). For this purpose, a well-graded sand was used. Another granular material was also proposed, which was produced from crushed pellet with similar well-graded granulometry. This idea could subsequently allow the possibility of moving towards mixture spindles based on a single diameter of pellets (e.g. a mixture based on intact 16mm pellets and crushed 16mm with an optimal spindle) for cost optimization (without sand addition). Pellet crushing can be advantageous in permeability terms, in comparison to clear sand. Regarding the material's composition, Chapter 6 proposed the use of bentonite content ranging between 30% and 40%, in order to obtain adequate swelling capacity. The use of different finer grains imposed a variation on mixtures total composition (i.e. clayey and sand content).

In this chapter, different pelletized mixtures containing COx/MX80 pellets (clayey medium) and finer grains are studied upon hydration using site water. The tested mixtures are presented in details on section 7.2. The investigation is conducted by varying the type of finer component, contained by the mixture. In particular, sand, crushed pellets and mixtures of them are tested, creating clay/sand mixtures in proportions of 70%/30% to 100%/0% respectively. On section 7.3, the adopted experimental methods and protocols are presented. The experiments on the pelletized material were performed in the French Alternative Energies and Atomic Energy Commission (CEA) for the account of Andra, where oedometric size cells were adapted (in respect with the pellet diameter). The results of swelling pressure and hydraulic conductivity are presented on section 7.4 and further analysed on section 7.5, focusing on the hydro-mechanical response of the finer material. The main outcomes of the hydro-mechanical behaviour are outlined on the conclusion part (section 7.6).

## 7.2 Tested materials and infiltrated fluids used in the experiments

The hydro-mechanical response of different pelletized mixtures was investigated. The tested trimodal granular mixtures were composed of pellets presenting diameter of 16 mm and 10 mm,

as well as finer product with grain sizes  $d \leq 2$  mm. The GSD was selected after the experimental study for density maximisation (section 5.3.2).

The used materials and their granulometry are illustrated on Figure 7-1. Fabricated pellets composed of CO<sub>x</sub>/MX80 mixtures in fractions of 60/40 and 70/30 (in total mass) are tested. Details regarding their composition, water content and measured intra-pellet dry density are presented on Table 7-1. As finer grains with  $d \leq 2$  mm, the well-graded sand (WGS) used in the framework of previous studies is investigated. An alternative product for the finer grain component was fabricated. Pellets of 16 mm diameter were crushed and the resulting granulometry was produced to follow similar GSD with that of the well-graded sand. Table 7-2 illustrates the granulometric characteristics and the water content of the used sand and crushed pellets (CP). It can be seen that both material present similar curvature coefficient,  $CC$ . Crushed pellets exhibit slightly well graded granulometry than the sand, as the uniformity coefficient  $CU$  implies ( $CU \geq 6$  and  $1 \leq CC \leq 3$ ).

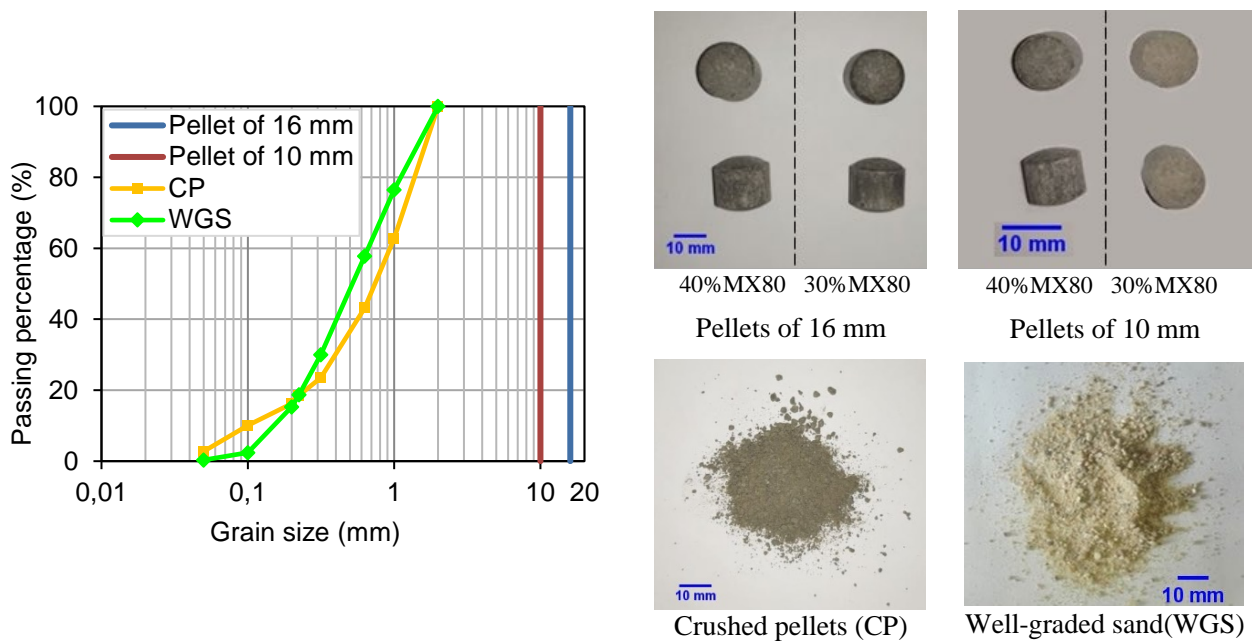


Figure 7-1 Grain size distribution and presentation of the materials used on the hydro-mechanical study of pelletized materials.

Table 7-1 Composition and physical parameters of the tested pelletized materials.

| Pellet diameter,<br>$d_i$ (mm) | Contained materials           | Water content,<br>$w$ (%) | Intra-pellet dry density,<br>$\rho_{d \text{ pellet}}$ (Mg/m <sup>3</sup> ) |
|--------------------------------|-------------------------------|---------------------------|---|
| 16                             | CO <sub>x</sub> /MX80 (60/40) | 9.4                       | 2.02  |
|                                | CO <sub>x</sub> /MX80 (70/30) | 8.6                       | 1.99  |
| 10                             | CO <sub>x</sub> /MX80 (60/40) | 7.3                       | 2.07  |
|                                | CO <sub>x</sub> /MX80 (70/30) | 6.9                       | 1.97  |

Table 7-2 Water content and granulometric parameters of the tested finer grains.

|                        | Water content,<br>$w$ (%) | $d_{max}$<br>(mm) | $d_{10}$<br>(mm) | $d_{60}$<br>(mm) | $CU$ | $CC$ |
|------------------------|---------------------------|-------------------|------------------|------------------|------|------|
| Well-graded sand (WGS) | 0.3                       | 2.0               | 0.12             | 0.61             | 5.1  | 1.2  |
| Crushed pellets (CP)*  | 7.2                       |                   | 0.10             | 0.90             | 9.0  | 1.8  |

\* from pellets of 30%MX80

The investigated pelletized mixtures are formed the optimal mixtures and the layering solution; by pellets of 16 mm and 10 mm and finer grains (sand and/or crushed pellets), in proportions of 60%, 10% and 30% (in total mass) respectively. As it was already highlighted, the presence of the finer grains with proportion of 30% is necessary to achieve a resulting packing dry density of  $1.60 \text{ Mg/m}^3$ . In this context, three mixtures were selected to be investigated. In particular:

- (a) **Mixture 1:** 16 mm -10 mm- sand in proportions of 60-10-30%,
- (b) **Mixture 2:** 16 mm -10 mm-crushed pellets in proportions 60-10-30%,
- (c) **Mixture 3:** 16 mm -10 mm- crushed pellets- sand in proportions 60-10-15-15%.

Mixture 1 contains 70% pellets and 30% sand (WGS), whereas mixture 2 contains 70% pellets and 30% crushed pellets (CP). On Mixture 3, the finer grains were composed of both crushed pellets and sand of equal fractions, corresponding to a proportion of 30% of mixture's total mass. For each mixture, the bentonite content inside the pellets was selected in a way to respect a total bentonite mass proportion of 30%. More specific details regarding the components and their composition are presented on Table 7-3. It can be seen that MX80 bentonite content is almost constant, slightly ranging between 28% and 31.5% of the total mass. COx argillite percentage varies more from 42% and 70%. On the other hand, the sand content ranges between 0 to 30%.

In general, the used materials can be classified in two main categories concerning the mineralogical characteristic:

- Clayey content, which refers to the COx/MX80 mixtures, and
- Sand content.

The hydration of the studied specimens was carried out by using solutions according to the design conditions (i.e. URL's groundwater). Therefore, site water (SW) was infiltrated into the materials. Table 7-4 presents the receipt used for the preparation of the synthetic solution according to Andra's indications, whereas Table 7-5 illustrates its ionic concentration and properties.

Table 7-3 Details of investigated pelletized mixtures.

|           | Diameters          | Form   | Proportion of component (%) | Composition               | Total proportion of materials (%)   |
|-----------|--------------------|--------|-----------------------------|---------------------------|-------------------------------------|
| Mixture 1 | 16 mm              | Pellet | 60                          | 60CO <sub>x</sub> /40MX80 | 42CO <sub>x</sub> /28MX80/30WGS     |
|           | 10 mm              | Pellet | 10                          | 60CO <sub>x</sub> /40MX80 |                                     |
|           | WGS, $d \leq 2$ mm | Powder | 30                          | sand                      |                                     |
| Mixture 2 | 16 mm              | Pellet | 60                          | 70CO <sub>x</sub> /30MX80 | 70CO <sub>x</sub> /30MX80           |
|           | 10 mm              | Pellet | 10                          | 70CO <sub>x</sub> /30MX80 |                                     |
|           | CP, $d \leq 2$ mm  | Powder | 30                          | 70CO <sub>x</sub> /30MX80 |                                     |
| Mixture 3 | 16 mm              | Pellet | 60                          | 60CO <sub>x</sub> /40MX80 | 53.5CO <sub>x</sub> /31.5MX80/15WGS |
|           | 10 mm              | Pellet | 10                          | 70CO <sub>x</sub> /30MX80 |                                     |
|           | CP, $d \leq 2$ mm  | Powder | 15                          | 70CO <sub>x</sub> /30MX80 |                                     |
|           | WGS, $d \leq 2$ mm | Powder | 15                          | sand                      |                                     |

WGS: well-graded sand, CP: crushed pellets

Table 7-4 Receipt for the preparation of synthetic waters.

| Component (g/L) | NaCl  | KCl   | NaHCO <sub>3</sub> | CaSO <sub>4</sub> .2H <sub>2</sub> O | MgSO <sub>4</sub> .7H <sub>2</sub> O | CaCl <sub>2</sub> .2H <sub>2</sub> O | Na <sub>2</sub> SO <sub>4</sub> |
|-----------------|-------|-------|--------------------|--------------------------------------|--------------------------------------|--------------------------------------|---------------------------------|
| SW              | 1.950 | 0.035 | 0.130              | 0.630                                | 1.020                                | 0.080                                | 0.700                           |

SW: Site water

Table 7-5 Ionic concentration and properties of infiltrated site water.

| Component (mmol/L) | Na <sup>+</sup> | Cl <sup>-</sup> | K <sup>+</sup> | HCO <sub>3</sub> <sup>-</sup> | Mg <sup>2+</sup> | SO <sub>4</sub> <sup>2-</sup> | Ca <sup>2+</sup> | <i>I</i> | pH  | <i>EC</i> (μS/cm) |
|--------------------|-----------------|-----------------|----------------|-------------------------------|------------------|-------------------------------|------------------|----------|-----|-------------------|
| SW                 | 44.8            | 34.9            | 0.5            | 1.5                           | 4.1              | 12.7                          | 4.2              | 83       | 7.9 | 547               |

SW: Site water, *I*: Ionic strength, *EC*: Electrical conductivity

### 7.3 Experimental method and set-up

The swelling capacity of the pelletized materials was investigated under constant volume conditions. The developed swelling pressure was measured, using an oedometric cell of large diameter,  $D=120$  mm ( $\sim 7.5 \cdot d_{max}$ ). For the hydro-mechanical testing of pelletized material, the need for suitable cell diameters can be challenging in term of test planning (e.g. number of tests, test duration). The used stainless-steel cell is presented on Figure 7-2. It includes also a light polymer piston and two porous disks to sandwich the prepared soil specimens.

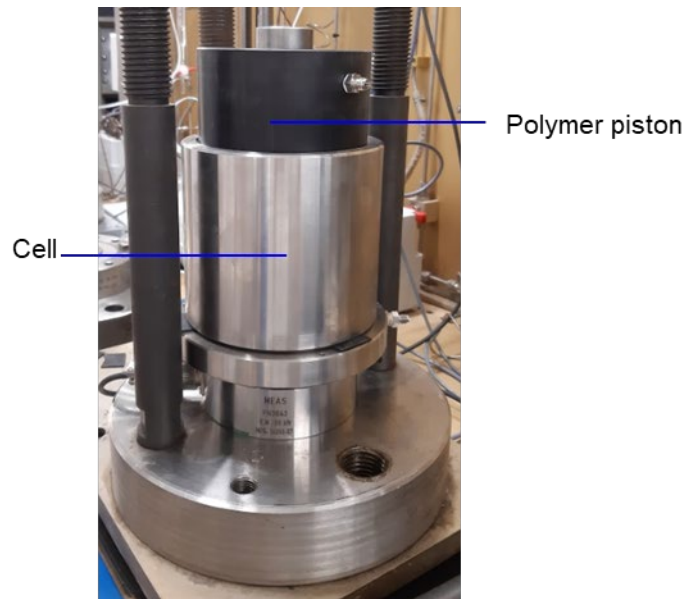


Figure 7-2 CEA cell of 120 mm in internal diameter used for the swelling pressure measurements of the pelletized materials.

### 7.3.1 Samples preparation

The steps followed on samples preparation are illustrated on Figure 7-3. Contrary to powdered mixtures, no compaction stress is applied to the pelletized material upon its preparation. The initial “zero” height,  $h_0$  which included the two porous disks and the piston was measured using a caliper. Once the specimen’s total mass ( $M_{sample}$ ) was deposited inside the cell, the new height was determined ( $h_1$ ). In parallel, an equivalent mixture was prepared for oven drying for 24 hours at 105°C in order to precisely determine the sample’s water content.

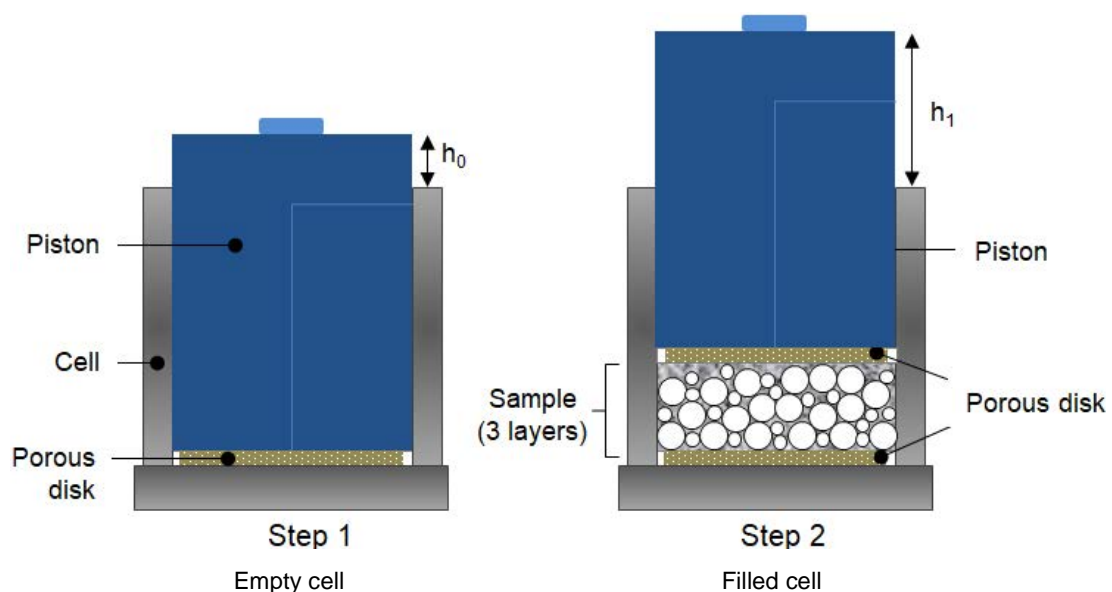


Figure 7-3 Preparation steps followed for the pelletized specimens.

The sample's initial dry density  $\rho_d$  was finally measured as:

$$\rho_d = \frac{M_{sample}}{A_{sample} \cdot H_0 \cdot (1 + w)} \quad (7.1)$$

where  $M_{sample}$  is the sample total mass,

$A_{sample}$  is the cross-sectional area of the specimen,

$w$  is the sample's water content and

$H_0$  is the sample height defined as  $h_1 - h_0$  from Figure 7-3.

Specimens were prepared in layers, based on observations reported on section 5.3.1.1. The grain sizes (pellets, sand or crushed pellets) were implemented at the target proportions by placing the diameters in order of size; pellets of 16 mm were the first placed, while pellets of 10 mm and finer grains were consecutively following. For each layer of GSD, the surface was carefully flattened using a brush, which aimed to improve the rearrangement of finer grains between voids formed by the pellets (i.e. inter-pellet void). In the case where both crushed pellets and sand were used (i.e. Mixture 3), the finer products were premixed together, before their placement. The method presented good repeatability in terms of the resulting dry density of the mixture ( $\approx 1.60 \text{ Mg/m}^3$ ). In the case of sand used as finer material, a slightly higher density could be achieved. Further details are given below.

The proper implementation of the desired GSD was assured by calculating the target quantities, after the 16 mm-sized pellets emplacement. The process was repeated three times in total (i.e. 3 layers), in order to result in a specimen with height  $H \approx 50 \text{ mm}$ . The decision was based on results obtained by Imbert and Villar (2006), regarding the minimum height necessary to avoid misleading scale effects on bentonite pellets samples. Approximately 1 kg of pelletized mixture was used to form each specimen.

The adopted protocol resulted in a minimum dry density,  $\rho_d$  of  $1.60 \text{ Mg/m}^3$ . Table 7-6 summarises the initial details for the tested samples. Two samples for Mixture 1 (pellets mixed with 30% sand) were prepared, presenting different dry densities ( $1.60 - 1.70 \text{ Mg/m}^3$ ). For Mixture 2 and Mixture 3, an initial dry density of around  $1.60 \text{ Mg/m}^3$  could be achieved. In fact, it was observed that when crushed pellets were used as finer grains, the resulting packing dry density was relatively lower than the sand alternative. The remark can be related to the slightly different granulometry that crushed pellets presented (i.e. higher percentage of fines). Additionally, the different mineralogical composition (crushing of clayey pellets) might lead to cohesion development between the crushed pellets, hindering materials compactness

(Vandewalle et al. 2007, Zou et al. 2011). On Figure 7-4, the prepared specimens are presented at an intermediate and at the final step of their preparation. Since the specimen preparation, sand appears to more easily penetrate between the emplaced pellets (Figure 7-4a), compared to the other cases (Figure 7-4b and Figure 7-4c), where pellets are less distinguished.

Table 7-6 Details of the pelletized samples tested on swelling under constant volume conditions.

| Sample Name    | Mixture | Sand content (%) | Initial water content, $w(\%)$ | Initial height $H_0$ (mm) | Initial dry density, $\rho_d$ (Mg/m <sup>3</sup> ) |
|----------------|---------|------------------|--------------------------------|---------------------------|--|
| 70P-30WGS-a    | 1       | 30               | 6.25                           | 49.03                     | 1.71   |
| 70P-30WGS-b    |         | 30               | 6.28                           | 50.52                     | 1.60   |
| 70P-30CP       | 2       | 0                | 8.06                           | 49.23                     | 1.64   |
| 70P-15CP-15WGS | 3       | 15               | 7.18                           | 49.96                     | 1.61   |

P: pellets, WGS: sand, CP: crushed pellets

### 7.3.2 Constant volume cell

The evolution of swelling pressure was determined using a constant-volume system developed by CEA (Figure 7-5). The cell containing the pelletized sample is placed on the base of a rigid metallic frame. A piston equipped with a load cell is placed on the upper part of the sample, in contact with the cell piston. Its position is fixed, blocking the sample's axial deformation and constant volume conditions are ensured. The developed swelling pressure is measured in the axial direction through the installed load cell. An LVDT is in contact with the cell piston to record potential axial displacements.

Site water (SW) was used to infiltrate the specimen from the cell's bottom part. A graduated burette was connected to apply hydraulic charge  $\Delta h$  of 40 cm, corresponding to injection pressure of 4 kPa (hydraulic gradient  $i \approx 8$ ). The test was considered terminated when the developed swelling pressure was approximately stabilised. In average, the samples hydration had duration of 30 days. The recorded axial deformation of the studied samples was ranging between 0.2% and 0.8%.



(a)



(b)



(c)

Figure 7-4 Photographs of the studied pelletized samples during preparation (left) and at the final preparation step (right): (a) Mixture 1 (70P-30WGS), (b) Mixture 2 (70P-30CP) and (c) Mixture 3 (70P-15CP-15WGS).

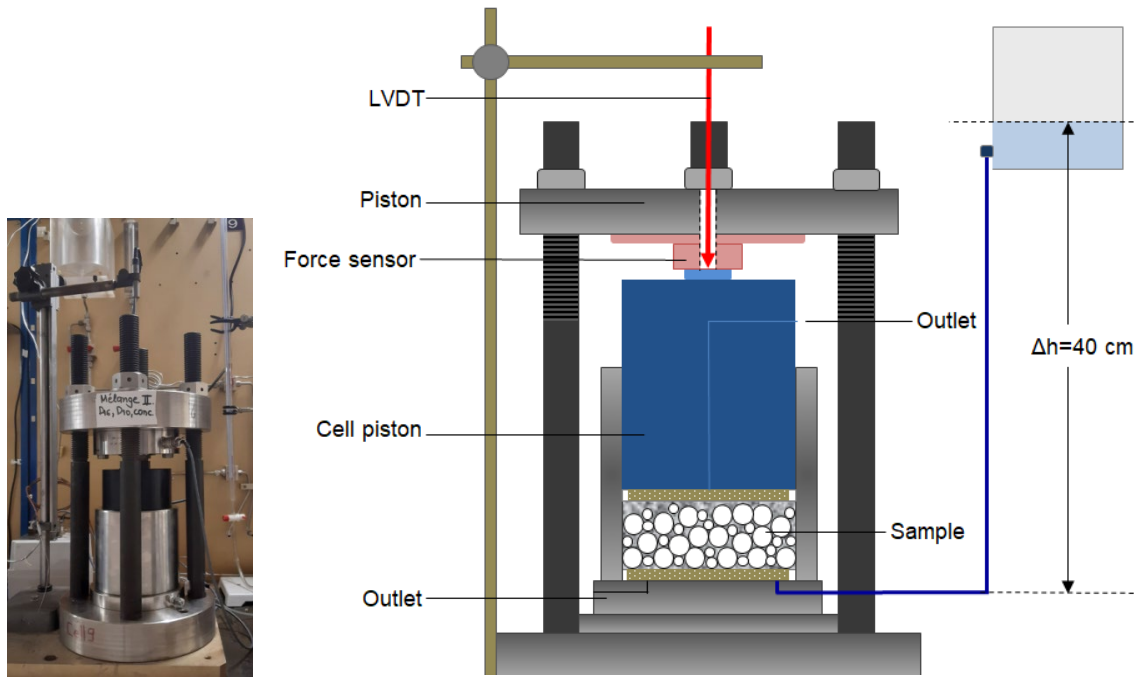


Figure 7-5 Experimental set-up used on swelling under constant volume tests on pelletized material.

### 7.3.3 Saturated hydraulic conductivity

After the stabilisation of the developed swelling pressure (i.e. the material is considered saturated), the hydraulic permeability was evaluated. Site water continued to infiltrate the sample under constant pressure and the flow rate was measured. Higher injection pressure than swelling pressure tests was imposed (7 and 100 kPa). In particular, the hydraulic charge of  $\Delta h = 40$  cm during the swelling pressure tests was increased during the hydraulic conductivity tests. On Mixture 1, with the highest sand content (30%), an injection pressure of 7 kPa (i.e. corresponding at hydraulic charge  $\Delta h$  of 70 cm) was adequate to infiltrate the specimen. On the rest of the pelletized samples, a pressure/volume controller was connected, injecting water with 100 kPa (i.e. corresponding hydraulic charge  $\Delta h$  of 10 m). In both cases, the injected volume was recorded and the flow rate was determined. The saturated hydraulic conductivity was computed assuming laminar flow, by applying the Darcy's law for incompressible fluids as:

$$K = \frac{Q \cdot H_0}{A_{sample} \cdot \Delta h} \quad (7.2)$$

where  $Q$  represents the average obtained flow rate ( $\text{m}^3/\text{s}$ ),

$A_{sample}$  is the cross-sectional area of the specimen ( $\text{m}^2$ ),

$H_0$  is the specimen's height (m) and

$\Delta h$  corresponds to the imposed hydraulic charge (m).

In addition, the exhibited intrinsic permeability of the pelletized medium was calculated as follows:

$$k = K \frac{\mu_{fluid}}{\rho_{fluid} \cdot g} \quad (7.3)$$

where  $\mu_{fluid}$  the dynamic viscosity of the water (Pa.s),

$\rho_{fluid}$  is the density of water (kg/m<sup>3</sup>) and

$g$  corresponds to the gravity (9.81 m/s<sup>2</sup>)

The tests were performed at constant laboratory temperature of 23 ± 1 °C.

## 7.4 Experimental results

### 7.4.1 Swelling pressure

The swelling pressure developed by the studied pelletized samples ( $D=120$  mm,  $H \approx 50$  mm), was evaluated at constant volume conditions, where no mechanical compaction was applied. The results for Mixture 1, Mixture 2 and Mixture 3 are presented below.

The experimental data of the pelletized mixtures containing 70% pellets (60% pellets of 16 mm containing 40%MX80 and 10% pellets of 10 mm containing 40%MX80) and 30% sand, prepared on different dry densities (Table 7-6) are given on Figure 7-6. A quick development of the swelling pressure is observed. It is clear that swelling pressure is almost stabilised during the first 24 h of hydration (Figure 7-6a). This kinetic suggest that site water infiltrates the sample very quickly, due to sand's presence (i.e. a rather permeable material) and leads to a relatively instant pellet hydration and swelling activation. Furthermore, the well-known dependency of compacted powders on the initial dry density is also observed for the investigated pelletized samples. An increase of dry density from  $\rho_d = 1.60$  Mg/m<sup>3</sup> to  $\rho_d = 1.70$  Mg/m<sup>3</sup> raised swelling pressure by 35%. Additionally, during the constant volume test, it was noticed that the injected water infiltrated the specimen's height very quickly for the sample with lower dry density  $\rho_d = 1.60$  Mg/m<sup>3</sup> (70P-30WGS-b), implying significant macroporosity and high hydraulic conductivity. Nevertheless, the final swelling pressures are considerably high for both samples (0.9 and 1.2 MPa), even if bentonite content is the lowest of the mixtures (28%MX80). These parameters and especially the effect of sand in the mixture are discussed on section 7.5.

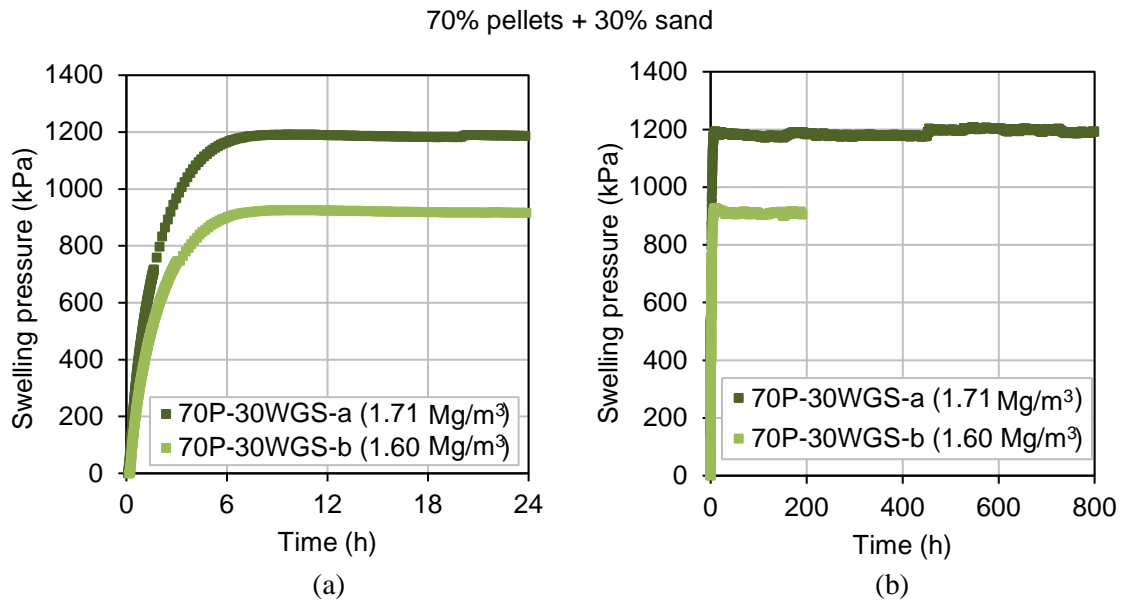


Figure 7-6 Evolution of swelling pressure over time for Mixture 1 (16 mm, 10 mm and sand) prepared at initial dry density of  $\rho_d = 1.60 \text{ Mg/m}^3$  and  $\rho_d = 1.70 \text{ Mg/m}^3$ : (a) during the first 24 h of hydration and (b) until the end of the test.

Figure 7-7 illustrates the results of 70% pellets (60% pellets of 16 mm containing 30%MX80 and 10% pellets of 10 mm containing 30%MX80) and 30% of crushed pellets (containing 30%MX80). A less rapid increase of swelling pressure with time compared to mixtures containing 30% of sand is observed in the beginning of hydration. Swelling pressure leads to a more stable evolution after approximately 10 days of hydration. This observation implies lowered initial macrovoids, which is related with the “non-inert role” of crushed pellets. For a hydration of 30 days, the developed swelling pressure is lower ( $\sim 0.35 \text{ MPa}$ ) than the pelletized specimen 70P-30WGS-b (i.e. 30% sand,  $\rho_d = 1.60 \text{ Mg/m}^3$ ), having similar initial dry density. A light evolution of the swelling pressure is observed even after 30 days, which nonetheless is still slow.

On Figure 7-8, the developed swelling pressure obtained by the mixture of 70% pellets (60% pellets of 16 mm containing 40%MX80 and 10% pellets of 10 mm containing 30%MX80), 15% of crushed pellets (containing 30%MX80) and 15% of sand is given. Mixture 3 was proposed as “intermediate” state between the two previous samples (i.e. the finer grains are composed of sand and crushed pellets). In this context, the developed kinetic shows a rapid increase of swelling pressure in the beginning of hydration, due to the rather permeable sand that allows water to quickly hydrate the sample. Nonetheless, the crushed pellets in the inter-pellet void hinder the water infiltration (i.e. lower permeability as clayey material) and therefore the swelling pressure gradually reduces. A slight peak, which was previously presented by the powdered mixtures, is observed on pelletized material before stabilisation, which might occur due to materials rearrangement. However, the latter needs further investigation. Swelling

pressure is stabilised after approximately 20 days of water infiltration, where a swelling stress of 0.48 MPa was obtained.

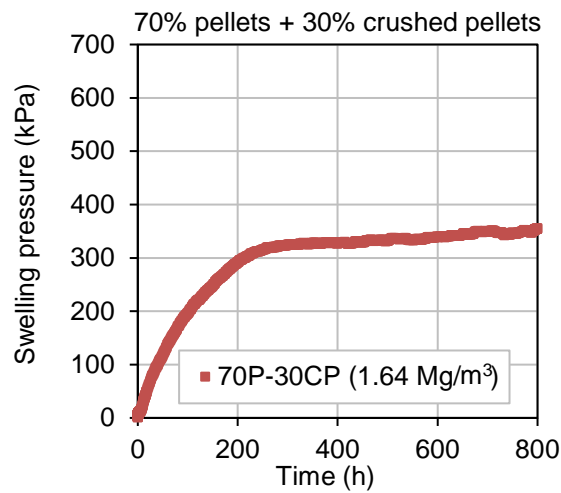


Figure 7-7 Evolution of swelling pressure over time for Mixture 2 (16 mm, 10 mm and crushed pellets) prepared at initial dry density of  $\rho_d = 1.64 \text{ Mg/m}^3$ .

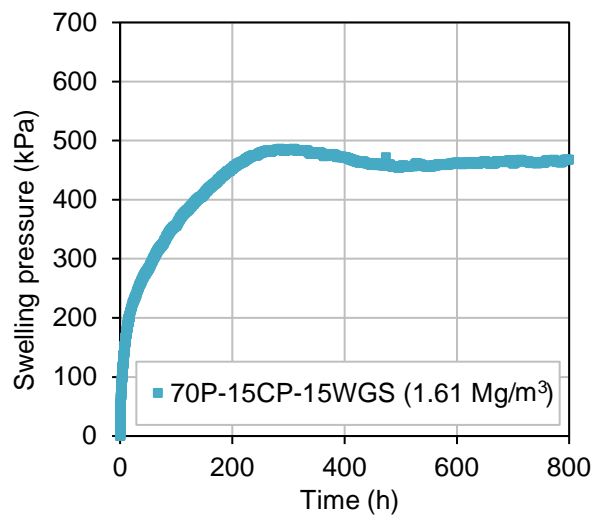


Figure 7-8 Evolution of swelling pressure over time for Mixture 3 (16 mm, 10 mm and sand/crushed pellets) prepared at initial dry density of  $\rho_d = 1.61 \text{ Mg/m}^3$ .

Figure 7-9 summarizes the swelling pressure developed by all tested samples hydrated for 30 days. The figure shows the composition and initial dry density of the tested mixtures. A clear effect of sand's presence is visible. When sand is not contained in the mixture, a slight variation of swelling pressure is observed. The final results are summarized on Table 7-7.

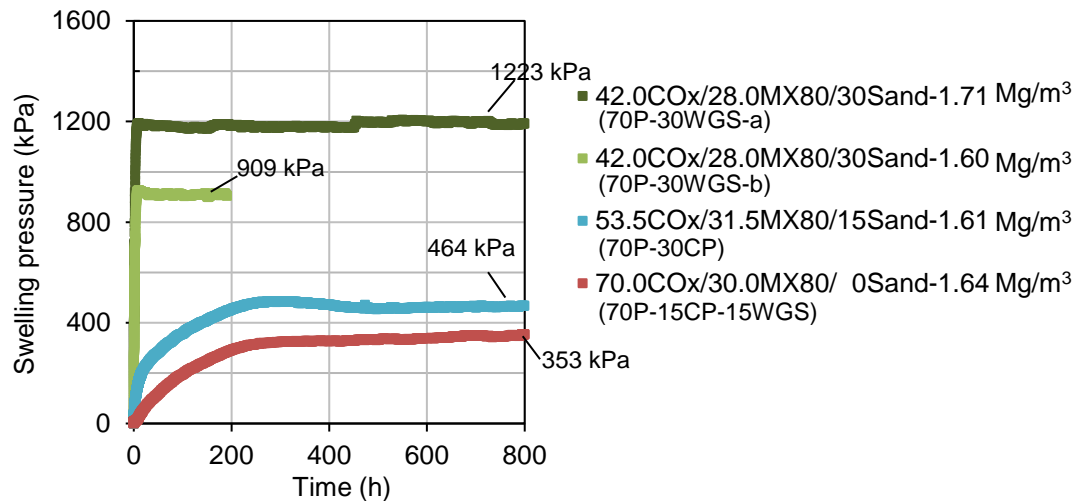


Figure 7-9 Evolution of swelling pressure for all investigated pelletized mixtures, focusing on the materials composition.

Table 7-7 Results of swelling pressure tests on pelletized samples hydrated under constant volume conditions (hydration of ~ 30 days).

| Sample Name    | Mixture | Clayey content (%) | Sand content (%) | Initial dry density, $\rho_d$ (Mg/m <sup>3</sup> ) | Final swelling pressure (kPa) |
|----------------|---------|--------------------|------------------|--|-------------------------------|
| 70P-30WGS-a    | 1       | 70                 | 30               | 1.71   | 1223.4                        |
| 70P-30WGS-b    |         |                    |                  | 1.60   | 909.4                         |
| 70P-30CP       | 2       | 100                | 0                | 1.64   | 352.9                         |
| 70P-15CP-15WGS | 3       | 85                 | 15               | 1.61   | 463.8                         |

P: pellets, WGS: well-graded sand, CP: crushed pellets

#### 7.4.2 Hydraulic conductivity

Following the stabilization of swelling pressure at approximately 30 days of hydration (i.e. 800 h), permeability tests were conducted on mixture 1 prepared at initial dry density of 1.71 Mg/m<sup>3</sup> (70P-30WGS-a), mixture 2 and mixture 3. It is reminded that during permeability measurement, mixture 1 was hydrated under lower injecting pressure (7 kPa), whereas on mixture 2 and 3 the injection pressure was increased to achieve a more rapid infiltration of the specimen (100 kPa). The flow rate under constant injection pressure was measured in terms of injected volume over time. The results are presented on Figure 7-10, Figure 7-11, Figure 7-12, for each studied mixture.

A steady flow rate is in average observed for all tested pelletized assemblies, showing that the samples were saturated. The pelletized sample composed of 30% sand (Figure 7-10) exhibited a perfectly linear relation flow rate since the beginning of the test. Mixture 2 presented a non-

linear relation of volume with time for a short period of injection time (Figure 7-11a), suggesting that the specimen was not yet fully saturated at the end of swelling pressure test. However it does not significantly affect the obtained result of swelling pressure. A slightly similar behaviour is observed on mixture 3, which is less prominent (Figure 7-12). As expected, the injected volume is clearly higher on mixture 1 (i.e. 30% of sand content) for a shorter amount of injection time (Figure 7-10).

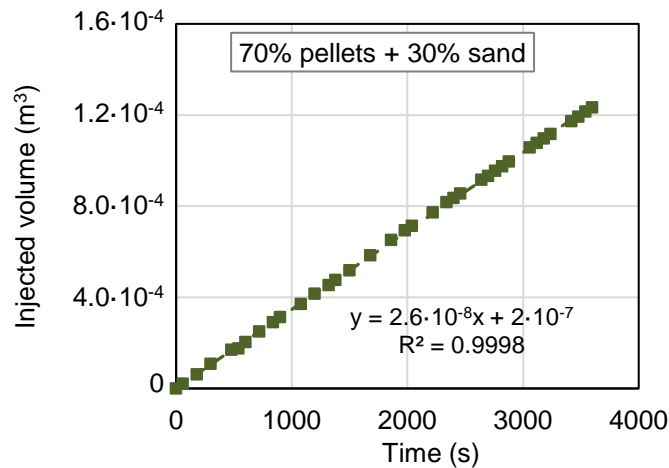


Figure 7-10 Evolution of injected water volume over time for Mixture 1 (16 mm, 10 mm and sand) prepared at initial dry density of  $\rho_d = 1.71 \text{ Mg/m}^3$ .

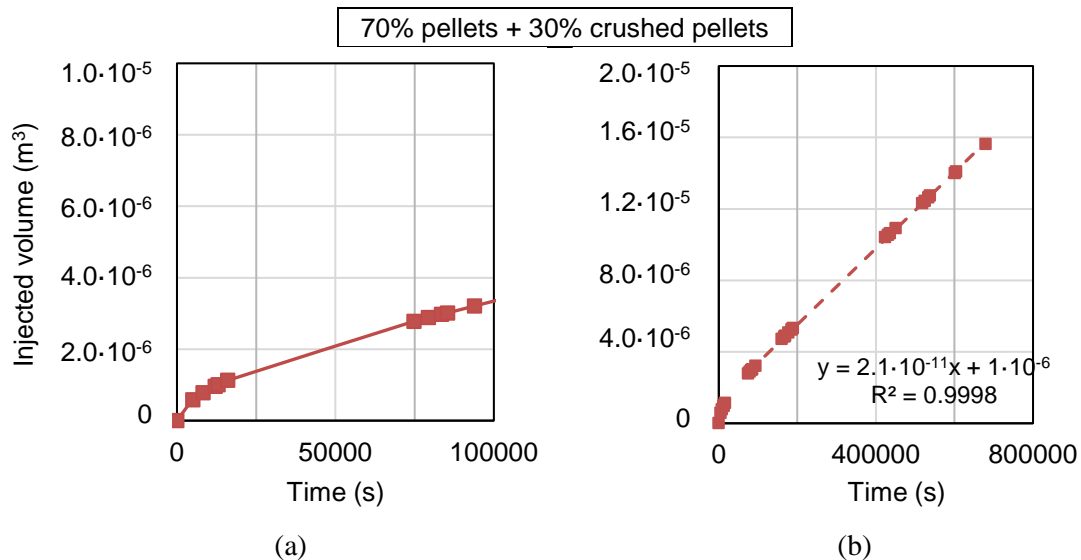


Figure 7-11 Evolution of injected water volume over time for Mixture 2 (16 mm, 10 mm and crushed pellets) prepared at initial dry density of  $\rho_d = 1.64 \text{ Mg/m}^3$ : (a) during 24 h of injection and (b) until the end of the test.

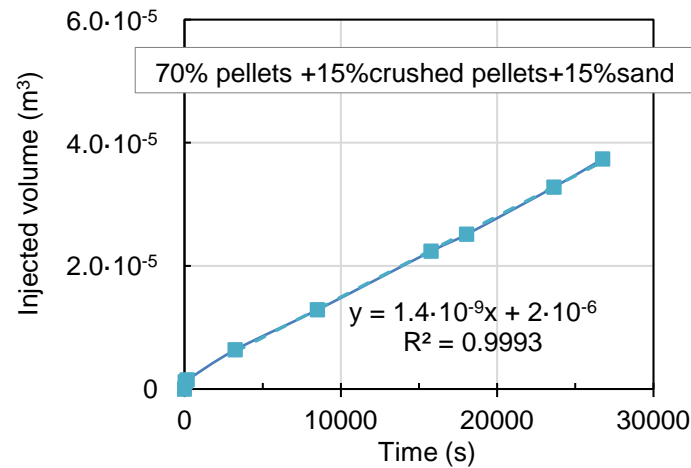


Figure 7-12 Evolution of injected water volume over time for Mixture 3 (16 mm, 10 mm and sand/crushed pellets) prepared at initial dry density of  $\rho_d = 1.61 \text{ Mg/m}^3$ .

The experimental values of saturated hydraulic conductivity and intrinsic permeability, obtained on this study for the different specimens are summarised on Table 7-8 together with details concerning the resulting dry density of the pelletized mixtures.

Table 7-8 Results of hydraulic conductivity tests on pelletized samples under constant volume conditions.

| Sample Name     | Mixture | Sand content (%) | Initial dry density, $\rho_d$ (Mg/m <sup>3</sup> ) | Average flow rate, $Q$ (m <sup>3</sup> /s) | Hydraulic conductivity, $K$ (m/s) | Intrinsic permeability, $k$ (m <sup>2</sup> ) |
|-----------------|---------|------------------|--|--|-----------------------------------|---|
| 70P-30WGS-a     | 1       | 30               | 1.71   | $2.59 \cdot 10^{-8}$                       | $1.65 \cdot 10^{-7}$              | $1.51 \cdot 10^{-12}$                         |
| 70P-30CP        | 2       | 0                | 1.64   | $2.13 \cdot 10^{-11}$                      | $9.27 \cdot 10^{-12}$             | $8.50 \cdot 10^{-17}$                         |
| 70P-15CP-15sand | 3       | 15               | 1.61   | $1.38 \cdot 10^{-9}$                       | $6.11 \cdot 10^{-10}$             | $5.60 \cdot 10^{-15}$                         |

P: pellets, WGS: well-graded sand, CP: crushed pellets

## 7.5 Discussion

### 7.5.1 Effect of finer grains type on hydro-mechanical behaviour

As it has been already clarified, the studied mixtures were prepared according to the optimum granulometry (16 mm, 10 mm, finer grains in proportions of 60%, 10%, 30%) that capable of maximising the resulting packing density. In that context, different types of finer grains were used (sand and/or crushed pellets) that consequently influenced the materials composition. The resulting material mixtures were governed by the two components of clayey and sand content.

The experimental study on the hydro-mechanical behaviour of pelletized material showed a clear effect of the finer grains composition (sand, crushed pellets). The obtained final swelling pressure values and the saturated hydraulic conductivity are discussed, as function of the implemented sand content. The corresponding percentage of the clayey materials (COx/MX80 mixtures) is also highlighted.

Figure 7-13 illustrates the results of the pelletized samples that presented a common dry density of  $\rho_d \approx 1.62 (\pm 0.02 \text{ Mg/m}^3)$  (i.e. 70P-30WGS-b, 70P-30CP and 70P-15CP-15sand). It can be seen that although sand is an inert material that does not provoke any swelling, it clearly increases the swelling pressure. These data in fact show that the sand selected as the pelletized mixture's finer component, blocks the COx/MX80 pellets (that tend to increase their volume upon hydration) and prevents their swelling. As a result, swelling pressure is developed. More precisely, the sand fills the inter-pellet void, creating an almost incompressible layer between the swelling pellets. The effect can be better visualised on Figure 7-14, where the specimen is presented as obtained at the end of swelling pressure test. COx/MX80 pellets have swollen filling all the available space, whereas sand has remained intact. The non-homogeneous distribution of the materials is visible also on the saturated state.

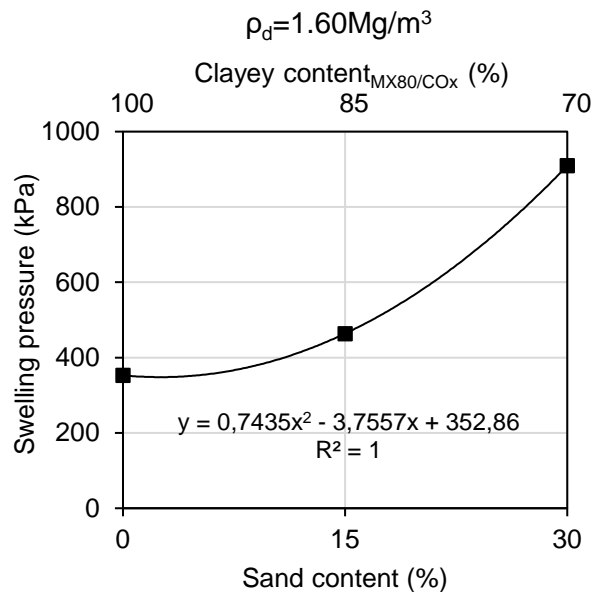


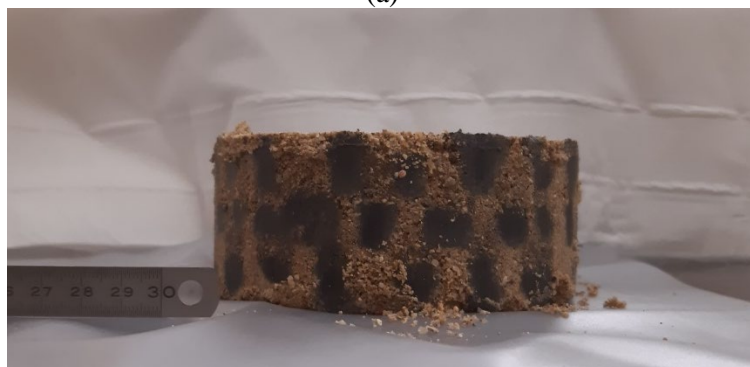
Figure 7-13 Variation of final swelling pressure with sand and clayey percentage contained in the pelletized mixture (mixture's initial dry density  $\rho_d \approx 1.60 \text{ Mg/m}^3$ ).

Contrary to sand, crushed pellets behave in a different manner upon their hydration. In particular, pellet crushing indicates that an amount of the fabricated material exhibits overconsolidated state (i.e. grains that resulted from breakage of highly-compacted material like pellets). However, fines in the form of powder, which are not consolidated, can also result. The present crushed pellets were produced to approximately follow a well-graded granulometry with

$d_{max} = 2$  mm (Figure 7-1). This fact implies that the amount of over-consolidated grains might be reduced. As a reminder, previous experimental studies showed that normally consolidated material presented collapse, while overconsolidated samples presented clear swelling (Figure 2-19). Therefore, the mixtures containing crushed pellets as finer grains introduce two phenomena upon water infiltration: the overconsolidated pellets present swelling and increase their volume (e.g. reducing their density), whereas crushed pellets tend to collapse (or merely do not exhibit swelling) and are free to be compressed by pellet swelling. This state creates less “fixed” volume conditions than when 30% of sand is contained and lower swelling pressure is developed upon hydration. The effect of collapse/compression is expected to be less significant when sand and crushed pellets are used, since sand always behaves as inert material.



(a)



(b)

Figure 7-14 Specimens of Mixture 1 (16 mm, 10 mm and sand) prepared at initial dry density of  $\rho_d = 1.60$  Mg/m<sup>3</sup> (70P-30WGS-b) at the end of swelling pressure test (D=120 mm/H=50 mm).

On Figure 7-15, the “intermediate” sample of Mixture 3, containing crushed pellets and sand as finer grains, is illustrated at the end of the test. A significantly more homogenised state compared to Figure 7-14 is observed, since lower sand content (15%) is mixed with crushed pellets (15%). The sample has been swollen during hydration and no macrovoids exist. The

imprint of the hydrated pellets is slightly visible at the end of the tests, due to different composition of pellets and the finer material. Sand grains can also be located.



Figure 7-15 Specimens of Mixture 3 (16 mm, 10 mm, crushed pellets and sand) prepared at initial dry density of  $\rho_d = 1.60 \text{ Mg/m}^3$  (70P-15CP-15WGS) at the end of swelling pressure and permeability test ( $D=120 \text{ mm}/H=50 \text{ mm}$ ).

Figure 7-16 presents the specimen of Mixture 2, containing pellets and crushed pellets. On that case as well, no voids are identified, demonstrating the materials swelling. A light pellet imprint is visible also in this mixture, exhibiting however a significantly more homogenized appearance, since only COx/MX80 (70/30) is contained.

The obtained hydraulic conductivity at saturation is illustrated also on Figure 7-17 as function of the implemented sand content. The mixture containing 30% of sand (sample 70P-30WGS-a) presented slightly higher initial dry density ( $\rho_d = 1.71 \text{ Mg/m}^3$ ) than the other samples ( $\rho_d = 1.62 \pm 0.02 \text{ Mg/m}^3$ ). Nonetheless, the experimental result is illustrated on the figure to better demonstrate the impact of sand on hydraulic conductivity. It is expected that for 30% of sand combined with a lower initial dry density ( $\sim 1.60 \text{ Mg/m}^3$ ) higher permeability would be obtained. An inverse behaviour is reported on the material's permeability in comparison to the developed swelling pressure. As expected, hydraulic conductivity clearly increases as sand

presence becomes more significant in the mixture. The effect is significant especially after 15% of imported sand content, where permeability is mainly governed by the sand that creates a preferential path for the water infiltration. On the other hand, an expected effect of clayey material content (COx/MX80) is observed: the higher the clay content, the lower the hydraulic conductivity. Permeability is not affected by the possible collapse of crushed pellets upon hydration ( $6 \cdot 10^{-10}$  m/s for 85% of COx/MX80,  $9.3 \cdot 10^{-12}$  m/s for pure COx/MX80).

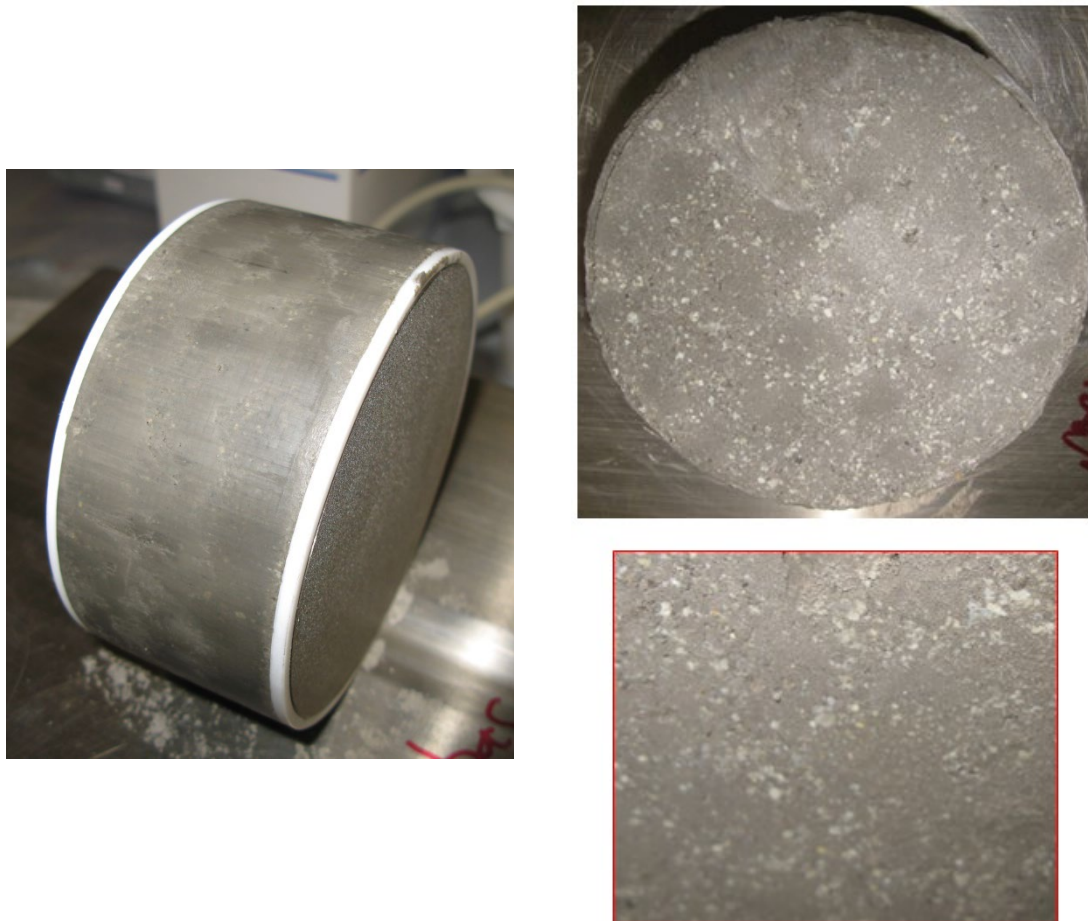


Figure 7-16 Specimens of Mixture 2 (16 mm, 10 mm, crushed pellets) prepared at initial dry density of  $\rho_d = 1.60$  Mg/m<sup>3</sup> (70P-30CP) at the end of swelling pressure and permeability test (D=120 mm/H=50 mm).

For the conducted testing period, sand addition appeared beneficial for swelling pressure development, but unfavourable for the materials self-sealing properties (i.e. low hydraulic conductivity). Figure 7-18 additionally shows the effect of sand presence on both parameters. An optimisation of sand content incorporated in the pelletized mixture could be further addressed in the future to fulfil the design requirements of a pelletized backfill.

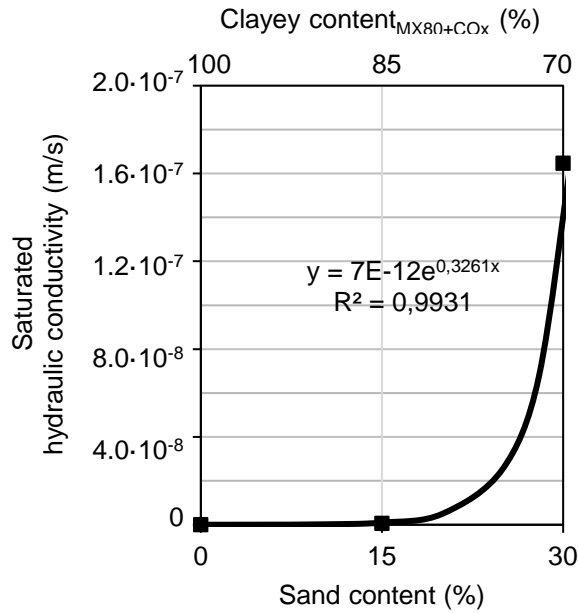


Figure 7-17 Variation of saturated hydraulic conductivity with sand and clayey percentage contained in the pelletized mixture.

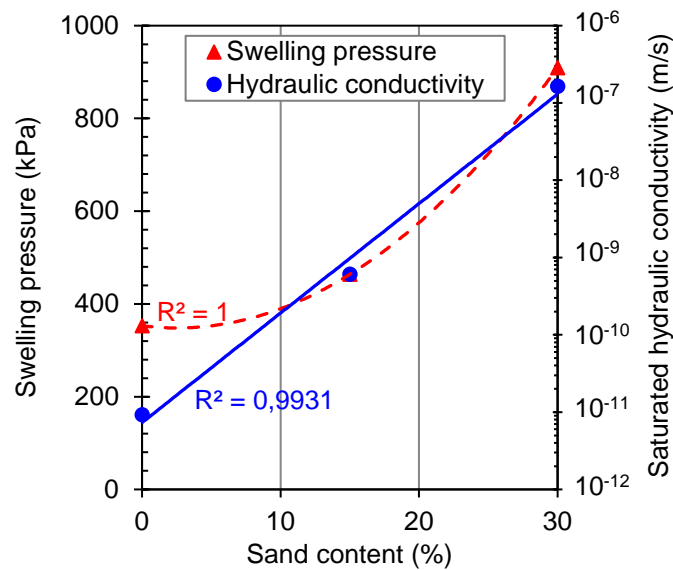


Figure 7-18 Swelling pressure and hydraulic conductivity developed by the investigated pelletized mixtures in relation to the sand content.

### 7.5.2 Clayey mixtures: pelletized material versus compacted powders

It was seen that the type of the implemented finer grain component has an important role on the hydro-mechanical response. Mixture 2 contained pellets and crushed pellets, which were both, composed of 70% COx argillite and 30% MX80 bentonite, pure clayey materials. In that

homogeneous condition, a comparison is conducted between CO<sub>x</sub>/MX80 pelletized material and CO<sub>x</sub>/MX80 compacted powders for similar initial dry densities.

Therefore, Figure 7-19 correlated the results of final swelling pressure for the pelletized and powdered mixture with the initial dry density. The results of CO<sub>x</sub>/MX80 compacted powders correspond to those presented on paragraph 6.4.3 for  $\rho_d=1.45 \text{ Mg/m}^3$  and  $1.60 \text{ Mg/m}^3$ , as well as to a supplementary test on higher density values ( $\rho_d \approx 1.70 \text{ Mg/m}^3$ ), which was carried out for the need of the present comparison. The exponential relation proposed for the specific results of powdered mixtures is also illustrated. No significant variation between pelletized and powdered CO<sub>x</sub>/MX80 mixtures is observed for similar density state. It is in agreement with previous studies on powdered material and pelletized material, both compacted at the same dry densities (Imbert and Villar 2006, Hoffmann et al. 2007, Karnland et al. 2008). Although here no compaction was applied on preparation of the pelletized material, a good correlation is obtained.

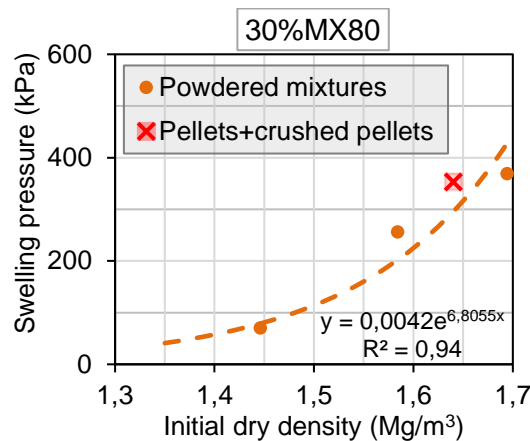


Figure 7-19 Final swelling pressure for CO<sub>x</sub>/MX80 powdered mixtures and pelletized sample composed of 30%MX80 (pellets and crushed pellets).

### 7.5.3 Pellets/Sand mixture: equivalent dry density of pellets

The effect of sand's presence on the pelletized sample was previously characterised as an inert inter-pellet layer that blocks the CO<sub>x</sub>/MX80 pellets (i.e. swelling material) (Mixture 1). In order to better evaluate the remark and assess the role of the sand as component of the pelletized mixture, an equivalent dry density is used to determine the resulting density of the "pure" pelletized material (i.e. clayey mixture). It is an attempt to simulate the corresponding density conditions at a compacted powder material and evaluate if a comparison with the pelletized mixture containing sand could be carried out as well.

Upon the material's emplacement, the pelletized sample containing pellets of 16 mm, 10 mm and sand, presents a total volume  $V_T$  corresponding to its measured height  $H_0$  (section 7.3.1)

and exhibits the overall dry density of the mixture ( $\rho_d$ ). The sand is considered as inert dry material. It is placed between the used pellets and presents an apparent/bulk density ( $\rho_{sand}$ ). The equivalent dry density of the pellets (*EPDD*) can be determined according to Figure 7-20. This density is defined as the ratio of the dry pelletized mass to the volume of pellets and the voids in the mixture. Similar concept were used by other studies on clay/sand powdered mixtures (Dixon et al. 1985, Lee et al. 2001).

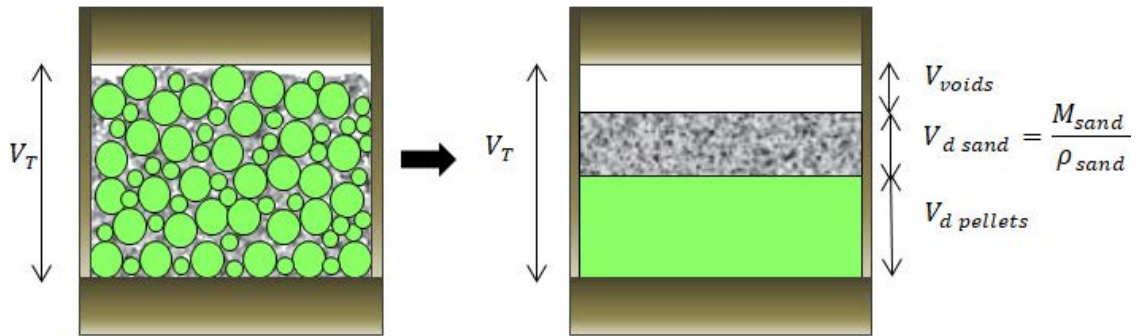


Figure 7-20 Equivalent state of pellet dry density for pelletized mixtures containing sand as finer gains.

The equivalent dry density of the pellets (*EPDD*) inside is calculated as:

$$EPDD = \frac{M_{d\ pellets}}{V_{d\ pellets} + V_{voids}} = \frac{M_{d\ pellets}}{V_T - V_{sand}} \quad (7.4)$$

where  $M_{d\ pellets}$  is the dry mass of the used pelletized material, calculated from the total mass of the 16 mm and 10 mm pellets, taking in account their respective water content as presented on Table 7-1,

$V_T$  is the total volume measured upon specimens preparation and

$V_{sand}$  the volume of sand calculated from the sand's apparent density.

The apparent density of the used dry sand was measured equal to  $\rho_{sand} = 1.50 \text{ Mg/m}^3$ . The measurement was determined by conducting multiple deposits of the dry sand, inside the cylindrical cell with diameter of 120 mm and recording its volume.

The hypothesis considers the sand as “incompressible” material. To reinforce the argument, uniaxial compression tests were performed on the used dry sand and are presented on Figure 7-21. The testing protocol was similar to that present on section 4.2.1.2, in the context of pelletizing process. However, lower stresses were applied (e.g. up to 2 MPa) in order to correspond to the magnitude of the developed swelling pressure. For comparison purposes, the results of COx argillite are also given. As it can be seen two materials behave in a significantly different manner. It can be seen that dry sand exhibits very low compressibility ( $C_C = 0.02$ ).

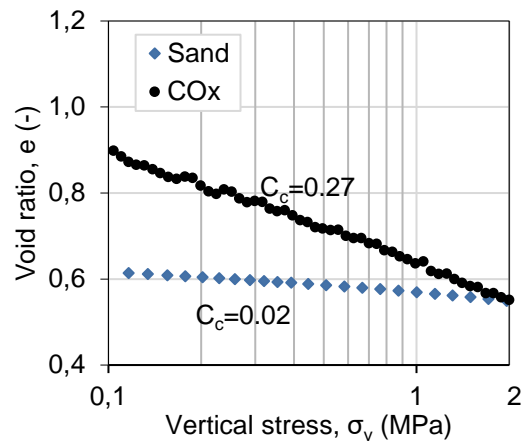


Figure 7-21 Variation of void ratio as function of vertical pressure (in logarithmic scale) for sand and COx argillite.

On this context, swelling pressure tests were conducted on COx/MX80 powdered mixtures compacted at the calculated equivalent dry density of pellets. A comparison between the tested pelletized mixtures containing 30% of sand (Mixture 1: 70P-30WGS-a and 70P-30WGS-b) and the equivalent powdered mixture was conducted. Since pellets of mixture 1 were composed of 60% COx and 40% MX80 (Table 7-3), powdered COx/MX80 mixtures with 40% MX80 were compacted. The corresponding equivalent dry densities  $EPDD$  were calculated as  $1.70 \text{ Mg/m}^3$  and  $1.80 \text{ Mg/m}^3$  for the pelletized mixtures dry density  $\rho_d$  of  $1.60$  and  $1.70 \text{ Mg/m}^3$  respectively. The results are presented on Figure 7-22, together with the results obtained by the considered pelletized mixtures. The data of the pelletized mixture have been limited in time (200 h) in order to compare them with the powdered mixtures. It is reminded that for the pelletized mixture containing 30% sand, the developed swelling pressure was almost stabilized during the first 24 h and no significant variation was then observed.

On Figure 7-22, a first observation regarding the swelling pressure kinetics of the compacted powders could be highlighted. For both powdered samples, swelling pressure increases until a stable final value, contrary to the increase/decrease/stabilisation pattern observed on specimens compacted on lower dry densities (Figure 6-16). The observation is in agreement with the decreased macropores that exist on higher dry densities, where no collapse occurs (Pusch 1982, Lloret and Villar 2007, Zeng et al. 2019).

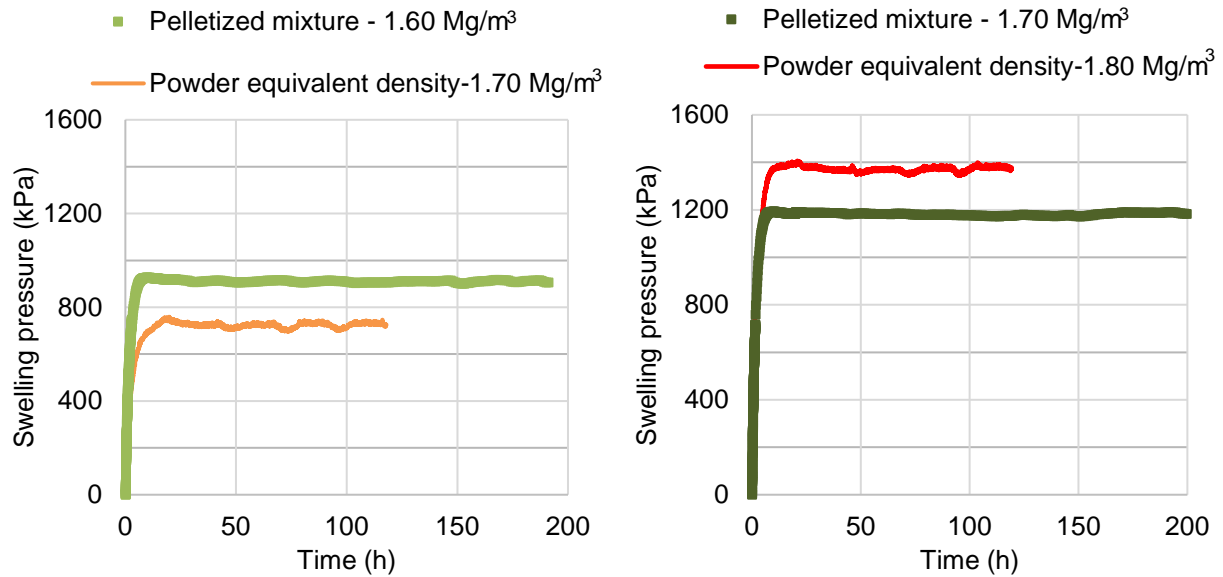


Figure 7-22 Swelling pressure developed by pelletized mixtures and powdered mixtures compacted at the equivalent pellet dry density.

Contrary to the pure clayey mixtures of paragraph 7.5.2, a variation of the developed pressures is observed for the pelletized material and the equivalent density state in powders. More precisely, an absolute error of 19.6% and 11.9% is obtained between pelletized and powder sample on Figure 7-22a and Figure 7-22b respectively. In other words, the swelling pressure is underestimated for  $\rho_d=1.60 \text{ Mg/m}^3$  and overestimated for  $\rho_d=1.70 \text{ Mg/m}^3$ . This heterogeneous behaviour suggests that an equivalent powder state is not possible to be defined on pelletized trimodal mixtures containing pure sand as component. In fact, pellets (16 mm and 10 mm) are not completely “saturated” by the sand and voids exist upon the emplacement state: for instance, inter-pellet voids where sand did not homogeneously penetrate (Figure 7-23). The phenomena can be intensified since the pelletized material is emplaced without mechanical compaction in the experiments, as well as in real gallery conditions. In that framework, the sand is not homogeneously distributed and probably does not present the same density over the specimen, as considered in the hypothesis. In the case of crushed pellets this phenomenon decreases, due to differences between clayey and sandy materials. Apart from the clear distinction in the hydro-mechanical behaviour of the two materials, segregation upon the emplacement is less possible to be obtained if crushed clayey pellets are used, due to electrostatic forces developed on clays or the similar friction of the different size components. In the future, the distribution of sand density should be more precisely evaluated, examining possible segregation phenomena.

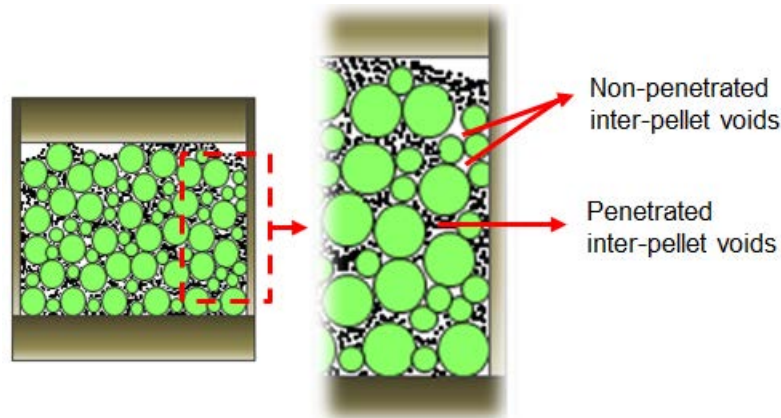


Figure 7-23 Local heterogeneity of sand's distribution upon the materials emplacement.

## 7.6 Conclusions

The hydro-mechanical response of three potential COx/MX80 pelletized mixtures, presented trimodal granulometric configurations, was studied. The swelling pressure and hydraulic conductivity were evaluated upon their emplacement condition. All samples presented common grain size distribution dictated by previous experimental study. The tested specimens were composed of 16 mm and 10 mm diameter pellets as well as a finer grain component ( $d \leq 2$  mm), in proportions of 60%, 10% and 30% respectively (in total mass). Sand and /or crushed pellets were suggested as finer grains, affecting the overall materials composition. Pellets and crushed pellets were composed of COx/MX80 mixtures (i.e. clayey materials). MX80 bentonite content of approximately 30% ( $\pm 2$ ) was used, whereas COx fraction was varied. For all conducted tests, the clayey content (COx argillite and MX80 bentonite) ranged between 70% and 100%, whereas sand content varied between 0% and 30% accordingly.

In accordance to the testing period, the main outcomes of the study are summarised below.

- The well-known swelling pressure augmentation at higher initial dry densities is obtained for pelletized samples presenting the same composition.
- The kinetic of swelling pressure evolution is directly connected with the reported hydraulic conductivity. As sand content increases (i.e. higher developed hydraulic conductivity), the material presents high macropores and the swelling pressure is developed almost instantly. On the other hand, for lower sand contents and higher presence of clayey material (i.e. less permeable sample), swelling pressure increases slowly until its final stabilization.
- A significant dependence on the used type of finer grains is presented: sand blocks the inter-pellet void, reinforcing constant volume conditions (i.e. swelling pressure

increase), whereas crushed pellets deform upon wetting, giving place to the swelling pellets for volume increase.

- Swelling pressure follows non-linear augmentation with sand content, whereas hydraulic conductivity increases approximately exponentially. After sand content of 15%, permeability is governed by the sand.
- For pure clayey pelletized samples, the developed swelling pressure is very close to the pressure reported by the powdered samples compacted at the same dry density. On the other hand, a corresponding state in powdered mixtures is difficult to be defined when sand exist in the inter-pellet voids. The latter highlights the essential role of the inevitable technological voids of emplacement, on the hydro-mechanical response.



## Chapter 8 - General conclusions and perspectives

Objective of the present PhD thesis is the proposition of a granular pelletized material, suitable to be implemented as backfill for the deep geological disposal facilities of the French Cigeo project. The backfill, as part of the repository's closure safety system, is installed to reinforce the overall structure's sealing characteristics upon groundwater infiltration and limit any possible propagation of the damaged zone around the drift.

In this context, the main parameters to investigate are the material's swelling capacity (i.e. swelling potential or swelling pressure) and hydraulic performance, which are both improved by achieving the maximum density of the installed material. Although swelling clays (e.g. MX80 bentonite) are traditionally used for these purposes, the large amount of backfill necessary to fill the remaining openings and the compatibility with the host rock, dictate the re-use of the excavated COx claystone. Additionally, COx presents some swelling characteristics, due to smectite found on the clay mineral.

Therefore, the pelletized material is suggested to be composed of COx/MX80 mixture, minimising as possible the bentonite presence. Part of the originality of the present investigation is the pelletization of COx argillite, which had not previously attempted and to our knowledge, no information was available. The study is focused on two levels:

- the most compacted packing state of a granular mixture, primarily affected by the material's granulometric parameters (GSD), and
- the hydro-mechanical response, which is provoked by the composing materials.

The following conclusions and perspectives are developed on that basis.

## 8.1 Conclusions

### 8.1.1 Pelletized GSD and resulting packing density

The selected GSD ( $d_i$  and  $\%d_i$  for  $i=\max, med, min$ ) was optimised to result in the maximum resulting packing dry density, by conducting gravitational deposits using numerical and experimental methods on various bimodal and trimodal samples. Therefore:

- (a) As a first step, numerical simulations using the discrete element method (DEM) are applied to adjust the pellet sizes and proportions inside the mixture. More precisely, the method Non-Smooth Contact Dynamics is adopted, considering mixtures composed of rigid dry spherical particles, subjected to deposit under gravity without applying additional compaction. The cell always presented sized 10 times larger than the maximum grain size, while the friction between particle/cell was neglected. Relatively low inter-particle friction angle was applied, which nonetheless varied when the specific parameter was investigated.
- (b) After concluding in the DEM optimum GSD, experiments using the fabricated sizes, as well as finer grains, examine further the packing state and the preparation protocol.

Volumetric proportions were considered equal to mass proportions, since the particle density corresponded to the pellet intra-pellet density ( $\rho_d^{pellet} = 2 \text{ Mg/m}^3$ ).

Both methods reached the following remarks:

- Optimum proportions  
In order to increase as possible the resulting packing density of bimodal and trimodal granular mixtures, optimum proportions can be imposed, independently to the actual sizes, with  $d_{max}$  to rank the highest fraction inside the mixture. For bimodal sample these proportions slightly vary between 60-70% for  $d_{max}$  and consequently 30-40% for  $d_{min}$ . For ternary samples, the densest state is achieved when the proportions criteria of  $\%d_{max} > \%d_{min} > \%d_{med}$  are fulfilled. More especially the proportions of 60%, 10% and 30% were selected as  $\%d_{max}$ ,  $\%d_{min}$  and  $\%d_{med}$  respectively.
- Effect of intermediate diameter  
The intermediate diameter  $d_{med}$  is independent to the maximum obtained density, therefore bimodal and trimodal configurations with common the extreme diameters  $d_{max}$  and  $d_{min}$  (but evidently in different proportions) present the same packing state.

- Effect of size ratio of minimum diameter

The parameter  $\alpha_{min} = \frac{d_{min}}{d_{max}}$  appears as the most decisive specification for maximizing the mixtures dry density; the lower the  $\alpha_{min}$ , the denser compactness is achieved. On bimodal samples, no variation in the maximum density is observed for  $\alpha_{min} > 0.6$ . Ternary mixtures having common  $\alpha_{min}$  and different imposed sizes exhibit low variation in the resulting compactness.

- Effect of deposit height

Numerical simulations investigating the effect of deposit height on the materials compactness, highlighted the increase of resulting packing density for more important deposit heights (i.e. higher initially kinetic energy).

- Effect of interactions particles/cell

Experimental data focusing on the impact of friction between sample and cell boundaries on the particles rearrangement show that direct deposit of a pre-blended granulometry presents lower compactness characteristics, than layering the desired granulometry. The cell form does not impact the density state, if the available volume is similar.

The DEM dictates that the optimum GSD is the trimodal sample of 16 mm, 10 mm and 4 mm in proportions of 60%, 10% and 30% respectively. A parametric study on that granulometry using the adopted numerical model, allowed the direct comparison of numerical and experimental data. The following outcomes are reported:

- Increase of inter-particle friction coefficient,  $\mu$  hinders the particle rearrangement and results in lower achieved densities independently to the imposed deposit height. The effect becomes insignificant for  $\mu > 0.6$ .
- The experimental layering method coincides with numerical results, due to similar boundary conditions (cell scale, sample/cell interactions). This indirect calibration that correlated the packing dry density with the numerical inter-particle friction characteristics indicates an inter-particle friction angle of 30°. The value is very close with the repose angle exhibited by the same granular sample.

Finally, finer grains ( $d \leq 2$  mm) of wide size range (e.g. well-graded sand) are essential to achieve higher packing densities (1.45-1.60 Mg/m<sup>3</sup>). The optimal granulometry of the pelletized mixture is determined in respect to the maximum density value, considering in parallel production criteria. Therefore the selected GSD for the pelletized assembly is:

- Pellets in diameters of 16 mm and 10 mm and well-graded sand prepared in layers of proportions of 60%, 10% and 30% in total mass.

### 8.1.2 COx/MX80 pellet fabrication

The characterisation of the studied soil materials shows a clear difference in the properties: COx is clay of medium plasticity, whereas MX80 bentonite is clay of extremely high plasticity, exhibiting high swelling and absorption capacity index properties. MX80 addition on COx affects the basic soil characteristics accordingly.

The fabrication of quasi-spherical pellets composed of COx/MX80 mixtures at target dry density of  $\rho_d^{pellet} = 2.0 \text{ Mg/m}^3$  is carried out for the first time, by applying the compression method, in order to produce diameter sizes of 16 mm, 10 mm and 4 mm. The mixtures compressibility is examined in two levels: by initially performing uniaxial oedometric compression tests on small soil cylindrical specimens ( $D=40 \text{ mm}$ ,  $H=40 \text{ mm}$ ) and by directly using the reconditioned tablet press machine on the target pellet size. However, the high compaction velocity at which the pellet machine operates (i.e. it is not possible to be simulated on the oedometric device), reveals a difference in material's behaviour.

At low displacement rates ( $0.04 \approx 0.85 \text{ mm/min}$ ), COx/MX80 mixtures compressibility is mainly governed by COx argillite compression characteristics ( $\leq 40\% \text{ MX80}$ ). MX80 bentonite content does not impact the materials behaviour at reception conditions. However, at higher water contents compaction is improved only when stresses lower than 10 MPa are applied, that do not correspond to the desired density. On these conditions, an important developed capillarity hinders the compaction at the necessary high stresses, which is observed also even at decreased displacement rates.

The actual pelletization is characterised as a challenging process that correlates parameters such as the pellet intactness, the target intra-pellet density and a sufficient long-term production. In that context, COx behaves as a non-easily pelletized material. The essential accessories of punch tools and moulds are firstly designed and then fabricated from materials (e.g. steel type) suitable to successfully carry out the mixtures compaction on the machine. The relatively complex pellet geometry (i.e. curvature of the spherical part on pellet's top and bottom) indicates the decrease of pellet's spherical height (i.e. volume of the spherical part  $\sim 10\%$  of the total pellet volume). A series of modifications are proposed to improve pellet production. Decrease of COx fines percentage at reception water content conditions increase the percentage of produced intact pellets. Conversely, increase of COx water content (approximately at 8.5%) appears as sufficient solution for an industrial pellet production. Nonetheless, since COx presence is the limiting factor on the pelletizing process, an insignificant reduction of the target intra-pellet density is proposed in order to optimise the fabrication of intact pellets.

Following the feedback from manufacturing and installation applications in galleries (REX sealing experiment), the proposed pelletized solution seems technologically feasible.

### **8.1.3 Hydro-mechanical response of compacted CO<sub>x</sub>/MX80 powdered and pelletized materials**

The hydro-mechanical response of CO<sub>x</sub>/MX80 mixtures ( $\leq 40\%$ MX80) is studied in both powdered and pelletized form. In the direction of a preliminary evaluation, pure CO<sub>x</sub>/MX80 powdered mixtures are compacted at the density range that a pelletized configuration is expected to present ( $\rho_d = 1.45 \sim 1.60 \text{ Mg/m}^3$ ). On the contrary, the actual selected granular mixture containing CO<sub>x</sub>/MX80 pellets of 16 mm and 10 mm as well as well-graded finer grains with  $d \leq 2 \text{ mm}$  (e.g. sand and/crushed pellets) is examined upon the conditions of emplacement, where no compaction efforts have been applied ( $\rho_d \approx 1.60 \text{ Mg/m}^3$ ).

In first case, the effect of MX80 bentonite content is investigated by conducting a parametric study for the CO<sub>x</sub>/MX80 powders hydro-mechanical and physicochemical properties. Plasticity index, free swelling capacity index and swelling capacity of compacted CO<sub>x</sub>/MX80 specimens (i.e. swelling pressure and swelling potential) become clearly more significant upon MX80 addition. The optimum compaction characteristics decrease with bentonite fraction, due to the swelling of MX80 particles upon wetting. Additionally, the use of synthetic solutions (i.e. site water and cementitious water) present a clear impact compared to pure demineralised water. The effect is related to salt presence that influences the clay interaction with water. Cementitious alkaline water seems to impact less significantly the material's swelling potential, but the overall results consider this difference as insignificant, probably due to the fact that despite their different chemical composition, the two solutions present very similar ionic strength. Therefore, in respect to the short-term testing period, no alkaline effect on materials swelling is suggested. Swelling potential tests performed with the modified CO<sub>x</sub>'s granulometry and sand, reveal no influence compared to the original argillite and bentonite materials. Both swelling pressure and swelling potential improvement is obtained on density maximization. An increase/decrease/stabilisation development of the swelling pressure is observed, which is more pronounced when MX80 content and initial dry density decreased, implying that higher macropores exist on higher CO<sub>x</sub> content. However, CO<sub>x</sub>/MX80 mixtures prepared at the optimum water content conditions (i.e. lower initial suction) do not present this peak on the swelling pressure kinetics. A slight effect of the initial water content conditions on the final pressure is obtained, especially for the higher bentonite content. Processed data of the swelling under constant vertical stress tests are conduct a preliminary analysis for the swelling potential

of CO<sub>x</sub>/MX80 backfill, emplaced at gallery conditions (gallery of 8 m diameter) if homogeneous density distribution is considered. The calculations correlate the logarithmic relation of the swelling potential with the vertical stress caused by the material's unit weight within the gallery's height, and thus propose mainly CO<sub>x</sub>/MX80 mixtures with bentonite content ranging between 30% and 40%.

For the pelletized material, the packing state is resulted from several mixtures of pellets with 16 mm and 10 mm diameter and finer grain component ( $d \leq 2$  mm) made of sand and/or crushed pellets, in proportions of 60%, 10% and 30%. In that framework, the mixture's total composition is constituted by the content of clayey (CO<sub>x</sub>/MX80 mixture: 70 – 100%) and sandy materials (0 – 30%), with MX80 total proportion to remains around 30% ( $\pm 2$ ) and CO<sub>x</sub> fraction slightly vary. A hydration of 30 days under constant volume conditions is conducted. The expected effect of density state on the developed swelling response is also obtained, regardless whether its variation has resulted from a simple materials deposition (i.e. no mechanical compaction). A significant effect of the imposed finer grain component on the hydro-mechanical performance is presented, presenting two antagonistic phenomena. The existing sand between the clayey swelling pellets emphasises the constant volume conditions increasing almost directly the developed swelling pressure ( $\sim 1$  MPa for a dry density of  $1.70 \text{ Mg/m}^3$ ), whereas crushed pellets as compressible material upon wetting, allow pellets to increase their volume more freely. On the other hand, sand's addition impacts almost exponentially the sealing characteristics (i.e. increase of hydraulic conductivity). In the case of pure clayey pelletized mixtures (e.g. CO<sub>x</sub>/MX80 pellets and crushed pellets), pelletized and powdered material presented very common final swelling pressure for the same mixtures dry density, verifying results of previous experimental studies. However, the experimental results show that a comparison of the pelletized material and the equivalent powdered state cannot be easily conducted when sand is added in the mixture, probably due to non-homogeneous distribution of the sand between the pellets upon the material's emplacement.

## 8.2 Perspectives

A series of tests regarding the maximization of the resulting packing density, as well as the evaluation of the desired hydro-mechanical performance (sufficient swelling capacity and low hydraulic conductivity) revealed a complex and almost antagonistic behaviour between these parameters. More precisely, it was seen that finer grains is essential requirement for the achievement of a dense state. Although the option of sand presents beneficial results in terms of swelling pressure, it is unfavourable for the developed permeability. On the other hand, the tested crushed pellets are able to compensate the negative effect of hydraulic conductivity,

without maintaining the swelling capacity. Taking into account both emplacement and hydrated conditions, the following suggestions are given for future consideration.

On the pelletized material's emplacement, where no hydration has occurred, the homogeneity of density distribution should be examined, considering tests on larger scale. These conditions allow the identification of possible phenomena of segregation and the propositions of suitable solutions. For example, since the numerical and experimental data of the present study showed that the resulting packing density is mainly governed by the two extreme imposed sizes (e.g.  $d_{max}$  and  $d_{min}$ ), coarse sized crushed pellets could be produced as the intermediate diameter  $d_{med}$ , with diameter between 10 mm and 2 mm. This proposition might contribute in avoiding possible segregation phenomena, while only one pellet size would be manufactured. However, it is not known if the crushing would impact swelling capacity. Furthermore, focusing on the finer component of the mixture,  $d_{min}$  ( $d \leq 2$  mm), an optimisation of the imposed sand content could be examined in more details. In parallel with the optimization of sand content, the influence of crushed pellets granulometry ( $d \leq 2$  mm) on swelling performance is suggested for further examination. Hence, the effect of the non-overconsolidated fines (i.e. almost powder) on the hydro-mechanical response will be assessed. Furthermore, a pelletized material made of technologically feasible larger diameters (in respect to the study's size ratio) is suggested for possible examination. This option might be favorable for large-scale industrial production and needs to be completed by an emplacement test analysis of reduced size (max diameter 1m).

Regarding the condition of hydration, the number and the relatively time-consuming tests allowed only the infiltration of site water on the swelling pressure tests performed at COx/MX80 powdered and pelletized mixtures. Even though the rest of the results suggested no significant impact, the influence of the alkaline cementitious solution should be assessed for these cases for a longer testing period, to evaluate the long-term chemical interactions.

An interesting and important parameter to explore - which is connected to the mechanical resistance of the backfill - is the behaviour of the saturated pelletized assembly on compression. Therefore, the experimental study on the material's compressibility is proposed under different considered hydration scenarios: free volume conditions, constant volume conditions, or a more realistic case where after the filling of a percentage of initial voids, constant volume conditions are applied. After the swelling stabilization, the material mechanical modulus can be measured by performing unloading and reloading cycles. These parameters are additionally useful for the numerical modelling of the backfill.

A parameter which was not included in the objectives of the present thesis is the gas production during the repository life, caused by the anaerobic corrosion of the metal. The developed gas

permeability of the selected backfill material should be examined in a way to limit the build up of gas pressure inside of the repository.

---

## References

- Adema, A., Yang, Y., and Boom, R. 2009. Coupled DEM-CFD modelling of the ironmaking blast furnace. *In* Proceedings of the 5th International Congress on the Science and Technology of Ironmaking (ICSTI).
- AFNOR. 1993. Soil : investigation and testing - Determination of Atterberg's limits - Liquid limit test using Casagrande apparatus - Plastic limit test on rolled thread. Association Française de Normalisation (AFNOR).
- AFNOR. 1995. Soil : investigation and testing - Atterberg limit determination - Part 1 : Liquid limit - Cone penetrometer method. Association Française de Normalisation (AFNOR).
- AFNOR. 1998. Soils : Investigation and testing - Measuring of the methylene blue adsorption capacity of a rocky soil - Determination of the methylene blue of a soil by means of the stain test. Association Française de Normalisation (AFNOR).
- AFNOR. 2002. Bentonitic geosynthetics - Determination of the swelling capacity of clay in bentonitic geosynthetics. Association Française de Normalisation (AFNOR).
- AFNOR. 2014. Soils : investigation and testing - Determination of the compaction reference values of a soil type - Standard Proctor test - Modified Proctor test. Association Française de Normalisation (AFNOR).
- Agus, S.S. 2005. An experimental study on hydro-mechanical characteristics of compacted bentonite-sand mixtures. PhD Thesis, Bauhaus-University Weimar.
- Akgün, H., and Koçkar, M.K. 2018. Evaluation of a sand bentonite mixture as a shaft/borehole sealing material. *Applied Clay Science*, **164**: 34–43. doi:10.1016/j.clay.2017.12.043.
- Al-Hashemi, H.M.B., and Al-Amoudi, O.S.B. 2018. A review on the angle of repose of granular materials. *Powder Technology*, **330**: 397–417. Elsevier.
- Al-Mhaidib, A.I. 1998. Swelling Behaviour of Expansive Shales from the Middle Region of Saudi Arabia. *Geotechnical & Geological Engineering*, **16**(4): 291–307. doi:10.1023/A:1008819025348.
- Alonso, E.E., Hoffmann, C., and Romero, E. 2010. Pellet mixtures in isolation barriers. *Journal of Rock Mechanics and Geotechnical Engineering*, **2**(1): 12–31. doi:10.3724/SP.J.1235.2010.00012.
- Alonso, E.E., Romero, E., and Hoffmann, C. 2011. Hydromechanical behaviour of compacted granular expansive mixtures: experimental and constitutive study. *Géotechnique*, **61**(4): 329–344. ICE Publishing. doi:10.1680/geot.2011.61.4.329.
- An, X.Z., Li, C.X., Yang, R.Y., Zou, R.P., and Yu, A.B. 2009. Experimental study of the packing of mono-sized spheres subjected to one-dimensional vibration. *Powder Technology*, **196**(1): 50–55.
- An, X.Z., Yang, R.Y., Zou, R.P., and Yu, A.B. 2008. Effect of vibration condition and inter-particle frictions on the packing of uniform spheres. *Powder Technology*, **188**(2): 102–109. Elsevier. doi:10.1016/j.powtec.2008.04.001.

- Andra. 2005. Dossier Synthesis - Evaluation of the feasibility of a geological repository in an argillaceous formation.
- Andra. 2013. The Cigéo project - Meuse/Haute-Marne reversible geological disposal facility for radioactive waste. Dupuis M.C, Gonnet F.M.
- Andra. 2016a. Safety Options Report - Post-Closure Part (DOS-AF). ANDRA.
- Andra. 2016b. Safety Options Report - Operating Part (DOS-Expl).
- Andra. 2019. Synthesis of 20 years Research, Development and Demonstration in Andra's Underground Research Laboratory in Bure for Cigéo Project - France.
- Armand, G., Conil, N., Talandier, J., and Seyedi, D.M. 2017. Fundamental aspects of the hydromechanical behaviour of Callovo-Oxfordian claystone: From experimental studies to model calibration and validation. *Computers and Geotechnics*, **85**: 277–286. doi:10.1016/j.compgeo.2016.06.003.
- Armand, G., Leveau, F., Nussbaum, C., de La Vaissière, R., Noiret, A., Jaeggi, D., Landrein, P., and Righini, C. 2014. Geometry and Properties of the Excavation-Induced Fractures at the Meuse/Haute-Marne URL Drifts. *Rock Mechanics and Rock Engineering*, **47**(1): 21–41. doi:10.1007/s00603-012-0339-6.
- Armand, G., Noiret, A., Zghondi, J., and Seyedi, D.M. 2013. Short-and long-term behaviors of drifts in the Callovo-Oxfordian claystone at the Meuse/Haute-Marne Underground Research Laboratory. *Journal of Rock Mechanics and Geotechnical Engineering*, **5**(3): 221–230.
- Arvidsson, A., Josefsson, P., and Eriksson, P. 2015. System design of backfill, Project results. TR-14-20.
- Baille, W., Tripathy, S., and Schanz, T. 2010. Swelling pressures and one-dimensional compressibility behaviour of bentonite at large pressures. *Applied Clay Science*, **48**(3): 324–333.
- Barast, G., Razakamanantsoa, A.-R., Djeran-Maigre, I., Nicholson, T., and Williams, D. 2017. Swelling properties of natural and modified bentonites by rheological description. *Applied Clay Science*, **142**: 60–68. doi:10.1016/j.clay.2016.01.008.
- Bell, F. 1993. *Engineering Treatment of Soils*. CRC Press, London.
- Broc, D., Plas, F., and Robinet, J.C. 1988. Mechanical properties of swelling Clays. *MRS Online Proceedings Library Archive*, **127**. Cambridge University Press. doi:10.1557/PROC-127-669.
- Castellanos, E., Villar, M.V., Romero, E., Lloret, A., and Gens, A. 2008. Chemical impact on the hydro-mechanical behaviour of high-density FEBEX bentonite. *Physics and Chemistry of the Earth, Parts A/B/C*, **33**: S516–S526. doi:10.1016/j.pce.2008.10.056.
- Chalermyanont, T., and Arrykul, S. 2005. Compacted sand-bentonite mixtures for hydraulic containment liners. *Songklanakarin Journal of Science and Technology*, **27**(2): 313–323.
- Chen, Y.-G., Dong, X.-X., Zhang, X.-D., Ye, W.-M., and Cui, Y.-J. 2018. Combined thermal and saline effects on the swelling pressure of densely compacted GMZ bentonite. *Applied Clay Science*, **166**: 318–326. doi:10.1016/j.clay.2018.10.001.
- Cho, G.C., Dodds, J., and Santamarina, J.C. 2006. Particle shape effects on packing density, stiffness and strength: natural and crushed Sands. *Journal of Geotechnical and Geoenvironmental Engineering*, **132**(5): 591–602. American Society of Civil Engineers. doi:10.1061/(ASCE)1090-0241(2006)132:5(591).
- Coetzee, C.J. 2016. Calibration of the discrete element method and the effect of particle shape. *Powder Technology*, **297**: 50–70. doi:10.1016/j.powtec.2016.04.003.
- Cuisinier, O., Deneele, D., and Masrouri, F. 2009. Shear strength behaviour of compacted clayey soils percolated with an alkaline solution. *Engineering Geology*, **108**(3): 177–188. doi:10.1016/j.enggeo.2009.07.012.
- Cuisinier, O., Deneele, D., Masrouri, F., Abdallah, A., and Conil, N. 2014. Impact of high-pH fluid circulation on long term hydromechanical behaviour and microstructure of compacted clay from the laboratory of Meuse-Haute Marne (France). *Applied Clay Science*, **88–89**: 1–9. doi:10.1016/j.clay.2013.12.008.

- Dang, K.D. 2007. Contribution à l'étude du comportement thermo-hydro-mécanique des matériaux argileux (bentonite MX80 et argilite du Callovo-oxfordienne). PhD Thesis, Rennes, INSA.
- Dardé, B. 2019. Experimental and numerical study of the hydromechanical behaviour of bentonite pellet-powder mixtures. PhD Thesis, Université Paris-Est.
- Darde, B., Roux, J.-N., Dangla, P., Pereira, J.-M., Tang, A.M., Talandier, J., and Vu, M.N. 2020. Modelling the hydromechanical behaviour of a granular expansive clayey soil upon hydration using discrete element method. *In CIGOS 2019, Innovation for Sustainable Infrastructure. Edited by C. Ha-Minh, D.V. Dao, F. Benboudjema, S. Derrible, D.V.K. Huynh, and A.M. Tang.* Springer, Singapore. pp. 871–876.
- Darde, B., Tang, A.M., Pereira, J.-M., Roux, J.-N., Dangla, P., Talandier, J., and Vu, M.N. 2018. Hydro-mechanical behaviour of high-density bentonite pellet on partial hydration. *Géotechnique Letters*, **8**(4): 330–335. ICE Publishing. doi:10.1680/jgele.18.00114.
- Davies, C.W., Davie, C.T., Charles, E.A., and White, M. 2017. Physicochemical and geotechnical alterations to MX-80 bentonite at the waste canister interface in an engineered barrier system. *Geosciences*, **7**(3). doi:10.3390/geosciences7030069.
- Deganutti, A., Tecca, P., and Genevois, R. 2011. Characterization of friction angles for stability and deposition of granular material. *In Italian Journal of Engineering and Environment: 5th International Conference on Debris-Flow Hazards: Mitigation, Mechanics, Prediction and Assessment.*
- Delage, P., Howat, M.D., and Cui, Y.J. 1998. The relationship between suction and swelling properties in a heavily compacted unsaturated clay. *Engineering Geology*, **50**(1): 31–48. doi:10.1016/S0013-7952(97)00083-5.
- Delage, P., Marcial, D., Cui, Y.J., and Ruiz, X. 2006. Ageing effects in a compacted bentonite: a microstructure approach. *Géotechnique*, **56**(5): 291–304. ICE Publishing. doi:10.1680/geot.2006.56.5.291.
- Di Maio, C., Santoli, L., and Schiavone, P. 2004. Volume change behaviour of clays: the influence of mineral composition, pore fluid composition and stress state. *Mechanics of Materials*, **36**(5): 435–451. doi:10.1016/S0167-6636(03)00070-X.
- Dixon, D., Sanden, T., Jonsson, E., and Hansen, J. 2011. Backfilling of deposition tunnels: Use of bentonite pellets. Swedish Nuclear Fuel and Waste Management Co.
- Dixon, D.A., Gray, M.N., and Thomas, A.W. 1985. A study of the compaction properties of potential clay—sand buffer mixtures for use in nuclear fuel waste disposal. *Engineering Geology*, **21**(3): 247–255. doi:10.1016/0013-7952(85)90015-8.
- Dodds, J.A. 1980. The porosity and contact points in multicomponent random sphere packings calculated by a simple statistical geometric model. *Journal of Colloid and Interface Science*, **77**(2): 317–327. doi:10.1016/0021-9797(80)90302-1.
- Farhat, Z.N., Ding, Y., Northwood, D.O., and Alpas, A.T. 1996. Effect of grain size on friction and wear of nanocrystalline aluminum. *Materials Science and Engineering: A*, **206**(2): 302–313. doi:10.1016/0921-5093(95)10016-4.
- García-Siñeriz, J.L., Villar, M.V., Rey, M., and Palacios, B. 2015. Engineered barrier of bentonite pellets and compacted blocks: State after reaching saturation. *Engineering Geology*, **192**: 33–45. doi:10.1016/j.enggeo.2015.04.002.
- Garitte, B., Weber, H., and Müller, H.R. 2015. LUCOEX – WP2 DELIVERABLE (D-N°:D2.3) Requirements, manufacturing and QC of the buffer components.
- Gatabin, C., Imbert, C., Treppe, N., and L'Hostis, V. 2014. FSS-1 : Conception des matériaux à base d'argile gonflante.
- Gens, A. 2019. Clays in natural and engineered barriers for nuclear waste disposal. *Geomechanics for Energy and the Environment*, **17**: 1–2. doi:10.1016/j.gete.2018.11.004.
- Gens, A., and Alonso, E.E. 1992. A framework for the behaviour of unsaturated expansive clays. *Canadian Geotechnical Journal*, **29**(6): 1013–1032. NRC Research Press. doi:10.1139/t92-120.

- Ghasemi, Y. 2017. Aggregates in concrete mix design. PhD Thesis, Luleå University of Technology.
- Ghazavi, M., Hosseini, M., and Mollanouri, M. 2008. A comparison between angle of repose and friction angle of sand. *In* The 12th International Conference for International Association for Computer Methods and Advances in Geomechanics (IACMAG). pp. 1–6.
- Head, K.H. 2006. Manual of Soil Laboratory Testing. CRC Press - Taylor & Francis Group.
- Herbert, H.-J., Kasbohm, J., Sprenger, H., Fernández, A.M., and Reichelt, C. 2008. Swelling pressures of MX-80 bentonite in solutions of different ionic strength. *Physics and Chemistry of the Earth, Parts A/B/C*, **33**: S327–S342. doi:10.1016/j.pce.2008.10.005.
- Hirjau, M., Nicoara, A.C., Hirjau, V., and Lupuleasa, D. 2011. Pelletization techniques used in pharmaceutical fields. *Practica Farmaceutică*, **4**(3).
- Hoffmann, C., Alonso, E.E., and Romero, E. 2004. Fabric changes of a pellet-based bentonite buffer material and their effects on mechanical behaviour. *In* Elsevier Geo-Engineering Book Series. *Edited by* O. Stephanson. Elsevier. pp. 341–346.
- Hoffmann, C., Alonso, E.E., and Romero, E. 2007. Hydro-mechanical behaviour of bentonite pellet mixtures. *Physics and Chemistry of the Earth, Parts A/B/C*, **32**(8): 832–849. doi:10.1016/j.pce.2006.04.037.
- Hoffmann, C., Romero, E., and Alonso, E.E. 2005. Combining different controlled-suction techniques to study expansive clays. *In* Proceedings of the international symposium on advanced experimental unsaturated soil Mechanics, Trento, Italy. Balkema. pp. 61–67.
- Hyodo, N., Adachi, N., Hino, M., Todaka, Y., and Oba, Y. 2018. Effect of grain size on friction coefficient under oil lubrication in nanostructured Fe fabricated by PVD and SPD methods. *Procedia Manufacturing*, **15**: 1693–1700. doi:10.1016/j.promfg.2018.07.266.
- IAEA. 2009. Geological disposal of radioactive waste: technological implications for retrievability. IAEA Vienna, Austria.
- Imbert, C., and Villar, M.V. 2006. Hydro-mechanical response of a bentonite pellets/powder mixture upon infiltration. *Applied Clay Science*, **32**(3–4): 197–209.
- Ito, H., and Komine, H. 2008. Dynamic compaction properties of bentonite-based materials. *Engineering Geology*, **98**(3): 133–143. doi:10.1016/j.enggeo.2008.01.005.
- Jacinto, A.C., Ledesma, A., and Demagistri, A. 2016. Effect of the clay–water interaction in the hydration of compacted bentonite used in engineered barriers. *Geomechanics for Energy and the Environment*, **8**: 52–61. doi:10.1016/j.gete.2016.10.002.
- Jean, M. 1999. The non-smooth contact dynamics method. *Computer Methods in Applied Mechanics and Engineering*, **177**(3–4): 235–257. Elsevier. doi:10.1016/S0045-7825(98)00383-1.
- Jean, M., and Moreau, J.J. 1992. Unilaterality and dry friction in the dynamics of rigid body collections. *In* 1st Contact Mechanics International Symposium. Lausanne, Switzerland. pp. 31–48.
- Johannesson, L.-E., Börgesson, L., Goudarzi, R., Sandén, T., Gunnarsson, D., and Svemar, C. 2007. Prototype repository: A full scale experiment at Äspö HRL. *Physics and Chemistry of the Earth, Parts A/B/C*, **32**(1): 58–76. doi:10.1016/j.pce.2006.04.027.
- Johnsson, A., and Sandén, T. 2013. System design of backfill – Pellet optimization. Svensk Kärnbränslehantering AB.
- Karnland, O., Nilsson, U., Weber, H., and Wersin, P. 2008. Sealing ability of Wyoming bentonite pellets foreseen as buffer material – Laboratory results. *Physics and Chemistry of the Earth, Parts A/B/C*, **33**: S472–S475. doi:10.1016/j.pce.2008.10.024.
- Karnland, O., Olsson, S., and Nilsson, U. 2006. Mineralogy and sealing properties of various bentonites and smectite-rich clay materials. SKB Stockholm.
- Karnland, O., Olsson, S., Nilsson, U., and Sellin, P. 2007. Experimentally determined swelling pressures and geochemical interactions of compacted Wyoming bentonite with highly alkaline solutions. *Physics and Chemistry of the Earth, Parts A/B/C*, **32**(1): 275–286. doi:10.1016/j.pce.2006.01.012.

- Kayabali, K., and Demir, S. 2011. Measurement of swelling pressure: direct method versus indirect methods. *Canadian Geotechnical Journal*, **48**(3): 354–364. NRC Research Press. doi:10.1139/T10-074.
- Kohno, M., Nara, Y., Kato, M., and Nishimura, T. 2018. Effects of clay-mineral type and content on the hydraulic conductivity of bentonite–sand mixtures made of Kunigel bentonite from Japan. *Clay Minerals*, **53**(4): 721–732. GeoScienceWorld. doi:10.1180/clm.2018.52.
- Komine, H., and Ogata, N. 1994. Experimental study on swelling characteristics of compacted bentonite. *Canadian Geotechnical Journal*, **31**(4): 478–490. NRC Research Press. doi:10.1139/t94-057.
- Komine, H., and Ogata, N. 1999. Experimental Study on Swelling Characteristics of Sand-Bentonite Mixture for Nuclear Waste Disposal. *Soils and Foundations*, **39**(2): 83–97. doi:10.3208/sandf.39.2\_83.
- Komine, H., and Ogata, N. 2003. New equations for swelling characteristics of bentonite-based buffer materials. *Canadian Geotechnical Journal*, **40**(2): 460–475. NRC Research Press. doi:10.1139/t02-115.
- Komine, H., Yasuhara, K., and Murakami, S. 2009. Swelling characteristics of bentonites in artificial seawater. *Canadian Geotechnical Journal*, **46**(2): 177–189. NRC Research Press. doi:10.1139/T08-120.
- Kraehenbuehl, F., Stoeckli, H.F., Brunner, F., Kahr, G., and Mueller-Vonmoos, M. 1987. Study of the water-bentonite system by vapour adsorption, immersion calorimetry and X-ray techniques: I. Micropore volumes and internal surface areas, following Dubinin's theory. *Clay Minerals*, **22**(1): 1–9. Cambridge University Press. doi:10.1180/claymin.1987.022.1.01.
- Kumar, S., and Santhanam, M. 2003. Particle packing theories and their application in concrete mixture proportioning: A review. *Indian concrete journal*, **77**(9): 1324–1331.
- Laird, D.A. 2006. Influence of layer charge on swelling of smectites. *Applied Clay Science*, **34**(1): 74–87. doi:10.1016/j.clay.2006.01.009.
- de Larrard, F. 1999. *Concrete mixture proportioning: a scientific approach*. CRC Press, London.
- Lavanya, K., Senthil, V., and Rathi, V. 2011. Pelletization technology: a quick review. *International Journal of Pharmaceutical Sciences and Research*, **2**(6): 1337. *International Journal of Pharmaceutical Sciences and Research*.
- Lee, J.O., Cho, W.J., Kang, C.H., and Chun, K.S. 2001. Swelling and hydraulic properties of Ca-bentonite for the buffer of a waste repository. *Technologies for the Management of Radioactive Waste from Nuclear Power Plants and Back End Nuclear Fuel Cycle Activities*,: 1–10.
- Liu, S., and Ha, Z. 2002. Prediction of random packing limit for multimodal particle mixtures. *Powder Technology*, **126**(3): 283–296. doi:10.1016/S0032-5910(02)00075-X.
- Liu, Z.-R., Ye, W.-M., Zhang, Z., Wang, Q., Chen, Y.-G., and Cui, Y.-J. 2019. Particle size ratio and distribution effects on packing behaviour of crushed GMZ bentonite pellets. *Powder Technology*, **351**: 92–101. doi:10.1016/j.powtec.2019.03.038.
- Lloret, A., and Villar, M.V. 2007. Advances on the knowledge of the thermo-hydro-mechanical behaviour of heavily compacted “FEBEX” bentonite. *Physics and Chemistry of the Earth, Parts A/B/C*, **32**(8): 701–715. doi:10.1016/j.pce.2006.03.002.
- Lloret, A., Villar, M.V., Sanchez, M., Gens Solé, A., Pintado Llurba, X., and Alonso Pérez de Agreda, E. 2003. Mechanical behaviour of heavily compacted bentonite under high suction changes.
- Londe, L., Dubois, J.-P., and Bauer, C. 2008. Repository Drift Backfilling Demonstrator. WM Symposia, 1628 E. Southern Avenue, Suite 9-332, Tempe, AZ 85282 (United States).
- Lyu, Q., Ranjith, P.G., Long, X., Kang, Y., and Huang, M. 2015. A review of shale swelling by water adsorption. *Journal of Natural Gas Science and Engineering*, **27**: 1421–1431. doi:10.1016/j.jngse.2015.10.004.
- Madsen, F.T., and Müller-Vonmoos, M. 1989. The swelling behaviour of clays. *Applied Clay Science*, **4**(2): 143–156. doi:10.1016/0169-1317(89)90005-7.

- 
- de Magistris, F.S., Silvestri, F., and Vinale, F. 1998. Physical and mechanical properties of a compacted silty sand with low bentonite fraction. *Canadian Geotechnical Journal*, **35**(6): 909–925. NRC Research Press. doi:10.1139/t98-066.
- Manca, D., Ferrari, A., and Laloui, L. 2015. Fabric evolution and the related swelling behaviour of a sand/bentonite mixture upon hydro-chemo-mechanical loadings. *Géotechnique*, **66**(1): 41–57. ICE Publishing. doi:10.1680/jgeot.15.P.073.
- Mangulkar, M.N., and Jamkar, S.S. 2013. Review of particle packing theories used for concrete mix proportioning. *Contributory Papers*, **141**.
- Marigo, M., and Stitt, E.H. 2015. Discrete element method (DEM) for industrial applications: comments on calibration and validation for the modelling of cylindrical pellets. *KONA Powder and Particle Journal*, **32**: 236–252. Hosokawa Powder Technology Foundation. doi:10.14356/kona.2015016.
- Marjavaara, P., Holt, E., and Sjoebloom, V. 2013. Customized bentonite pellets. Manufacturing, performance and gap filling properties. Posiva Oy.
- Marshall, J.S., and Dhir, V.K. 1986. On the prediction of porosity of beds composed of mixtures of spherical particles. *Chemical Engineering Communications*, **48**(4–6): 261–285. Taylor & Francis. doi:10.1080/00986448608910018.
- Massat, L., Cuisinier, O., Bihannic, I., Claret, F., Pelletier, M., Masrouri, F., and Gaboreau, S. 2016. Swelling pressure development and inter-aggregate porosity evolution upon hydration of a compacted swelling clay. *Applied Clay Science*, **124–125**: 197–210. doi:10.1016/j.clay.2016.01.002.
- Mayne, P.W., and Kulhawy, F.H. 1982. Ko- OCR Relationships in Soil. *Journal of the Soil Mechanics and Foundations Division*, **108**(6): 851–872.
- Mayor, J.-C., García-Siñeriz, J.L., Alonso, E., Alheid, H.J., and Blumbling, P. 2005. Engineered barrier emplacement experiment in Opalinus Clay for the disposal of radioactive waste in underground repositories. *Empresa Nacional de Residuos*.
- Middelhoff, M., Cuisinier, O., Masrouri, F., Talandier, J., and Conil, N. 2020. Combined impact of selected material properties and environmental conditions on the swelling pressure of compacted claystone/bentonite mixtures. *Applied Clay Science*, **184**: 105389. doi:10.1016/j.clay.2019.105389.
- Mishra, A.K., Ohtsubo, M., Li, L.Y., Higashi, T., and Park, J. 2009. Effect of salt of various concentrations on liquid limit, and hydraulic conductivity of different soil-bentonite mixtures. *Environmental Geology*, **57**(5): 1145–1153. doi:10.1007/s00254-008-1411-0.
- Mitchell, J.K., and Soga, K. 2005. *Fundamentals of soil behavior*. John Wiley & Sons New York.
- Mohajerani, M., Delage, P., Monfared, M., Tang, A.M., Sulem, J., and Gatmiri, B. 2011. Oedometric compression and swelling behaviour of the Callovo-Oxfordian argillite. *International Journal of Rock Mechanics and Mining Sciences*, **48**(4): 606–615. doi:10.1016/j.ijrmms.2011.02.016.
- Molinero Guerra, A., Aïmedieu, P., Bornert, M., Cui, Y.-J., Tang, A.M., Sun, Z., Mokni, N., Delage, P., and Bernier, F. 2018. Analysis of the structural changes of a pellet/powder bentonite mixture upon wetting by X-ray computed microtomography. *Applied Clay Science*, **165**: 164–169. doi:10.1016/j.clay.2018.07.043.
- Molinero Guerra, A., Cui, Y.-J., He, Y., Delage, P., Mokni, N., Tang, A.M., Aïmedieu, P., Bornert, M., and Bernier, F. 2019. Characterization of water retention, compressibility and swelling properties of a pellet/powder bentonite mixture. *Engineering Geology*, **248**: 14–21. doi:10.1016/j.enggeo.2018.11.005.
- Molinero Guerra, A., Mokni, N., Delage, P., Cui, Y.-J., Tang, A.M., Aïmedieu, P., Bernier, F., and Bornert, M. 2017. In-depth characterisation of a mixture composed of powder/pellets MX80 bentonite. *Applied Clay Science*, **135**: 538–546. doi:10.1016/j.clay.2016.10.030.
- Molinero-Guerra, A., Delage, P., Cui, Y.-J., Mokni, N., Tang, A.M., Aïmedieu, P., Bernier, F., and Bornert, M. 2019. Water-retention properties and microstructure changes of a
-

- 
- bentonite pellet upon wetting/drying; application to radioactive waste disposal. *Géotechnique*, **70**(3): 199–209. ICE Publishing. doi:10.1680/jgeot.17.P.291.
- Muley, S., Nandgude, T., and Poddar, S. 2016. Extrusion–spheronization a promising pelletization technique: In-depth review. *Asian Journal of Pharmaceutical Sciences*, **11**(6): 684–699. doi:10.1016/j.ajps.2016.08.001.
- Müller, H.R., Garitte, B., Vogt, T., Köhler, S., Sakaki, T., Weber, H., Spillmann, T., Hertrich, M., Becker, J.K., and Giroud, N. 2017. Implementation of the full-scale emplacement (FE) experiment at the Mont Terri rock laboratory. *Swiss Journal of Geosciences*, **110**(1): 287–306.
- Muntohar, A.S. 2004. Swelling and compressibility characteristics of soil-bentonite mixtures. *Civil Engineering Dimension*, **5**(2): pp-93.
- Nader, F., Silvani, C., and Djeran-Maigre, I. 2017. Grain breakage under uniaxial compression using a three-dimensional discrete element method. *Granular Matter*, **19**(3): 53.
- Noiret, A., Bethmont, S., Bosgiraud, J.-M., and Foin, R. 2016. DOPAS Work Package 4 Deliverable 4.8 FSS Experiment Summary Report.
- Norrish, K. 1954. The swelling of montmorillonite. *Discussions of the Faraday society*, **18**: 120–134.
- Pasquiou, A. 2001. Pellets d'argiles gonflantes. Elaboration et caractérisation hydromécanique. PhD Thesis, Université des Sciences et Technologie de Lille.
- Pusch, R. 1980. Swelling pressure of highly compacted bentonite. Svensk Kaernbraenslefoersoerjning AB.
- Pusch, R. 1982. Mineral–water interactions and their influence on the physical behavior of highly compacted Na bentonite. *Canadian Geotechnical Journal*, **19**(3): 381–387. NRC Research Press. doi:10.1139/t82-041.
- Pusch, R., Bluemling, P., and Johnson, L. 2003. Performance of strongly compressed MX-80 pellets under repository-like conditions. *Applied Clay Science*, **23**(1): 239–244. doi:10.1016/S0169-1317(03)00108-X.
- Pusch, R., and Yong, R.N. 2006. Microstructure of smectite clays and engineering performance. CRC Press.
- Rao, S.M. 2006. Identification and classification of expansive soils. Taylor and Francis, London.
- Razakamanantsoa, A.R., Barast, G., and Djeran-Maigre, I. 2012. Hydraulic performance of activated calcium bentonite treated by polyionic charged polymer. *Applied Clay Science*, **59–60**: 103–114. doi:10.1016/j.clay.2012.01.022.
- Razakamanantsoa, A.R., and Djeran-Maigre, I. 2016. Long term chemo-hydro-mechanical behavior of compacted soil bentonite polymer complex submitted to synthetic leachate. *Waste Management*, **53**: 92–104. doi:10.1016/j.wasman.2016.04.023.
- Ridley, A.M. 1993. The measurement of soil moisture suction. PhD Thesis, University of London.
- Robinet, J.C., Gatabin, C., Imbert, C., and Michau, N. 2003. Study of the effectes of an alkaline plume on the hydraulic and hydro-mechanical properties of the bentonite MX80- Final Report ANDRA C.RP.0EUG.02.009.
- Robinet, J.-C., Sardini, P., Coelho, D., Parneix, J.-C., Prêt, D., Sammartino, S., Boller, E., and Altmann, S. 2012. Effects of mineral distribution at mesoscopic scale on solute diffusion in a clay-rich rock: Example of the Callovo-Oxfordian mudstone (Bure, France). *Water Resources Research*, **48**(5). doi:10.1029/2011WR011352.
- Romero, E. 2013. A microstructural insight into compacted clayey soils and their hydraulic properties. *Engineering Geology*, **165**: 3–19. doi:10.1016/j.enggeo.2013.05.024.
- Romero, E., Della Vecchia, G., and Jommi, C. 2011. An insight into the water retention properties of compacted clayey soils. *Géotechnique*, **61**(4): 313–328. ICE Publishing. doi:10.1680/geot.2011.61.4.313.
- Romero, E., Gens, A., and Lloret, A. 1999. Water permeability, water retention and microstructure of unsaturated compacted Boom clay. *Engineering Geology*, **54**(1): 117–127. doi:10.1016/S0013-7952(99)00067-8.
-

- Rosato, A.D., Dybenko, O., Horntrop, D.J., Ratnaswamy, V., and Kondic, L. 2010. Microstructure evolution in density relaxation by tapping. *Physical Review E*, **81**(6): 061301. American Physical Society. doi:10.1103/PhysRevE.81.061301.
- Saba, S., Barnichon, J.-D., Cui, Y.-J., Tang, A.M., and Delage, P. 2014a. Microstructure and anisotropic swelling behaviour of compacted bentonite/sand mixture. *Journal of Rock Mechanics and Geotechnical Engineering*, **6**(2): 126–132. doi:10.1016/j.jrmge.2014.01.006.
- Saba, S., Delage, P., Lenoir, N., Cui, Y.J., Tang, A.M., and Barnichon, J.-D. 2014b. Further insight into the microstructure of compacted bentonite–sand mixture. *Engineering Geology*, **168**: 141–148. doi:10.1016/j.enggeo.2013.11.007.
- Saiyouri, N., Hicher, P.Y., and Tessier, D. 2000. Microstructural approach and transfer water modelling in highly compacted unsaturated swelling clays. *Mechanics of Cohesive-frictional Materials*, **5**(1): 41–60. Wiley. doi:10.1002/(SICI)1099-1484(200001)5:1<41::AID-CFM75>3.0.CO;2-N.
- Saiyouri, N., Tessier, D., and Hicher, P.Y. 2004. Experimental study of swelling in unsaturated compacted clays. *Clay Minerals*, **39**(4): 469–479. GeoScienceWorld. doi:10.1180/0009855043940148.
- Schanz, T., and Tripathy, S. 2009. Swelling pressure of a divalent-rich bentonite: Diffuse double-layer theory revisited. *Water Resources Research*, **45**(5). doi:10.1029/2007WR006495.
- Seiphoori, A. 2014. Thermo-hydro-mechanical characterisation and modelling of MX-80 granular bentonite. PhD Thesis, École Polytechnique Fédérale de Lausanne.
- Seiphoori, A., Ferrari, A., and Laloui, L. 2014. Water retention behaviour and microstructural evolution of MX-80 bentonite during wetting and drying cycles. *Géotechnique*, **64**(9): 721–734. ICE Publishing. doi:10.1680/geot.14.P.017.
- Shariatmadari, N., Salami, M., and Karimpour-Fard, M. 2011. Effect of inorganic salt solutions on some geotechnical properties of soil-bentonite mixtures as barriers. *International Journal of Civil Engineering*, **9**(2): 102–110.
- Shirazi, S.M., Wiwat, S., Kazama, H., Kuwano, J., and Shaaban, M.G. 2011. Salinity effect on swelling characteristics of compacted bentonite. *Environment Protection Engineering*, **37**(2): 65–74.
- Siddiqua, S., Blatz, J., and Siemens, G. 2011. Evaluation of the impact of pore fluid chemistry on the hydromechanical behaviour of clay-based sealing materials. *Canadian Geotechnical Journal*, **48**(2): 199–213. NRC Research Press. doi:10.1139/T10-064.
- Silbert, L.E., Ertas, D., Grest, G.S., Halsey, T.C., and Levine, D. 2002. Geometry of frictionless and frictional sphere packings. *Physical Review E*, **65**(3): 031304. American Physical Society. doi:10.1103/PhysRevE.65.031304.
- SKB. 2011. Backfilling of deposition tunnels: Use of bentonite pellets. SKB P-11-44.
- Sridharan, A., Rao, A.S., and Sivapullaiah, P.V. 1986. Swelling Pressure of Clays. *Geotechnical Testing Journal*, **9**(1): 24–33. ASTM International. doi:10.1520/GTJ10608J.
- Standish, N., and Borger, D.E. 1979. The porosity of particulate mixtures. *Powder Technology*, **22**(1): 121–125. doi:10.1016/0032-5910(79)85014-7.
- Standish, N., and Collins, D.N. 1983. The permeability of ternary particulate mixtures for laminar flow. *Powder Technology*, **36**(1): 55–60. doi:10.1016/0032-5910(83)80008-4.
- Stastka, J., and Smutek, J. 2015. Experimental works with bentonite pellets at the CEG. *In Proceedings of the LUCOEX conference and workshop–full-scale demonstration tests in technology development of repositories for disposal of radioactive waste*. pp. 179–184.
- Stastka, J., Svoboda, J., and Vasicek, R. 2019. Bentonite Pellets in the Construction of a Deep Geological Repository.
- Stoltz, G., Cuisinier, O., and Masroui, F. 2012. Multi-scale analysis of the swelling and shrinkage of a lime-treated expansive clayey soil. *Applied Clay Science*, **61**: 44–51. doi:10.1016/j.clay.2012.04.001.

- 
- Sun, H., Mařín, D., Najser, J., Neděla, V., and Navrátilová, E. 2018. Bentonite microstructure and saturation evolution in wetting–drying cycles evaluated using ESEM, MIP and WRC measurements. *Géotechnique*, **69**(8): 713–726. ICE Publishing. doi:10.1680/jgeot.17.P.253.
- Tang, A.-M., Cui, Y.-J., Eslami, J., and Défossez, P. 2009. Analysing the form of the confined uniaxial compression curve of various soils. *Geoderma*, **148**(3): 282–290. doi:10.1016/j.geoderma.2008.10.012.
- Tang, C.S., Tang, A.M., Cui, Y.-J., Delage, P., Schroeder, C., and De Laure, E. 2011a. Investigating the swelling pressure of compacted crushed-Calovo-Oxfordian claystone. *Physics and Chemistry of the Earth, Parts A/B/C*, **36**(17–18): 1857–1866.
- Tang, C.S., Tang, A.M., Cui, Y.-J., Delage, P., Schroeder, C., and Shi, B. 2011b. A study of the hydro-mechanical behaviour of compacted crushed argillite. *Engineering geology*, **118**(3–4): 93–103.
- Teodori, S.P., Weber, H.P., Köhler, S., Mueller, H.R., Ploetze, M., and Holl, M. 2012. Granular bentonite production as buffer material for a full-scale emplacement ('FE') experiment. *Clays in natural and engineered barriers for radioactive waste confinement - 5 International meeting Book of abstracts*, (p. 923). France,.
- Terzaghi, K. 1943. *Theoretical Soil Mechanics*. JohnWiley & Sons. John Wiley & Sons New York.
- Tu, S.Q. 2011. Contribution à l'étude du comportement thermo hydro mécanique des bouchons d'alvéole et scellements de galerie dans les ouvrages de stockages de déchets radioactifs. PhD Thesis, INSA de Rennes.
- Unikowski, Z.R. 1982. Influence des argiles sur les propriétés des mortiers de ciment. *Laboratoire Central des Ponts et Chaussées*, (110): 4–82.
- Vaid, Y.P., and Negussey, D. 1984. Relative Density of Pluviated Sand Samples. *Soils and Foundations*, **24**(2): 101–105. doi:10.3208/sandf1972.24.2\_101.
- de la Vaissière, R., Conil, N., Morel, J., Leveau, F., Gatabin, C., Garcia-Sineriz, J.L., Habos, H., Rey, M., Piedevache, M., Helminger, B., and Balland, C. 2014. Design and construction of a large-scale sand-bentonite seal in the Meuse/Haute Marne underground research laboratory: NSC experiment. *Bundesanstalt für Geowissenschaften und Rohstoffe (BGR)*. pp. 133–135.
- Van Geet, M., Volckaert, G., and Roels, S. 2005. The use of microfocus X-ray computed tomography in characterising the hydration of a clay pellet/powder mixture. *Applied Clay Science*, **29**(2): 73–87. doi:10.1016/j.clay.2004.12.007.
- Vandewalle, N., Lumay, G., Gerasimov, O., and Ludewig, F. 2007. The influence of grain shape, friction and cohesion on granular compaction dynamics. *The European Physical Journal E*, **22**(3): 241–248. doi:10.1140/epje/e2007-00031-0.
- Villar, M.V. 2002. Thermo-hydro-mechanical characterisation of a bentonite from Cabo de Gata. A study applied to the use of bentonite as sealing material in high level radioactive waste repositories. *Publicación Técnica ENRESA*, **1**(2002): 258.
- Villar, M.V. 2005. MX-80 bentonite. Thermo-hydro-mechanical characterisation performed at CIEMAT in the context of the Prototype Project. *Informes Técnicos CIEMAT*, **1053**: 39.
- Villar, M.V., Gómez-Espina, R., and Gutiérrez-Nebot, L. 2012. Basal spacings of smectite in compacted bentonite. *Applied Clay Science*, **65–66**: 95–105. doi:10.1016/j.clay.2012.05.010.
- Villar, M.V., Gómez-Espina, R., and Lloret, A. 2010. Experimental investigation into temperature effect on hydro-mechanical behaviours of bentonite. *Journal of Rock Mechanics and Geotechnical Engineering*, **2**(1): 71–78. doi:10.3724/SP.J.1235.2010.00071.
- Villar, M.V., and Lloret, A. 2007. Dismantling of the first section of the FEBEX in situ test: THM laboratory tests on the bentonite blocks retrieved. *Physics and Chemistry of the Earth, Parts A/B/C*, **32**(8): 716–729. doi:10.1016/j.pce.2006.03.009.
- Villar, M.V., and Lloret, A. 2008. Influence of dry density and water content on the swelling of a compacted bentonite. *Applied Clay Science*, **39**(1–2): 38–49.
-

- Wang, L., Bornert, M., Chanchole, S., and Héripré, E. 2013a. Experimental investigation of the free swelling of crushed argillite. *Géotechnique Letters*, **3**(2): 89–92. ICE Publishing. doi:10.1680/geolett.13.00012.
- Wang, Q., Cui, Y.-J., Tang, A.M., Delage, P., Gatmiri, B., and Ye, W.-M. 2014. Long-term effect of water chemistry on the swelling pressure of a bentonite-based material. *Applied Clay Science*, **87**: 157–162. doi:10.1016/j.clay.2013.10.025.
- Wang, Q., Minh Tang, A., Cui, Y.-J., Delage, P., Barnichon, J.-D., and Ye, W.-M. 2013b. The effects of technological voids on the hydro-mechanical behaviour of compacted bentonite–sand mixture. *Soils and Foundations*, **53**(2): 232–245. doi:10.1016/j.sandf.2013.02.004.
- Wang, Q., Tang, A.M., Cui, Y.-J., Delage, P., and Gatmiri, B. 2012. Experimental study on the swelling behaviour of bentonite/claystone mixture. *Engineering Geology*, **124**: 59–66. doi:10.1016/j.enggeo.2011.10.003.
- Wei, H., Ge, Y., Li, M., Li, Y., Saxén, H., He, Z., and Yu, Y. 2020. DEM study of the porosity distribution of pellet sandpile formed by ternary size particles. *Powder Technology*, **360**: 1337–1347. Elsevier. doi:10.1016/j.powtec.2019.11.017.
- Westman, A.E.R., and Hugill, H.R. 1930. The packing of particles. *Journal of the American Ceramic Society*, **13**(10): 767–779.
- Wiącek, J. 2016. Geometrical parameters of binary granular mixtures with size ratio and volume fraction: experiments and DEM simulations. *Granular Matter*, **18**(3): 42.
- Xu, Z., Xu, N., and Wang, H. 2019. Effects of Particle Shapes and Sizes on the Minimum Void Ratios of Sand. *Advances in Civil Engineering*, **2019**: 1–12. doi:10.1155/2019/5732656.
- Ye, W.M., Zheng, Z.J., Chen, B., Chen, Y.G., Cui, Y.J., and Wang, J. 2014. Effects of pH and temperature on the swelling pressure and hydraulic conductivity of compacted GMZ01 bentonite. *Applied Clay Science*, **101**: 192–198. doi:10.1016/j.clay.2014.08.002.
- Yi, L.Y., Dong, K.J., Zou, R.P., and Yu, A.B. 2011. Coordination Number of the Packing of Ternary Mixtures of Spheres: DEM Simulations versus Measurements. *Industrial & Engineering Chemistry Research*, **50**(14): 8773–8785. American Chemical Society. doi:10.1021/ie200765h.
- Yigzaw, Z.G., Cuisinier, O., Massat, L., and Masrouri, F. 2016. Role of different suction components on swelling behavior of compacted bentonites. *Applied Clay Science*, **120**: 81–90. doi:10.1016/j.clay.2015.11.022.
- Yu, A.B., and Standish, N. 1987. Porosity calculations of multi-component mixtures of spherical particles. *Powder Technology*, **52**(3): 233–241. doi:10.1016/0032-5910(87)80110-9.
- Yu, A.-B., Zou, R.-P., and Standish, N. 1992. Packing of Ternary Mixtures of Nonspherical Particles. *Journal of the American Ceramic Society*, **75**(10): 2765–2772. doi:10.1111/j.1151-2916.1992.tb05502.x.
- Yven, B., Sammartino, S., Geraud, Y., Homand, F., and Villieras, F. 2007. Mineralogy, texture and porosity of Callovo-Oxfordian argillites of the Meuse/Haute-Marne region (eastern Paris Basin). *Mémoires de la Société géologique de France*, **178**(1): 73–90.
- Zeng, Z., Cui, Y.-J., Zhang, F., Conil, N., and Talandier, J. 2019. Investigation of swelling pressure of bentonite/claystone mixture in the full range of bentonite fraction. *Applied Clay Science*, **178**: 105137. doi:10.1016/j.clay.2019.105137.
- Zeng, Z., Cui, Y.-J., Zhang, F., Conil, N., and Talandier, J. 2020. Effect of technological voids on the swelling behaviour of compacted bentonite/claystone mixture. *Canadian Geotechnical Journal*, NRC Research Press. doi:10.1139/cgj-2019-0339.
- Zhang, C.-L. 2014. Characterization of excavated claystone and claystone–bentonite mixtures as backfill/seal material. *Geological Society, London, Special Publications*, **400**(1): 323–337. Geological Society of London. doi:10.1144/SP400.28.
- Zhang, C.-L., and Kröhn, K.-P. 2019. Sealing behaviour of crushed claystone–bentonite mixtures. *Geomechanics for Energy and the Environment*, **17**: 90–105. doi:10.1016/j.gete.2018.09.004.

- 
- Zhang, H.-Y., Cui, S.-L., Zhang, M., and Jia, L.-Y. 2012. Swelling behaviors of GMZ bentonite–sand mixtures inundated in NaCl–Na<sub>2</sub>SO<sub>4</sub> solutions. *Nuclear Engineering and Design*, **242**: 115–123. doi:10.1016/j.nucengdes.2011.10.042.
- Zhang, Z., Ye, W.-M., Liu, Z.-R., Chen, B., and Cui, Y.-J. 2018. Influences of PSD curve and vibration on the packing dry density of crushed bentonite pellet mixtures. *Construction and Building Materials*, **185**: 246–255. doi:10.1016/j.conbuildmat.2018.07.096.
- Zhang, Z.P., Liu, L.F., Yuan, Y.D., and Yu, A.B. 2001. A simulation study of the effects of dynamic variables on the packing of spheres. *Powder Technology*, **116**(1): 23–32. doi:10.1016/S0032-5910(00)00356-9.
- Zheng, J., Carlson, W.B., and Reed, J.S. 1995. The packing density of binary powder mixtures. *Journal of the European Ceramic Society*, **15**(5): 479–483. doi:10.1016/0955-2219(95)00001-B.
- Zhou, Y.C., Xu, B.H., Yu, A.B., and Zulli, P. 2002. An experimental and numerical study of the angle of repose of coarse spheres. *Powder Technology*, **125**(1): 45–54. doi:10.1016/S0032-5910(01)00520-4.
- Zou, R.P., Gan, M.L., and Yu, A.B. 2011. Prediction of the porosity of multi-component mixtures of cohesive and non-cohesive particles. *Chemical engineering science*, **66**(20): 4711–4721.
- Zou, R.P., and Yu, A.B. 1996. Evaluation of the packing characteristics of mono-sized non-spherical particles. *Powder Technology*, **88**(1): 71–79. doi:10.1016/0032-5910(96)03106-3.



---

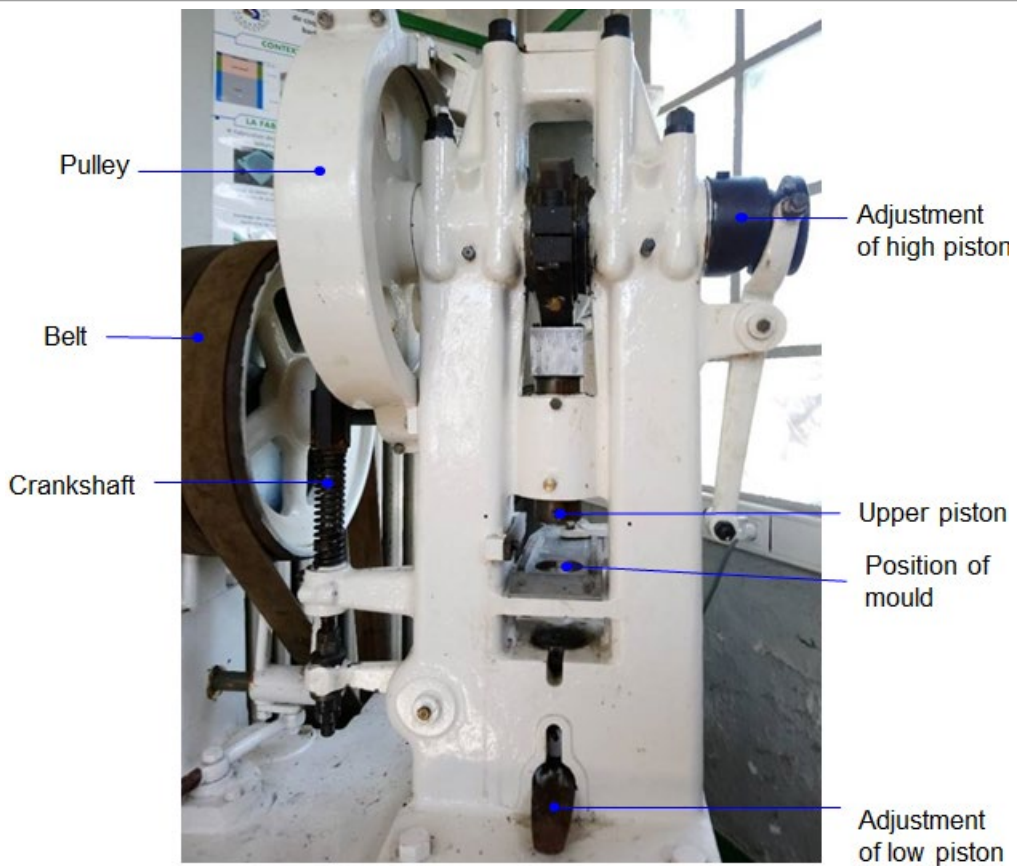
## Appendix A: Tablet machine

The reconditioned tablet machine used for the pelletization (Figure A-1) and the designs of the fabricated accessories are presented in more details.

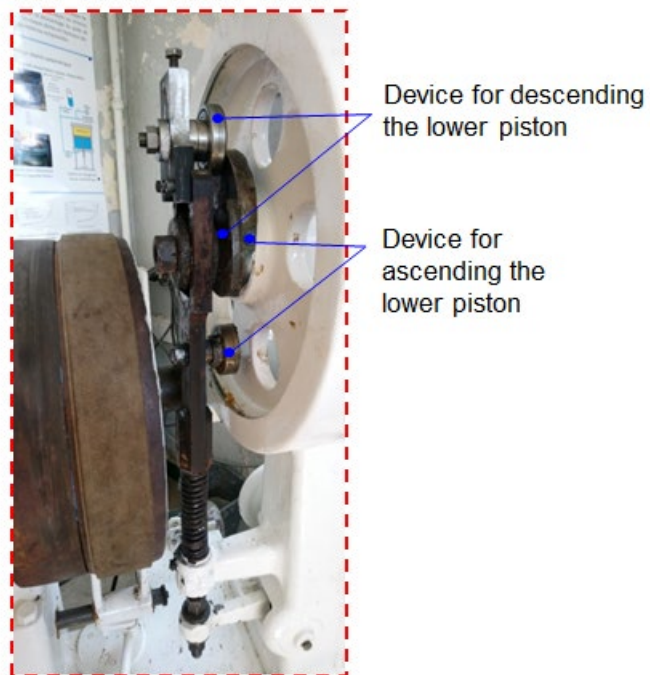
The table press (Frogerais 1B) was reconditioned for the needs of the present project. The machine consists of a motor that drives a pulley on the axis of the crankshaft via a belt. A second pulley is activated by the transfer of the belt, which triggers two pistons in the upper and bottom part of a metallic frame. The pistons are responsible for the material's compaction. On Figure A-2, the different parts of the tablet machine are described, showing also the devices responsible for the adjustment of the pistons position. Figure A-3 presents the funnel through which the material is inserted and the moving mechanism that deposit the raw material inside the mould.



Figure A-1 Frogerais 1B tablet press machine used for the pellet fabrication.



(a)



(b)

Figure A-2 Description of (a) the machine's different parts and (b) the mechanisms allowing the lower piston's movement.

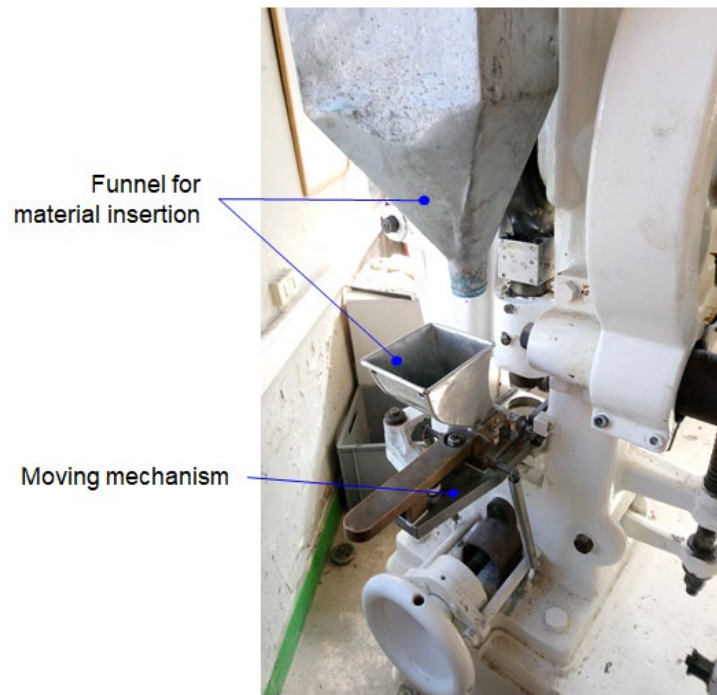


Figure A-3 Description of the machine's pack part.

Specific accessories of the pellet machine were necessary to carry out the fabrication of the target sizes. Moulds and punch tools were meticulously designed to produce the pellets of quasi-spherical shape, having diameters of 16 mm, 10 mm and 4 mm. In particular, the accessories for the diameter of 10 mm were already available upon the purchase of the tablet machine. Therefore, in this case only the punch tools were designed, since modifications on the curvature radius of the punch tool's edge were finally necessary for the CO<sub>x</sub>/MX80 mixtures.



## Appendix B: Examination of pellet production in semi-industrial scale

The report presents in details the experimental data regarding the pellet production. The details concern the measured intra-pellet density, the percentage of produced intact pellet and the ease level of compaction. The observed type of pellet damage is also listed. The results concerning the effect of COx initial state on the pellet production are given on Table B-1 and Table B-2. Table B-3 and Table B-4 illustrate the influence of COx/MX80 mixtures water content and MX80 content contained in the mixture respectively. On each table, the most favourable conditions were highlighted in red colour.

Table B-1 Effect of COx argillite's granulometry with original water content conditions on the pellet production.

| Pellet diameter (mm)  | Punch tool position  |                      | MX80 content   | COx granulometry  | COx water content, w | Intra-pellet dry density, $\rho_{d\text{ pellet}}$ (Mg/m <sup>3</sup> ) | Ease of compaction | Percentage of intact pellets (%) | Observations  |
|---|----------------------|----------------------|----------------|---|----------------------|---|--------------------|----------------------------------|---|
|   | Upper <sup>(a)</sup> | Upper <sup>(b)</sup> |                |   |                      |   |                    |                                  |   |
| 10  | 9                    | 17                   | 40%MX80        | Doriginal (30% <200 $\mu\text{m}$ )                           | Initial              | -   | Very difficult     | -                                | Pellet de-cohesion upon decompaction from the machine |
| 10  | 9                    | 17                   | 40%MX80        | D20 (20% <200 $\mu\text{m}$ )                                 | Initial              | -   | Very difficult     | 50                               | Pellet de-cohesion upon decompaction from the machine |
| 10  | 9                    | 17                   | 40%MX80        | D30 (30% <200 $\mu\text{m}$ )                                 | Initial              | -   | Difficult          | 50                               | Pellet de-cohesion upon decompaction from the machine |
| <b>10</b>   | <b>9</b>             | <b>17</b>            | <b>40%MX80</b> | <b>D10 = Dmodified (10% &lt;200 <math>\mu\text{m}</math>)</b> | <b>Initial</b>       | <b>2.05</b>   | <b>Easy</b>        | <b>100</b>                       | <b>-</b>  |
| <sup>(a)</sup> indicated on the adjustment ring<br><sup>(b)</sup> depth of filling height in mm<br>Initial: water content of reception conditions<br>Doriginal: COx original granulometry at the reception, Dmodified: 10% <200 $\mu\text{m}$ |                      |                      |                |   |                      |   |                    |                                  |   |

Table B-2 Effect of COx argillite's water content on pellet production.

| Pellet diameter (mm) | Punch tool position  |                      | MX80 content | COx granulometry | COx water content, w | Mixture's water content (%) | Ease of compaction | Percentage of intact pellets (%) | Observations  |
|----------------------|----------------------|----------------------|--------------|------------------|----------------------|-----------------------------|--------------------|----------------------------------|---|
|                      | Upper <sup>(a)</sup> | Upper <sup>(b)</sup> |              |                  |                      |                             |                    |                                  |   |
| 16                   | N°3+1/2              | 25 mm                | 30%MX80      | Dmodified        | Initial              | 7.85                        | Easy               | 95                               | -   |
| 16                   | N°3+1/2              | 25 mm                | 30%MX80      | Doriginal        | Initial              | 8.30                        | Very difficult     | -                                | Pellet de-cohesion upon decompaction from the machine |
| 16                   | N°3+1/2              | 25 mm                | 30%MX80      | Doriginal        | 7.30                 | 8.67                        | Difficult          | 35                               | Material attachment                                   |
| 16                   | N°3+1/2              | 25 mm                | 30%MX80      | Doriginal        | 7.79                 | 9.04                        | Difficult          | 65                               | Material attachment                                   |
| 16                   | N°3+1/2              | 25 mm                | 30%MX80      | Doriginal        | 8.15                 | 9.10                        | Difficult          | 80                               | Material attachment                                   |
| 16                   | N°3+1/2              | 25 mm                | 30%MX80      | Doriginal        | 8.30                 | 9.30                        | Difficult          | 90                               | Material attachment                                   |
| 16                   | N°3+1/2              | 25 mm                | 30%MX80      | Doriginal        | 8.53                 | 9.47                        | Easy               | 95                               | Slight material attachment                            |
| 16                   | N°3+1/2              | 25 mm                | 30%MX80      | Doriginal        | 8.70                 | 9.51                        | Difficult          | 90                               | Material attachment                                   |
| 16                   | N°3+1/2              | 25 mm                | 30%MX80      | Doriginal        | 9.07                 | 9.63                        | Difficult          | 50                               | Material attachment                                   |

<sup>(a)</sup> indicated on the adjustment ring  
<sup>(b)</sup> depth of filling height in mm  
Initial: water content of reception conditions, Dmodified: 10%<200 µm, Doriginal: original COx granulometry

Table B-3 Effect of COx/MX80 mixtures water content on pellet production.

| Pellet diameter (mm) | Punch tool position  |                      | MX80 content   | COx granulometry | Mixture's water content (%)       | Intra-pellet dry density, $\rho_{d\ pellet}$ (Mg/m <sup>3</sup> ) | Ease of compaction | Percentage of intact pellets (%) | Observations  |
|----------------------|----------------------|----------------------|----------------|------------------|-----------------------------------|---|--------------------|----------------------------------|---|
|                      | Upper <sup>(a)</sup> | Upper <sup>(b)</sup> |                |                  |                                   |   |                    |                                  |   |
| 10                   | 9                    | 17                   | 40%MX80        | Dmodified        | 6.15 < w <sub>initial</sub>       | 2.03  | Very difficult     | -                                | Pellet de-cohesion upon decompaction from the machine |
| <b>10</b>            | <b>9</b>             | <b>17</b>            | <b>40%MX80</b> | <b>Dmodified</b> | <b>7.85 = w<sub>initial</sub></b> | <b>2.07</b>   | <b>Easy</b>        | <b>100</b>                       | <b>-</b>  |
| 10                   | 9                    | 17                   | 40%MX80        | Dmodified        | 12.84 > w <sub>initial</sub>      | 1.98  | Easy               | 5                                | Material attachment                                   |

<sup>(a)</sup> indicated on the adjustment ring  
<sup>(b)</sup> depth of filling height in mm  
 Doriginal: COx original granulometry at the reception, w<sub>initial</sub> : COx/MX80 water content of reception conditions

Table B-4 Effect of MX80 bentonite content on pellet production.

| Pellet diameter (mm) | Punch tool position  |                      | MX80 content   | COx granulometry | COx water content, w | Intra-pellet dry density, $\rho_{d\ pellet}$ (Mg/m <sup>3</sup> ) | Ease of compaction | Percentage of intact pellets (%) | Observations               |
|----------------------|----------------------|----------------------|----------------|------------------|----------------------|---|--------------------|----------------------------------|----------------------------|
|                      | Upper <sup>(a)</sup> | Upper <sup>(b)</sup> |                |                  |                      |   |                    |                                  |                            |
| <b>10</b>            | <b>9</b>             | <b>17</b>            | <b>40%MX80</b> | <b>Dmodified</b> | <b>Initial</b>       | <b>2.05</b>   | <b>Easy</b>        | <b>100</b>                       | <b>-</b>                   |
| 10                   | 8+1/3                | 16.5                 | 30%MX80        | Dmodified        | Initial              | 2.05  | Difficult          | 75                               | Material attachment        |
| <b>10</b>            | <b>7+2/3</b>         | <b>16</b>            | <b>30%MX80</b> | <b>Dmodified</b> | <b>Initial</b>       | <b>1.95</b>   | <b>Difficult</b>   | <b>80</b>                        | <b>Material attachment</b> |
| 10                   | 7+2/3                | 16                   | 20%MX80        | Dmodified        | Initial              | 2.03  | Very difficult     | 50                               | Material attachment        |

<sup>(a)</sup> indicated on the adjustment ring  
<sup>(b)</sup> depth of filling height in mm  
 Dmodified: 10%<200  $\mu$ m, Initial: water content of reception conditions



---

# Résumé de thèse

## 1. Introduction – Contexte

Dans le cadre de la gestion des déchets radioactifs à haute activité à vie longue, le stockage profond est considéré comme une solution sûre et respectueuse de l'environnement. En France, l'Andra (Agence Nationale pour la gestion de déchets radioactifs) est en charge du projet «Cigéo» (Centre industriel de stockage géologique), solution de référence conçue pour stocker ces déchets à une profondeur de 500 mètres dans la formation argileuse du Callovo-Oxfordien (COx) dans l'est du bassin parisien. La sûreté à long terme du stockage repose sur la capacité de confinement de la couche du Callovo-Oxfordien. La création d'un réseau de galeries, d'ouvrages d'accès et d'alvéoles de stockage pourrait induire des chemins préférentiels d'écoulement d'eau dans et le long de ces ouvrages. Le remblaiement des galeries et la mise en place localement de scellements à base d'argiles gonflantes sont conçus pour empêcher / limiter la circulation d'eau dans les installations en après fermeture.

Parmi les solutions étudiées, l'Andra envisage la mise en place de mélanges à base de COx remanié et d'argile gonflante (bentonite MX80), sous la forme de pellets, pour le remblaiement des galeries. L'option pelletisée présente des avantages opérationnels, par la réutilisation du COx excavé qui bénéficie d'une bonne compatibilité géochimique avec la roche environnante tout en minimisant l'utilisation d'un matériau commercial. L'assemblage de pellets est mis en place dans les galeries à l'état sec, présentant ainsi une structure granulaire, qui est progressivement homogénéisée par le gonflement lors de l'hydratation par l'eau provenant de la roche hôte.

La motivation de cette thèse était d'examiner la faisabilité de mettre en œuvre un matériau en pellets constitué de COx, dopé avec de la bentonite MX80, ainsi que la réponse hydromécanique du mélange dans les conditions d'environnement du stockage. L'étude comprend la conception, la fabrication et l'analyse du mélange granulaire utilisé. Les pellets doivent être fabriqués à une échelle semi-industrielle, en utilisant pour la première fois l'argilite du COx.

Plus précisément, les objectifs se concentrent principalement sur les aspects suivants:

1. La sélection du mélange des pellets selon la granulométrie, qui maximise la densité de la mise en place (conditions optimales).
2. La fabrication des pellets COx/MX80 pour la granulométrie optimale choisie.
3. L'évaluation expérimentale hydromécanique (pression de gonflement, potentiel de gonflement) des mélanges COx/MX80 en poudre, en fonction de la densité cible de l'assemblage des pellets.
4. L'étude hydromécanique (pression de gonflement et conductivité hydraulique) sur les assemblages de pellets, proposés selon l'optimisation de la granulométrie.

## 2. Etat de l'art et stratégie proposée par cette thèse

L'argilite du COx remaniée est envisagée comme matériau potentiellement réutilisable, pour le remblaiement des galeries. Les mises en forme en lien avec une solution industrielle d'installation dans le stockage et son utilisation en mélange pour accroître ses performances hydromécaniques font l'objet d'études poussées. Ce travail de thèse se concentre sur une des solutions potentielles à savoir la pelletisation d'un mélange de COx/MX80. Dans un premier

---

temps, une revue bibliographique sur l'identification des paramètres essentiels pour la mise en œuvre des pellets d'argilite/bentonite a été effectuée.

Les faibles propriétés de gonflement du COx nécessitent de l'utiliser en mélange avec une argile gonflante ici la MX80 pour répondre aux exigences de conception en termes de potentiel de gonflement. Néanmoins, le pourcentage de bentonite MX80 ne doit pas excéder 50% afin de minimiser les coûts des remblais. Dans ce cadre, plusieurs paramètres affectent la réponse finale du matériau conformément aux exigences de Cigéo :

- Teneur en bentonite (%MX80),
- État de compactage initial (la densité sèche du matériau),
- Compositions chimiques des eaux infiltrées (eaux souterraines et conditions alcalines).

Des études antérieures (Hoffman et al. 2005, Imbert and Villar 2006, Karnland et al. 2008) montrent que les pressions de gonflement sont indépendantes de l'état initial (poudres ou granulaires) et sont gouvernées par la densité sèche finale. La réponse hydromécanique des pellets de bentonite est identique à celle du matériau «en poudre» pour les mêmes densités. Aucune étude n'a été réalisée sur le comportement hydromécanique des pellets COx/bentonite.

Cette étude porte sur l'état de compacité (densité de la mise en place) du matériau granulaire, pour atteindre la cible des propriétés de gonflement souhaitées. La relation de gonflement avec la densité sera réalisée sur des mélanges poudre de COx/MX80. En plus, le matériau en pellets sera fabriqué pour aboutir à la densité souhaitée, à partir des caractéristiques granulométriques et le protocole de mise en œuvre.

Dans ce cadre, le programme expérimental suivant a été proposé:

1. Étude numérique en utilisant la méthode DEM, sur l'optimisation de la distribution granulométrique, afin d'obtenir l'état le plus dense.
2. La fabrication de pellets COx/MX80, pour les tailles sélectionnées par la DEM.
3. Étude expérimentale permettant d'une part d'évaluer l'étude numérique de l'assemblage des pellets préconisé par la DEM, et d'autre part, une augmentation de la densité par des essais supplémentaires en faisant appel à des matériaux non pelletisés (concassés de pellets et sable).
4. Evaluation de la densité de mise en place à partir des poudres des mélanges COx/MX80 pour atteindre les propriétés de gonflement souhaitées.
5. Etude expérimentale sur le comportement hydromécanique de pellets COx/MX80 sur la granulométrie sélectionnée.

---

### 3. Etude numérique sur l'optimisation de l'assemblage de pellets

La granulométrie optimale vise à obtenir une densité maximale. Dans ce contexte, des simulations numériques par la méthode des éléments discrets (DEM) ont été mises en œuvre afin de réaliser des dépôts gravitationnels des échantillons constitués de sphères de différents diamètres. Ainsi chaque simulation numérique permet d'évaluer la densité de mise en place. L'outil numérique utilisé est le logiciel libre LMGC<sup>90</sup>, qui se base sur la méthode NSCD (Non-Smooth Contact Dynamics) aux collections de corps rigides et/ou déformables (Jean 1999). Les forces de contact sont décrites par la loi de Signorini, qui identifie un système binaire unique candidat/antagoniste. Il s'agit d'une loi de contact unilatéral non régulière, en considérant des corps impénétrables. La loi de frottement de Coulomb s'applique en cas de contact sec sans cohésion entre les particules.

Une granulométrie ( $d_i$ , % $d_i$ ) prédéfinie est générée et déposée par une hauteur fixée dans un conteneur rectangulaire de dimensions données ( $l_x = l_y = l_z = 10 \cdot d_{max}$ ). Initialement, l'échantillon de sphères rigides, est généré avec une densité faible à l'intérieur des cinq parois de la boîte. La 6<sup>ème</sup> paroi est en contact avec la sphère qui se trouve à position la plus haute, ce qui permet de déterminer la hauteur de l'échantillon. Le coefficient de frottement inter-particules est également donné. Le frottement des particules avec la cellule est négligé. Lorsque l'énergie cinétique devient égale à zéro, le réarrangement des particules est terminé. À la fin du dépôt, et ayant extrait le volume final (résultats globaux), le volume des sphères solides est recalculé à l'aide d'une paroi fictive, réduisant les effets des bords et d'échelle et essayant de s'approcher au mieux des conditions qui règnent *in situ* dans les galeries (résultats recalculés).

Des échantillons bimodaux et trimodaux ont été testés. Les tailles des sphères étaient compatibles avec la pelletisation, ainsi qu'avec les moyens de mesure du laboratoire. L'impact des proportions volumétriques (% $d_i$ ) et du rapport de taille  $\alpha_i$  ( $d_i/d_{max}$ ) sur l'état le plus dense est évalué ultérieurement. L'effet du dépôt et de l'angle de frottement a été examiné sur la granulométrie optimale.

Les résultats des simulations numériques ont montré un impact des différentes méthodes de calcul de la densité (résultats globaux et recalculés) : les résultats recalculés présentent un état plus dense que les résultats globaux. Cependant, dans les deux cas, le modèle a présenté une répétabilité élevée en termes de granulométrie générée et de densité. Ces simulations ont permis d'établir les conclusions suivantes :

- Echantillons bimodaux : la densité maximale a été observée pour les pourcentages volumiques de diamètre maximal (% $d_{max}$ ) de 60 à 70%. La densité maximale a été obtenue lorsque le rapport de taille  $\alpha_{min}$  diminuait, tandis que pour  $\alpha_{min} > 0,6$ , l'effet sur la densité était moins significative.
- Echantillons trimodaux : l'état le plus dense était présenté lorsque % $d_{max}$  > % $d_{min}$  > % $d_{med}$ . Des vides plus faibles sont observés avec la diminution de la taille minimale des particules ( $\alpha_{min}$ ), en raison de la pénétration des petits grains dans les vides créés par les gros grains. Pour un rapport de taille constant  $\alpha_{min}$ , une très faible variation de la densité sèche maximale a été obtenue (<1%).
- La densité maximale obtenue est indépendante du diamètre intermédiaire. Plus précisément, pour les configurations bimodales et trimodales avec  $d_{max}$  et  $d_{min}$  communs, la même densité a été obtenue avec des proportions volumétriques différentes.

- 
- Une amélioration de la densité est observée avec l'augmentation de la hauteur du dépôt induit par une énergie cinétique plus grande produisant un meilleur réarrangement des particules.
  - L'augmentation du frottement inter-particules empêche le glissement et le réarrangement des particules.
    - ✓ Les tailles de 16-10-4 mm dans des proportions de 60%-10%-30% ont été sélectionnées comme granulométrie DEM optimale. Ils ont conduit à l'une des densités recalculées les plus élevées (erreur absolue de 0,7% par rapport à la valeur de densité maximale observée) et ils ont été considérés comme plus compatibles avec les moyens techniques de pelletisation.

#### 4. Etude sur le processus de pelletisation

Le chapitre se concentre sur la fabrication de pellets de mélanges de COx/MX80 dans des conditions semi-industrielles. Dans le domaine pharmaceutique et plus précisément dans l'industrie des poudres, la méthode de compression est l'une des techniques principales, utilisée pour créer des pellets. Cette technique a été aussi adoptée pour fabriquer des pellets à base d'argile. Dans ce contexte, les mélanges de COx/MX80 en poudre (à l'état de la réception) ont été compactés aux diamètres souhaités, en utilisant une machine à comprimés reconditionnée. Les tailles des pellets cibles sont les diamètres optimaux (16 mm, 10 mm, 4 mm) selon l'étude numérique.

Au début, les mélanges de COx/MX80 sont caractérisés en termes des propriétés d'indice standard (limites d'Atterberg, capacité d'absorption d'eau, indice de gonflement libre). La compressibilité des mélanges a été aussi étudiée, afin de simuler le comportement mécanique du matériau pendant la pelletisation. En parallèle, une presse à comprimés Frogerais reconditionnée, avec ses accessoires a été mise en œuvre pour produire des pellets de taille 16 mm, 10 mm et 4 mm. La production est analysée en fonction de différents paramètres (forme des poinçons, nature des aciers utilisés et traitement thermique associés, teneur en eau des mélanges etc...).

La caractérisation des matériaux a montré que la bentonite MX80 présente un indice de plasticité extrêmement élevé. En revanche, l'argilite du COx est une argile d'indice de plasticité moyen. L'ajout de bentonite dans le mélange COx/MX80 montre que la MX80 augmente la plasticité du mélange, tandis que l'indice de gonflement libre devient plus important.

Les essais de compression œdométrique ( $D = 40$  mm,  $H = 40$  mm) ont été réalisés afin d'évaluer le module de compressibilité œdométrique et la relation pression de compactage-densité sèche. Il a été constaté qu'une pression verticale d'environ 30 MPa est nécessaire pour obtenir une masse volumique sèche de l'ordre de 2.0 Mg/m<sup>3</sup>. Notons ici, que la fabrication des pellets est différente du compactage quasi statique qui définit un ordre de grandeur de la pression de compactage, puisqu'elle est effectuée à grande vitesse. Les remarques suivantes peuvent être soulignées par l'étude du compactage :

- La compressibilité œdométrique des mélanges COx/MX80 en poudre n'est pas ou peu influencée par le pourcentage de bentonite du mélange. La compressibilité est principalement gouvernée pas le COx, cependant, la présence de la MX80 insère des

---

vides initiaux et nécessite une contrainte verticale plus élevée pour atteindre la densité du COx seul.

- La teneur en eau comprise entre 8 à 10% permet d'augmenter la compressibilité et par conséquent d'améliorer la fabrication des pellets. En revanche pour des teneurs en eau plus élevées (~15%), la saturation en eau des espaces interfoliaires produit un gonflement qui s'oppose à la pression de compactage nécessitant des contraintes plus élevées. Ce comportement est également observé lorsque la vitesse de compactage diminue.

La machine à pellets fonctionne aux vitesses de compactage plus élevées ; la formation des pellets est réalisée à la suite d'un « choc ». Le matériau initial est compacté sous forme quasi-sphérique avec une partie cylindrique et deux parties sphériques sur la partie supérieure et inférieure. Les accessoires nécessaires (matrices, poinçons) ont été conçus et fabriqués pour les tailles cibles. Les premiers essais de fabrication des mélanges COx/MX80 se sont avérés décevants notamment par la présence de grains fins durs du COx provoquant les coincements des poinçons dans les matrices. Des outils de poinçonnage et des matrices ont été fabriqués de nouveau à partir d'aciers capables de résister à l'abrasion des particules fines du COx. Après un long processus de recherche d'aciers adaptés ainsi que la géométrie des poinçons, la productivité de la pelletisation a été optimisée, permettant la production de pellets intacts et à forte densité en grande quantité. En plus de ces paramètres que sont la nature des aciers et la géométrie des poinçons, deux autres paramètres ont permis d'accroître la production de la fabrication des pellets:

- La diminution des particules du COx inférieurs à 200  $\mu\text{m}$  a facilité la fabrication de pellets intacts, en gardant la teneur en eau de réception. Cependant, une légère augmentation de la teneur en eau d'origine du COx est apparue comme une solution suffisante pour une production industrielle réussie de granulés.
- L'ajout de COx était un paramètre limitant pour la réalisation des granulés. Par conséquent, une réduction insignifiante de la densité intra-pellet (~5%) a été proposée pour obtenir une fabrication de pellets intacts.

## **5. Etude expérimentale sur l'optimisation de la densité de la mise en place de l'assemblage de pellets**

Après avoir défini la granulométrie optimale par la DEM, une étude expérimentale a été effectuée, afin d'évaluer les biais éventuels entre expérience et modélisation. L'optimisation de la densité a été réalisée à l'aide de dépôts gravitationnels à une échelle très comparable avec celle des simulations. Contrairement aux simulations DEM où la granulométrie est générée en proportions volumiques, l'étude expérimentale travaille en termes de masse totale. La masse volumique intra-pellet sèche était généralement considérée comme 2,0  $\text{Mg/m}^3$ . La comparaison expérience/ modélisation est satisfaisante et reproduit bien les différentes proportions.

Les pellets fabriqués de diamètres de 16 mm, 10 mm and 4 mm ont été testées. De plus, deux types de sable ont été testés : un bien-gradués (WGS) et un mal-gradués avec (PGS) avec des grains inférieurs à 2mm. L'objectif de ces essais a été double : examiner l'effet de la présence d'un matériau « plus fin » dans le mélange de pellets, ainsi que l'influence de sa granulométrie sur la densité de la mise en place. La densité a été mesurée en utilisant deux types de cellules, qui présentent un volume total similaire : un conteneur cubique ( $l_x =$

---

$l_y = 160$  mm,  $l_z = 180$  mm) comme celui utilisé pour les simulations de DEM, et un conteneur cylindrique ( $D \approx 0.155$  m,  $H \approx 0.165$  m). Les dépôts ont été réalisés en préparant des échantillons prémélangés et des échantillons par couches, permettant d'évaluer les effets possibles du protocole de mise en œuvre. Des échantillons bimodaux (16 mm-4 mm), trimodaux (16 mm-10 mm-4 mm, 16 mm-10 mm-WGS, 16mm-4mm-WGS, 16mm-4mm-PGS) et multimodaux (16 mm-10mm-4mm-WGS) ont été testés.

Une discussion détaillée sur les résultats expérimentaux obtenus ainsi que les résultats numériques obtenus au chapitre 3, a permis d'élaborer les conclusions suivantes :

- Le protocole adopté pour la mise en place impacte la densité. Les échantillons préparés par couches présentent un état plus dense que ceux prémélangés. Les interactions des particules sur les parois de la cellule sont plus faibles dans le cas de la méthode par couches.
- La densité du mélange granulaire n'était pas affectée par la forme de la cellule utilisée (cubique/cylindrique).
- Les masses volumiques expérimentales résultantes de la granulométrie optimale obtenues par la DEM (16 mm-10 mm-4 mm en proportions de 60-10-30%) sont:
  - o En général faible ( $\sim 1.30$  Mg/m<sup>3</sup>) pour les deux protocoles de mise en place.
  - o La comparaison avec les calculs numériques de l'étude paramétrique du chapitre 3 a montré que les résultats expérimentaux par couches sont proches des résultats globaux de la DEM. Pour rappel, ces interactions sont négligées sur les simulations de DEM et elles sont faibles pour la préparation par couches.
  - o La comparaison simulations-expériences a permis de déterminer le coefficient de frottement inter-particules, qui a été considéré comme approximativement égal à  $\mu=0,6$  ( $\varphi=30^\circ$ ). Cette valeur est similaire à celle obtenue l'angle de la formation d'un tas du mélange de pellets.
- L'augmentation de la masse volumique du matériau granulaire (1.45-1.60 Mg/m<sup>3</sup>) a été obtenue par l'ajout des grains « plus fin » ( $d < 2$ mm, sable WGS).
- La masse volumique la plus élevée a été réalisée pour deux échantillons trimodaux préparés par couches : 16 mm, 4 mm et sable bien-gradué et 16 mm, 10 mm et sable bien-gradué en proportions de 60%, 10 % et 30% de la masse totale.
  - ✓ La gamme de masse volumique de mise en place qui nous intéresse est d'environ 1,45 à 1,60 Mg/m<sup>3</sup>.
  - ✓ La fabrication de pellets de 4 mm étant plus compliquée (seuls les pellets de bentonite MX80 de diamètres 16 mm et 10mm ont été fabriqués (production chronophage). La granulométrie retenue est de type trimodal de 16 mm, 10 mm et sable bien-gradué (c'est-à-dire composant de grain plus fin) préparé en couches avec les proportions de 60%, 10% et 30% en masse totale.

---

## 6. Etude hydromécanique COx/MX80 à partir de mélanges COx/MX80 en poudre compactées

Les caractéristiques de gonflement (pression de gonflement, potentiel de gonflement) du matériau COx/MX80 sont indépendantes de leur mise en forme (briques, pellets, etc.) et ne dépendent que de la densité sèche (Imbert et Villar, 2006; Hoffmann et al., 2007; Karnland et al., 2008). Ainsi l'évaluation des caractéristiques hydromécaniques (pression de gonflement ou potentiel de gonflement) a été réalisée sur les mélanges en poudre de COx/MX80 ( $\leq 40\%$ MX80) sur des chemins œdométriques pour une gamme de densités attendues pour le remblai entre 1,45-1,60 Mg/m<sup>3</sup>.

Les propriétés physicochimiques (indices de plasticité, indice de gonflement libre, caractéristiques de compactage dynamique) ainsi que la capacité de gonflement à volume constant (pression de gonflement) et à contrainte constante (potentiel de gonflement) ont été déterminées. Pour les deux types d'essais œdométriques, les échantillons de COx/MX80 en poudre ont été compactés aux masses volumiques de 1,45 Mg/m<sup>3</sup> et 1,60 Mg/m<sup>3</sup>. Pour certains essais, l'argilite du COx et la bentonite MX80 ont la teneur en eau de réception ( $w_{COx} \approx 6\%$ ,  $w_{MX80} \approx 12\%$ ). Trois chimies de l'eau interstitielle ont été utilisées pour l'hydratation: eau déminéralisée, eau du site et eau cimentaire (représentative de l'eau du site passant à travers les revêtements de béton). Les essais sur les poudres de COx/MX80 ont été focalisés sur :

- Le pourcentage de bentonite dans le mélange COx/MX80,
- La densité sèche initiale,
- La nature chimique du fluide de saturation (eau de site, eau déminéralisée et eau cimentaire).

L'ensemble des résultats obtenus sur les mélanges COx/MX80 indiquent :

- L'indice de plasticité (limites d'Atterberg) et l'indice de gonflement libre augmentent avec l'augmentation de la teneur en bentonite introduite dans le mélange.
- La densité sèche maximale (Proctor) diminue avec l'augmentation du pourcentage de MX80.
- La chimie de l'eau interstitielle impacte les propriétés de gonflement : l'eau de site et l'eau cimentaire entraînent une diminution du gonflement, par rapport à l'eau déminéralisée.

Les propriétés de gonflement observées à partir des essais sur les mélanges compactés COx/MX80 (c'est-à-dire potentiel de gonflement et pression de gonflement) pour des masses volumiques comprises entre 1,45 à 1,60 Mg/m<sup>3</sup> ont permis d'établir que :

- La pression de gonflement et le potentiel de gonflement augmentent avec l'augmentation de la densité sèche.
- Le potentiel de gonflement suit une augmentation linéaire avec le pourcentage de bentonite.
- La pression de gonflement augmente de manière non-linéaire avec le pourcentage de la MX80.
- Une relation logarithmique du potentiel de gonflement avec la contrainte verticale appliquée a été obtenue, pour tous les mélanges COx/MX80 étudiés hydratés avec de l'eau du site.
- Aucun effet prononcé de la solution alcaline n'a été observé, par rapport à l'eau de site.

- 
- La pression de gonflement présente une augmentation jusqu'à un pic, suivie d'une décroissance et une stabilisation. Ce phénomène a été plus marqué avec la diminution du pourcentage de MX80 et de la densité sèche initiale. Pour les mélanges préparés aux teneurs en eau correspondant aux valeurs optimales de compactage optimales (Proctor standard), cette cinétique n'a pas été observée. Par contre, une faible diminution de la pression de gonflement a été obtenue pour l'augmentation de la teneur en eau, en particulier pour les pourcentages de bentonite plus élevés.
  - L'étude du scellement (reprise des vides en clés de voute) des galeries de diamètre 8 m, avec le matériau COx/MX80 a été investiguée. La méthode considère que la contrainte appliquée sur le remblai est due à son poids propre. Les calculs ont montré que le scellement des galeries peut être obtenu avec les mélanges COx/MX80 entre 30% et 40% de la MX80.

## 7. Etude hydromécanique des mélanges COx/MX80 sous forme de pellets

Le comportement hydromécanique de l'assemblage de pellets de COx/MX80 a été étudié, avec une mise en place par couches et sans appliquer un compactage mécanique. La pression de gonflement développée est mesurée à volume constant, ainsi que la conductivité hydraulique (perméabilité) à la saturation.

Tous les matériaux testés sont formés selon la granulométrie optimale retenue au chapitre 5. En particulier, des échantillons composés de pellets de 16 mm, de pellets de 10 mm et de grains plus fins ( $d < 2$  mm) sont préparés par couches, en proportions de 60%, 10% et 30% en masse totale. Deux types de grains plus fins ont été utilisés : du sable bien-gradué et du concassé de pellets, présentant une granulométrie très similaire. Des mélanges contenant du sable, du concassé et des mélanges des deux à proportions égales ont été étudiés. La variation des matériaux utilisés peut être catégorisée en fonction de leur caractéristique minéralogique: le matériau argileux correspondant aux mélanges de COx/MX80, et le matériau sableux correspondant à la teneur en sable incorporée. En total, la teneur en bentonite MX80 est presque constante comprise entre 28% et 32,5%, le pourcentage du COx varie plus entre 42% et 70%, et la teneur en sable est comprise entre 0 et 30%.

Les essais ont été réalisés à volume constant, en utilisant une cellule de 120 mm de diamètre intérieur, et une hauteur d'environ 50 mm, correspondant à trois couches de matériau. Les échantillons ont été hydratés avec de l'eau du site et il a été permis d'établir que :

- La pression de gonflement augmente avec l'accroissement de la densité sèche.
- La cinétique de la pression de gonflement est liée à la conductivité hydraulique. Lorsque la teneur en sable augmente (c'est-à-dire une conductivité hydraulique plus élevée), la pression de gonflement se développe de manière presque instantanée. En revanche, dans le cas du concassé (c'est-à-dire un échantillon moins perméable), la cinétique de l'évolution de la pression de gonflement est plus lente.
- Une dépendance significative sur la pression de gonflement selon le type de grains plus fins (sable ou concassé de pellets) a été observée. Les échantillons constitués de 30% de sable présentent des pressions de gonflement plus élevées.
- La pression de gonflement suit une augmentation non linéaire avec la teneur en sable.
- La conductivité hydraulique augmente de manière exponentielle avec le pourcentage de sable. En revanche à partir de 15%, la perméabilité est régie par le sable.

- 
- Pour les échantillons de mélanges de pellets CO<sub>x</sub>/MX80 et concassé de pellets, la pression de gonflement développée est très proche de la pression de gonflement des échantillons en poudre compactés à la même densité sèche.

## 8. Conclusions

Les conclusions générales sont développées sous les aspects suivants.

### Granulométrie optimale

La compacité d'un matériau granulaire a été examinée en termes de distribution granulométrique par étude numérique et expérimentale :

- Un fuseau trimodal et bimodal de pellets peut mener à la même densité si les deux tailles extrêmes restent semblables.
- Le rapport de taille est un paramètre essentiel, qui contrôle la densité de l'assemblage.
- La masse volumique du mélange granulaire >1,45 Mg/m<sup>3</sup> est obtenue seulement avec des pellets et des grains « plus fin » (d<2mm) possédant une granulométrie bien-graduée (par exemple un sable).
- Le mélange retenu constitué de pellets de diamètres 16 mm et 10 mm et de sable bien-gradué est mis en place par couches avec les proportions de 60%, 10% et 30% en masse.

### Fabrication des pellets

Des mélanges de CO<sub>x</sub>/MX80 en poudre ont été compactés pour fabriquer des pellets de 16 mm, 10 mm et 4 mm, en utilisant une machine à comprimés reconditionnée pour la présente étude. Le CO<sub>x</sub> est une argile de moyenne plasticité, contrairement à la MX80 qui présente une plasticité extrêmement élevée. La fabrication des pellets à base de CO<sub>x</sub> contenant des particules fines abrasives a nécessité de nombreuses adaptations portant sur le choix des aciers et des géométries des poinçons, des matrices et de la teneur en eau du mélange. C'est ainsi que la forme sphérique des extrémités des poinçons a nécessité de nombreux ajustements. Il en a résulté la réalisation d'un grand nombre de poinçons pour obtenir une bonne productivité de pellets (nombre de pellets intacts/ nombre de pellets fabriqués). Après tous ces ajustements la fabrication des pellets a été réalisée pour une masse volumique de l'ordre de 2,0 Mg/m<sup>3</sup>.

### Etude hydromécanique

Le comportement hydromécanique des mélanges CO<sub>x</sub>/MX80 (≤40% MX80) est étudié sur des poudres et des assemblages de pellets, pour la même gamme de densité. L'ensemble des essais réalisés ont permis d'établir que :

- L'augmentation de la bentonite dans le mélange, augmente la capacité de gonflement.
- Pas de variation significative des propriétés de gonflement entre l'eau du site et la solution alcaline.
- Les échantillons de pellets et de poudres compactés à la même densité, avec les mêmes pourcentages des constituants CO<sub>x</sub>/MX80, présentent les mêmes pressions de gonflement.
- L'ajout de sable dans le mélange pellets CO<sub>x</sub>/MX80 entraîne une augmentation de la pression de gonflement.
- L'introduction de sable au sein des pellets augmente considérablement la conductivité hydraulique.
- Une optimisation sur le pourcentage de sable dans les pellets en terme de conductivité hydraulique et de pression d'entrée d'air devra être menée au regard des caractéristiques hydromécaniques souhaitées pour le remblai.





FOLIO ADMINISTRATIF

THESE DE L'UNIVERSITE DE LYON OPEREE AU SEIN DE L'INSA LYON

NOM : TYRI

DATE de SOUTENANCE : 07/01/2021

Prénoms : Danai Panagiota

TITRE : Contribution to the study of pelletized mixture composed of COx argillite and MX80 bentonite as backfill for geological repositories

NATURE : Doctorat

Numéro d'ordre : 2021LYSEI001

Ecole doctorale : Mécanique – Energétique – Génie Civil - Acoustique

Spécialité : Génie Civil

**RESUME :**

The safe operation of geological disposal facilities for radioactive waste indicates the galleries progressive closure, by installing sealing and backfill materials. In French concept of radioactive waste disposal, crushed excavated Callovo-Oxfordian (COx) argillite with bentonite additive (MX80) in pelletized form is considered as backfill material, due to operational advantages. The pelletized mixture is emplaced inside the galleries at dry state, presenting initially a granular structure, gradually homogenised, due to swelling upon hydration from the groundwater of the surrounding rock.

Objective of the PhD thesis is the determination and fabrication of the pelletized mixture, as well as the analysis of its hydro-mechanical behaviour. The pelletized granulometry is selected to result in the highest possible packing density, defining the optimum grain size distribution (GSD). The implemented COx/MX80 backfill needs to produce adequate swelling capacity and low hydraulic conductivity.

Numerical and experimental gravitational deposits are conducted, to study the compactness of a granular material, without mechanical compaction. Simulations using the Discrete Element Method (DEM) investigate the granulometric effect on the granular material's packing state, determining an optimum GSD. Supplementary experiments are used to evaluate and finalise the granulometric selection maximising the resulting density. Both studies investigate the effect of additional parameters (implementation protocol, inter-particle friction, deposit height,...) on the packing state.

The pelletization of the selected GSD is performed for the first time on COx/MX80 powdered mixtures, by applying the compression method on a reconditioned tablet machine. The process is analysed to successfully fabricate pellets and optimise the challenging pellet production.

COx/MX80 mixtures hydro-mechanical behaviour is experimentally investigated by performing infiltration tests under free and confined volume conditions. A parametric study on various powdered mixtures is conducted to characterise the materials physicochemical properties and evaluate their swelling capacity at densities expected on the backfill implementation. On the other hand, the finalised pellets assembly on various compositions is directly tested in terms of swelling pressure and hydraulic conductivity.

MOTS-CLÉS : pellets, Callovo-Oxfordian claystone, MX80-bentonite, maximum packing density, optimum grain size distribution, DEM, hydro-mechanical behavior, swelling potential, swelling pressure, hydraulic conductivity

Laboratoire (s) de recherche : GEOMAS

Directeur de thèse: Irini DJERAN-MAIGRE

Président de jury : Daniel LEVACHER

**Composition du jury :**

Philippe COSENZA, Christophe LANOS, Daniel LEVACHER, Polyxeni KALLIOGLOU, Frédéric PLAS, Jad ZGHONDI, Irini DJERAN-MAIGRE, Jean-Claude ROBINET, Christophe IMBERT